



UNIVERSIDAD DE CHILE  
FACULTAD DE CIENCIAS FÍSICAS Y MATEMÁTICAS  
DEPARTAMENTO DE GEOLOGÍA

FUENTES Y RESERVORIOS DE YODO NATURAL Y ANTROPOGÉNICO  
EN EL DESIERTO DE ATACAMA, NORTE DE CHILE

**TESIS PARA OPTAR AL GRADO DE DOCTOR EN CIENCIAS, MENCIÓN  
GEOLOGÍA**

FERNANDA CAROLINA ÁLVAREZ AMADO

PROFESOR GUÍA:  
MARTIN REICH MORALES

MIEMBROS DE LA COMISIÓN:  
GABRIEL VARGAS EASTON  
GLEN SNYDER  
DOLORINDA DANIELE

SANTIAGO DE CHILE  
MARZO 2015

RESUMEN DE LA TESIS PARA OPTAR AL GRADO  
DE: Doctor en Ciencias, Mención Geología  
POR: Fernanda Carolina Álvarez Amado  
FECHA: 02/03/2015  
PROFESOR GUÍA: Martin Reich Morales

## **FUENTES Y RESERVORIOS DE YODO NATURAL Y ANTROPOGÉNICO EN EL DESIERTO DE ATACAMA, NORTE DE CHILE**

El Desierto de Atacama, ubicado en el norte de Chile corresponde al desierto más árido del planeta. En esta región se encuentran las mayores reservas de yodo a nivel mundial y a su vez corresponde a la principal provincia productora de este elemento. El origen de este enriquecimiento ha sido motivo de controversia y diferentes procesos han sido propuestos para explicar la presencia de yodo en Atacama, involucrando principalmente fuentes marinas y eólicas. Sin embargo, debido a la escasez de datos geoquímicos e isotópicos de yodo en la región, su origen aún no ha sido dilucidado. De acuerdo a lo anterior, el objetivo de esta tesis consiste en determinar las fuentes naturales y antropogénicas de yodo en reservorios superficiales de la región de Atacama.

Los resultados obtenidos en esta investigación comprueban que existe un fuerte enriquecimiento de yodo en la zona, el cual se extiende desde la Depresión Central hasta la Cordillera Occidental. Las razones isotópicas  $^{129}\text{I}/\text{I}$  obtenidas en rocas y suelos indican que el yodo deriva de un proceso de mezcla de diferentes fuentes, incluyendo fluidos profundos enriquecidos en contenido orgánico con variables aportes de fluidos volcánicos y meteóricos pre-antropogénicos. De manera consistente, la señal isotópica medida en aguas superficiales y subterráneas, en conjunto con las concentraciones de halógenos, sugieren la presencia de un fluido inicial enriquecido en yodo, el cual habría sido diluido por agua meteórica. Sin embargo, a diferencia de lo que indica la señal isotópica en rocas y suelos, la mayoría de las razones isotópicas observadas en aguas indican que existe una componente antropogénica.

Se propone que la principal fuente orgánica de yodo en rocas, suelos, aguas superficiales y subterráneas de Atacama, corresponde a las secuencias sedimentarias marinas del Jurásico, donde el yodo proviene del agua de poros o desde las facies carbonatadas, y es extraído a través del flujo subterráneo. Por otro lado, la componente antropogénica proviene de dos fuentes distintas: (1)  $^{129}\text{I}$  liberado por ensayos nucleares en el Océano Pacífico Central ( $^{129}\text{I}/\text{I} = 12000 \times 10^{-15}$ ); y (2)  $^{129}\text{I}$  liberado por plantas de procesamiento nuclear ubicadas en el hemisferio norte ( $^{129}\text{I}/\text{I} = 97000 \times 10^{-15}$ ).

Por lo tanto, se concluye la existencia de múltiples fuentes de yodo en el Desierto de Atacama, descartando que provenga exclusivamente de una fuente atmosférica, resaltando la importancia del drenaje subterráneo en los procesos de transporte y depositación en márgenes continentales.

***A mi Siste y mi tío Beto por estar siempre presentes,  
porque sé todo lo que me quisieron y por los hermosos  
recuerdos llenos de sentimiento que tengo junto a ustedes.***

*“... vivir la vida y aceptar el reto,  
recuperar la risa, ensayar el canto,  
bajar la guardia y extender las manos,  
desplegar las alas e intentar de nuevo,  
celebrar la vida y retomar los cielos,*

*No te rindas por favor no cedas,  
aunque el frío queme,  
aunque el miedo muerda,  
aunque el sol se ponga y se calle el viento,  
aún hay fuego en tu alma,  
aún hay vida en tus sueños...”*

***Mario Benedetti - No te rindas***

# Agradecimientos

Si hoy escribo estas palabras es gracias a mi familia, sé que cada vez que los necesite ustedes estarán ahí. Mauri, mi compañero y amor de la vida... gracias por estar a mi lado en este camino, por apoyarme incondicionalmente, por sentir y construir conmigo, por el hermoso futuro que nos aguarda... te amo. Mami y Papi, gracias por el gran esfuerzo que hacen día a día, el cual me ha permitido empezar y terminar esta etapa, Lila por poner el hombro y mantenernos unidos, Papi por trabajar tanto por nosotros, los quiero mucho. Lore, Nati y Javier, gracias por crecer conmigo, por alegrarme la vida, los amo, los apoyo en todo y admiro que sean personas conscientes de las injusticias de este mundo y que eso les duela. Gracias a mi siste, mi tío Pepín, mi tío Beto, mis primos Alberto, Nico y Pame, a la pequeña Sofi, y toda mi familia de San Antonio, son muy importantes para mí. También quiero agradecer a mi tía Maura por la compañía y apoyo. Gracias a mi familia de San Javier, donde he encontrado un segundo hogar.

Agradezco a Martin por confiar en mí, por apoyarme y entender siempre cuando tuve problemas, porque en conjunto al grupo de trabajo me enseñaron una buena y motivante forma de hacer ciencia. Gracias Coni por estar a mi lado todos los días y Alida por la ayuda en terreno y laboratorio. Oscar, Pablín, Dani, Camilo, Vladi y Laura gracias por escucharme, por enseñarme, por discutir conmigo y ayudarme a terminar este trabajo. Agradezco a Glen, por su disposición, su guía, por compartir su conocimiento y por recibirme en su casa. Gracias a Gabriel y Linda por sus comentarios y discusiones. También quisiera agradecer a todos los funcionarios y profesores del Departamento, en especial a Pancho por recibirme en geo general, a Maritza, Blanca, Mery Rose, Cristi, Vero, Kilo, Jaime y Rosita por su ayuda en estos 10 años. Sin el apoyo de ustedes esta tesis jamás hubiese terminado.

Durante mi vida he conocido muy buenas personas, grandes amigas y amigos, son muchos los momentos de alegría que atesoro junto a ustedes y otros tantos de pena en los que nunca fallaron. Muchas gracias a mis amigas del cole, las mejores, en especial Milu y Thiare por estar siempre que lo necesito, por traer al mundo a la pequeña Valentina. A mis grandes amigos de la u: Laja, Sally y Jorge. A mis amigas de geo: Caro, Chica, Paula, Vivi, Melu, Feña L, Pajariño, Atax, Chicho, Ismi, Cindy, Nico P, Feña A, Chala y Manu. A mis compañeritos de oficina, los que hicieron posible en el día a día, sacar esta tesis adelante: Feli, Monse, Coni, Oscar, Pablín, Dani, Mane, Pelao, Claudio, Mumo, Pame, Checho, Alida, Viole, Mary, Boyce y todos los demás.

Una parte muy importante de mi vida es el *basket*, a través de este deporte he conocido gente hermosa. Gracias a mi lindo equipo, a mis compañeras, que las extrañaré demasiado y a mis amigas Roci, Rucia, Vale, Giss, Nico, Dani y Juli. Gracias a mi *coach* y amigo Julio y al resto de los chiquillos. Gracias a todos por ser equipo dentro y fuera de la cancha.

También quiero agradecer a todas quienes llevan un mundo nuevo en sus corazones, a los y las que lucharon sin miedo el 2006, el 2011 y lo siguen haciendo, a los que conocen que este sistema, injusto y egoísta, es sólo una realidad transitoria, a quienes construyendo organización mantienen viva la esperanza.

Agradezco a las fuentes de financiamiento: Beca de Doctorado Nacional 2010 CONICYT, Proyecto FONDECYT 1100014 "Origin and age of iodine in supergene zones of copper deposits and in the nitrate ore fields of the Atacama Desert" , Proyecto FONDAP 15090013 a través del Centro de Excelencia en Geotermia de los Andes, y Proyecto Núcleo Milenio NC130065 "Metal tracing along subduction".

# Tabla de contenido

Capítulo I. Introducción .....	1
I.1 Publicaciones y resúmenes resultantes de esta investigación .....	4
I.1.1 Publicaciones .....	4
I.1.2 Resúmenes presentados en conferencias .....	5
I.2 Bibliografía .....	5
Capítulo II. Antecedentes geológicos y climáticos .....	7
II.1 Marco geológico .....	7
II.1.1 Cordillera de la Costa .....	7
II.1.2 Depresión Central .....	9
II.1.3 Precordillera .....	10
II.1.4 Depresión Subandina y Cordillera Occidental .....	11
II.2 Antecedentes climáticos .....	13
II.3 Bibliografía .....	14
Capítulo III. Metodologías y obtención de datos .....	18
III.1 Metodología en terreno .....	18
III.1.1 Muestras de roca y suelo .....	20
III.1.2 Muestras de agua .....	22
III.2 Metodología de muestreo en laboratorio .....	25
III.2.1 Comportamiento geoquímico .....	26
III.2.2 Sistema isotópico del yodo $^{129}\text{I}$ .....	27
III.2.3 Procedimientos analíticos: Concentraciones de halógenos .....	31
III.2.4 Extracción de yodo y medición de razones isotópicas $^{129}\text{I}$ .....	32
III.3 Bibliografía .....	39
Capítulo IV. Iodine in supergene copper blankets: a case study from the giant Chuquicamata porphyry deposit .....	42
IV.1 Abstract .....	42
IV.2 Introduction .....	42

IV.3	Iodine in the study area and samples.....	43
IV.4	Iodine geochemistry and the <sup>129</sup> I isotopic system.....	44
IV.5	Results .....	47
IV.6	Discussion.....	47
IV.7	Conclusion .....	50
IV.8	References.....	50
Capítulo V. Iodine in nitrate deposits from the Antofagasta districts .....		54
V.1	Abstract.....	54
V.2	Introduction .....	54
V.3	Results .....	55
V.4	Discussion.....	56
V.5	Conclusion .....	58
V.6	References.....	59
Capítulo VI. Sources of natural and anthropogenic iodine in natural waters from the Atacama Desert, northern Chile .....		61
VI.1	Abstract.....	61
VI.2	Introduction .....	62
VI.3	Climatic and hydrological setting.....	63
VI.4	Sampling materials.....	64
VI.5	Results .....	66
VI.6	Discussion.....	68
VI.6.1	Halogen concentrations.....	68
VI.6.2	<sup>129</sup> I concentrations and <sup>129</sup> I/I isotopic ratios .....	72
VI.6.3	Relative contributions of pre-anthropogenic vs. Anthropogenic sources for iodine in Atacama waters .....	75
VI.6.4	Local hydrological cycle of iodine .....	76
VI.7	Conclusions.....	78
VI.8	References.....	79
Capítulo VII. Sources, sinks and long-term cycling of iodine in the hyperarid Atacama continental margin .....		86

VII.1	Abstract .....	86
VII.2	Introduction .....	87
VII.3	Background .....	88
VII.3.1	Geological setting .....	88
VII.3.2	Climatic and hydrologic setting.....	89
VII.3.3	Iodine-rich nitrate soils and supergene copper deposits.....	91
VII.4	Sample material and analytical methods.....	94
VII.5	Results .....	95
VII.5.1	Iodine concentrations .....	95
VII.5.2	<sup>129</sup> I/I isotopic ratios .....	96
VII.6	Discussion .....	99
VII.6.1	Distribution of iodine in Atacama .....	99
VII.6.2	Sources of iodine.....	103
VII.6.3	Fluid mixing and timescales of groundwater flow .....	105
VII.6.4	Tectonic, climatic and metallogenic implications .....	108
VII.7	Conclusion .....	111
VII.8	References.....	112
Capítulo VIII.	Conclusiones .....	124
Apéndice A.	Publicaciones .....	126
A.1	Using iodine isotopes to constrain supergene fluid sources in arid regions: insights from the Chuquicamata oxide blanket .....	127
A.2	Climate change and tectonic uplift triggered the formation of the Atacama Desert's giant nitrate deposits.....	136
Apéndice B.	Resúmenes de congresos.....	140
B.1	Annual Goldschmidt Conference, Prague, Czech Republic, 2011 .....	140
B.2	XVIII Congreso Geológico Chileno, Antofagasta, Chile, 2012 .....	141
B.3	AGU Meeting of the Americas, Cancun, Mexico, 2013.....	142
B.4	Annual Goldschmidt Conference, Florence, Italy, 2013.....	144
B.5	Annual Goldschmidt Conference, Sacramento, USA, 2014.....	145

# Índice de figuras

II.1	Unidades morfoestructurales y zonas climáticas del Desierto de Atacama .....	9
II.2	Mapa geológico del área de estudio .....	12
III.1	Sitios de muestreo .....	19
III.2	Ocurrencia de depósitos de nitratos .....	21
III.3	Afloramientos de secuencias sedimentarias.....	22
III.4	Tipos de agua muestreados .....	23
III.5	Medición de parámetros <i>in situ</i> y filtrado de muestras.....	24
III.6	Colecto de agua de lluvia .....	25
III.7	Ciclo geoquímico del yodo en márgenes continentales.....	27
III.8	Sistemática de las dataciones con $^{129}\text{I}$ .....	29
III.9	Rangos de valores del sistema isotópico del yodo .....	30
IV.1	Ubicación del distrito de Chuquicamata, muestra de marshita (Cul) .....	44
IV.2	Modos de producción natural de $^{129}\text{I}$ .....	46
IV.3	Razones isotópicas $^{129}\text{I}/\text{I}$ en marshita y muestras de suelos de Chuquicamata .	47
IV.4	Modelo geoquímico de mezcla .....	49
V.1	Razones isotópicas $^{129}\text{I}/\text{I}$ en depósitos de nitratos.....	56
V.2	Modelo genético del origen de nitratos .....	58
VI.1	Sitios de muestreo .....	65
VI.2	Razones isotópicas $^{129}\text{I}/\text{I}$ según el reservorio .....	68
VI.3	Diagrama de yodo versus cloro .....	70
VI.4	Diagrama de bromo versus cloro.....	71
VI.5	Diagrama $\text{I}/\text{Cl}$ versus $\text{Br}/\text{Cl}$ .....	72
VI.6	Concentraciones de $^{129}\text{I}$ y razones isotópicas $^{129}\text{I}/\text{I}$ , comparación con datos mundiales .....	74



VI.7	Diagrama de mezcla $^{129}\text{I}/\text{I}$ versus $1/\text{I}$ .....	76
VI.8	Ciclo hidrológico del yodo en el Desierto de Atacama.....	77
VII.1	Unidades morfoestructurales, mapa de precipitación y sitios de muestreo .....	91
VII.2	Afloramientos de reservorios sólidos y distribución de las razones $^{129}\text{I}/\text{I}$ .....	94
VII.3	Razones isotópicas $^{129}\text{I}/\text{I}$ según el reservorio .....	99
VII.4	Rangos de concentración de yodo en reservorios del Desierto de Atacama....	101
VII.5	Perfil de suelo de nitrato representativo, concentraciones de yodo y razones $^{129}\text{I}/\text{I}$ .....	102
VII.6	Diagrama de mezcla $^{129}\text{I}/\text{I}$ versus $1/\text{I}$ .....	105
VII.7	Modelo geoquímico de mezcla .....	108

# Índice de tablas

VI.1	Resultados analíticos de concentraciones de halógenos y razones isotópicas $^{129}\text{I}/\text{I}$ en muestras de agua .....	67
VII.1	Resultados analíticos de concentraciones de yodo y razones isotópicas $^{129}\text{I}/\text{I}$ en suelos, sedimentos y rocas.....	97
VII.2	Resultados analíticos de concentraciones de yodo y parámetros geoquímicos en muestras de agua .....	98

# Capítulo I.

# Introducción

El yodo (I) es un elemento químico esencial para el desarrollo de la vida. Este elemento es considerado un micronutriente fundamental para la subsistencia y el crecimiento de humanos y otros organismos.

Actualmente el yodo tiene aplicaciones en diferentes áreas. En la medicina, es utilizado como componente principal en medios de contraste en exámenes de rayos X y en antisépticos. Además, actúa como catalizador en la síntesis de productos farmacéuticos. En la industria, el yodo es utilizado como biocida para contrarrestar la acción de organismos considerados nocivos para la salud. Recientemente, el yodo ha adquirido importancia en el área tecnológica, siendo ampliamente usado en la fabricación de polarizadores de cámaras fotográficas y pantallas de cristal-líquido (LCD). Este variado y moderno rango de aplicaciones ha potenciado el interés económico de este elemento en las últimas décadas.

Alrededor del 90% del yodo en el mundo es producido por Chile (~55%) y Japón (~35%). Chile, además de ser el principal productor de yodo a nivel mundial, posee las mayores reservas de este elemento, específicamente en los suelos de nitratos o “caliche” del Desierto de Atacama, norte de Chile.

En cuanto a sus propiedades químicas, el yodo es un elemento perteneciente al grupo de los halógenos, por lo tanto, comparte ciertas características con el cloro (Cl) y el bromo (Br). Sin embargo, debido a su gran radio iónico (2.16 Å), rara vez es incorporado a fases minerales y tiende a permanecer en solución acuosa por mayor tiempo que los otros halógenos. Por otro lado, debido a su naturaleza fuertemente biofílica, el yodo se concentra preferentemente en fluidos de origen orgánico, por lo que, a diferencia del cloro, no es considerado un elemento conservativo en sistemas acuosos.

La distribución global de yodo está dominada por el sistema marino, en particular por los sedimentos del fondo oceánico, que contienen alrededor del ~70% del yodo total en la corteza y presentan concentraciones que varían desde los 200 hasta los 1300 ppm (Wong, 1991; Muramatsu & Wedepohl, 1998). En contraste, el agua de mar tiene una concentración promedio de yodo de 0,05 ppm, cuatro órdenes de magnitud más baja que la concentración en sedimentos marinos. Si bien la cantidad de yodo disponible en ambientes marinos y su distribución global están bien acotadas (Muramatsu y Wedepohl, 1998; Baker *et al.*, 2001), pocos casos de concentraciones elevadas en rocas, suelos y aguas de la corteza continental han sido reportados, con ocurrencias de minerales de yodo restringidas a ambientes hiperáridos.

Como se mencionó anteriormente, uno de estos casos corresponde al Desierto de Atacama, el cual alberga depósitos con algunas de las concentraciones más altas de yodo conocidas en ambientes continentales (Ericksen, 1981). En esta área, la ocurrencia

de minerales se restringe a: (1) Zonas supérgenas en depósitos de cobre y (2) Suelos de nitratos ubicados al este de la Cordillera de la Costa.

En zonas supérgenas de depósitos de cobre en la Cordillera de la Costa (e.g., Mantos de la Luna), Depresión Central (e.g., Spence) y Precordillera (e.g., Chuquicamata y Escondida) se han reportado minerales con yodo. Por ejemplo, Jarrell (1939) confirma la ocurrencia de *marshita* (CuI) en Chuquicamata, asociada fuertemente a la atacamita. Minerales de yodato y cobre también se han reportado en la zona de óxidos de Chuquicamata, entre ellos la *salesita* (Cu(IO<sub>3</sub>)(OH)) y *bellingierita* (Cu<sub>3</sub>(IO<sub>3</sub>)<sub>6</sub>·2H<sub>2</sub>O) (Jarrell et al., 1944). En estos trabajos se menciona el avistamiento de nubes de color púrpura durante tronaduras, las cuáles reflejan un contenido considerable de yodo. Por otro lado, se han reconocido anomalías geoquímicas de yodo en aguas subterráneas y suelos asociados a estos yacimientos, donde valores anómalos de yodo coexisten con cloruros de cobre y sulfatos, entre otras fases oxidadas de cobre (e.g., Cameron et al., 2010). Reich et al. (2009) reportaron la ocurrencia de inclusiones de yodargirita en cristales de calcosina de Mantos de la Luna, sugiriendo que habrían precipitado a partir de fluidos reducidos ricos en yodo.

Los depósitos de nitratos constituyen la principal fuente de yodo a nivel mundial, reportándose concentraciones de yodo que sobrepasan en tres a cuatro órdenes de magnitud la concentración promedio de la corteza continental (120 ppb, Muramatsu y Wedepohl, 1998). En estos depósitos el yodo forma minerales de yodato (IO<sub>3</sub><sup>-</sup>), los que se presentan asociados a nitratos (NO<sub>3</sub><sup>-</sup>), cloruros (Cl<sup>-</sup>), sulfatos (SO<sub>4</sub><sup>2-</sup>), y en menor medida con percloratos (HClO<sub>4</sub>) y cromatos (CrO<sub>4</sub><sup>2-</sup>), (Ericksen, 1981).

Por otro lado, el origen del yodo en estos depósitos ha sido materia de debate, sin ser esclarecido aún. Algunos autores han propuesto una fuente atmosférica para el yodo en los nitratos, donde éste sería liberado como yodato desde compuestos orgánicos presentes en el *spray* marino y/o partículas de aerosol, precipitando luego desde la atmósfera a la superficie de la Depresión Central (Ericksen, 1983; Michalski *et al.*, 2004). Sin embargo, datos preliminares de isótopos de yodo en estos suelos se asemejan a razones isotópicas reportadas en fluidos de antearco, sugiriendo que el yodo presente en Atacama no proviene exclusivamente de una fuente atmosférica-marina y reflejaría el aporte de una fuente más profunda, diferente a la de nitratos o sulfatos (Fehn *et al.*, 2007). Por otro lado, en zonas de yacimientos supérgenos de cobre no existen datos isotópicos que soporten una hipótesis en particular.

De esta manera, la escasez de datos geoquímicos e isotópicos en la zona no ha permitido determinar cuáles son las fuentes de yodo y cómo actúan los procesos de transporte, precipitación y fijación de yodo en la región de Atacama. Debido a este vacío de información, hasta la fecha no ha sido posible explicar la presencia de concentraciones anómalas y cómo éstas se distribuyen en la región. Así, este inexplorado enriquecimiento de yodo en conjunto con la convergencia de factores geológicos y climáticos únicos en el

Desierto de Atacama constituyen una importante oportunidad para investigar el origen y comprender el ciclo geoquímico del yodo en ambientes continentales

El objetivo general de esta investigación consiste en determinar las fuentes de yodo en los distintos reservorios del Desierto de Atacama, para lo cual se utilizarán métodos geoquímicos e isotópicos, con especial énfasis en la aplicación del sistema isotópico de  $^{129}\text{I}$  en muestras de origen sólido y líquido. Además, debido al carácter biofílico del yodo, este elemento resulta muy útil no sólo para datar sino que también para trazar fluidos orgánicos, por lo tanto, a través del sistema isotópico del yodo y su relación con otros halógenos, se pretende estudiar la migración de fluidos a escala regional y su relación con la historia climática, hidrológica y geodinámica del Desierto de Atacama.

En el Capítulo IV se investiga el origen del yodo en minerales y suelos presentes en zonas supérgenas de yacimientos de cobre. Además, se discute la aplicabilidad del sistema isotópico del yodo como trazador de fluidos supérgenos. La integración de los datos obtenidos con modelos geoquímicos se utiliza para estimar la escala de tiempo de circulación de fluidos durante el enriquecimiento supérgeno en el norte de Chile.

En el Capítulo V se estudia el origen del yodo en los suelos de nitratos. Los datos presentados en esta sección corresponden a razones isotópicas medidas en muestras de la región de Antofagasta ( $23^{\circ}$ - $24^{\circ}\text{S}$ ), las cuales son analizadas con el fin de plantear un modelo genético capaz de explicar la presencia simultánea de las diferentes componentes (*i.e.*, nitratos, sulfatos, percloratos, yodatos y cromatos). Este modelo propone la existencia de múltiples fuentes para estos depósitos e incorpora el subestimado rol de las aguas subterráneas en su proceso de formación. Además, se investiga la posible relación entre las condiciones tectónicas, hidrológicas y climáticas desarrolladas en el Desierto de Atacama con la formación y preservación de los suelos de nitratos.

En el Capítulo VI se reporta por primera vez en Sudamérica la señal química e isotópica de yodo en aguas superficiales. Debido a que en los capítulos anteriores se propone una importante participación de aguas subterráneas en el origen del yodo, se estudian las concentraciones y razones de  $^{129}\text{I}/\text{I}$  en muestras de agua de mar, ríos, salares, aguas subterráneas, manantiales de alta y baja temperatura y agua de lluvia. El análisis de estos datos demuestra que existe un fluido rico en contenido orgánico que aporta yodo a las aguas naturales del Desierto de Atacama. Por otro lado, las razones isotópicas indican la influencia de una fuente atmosférica y antropogénica de yodo en la región, sugiriendo un transporte a gran escala de  $^{129}\text{I}$ , donde gran parte de este radioisótopo provendría desde el Océano Pacífico Central y el Hemisferio Norte.

En el Capítulo VII se investiga la distribución de yodo a escala regional. Los datos analizados en esta sección corresponden a concentraciones de yodo y razones isotópicas en muestras de rocas, suelos, sedimentos y aguas naturales del Desierto de Atacama ( $19.5^{\circ}$ - $24^{\circ}\text{S}$ ). Con esta información se identifican las zonas más enriquecidas

en yodo y se analiza cómo la distribución de éste puede relacionarse a procesos de transporte y precipitación. A partir de un análisis integrado se discute cuáles son específicamente las fuentes de yodo y cuánto aportan cada una de éstas en los diferentes reservorios del Desierto de Atacama. Estos datos, en conjunto con el desarrollo de modelamiento geoquímico, permiten estudiar procesos de migración y mezcla de fluidos a escala de decenas de millones de años. Además, se discute la relación entre la distribución geoquímica e isotópica del yodo con la evolución geodinámica y climática desarrollada en el Desierto de Atacama.

Finalmente, en el Capítulo VIII se presentan las conclusiones generales de esta investigación. Basados en las discusiones e interpretaciones de los capítulos anteriores, se propone el modelo final de origen, distribución y preservación de yodo en los reservorios el Desierto de Atacama. Además se indica los estudios futuros que podrían realizarse para complementar esta investigación.

## **I.1 Publicaciones y resúmenes resultantes de esta investigación**

### **I.1.1 Publicaciones**

Reich M., Snyder G. T., Álvarez F., Pérez A., Palacios C., Vargas G., Cameron E. M., Muramatsu Y. y Fehn U. (2013) Using iodine isotopes to constrain supergene fluid sources in arid regions: insights from the Chuquicamata oxide blanket. *Econ. Geol.* 108, 163-171. **Capítulo IV. Apéndice A.**

Pérez-Fodich A., Reich M., Álvarez F., Snyder G. T., Schoenberg R., Vargas G., Muramatsu Y. y Fehn U. (2014) Climate change and tectonic uplift triggered the formation of the Atacama Desert's giant nitrate deposits. *Geology* 42, 251-254. **Capítulo V. Apéndice A.**

Álvarez F., Reich M., Pérez-Fodich A., Snyder G. T. Sources of natural and anthropogenic iodine in natural waters from the Atacama Desert, northern Chile. En preparación. **Capítulo VI.**

Álvarez F., Reich M., Pérez-Fodich A., Snyder G. T., Muramatsu Y., Vargas G., y Fehn U. (2015) Sources, sinks and long-term cycling of iodine in the hyperarid Atacama continental margin. *Geochim. Cosmochim. Acta* (aceptado). **Capítulo VII.**

## I.1.2 Resúmenes presentados en conferencias

Reich M., Álvarez F., Pérez A., Snyder G. T., Palacios C., Vargas G., Muramatsu Y., Cameron E. M. y Fehn U. (2011) The  $^{129}\text{I}$  isotopic composition of supergene iodine minerals in Chile and Australia. *Annual Goldschmidt Conference, Prague, Czech Republic*. **Apéndice B.**

Álvarez F., Pérez A., Snyder G. T., Vargas G., Muramatsu Y. y Reich M. (2012) Origen del yodo en el Desierto de Atacama:  $^{129}\text{I}$  como trazador de fluidos en procesos geodinámicos. *XVIII Congreso Geológico Chileno, Antofagasta*. **Apéndice B.**

Álvarez F., Pérez A., Snyder G. T., Vargas G., Muramatsu Y. y Reich M. (2013) Source and sinks of natural and anthropogenic iodine in the hyperarid Atacama Desert of northern Chile. *AGU Meeting of the Americas, Cancun, Mexico*. **Apéndice B.**

Álvarez F., Reich M., Pérez A., Snyder G. T., Vargas G., Muramatsu Y. y Fehn U. (2013) Sources, sinks and long-term cycling of iodine in a hyperarid continental margin. *Annual Goldschmidt Conference, Florence, Italy*. **Apéndice B.**

Álvarez F., Reich M., Pérez A., Snyder G. T., Vargas G., Muramatsu Y. y Fehn U. (2014) Natural and anthropogenic iodine in Atacama: sources, sinks and cycling of iodine in a hyperarid continental margin. *Annual Goldschmidt Conference, Sacramento, USA*. **Apéndice B.**

## I.2 Bibliografía

Baker A. R., Tunnicliffe C. y Jickells T. D. (2001) Iodine speciation and deposition fluxes from the marine atmosphere. *J. Geophys. Res.* **106**, 28743-28749.

Cameron E. M., Leybourne M. I., Reich M. y Palacios C. (2010) Geochemical anomalies in northern Chile as a surface expression of the extended supergene metallogenesis of buried copper deposits. *Geochem-Explor. Env.* **10**, 1-14.

Ericksen G. E. (1981) Geology and origin of the Chilean nitrate deposits. *U.S. Geol. Surv. Prof. Paper 1188-B*. Unites States Government Printing Office, Washington.

Fehn U. Moran J. E., Snyder G. T. y Muramatsu Y. (2007) The initial  $^{129}\text{I}/\text{I}$  ratio and the presence of "old" iodine in continental margins. *Nucl. Instrum. Meth. B.* **259**, 496-502.

Jarrell O. (1939) Marshite and other minerals from Chuquicamata, Chile. *Am. Miner.* **24**, 629-635.

Jarrell O. (1944) Oxidation at Chuquicamata, Chile. *Econ. Geol.* **39**, 251-286.

- Michalski G., Bohlke J. K. y Thiemens M. (2004) Long term atmospheric deposition as the source of nitrate and other salts in the Atacama Desert, Chile: New evidence from mass independent oxygen isotopic compositions. *Geochim. Cosmochim. Acta* **68**, 4023-4038.
- Muramatsu Y. y Wedepohl K. H. (1998) The distribution of iodine in the earth's crust. *Chem. Geol.* **147**, 201-216.
- Pérez-Fodich A., Reich M., Álvarez F., Snyder G. T., Schoenberg R., Vargas G., Muramatsu Y. y Fehn U. (2014) Climate change and tectonic uplift triggered the formation of the Atacama Desert's giant nitrate deposits. *Geology* **42**, 251-254.
- Reich M., Palacios C., Alvear M., Cameron E. M., Leybourne M. I. y Deditius A. (2009a) Iodine-rich waters involved in supergene enrichment of the Mantos de la Luna argentiferous copper deposit, Atacama Desert, Chile. *Miner. Deposita* **44**, 719-722.
- Reich M., Snyder G. T., Álvarez F., Pérez A., Palacios C., Vargas G., Cameron E. M., Muramatsu Y. y Fehn U. (2013) Using iodine isotopes to constrain supergene fluid sources in arid regions: insights from the Chuquicamata oxide blanket. *Econ. Geol.* **108**, 163-171.
- Wong G. T. F. (1991) The marine geochemistry of iodine. *Rev. Aquatic. Sci.* **4**, 45-73.
- Zhou J. y Lau K. M. (1998) Does a monsoon climate exist over South America. *J. Clim.* **11**, 1020-1040.



## Capítulo II. Antecedentes geológicos y climáticos

El Desierto de Atacama se extiende en el Norte Grande de Chile y forma una parte importante de la porción más árida del Desierto de Chile-Perú. Se encuentra ubicado entre los Andes Centrales y el Océano Pacífico (Fig. II.1). La zona de estudio se enmarca en las regiones de Tarapacá y Antofagasta entre los 19°S y 24°S.

### II.1 Marco geológico

El contexto tectónico de la zona de estudio corresponde a un margen convergente, donde la placa oceánica de Nazca es subductada bajo la placa continental Sudamericana. Esta configuración tectónica habría sido adquirida hace aproximadamente 25 Ma (e.g. Pardo-Casas and Molnar, 1987). La actual tasa de convergencia es ~7.8 cm/yr (DeMetes *et al.*, 1994; Angermann *et al.*, 1999).

En este sector, se identifican al menos 5 unidades morfoestructurales principales: Cordillera de la Costa, Depresión Central, Precordillera, Cordillera Occidental, Altiplano y Puna (Fig. II.1A). Estas unidades son el resultado de la deformación compresiva producida durante el Cenozoico (Allmendinger *et al.*, 1997). Además, su distribución espacial presenta una íntima relación entre la ubicación de los arcos magmáticos desarrollados a partir del Jurásico durante el Ciclo Andino (Charrier *et al.*, 2002).

Por otro lado, durante el Ciclo Andino, importantes estructuras paralelas al margen se han asociado a la partición de la deformación ocasionada por la oblicuidad de la convergencia. Dos sistemas principales destacan: Sistema de Fallas de Atacama (SFA) en la Cordillera de la Costa, desarrollado durante el Jurásico Superior-Cretácico Inferior (Scheuber y Gonzalez, 1999; Scheuber y Andriessen, 1990; Gonzalez, 1996) y el Sistema de Fallas de Domeyko (SFD) en el sector de Precordillera, iniciado durante el Paleógeno (Amilibia *et al.*, 2008). Estas estructuras corresponden a sistemas estructurales de primer orden que controlarían el ascenso de magmas y fluidos (Maksaev y Zentilli, 1999).

A continuación se describe la evolución geológica desarrollada en la zona de estudio desde el Paleozoico al Reciente, a partir de las unidades morfoestructurales mencionadas (Fig. II.2).

#### II.1.1 Cordillera de la Costa

La Cordillera de la Costa en el norte de Chile es una franja de 700 km de largo que alcanza elevaciones de 1800 m. Las rocas más antiguas corresponden a afloramientos menores del basamento paleozoico representado por secuencias metaturbidíticas de la

Formación El Toco, desarrolladas durante el Devónico (Bahlburg *et al.*, 2009). Sobreyacen a tales secuencias, escasos afloramientos de rocas volcanoclásticas del Triásico (Suárez y Bell, 1992; Marinovic *et al.*, 1995) y sedimentitas marinas del Jurásico Inferior de la Formación Pan de Azúcar (Naranjo y Puig, 1984).

La mayor parte de la Cordillera de la Costa está conformada por rocas volcánicas y plutónicas que sobreyacen e intruyen las unidades antes mencionadas. Estas rocas representan el arco magmático del Jurásico-Cretácico Inferior y las unidades correspondientes se conocen como Formación La Negra en el sector de Antofagasta, Tocopilla y Baquedano (García, 1967) y Formación Oficina Viz en el área de Iquique y Pisagua (Thomas, 1970; Silva, 1977). Por otra parte, el volcanismo del Cretácico Inferior es representado por la Formación Aeropuerto, la cual se ubica principalmente en el margen oriental de la Cordillera de la Costa. Esta unidad consiste en afloramientos de poca extensión compuestos por rocas volcánicas y volcanoclásticas con intercalaciones marinas que sobreyacen de manera concordante las volcanitas de la Formación La Negra (Ulriksen, 1979; Naranjo y Puig, 1984; Marinovic *et al.*, 1995).

El volcanismo jurásico consiste principalmente en lavas porfíricas de composición andesítica y andesítica-basáltica (Oliveros *et al.*, 2006). Por otro lado, importantes cuerpos graníticos y gabroicos agrupados en el Batolito Costero (Jurásico Superior-Cretácico Inferior), intruyen tales secuencias volcánicas (Marinovic *et al.*, 1995).

Contemporáneo al desarrollo del arco magmático, se desarrollaron cuencas de trasarco en las actuales Cordillera de la Costa y Precordillera (Mpodozis y Ramos, 2008). Estas cuencas preservan rocas sedimentarias de origen marino, comúnmente fosilíferas, que representan un ciclo de transgresión-regresión (Charrier *et al.*, 2002). En la Cordillera de la Costa, estas secuencias afloran principalmente entre Iquique y Pisagua, donde corresponden a las formaciones Caleta Ligate (Bajociano), El Godo (Bajociano-Oxfordiano) y Santa Rosa (Oxfordiano Superior), desarrolladas durante el Jurásico Medio a Superior. Estas unidades han sido agrupadas en el Grupo Huantajaya (Kossler, 1998).

Los depósitos semiconsolidados más jóvenes presentes en la Cordillera de la Costa corresponden a gravas, arenas, limos y arcillas de origen aluvial, agrupadas en las Gravas de Alto Hospicio asignadas al Oligoceno-Pleistoceno en las cercanías de Iquique y a depósitos evaporíticos de sales y yeso con nitratos subordinados del Pleistoceno-Holoceno (Formación Soledad, Blanco *et al.*, 2012).

Por otro lado, el rasgo estructural de primer orden en la Cordillera de la Costa corresponde al Sistema de Fallas de Atacama (SFA), el cual se extiende por cerca de 1.000 km entre La Serena e Iquique (Naranjo, 1987; Arabasz, 1968; Brown *et al.*, 1993). Este sistema describe segmentos cóncavos al oeste con una orientación general nortesur. La actividad principal de este sistema corresponde a fallamiento de rumbo sinistral desarrollado durante el Cretácico Inferior, asociado a una fuerte oblicuidad en la subducción (Scheuber y Gonzalez, 1999). Durante el Mioceno medio, la actividad del

Sistema de Fallas de Atacama correspondería a fallamiento normal (Naranjo, 1987; Herve, 1987).

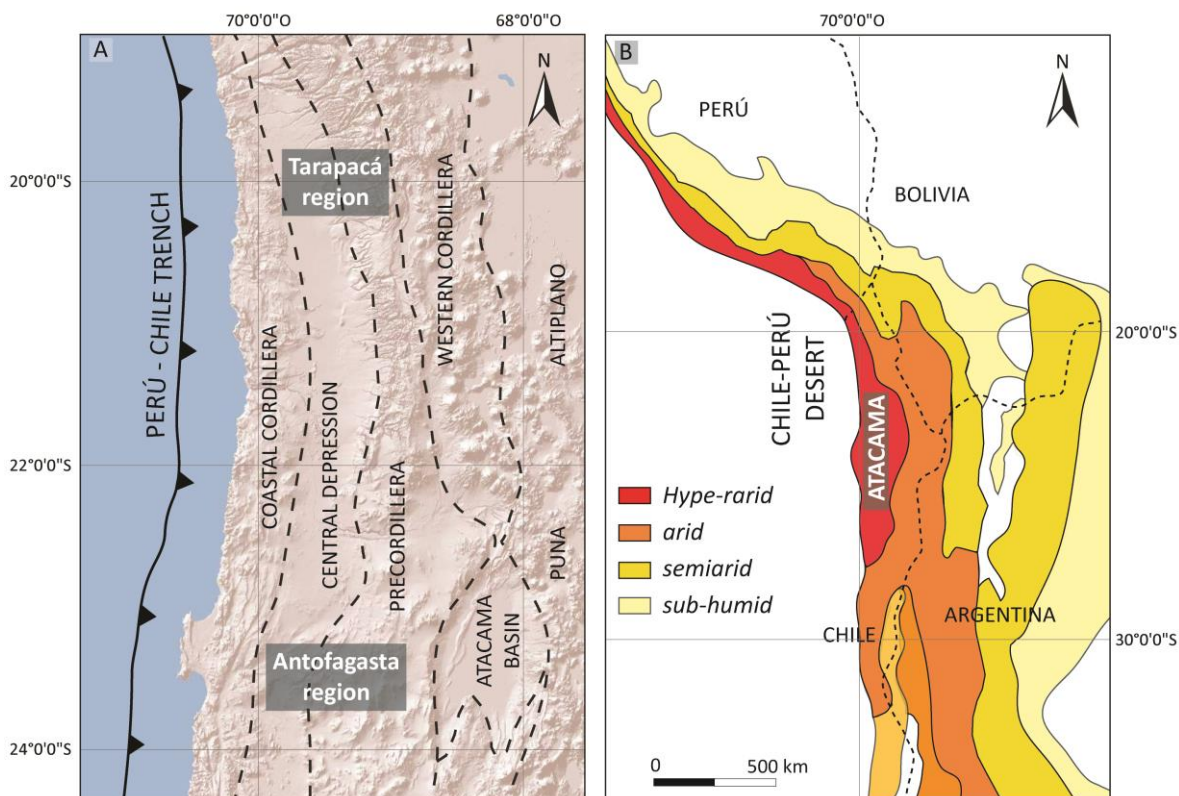


Figura II.1. (A) Mapa topográfico con las principales unidades morfoestructurales (B) Mapa con las zonas climáticas actuales del margen occidental de Sudamérica (Hartley y Chong, 2002).

## II.1.2 Depresión Central

Durante el inicio del Cretácico Tardío se habría desarrollado una reconfiguración de placas (Fase Peruana o Subhercínica) que dio como resultado la migración del arco magmático hacia la posición de la actual Depresión Central (Vicente *et al.*, 1973; Charrier *et al.*, 2002). Las unidades que afloran principalmente corresponden al arco volcánico del Cretácico Superior-Paleoceno, representado por afloramientos de rocas volcánicas y volcanoclásticas de las formaciones Cerro Empexa (Cretácico Superior) en las cercanías de Iquique (Blanco *et al.*, 2012; Galli, 1968), Quebrada Mala al este de Antofagasta y Augusta Victoria (Cretácico Superior-Eoceno) al sur de Antofagasta (Marinovic *et al.*, 1995; García, 1967). Estas rocas corresponden litológicamente a lavas basálticas a riolíticas, tobas, brechas y aglomerados piroclásticos junto a depósitos volcanoclásticos, las cuales sobreyacen en contacto discordante a secuencias del Jurásico-Cretácico Inferior o del Permo-Triásico y se habrían acumulado en una serie de cuencas extensionales de intra-arco (Charrier *et al.*, 2002).

La Depresión Central es cubierta por amplios mantos de gravas mal seleccionadas localmente cementadas, las cuales se intercalan típicamente con niveles de ignimbritas. Estas unidades sobreyacen en discordancia de erosión a las unidades mesozoicas mencionadas anteriormente. Se conocen con el nombre de Gravas de Alto Hospicio (Mioceno-Plioceno) y Formación El Diablo (Mioceno Medio) en las cercanías de Iquique (Blanco *et al.*, 2012), Formación Pampa de Mulas (Oligoceno-Mioceno) en el sector de Antofagasta (Chong, 1973; Marinovic *et al.*, 1995) y Gravas de Atacama (Oligoceno-Mioceno) al sur de Antofagasta (Naranjo y Puig, 1984). Finalmente, depósitos semi-consolidados de origen aluvial, coluvial y de piedemonte del Pleistoceno-Holoceno, cubren en discordancia erosiva la mayor parte de las unidades mencionadas.

### **II.1.3 Precordillera**

Este dominio aloja las rocas más antiguas del segmento andino en Chile. Rocas pertenecientes al basamento Precámbrico estarían representadas por aislados afloramientos de rocas plutónicas y metamórficas en la Sierra de Limón Verde y por el Complejo Metamórfico de Choja en la Sierra de Moreno (Damm *et al.*, 1990 in Charrier *et al.*, 2002). El Basamento Paleozoico corresponde a rocas volcánicas intermedias y ácidas del Devónico-Carbonífero correspondientes a las siguientes formaciones: Quipisca a la latitud de Tocopilla (Galli, 1968), Collahuasi a los 21°15' S (Vergara y Thomas, 1984), Agua Dulce y La Tabla en la Cordillera de Domeyko de la Región de Antofagasta (Marinovic *et al.*, 1995; García, 1967). Estas unidades son sobreyacidas en discordancia por secuencias sedimentarias de plataforma marina desarrolladas durante el Carbonífero Tardío al Pérmico Tardío, correspondientes a las formaciones Juan de Morales (Galli, 1956) y Cerro El Árbol (Marinovic *et al.*, 1995) en el extremo occidental de la Cordillera de Domeyko.

El registro mesozoico comprende escasas secuencias pertenecientes al Triásico ubicadas al sur de Antofagasta. Éstas se encuentran en contacto discordante sobre el basamento Paleozoico (formaciones Sierra de Varas, Agua Dulce y Estratos Cerro Guanaco; Marinovic *et al.*, 1995). La transgresión marina en Precordillera comienza en el Triásico Superior, representada por secuencias calcáreas ricas en material fosilífero de la Formación Profeta (Triásico Superior-Jurásico Inferior; Chong, 1977) y continúa en el Jurásico Temprano con las formaciones calcáreas-siliciclásticas, Longacho y Chacarillas en el sector de Arica e Iquique (Jurásico Inferior-Cretácico Inferior, Galli, 1968) y al noreste de Antofagasta con las formaciones marinas Quinchamale (Ladino, 1998) y Sierra El Cobre (Tobar, 1966). Hacia el este, se exponen secuencias predominantemente calcáreas y fosilíferas del Bajociano-Kimeridgiano del Grupo Caracoles conformada por cinco formaciones: Torcazas, Caracoles, Doralisa, Millonaria y Honda (García, 1967). Rocas del Cretácico sobreyacen discordantemente las unidades anteriormente mencionadas y están representadas por secuencias volcánicas y volcanoclásticas de las formaciones Cerro Empexa e Incache (Charrier *et al.*, 2002) y escasas rocas

sedimentarias clásticas continentales de las formaciones Tolar (Maksaev, 1978) y Santa Ana (Naranjo y Puig, 1984).

El rasgo estructural más relevante en este dominio consiste en el Sistema de Fallas de Domeyko o Falla Oeste, el cual se extiende al norte y sur del río Loa y se ubica en el eje del arco magmático del Cretácico Superior-Eoceno en Precordillera. Este sistema presenta fallamiento tanto sinestral como dextral asociada al cambio de la oblicuidad de la subducción desarrollada durante el Paleoceno (Tomlinson y Blanco, 1997; Reutter, 2001; Maksaev, 1990). Numerosos sistemas de pórfidos cupríferos del Paleoceno (Eoceno medio-Oligoceno temprano) se distribuyen a lo largo de este sistema en el área de este estudio: Rosario, Collahuasi-Ujina, Quebrada Blanca, El Abra, Chuquicamata, Mina Sur, Saldívar, La Escondida (Charrier *et al.*, 2002).

#### **II.1.4 Depresión Subandina y Cordillera Occidental**

La Depresión Subandina o “Depresión de Salares” corresponde a una cuenca tectónica elongada ubicada entre la Cordillera de Domeyko y el Altiplano entre las latitudes 21°-27°S. En el área de estudio esta unidad alberga los siguientes salares: Carcote, Acotan, Atacama, Imilac, Punta Negra y Pajonales (Charrier *et al.*, 2002), constituyendo el Salar de Atacama el de mayor extensión, ubicado a 2300 m. de altura en una llanura plana de un drenaje fosilizado (Muñoz *et al.*, 2002).

La Cordillera Occidental, ubicada en el borde occidental de Altiplano-Puna constituye el actual arco magmático y aloja principalmente depósitos volcánicos y volcanoclásticos correspondiente al volcanismo desarrollado desde el Mioceno al Reciente. Amplios depósitos de flujos piroclásticos (brechas piroclásticas y lahares) cubren las unidades litoestratigráficas más antiguas hacia el borde oriental de la Cordillera Occidental, mientras que en su borde occidental se presentan principalmente tobas, las cuales se intercalan con los depósitos de origen fluvio-aluvial de la Depresión Subandina (Charrier *et al.*, 2002). Numerosos centros volcánicos de estratovolcanes se alinean definiendo la orientación principal de esta unidad morfológica. Además, afloramientos locales de basamento Paleozoico (formaciones La Tabla y Zorritas) afloran hacia el sur del Salar de Punta Negra en la Región de Antofagasta (Gardeweg *et al.*, 1993).

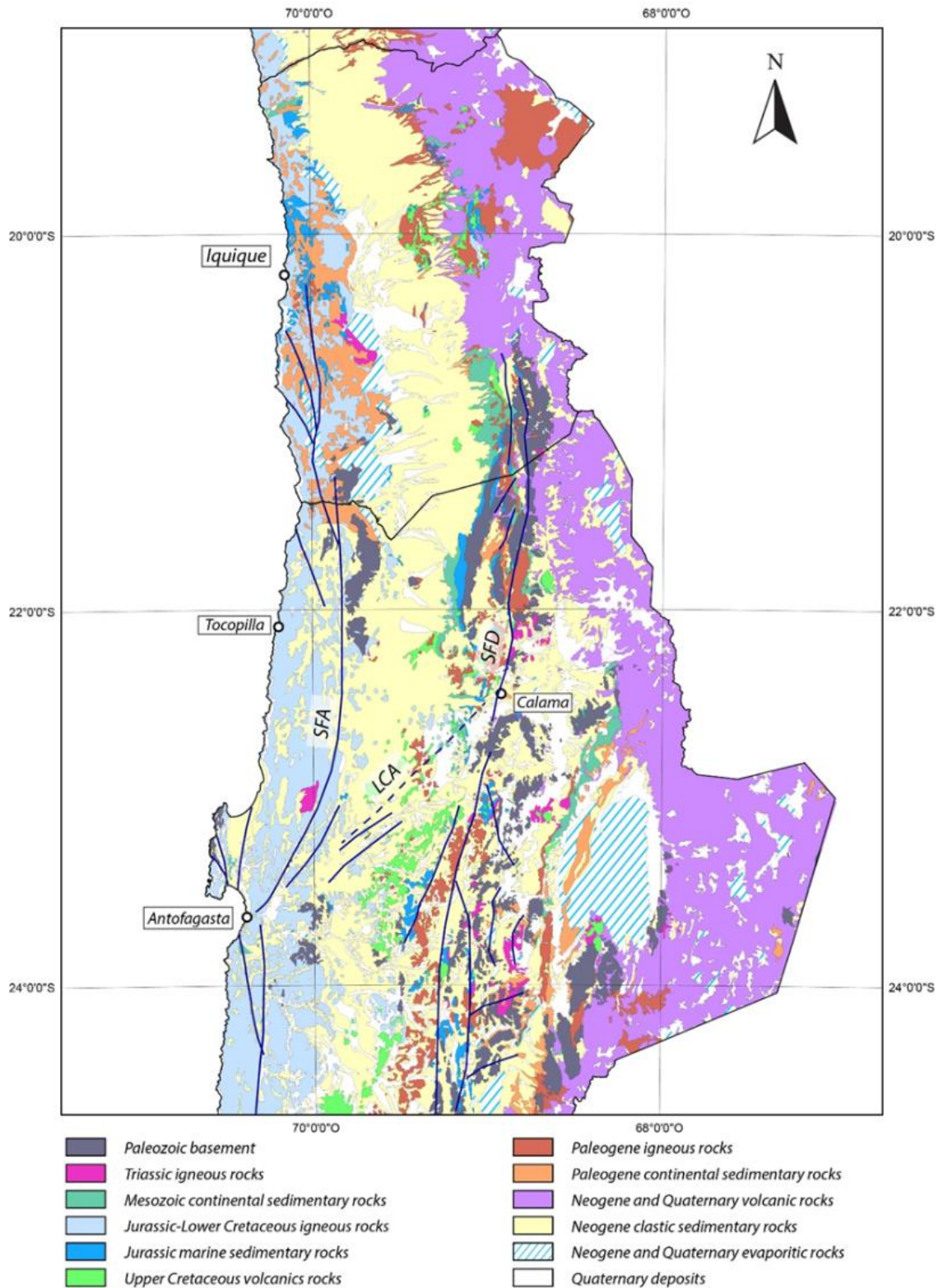


Figura II.2. Mapa geológico del área de estudio. SFA: Sistema de Fallas de Atacama. SFD: Sistema de Fallas de Domeyko. LCA: Lineamiento Antofagasta-Calama. Modificado de SERNAGEOMIN (2002).

## II.2 Antecedentes climáticos

El Desierto de Atacama corresponde al desierto más árido de la Tierra, constituyendo una gran parte del margen occidental de Sudamérica (Fig. II.1B). El Desierto de Atacama se extiende entre las latitudes 15°S y 25°S, abarcando desde el nivel del mar hasta el borde occidental de la Cordillera de los Andes, sin embargo, su núcleo hiperárido se localiza en la Cordillera de la Costa y Depresión Central. Esta zona de extrema hiperaridez prácticamente no recibe precipitaciones, con tasas que no superan los 2 mm/año. (Dirección Meteorológica de Chile, 2000). Se han reportado dispersos eventos de lluvia que ocurren a la escala de decenas de años, estos escasos aportes son rápidamente contrarrestados por el alto potencial de evapotranspiración (Houston y Hartley, 2003; McKay *et al.*, 2003; Garreaud *et al.*, 2010).

Las actuales condiciones de hiperaridez en el Desierto de Atacama se deben a la confluencia de cuatro factores principales (Hartley y Chong, 2002; Houston y Hartley, 2003): (a) La posición latitudinal de esta región, pues el Desierto de Atacama se ubica en el borde este del Pacífico Subtropical donde existe una zona de alta subsidencia atmosférica (Celda de Hadley) lo cual reduce significativamente la convección y por ende las precipitaciones; (b) La ubicación continental del Desierto de Atacama, ya que éste se encuentra a más de 2000 km de la fuente de humedad del Amazona-Atlántico; (c) La presencia de la Cordillera de los Andes, debido a su continuidad y gran elevación, la cordillera bloquea la humedad y precipitaciones desde el Océano Atlántico, este efecto se conoce como “sombra de lluvias” o “*rain-shadow effect*”; y (d) La presencia de la Corriente de Humboldt, esta corriente transporta masas de agua fría desde latitudes mayores hacia el norte a lo largo de toda la costa chilena, las que luego ascienden a la superficie (proceso conocido como surgencia) y provocan una inversión de temperatura que atrapa la humedad bajo los 800 m.s.n.m., impidiendo precipitaciones en la costa occidental.

A pesar del clima hiperárido dominante en la región, el Desierto de Atacama recibe diversos aportes de humedad y precipitaciones provenientes de diferentes fuentes según su posición y altura. En la Depresión Central, desde 300 hasta 1000 m.s.n.m., el margen occidental del Desierto de Atacama se ve principalmente afectado por una humedad constante que penetra en forma de niebla o *spray* marino formado bajo la capa de inversión (Rundel *et al.*, 1991). Por otro lado, a lo largo del margen oriental del Desierto de Atacama se recibe mayor cantidad de humedad y precipitaciones, las cuales están asociadas con el Monzón Sudamericano de Verano, donde corrientes que provienen desde el Amazonas generan las precipitaciones (Garreaud *et al.*, 2003). En la base de los Andes Centrales (~2500 m) éstas superan los 20 mm/año. Más hacia el este, entre los 2700 a 3500 m.s.n.m., las precipitaciones alcanzan los 300 mm/año y el clima varía de hiperárido a árido-semiárido (Garreaud *et al.*, 2003).

## II.3 Bibliografía

- Allmendinger R. W., Jordan T. E., Kay S. M. y Isacks B. L. (1997) Altiplano-Puna plateau of the Central Andes. *Annu. Rev. Earth Planet. Sci.* **25**, 139-174.
- Amilibia A., Sàbat F. y McClay K. (2008) The role of inherited tectono-sedimentary architecture in the development of the central Andean mountain belt: Insights from the Cordillera de Domeyko. *J. Struct. Geol.* **30**, 1520-1539.
- Angermann D., Klotz J. and Reigber C. (1999) Space-geodetic estimation of the Nazca-South America Euler vector. *Earth Planet. Sci. Lett.* **171**, 329-334.
- Arabasz W. (1968) Geologic structure of the Taltal Area, Northern Chile, in relation to the earthquake of December 28, 1966. *Bull. Seismol. Soc. Am.* **58**, 835-842.
- Bahlburg H., Vervoort J. D., Du Frane S. A., Bock B., Augustsson C. y Reimann C. (2009) Timing of crust formation and recycling in accretionary orogens: Insights learned from the western margin of South America. *Earth-Science Rev.* **97**, 215-241.
- Blanco N., Vásquez P., Sepúlveda F., Tomlinson A. J., Quezada A. y Ladino M. (2013) Levantamiento geológico para el fomento de la exploración de los recursos minerales e hídricos de la Cordillera de la Costa, Depresión Central y Precordillera de la Región de Tarapacá (20°-21°S). Servicio Nacional de Geología y Minería, Informe Registrado.
- Brown M., Diaz F. y Grocott J. (1993) Displacement history of the Atacama fault system 25° 00'-27° 00' S, northern Chile. *Geol. Soc. Am. Bull.* **105**, 1165-1174.
- Charrier R., Pinto L. y Rodriguez M. P. (2002) Tectonostratigraphic evolution of the Andean Orogen in Chile. In *The Geology of Chile*, 21-114.
- Chong G. (1977) Contribution to the knowledge of the Domeyko range in the Andes of northern Chile. *Geol. Rundschau* **66**, 374-404.
- Chong G. (1973) Reconocimiento Geológico del Área Catalina, Sierra de Varas y estratigrafía del Jurásico del Profeta, Provincia de Antofagasta. Universidad de Chile, Departamento de Geología, pp. 284.
- Damm W., Pichowiak S., Harmon R. S., Todt W., Kelley S., Omarini R. y Niemeyer H. (1990) Pre-Mesozoic evolution of the Central Andes, the basement revisited. eds. K. S. Mahlburg y C. W. Rapela. *Geol. Soc. Am. Spec. Pap.* **241**, 101-126.
- DeMets C., Gordon R. G., Argus D. F. and Stein S. (1994) Effect of recent revisions to the geomagnetic reversal timescale, *Geophys. Res. Lett.* **21**, 2191-2194.



- Galli C. (1968) Cuadrángulo Juan de Morales, Provincia de Tarapacá, escala 1:50.000. Carta Geológica de Chile, Instituto de Investigaciones Geológicas, Chile.
- Galli C. (1956) Nota sobre el hallazgo del Paleozoico superior en la Provincia de Tarapacá. *Rev. Miner.* **12**, 14-26.
- García F. (1967) Geología del Norte Grande de Chile. In *Simposium sobre Geosinclinal Andino*, pp. 138.
- Gardeweg P., Ramirez R. y Davidson M. (1993) Mapa geológico del área del Salar de Punta Negra y del volcan Lullaillaco (1:100.000). Región de Antofagasta.
- Garreaud R., Vuille M. y Clement A.C. (2003) The climate of the Altiplano: observed current conditions and mechanisms of past changes. *Palaeogeogr. Palaeoclimatol. Palaeoecol.* **194**, 5-22.
- Garreaud R., Molina A. y Farias M. (2010) Andean Uplift and Atacama Hyperaridity: A Climate Modeling Perspective. *Earth Planet. Sc. Lett.* **292**, 39-50.
- Gonzalez G. (1996) Evolución tectónica de la Cordillera de la Costa de Antofagasta (Chile): Con especial referencia a las deformaciones sinmagmáticas del Jurásico-Cretácico Inferior. *Berliner geowiss. Abh.* **181**, pp. 111.
- Grocott J. y Taylor G. (2002) Magmatic arc fault systems, deformation partitioning and emplacement of granitic complexes in the Coastal Cordillera, north Chilean Andes (25 30' S to 27 00' S). *J. Geol. Soc. London.* **159**, 425-443.
- Hartley A. J. y Chong G. (2002) Late Pliocene age for the Atacama Desert: Implications for the desertification of western South America. *Geology* **30**, 43-46.
- Herve M. (1987) Movimiento normal de la falla Paposo, zona de Falla Atacama, en el Mioceno, Chile. *Andean Geol.*, 31-36.
- Houston J. y Hartley A.J. (2003) The Central Andean west-slope rainshadow and its potential contribution to the origin of hyper-aridity in the Atacama Desert. *Int. J. Climatol.* **23**, 1453-1464.
- Kossler A. (1998) Der Jura in der Küstenkordillere von Iquique (Nordchile) – Paläontologie, Lithologie, Stratigraphie, Paläogeographie. *Berliner geowiss. Abh.* **A**, 1-226.
- Ladino M. (1998) Geología de la parte oriental de los Cuadrángulos Quebrada Chug-Chug y Cerros de Montecristo, Región de Antofagasta, Chile. Universidad de Chile.
- Maksaev V. (1978) *Cuadrangulo Chitigua y sector oriental del Cuadrangulo Cerro Palpana*, Región de Antofagasta. Escala 1:50.000., Santiago.

- Maksaev V. (1990) Metallogeny, geological evolution and thermochronology of the Chilean Andes between latitudes 21° and 26° south, and the origin of the major porphyry copper deposits. Ph. D. Thesis, Dalhousie University.
- Maksaev V. y Zentilli M. (1999) Fission track thermochronology of the Domeyko Cordillera, northern Chile: implications for Andean tectonics and Porphyry Copper Metallogenesis. *Explor. Min. Geol.* **8**, 65-89.
- Marinovic, N; Smoje, L; Maksaev, V; Hervé, M.; Mpodozis, C. (1995) Hoja Aguas Blancas, Región de Antofagasta. Servicio Nacional de Geología y Minería, Carta Geológica de Chile 70. Santiago.
- McKay C. P., Friedmann E.I., Gomez-Silva B., Caceres-Villanueva L., Andersen D. T. y Landheim, R. (2003) Temperature and moisture conditions for life in the extreme arid region of the Atacama Desert: four years of observations including the El Niño of 1997-1998. *Astrobiology* **3**, 393-406.
- Mpodozis C. y Ramos V. (2008) Tectónica jurásica en Argentina y Chile: extensión, subducción oblicua, rifting, deriva y colisiones. *Rev. Asoc. Geológica Argentina* **63**, 481-497.
- Muñoz N., Charrier R. y Jordan T. (2002) Interactions between basement and cover during the evolution of the Salar de Atacama Basin, northern Chile. *Andean Geol.* **29**, 55-80.
- Naranjo J. A. (1987) Interpretación de la actividad cenozoica superior a lo largo de la Zona de falla de Atacama, Norte de Chile. *Andean Geol.* **31**, 43-55.
- Naranjo, J. A.; Puig, A. (1984) Hojas Taltal y Chañaral, Regiones de Antofagasta y Calama. Carta Geológica de Chile, No. 62-63. Servicio Nacional de Geología y Minería, escala 1:250.000.
- Oliveros V., Féraud G., Aguirre L., Fornari M. y Morata D. (2006) The Early Andean Magmatic Province (EAMP): 40Ar/39Ar dating on Mesozoic volcanic and plutonic rocks from the Coastal Cordillera, northern Chile. *J. Volcanol. Geotherm. Res.* **157**, 311-330.
- Pardo-Casas F. and Molnar P. (1987) Relative motion of the Nazca (Farallon) and South American Plate since Late Cretaceous time. *Tectonics* **6**, 233-248.
- Reutter K. J. (2001) Le Ande centrali: elemento di un'orogenesi di margine continentale attivo. *Acta Nat. l'Ateneo Parm.* **37**, 5-37.

- Rundel P. W., Dillon M. O., Palma B. Mooney H. A., Gulmon S. L. y Ehleringer J. R. (1991) The phytogeography and ecology of the coastal Atacama and Peruvian deserts. *ALISO* **13**, 1-49.
- Scheuber E. y Andriessen P. a. M. (1990) The kinematic and geodynamic significance of the Atacama fault zone, northern Chile. *J. Struct. Geol.* **12**, 243-257.
- Scheuber E. y Gonzalez G. (1999) Tectonics of the Jurassic-Early Cretaceous magmatic arc of the north Chilean Coastal Cordillera (22°–26° S): A story of crustal deformation along a convergent plate. *Tectonics* **18**, 895-910.
- Scheuber E., Hammerschmidt K. y Friedrichsen H. (1995) <sup>40</sup>Ar/<sup>39</sup>Ar and Rb-Sr analyses from ductile shear zones from the Atacama Fault Zone, northern Chile: the age of deformation. *Tectonophysics* **250**, 61-87.
- Silva L. I. (1977) Geología de las Hojas Pisagua y Zapiga, Provincia de Iquique, Tarapacá, I Región, Chile, Instituto de Investigaciones Geológicas, Santiago, Carta Geológica de Chile, 1:100.000.
- Suárez M. y Bell C. (1992) Triassic rift-related sedimentary basins in northern Chile (24°-29°S). *J. South Am. Earth Sci.* **6**, 109-121.
- Thomas A. (1970) Cuadrángulos Iquique y Caleta Molle, Provincia de Tarapacá., Instituto de Investigaciones Geológicas de Chile, Carta Geológica de Chile, 21-22.
- Tobar A. (1966) Estratigrafía del área de Baquedano-Rencoret, Provincia de Antofagasta. Tesis Doctoral, Universidad de Chile, Santiago, pp. 69.
- Tomlinson A. J. y Blanco N. (1997) Structural evolution and displacement history of the West fault System, Precordillera, Chile: Part 1, synmineral history. In *Proceedings 8th Congreso Geológico Chileno* Antofagasta. pp. 1873-1877.
- Vergara H. y Thomas A. (1984) Hoja Collacagua, Región de Tarapacá, Chile, *escala 1:250.000*, Servicio Nacional de Geología y Minería, **59**. pp. 79.
- Vicente J., Charrier R., Davidson J., Mpodozis A. C. y Rivano S. (1973) La Orogénesis Subhercínica: Fase mayor de la evolución paleogeográfica y estructural de los Andes Argentino Chilenos centrales. In *5th Congreso Geológico Argentino* Buenos Aires. pp. 81-98.

## **Capítulo III. Metodologías y obtención de datos**

El presente estudio considera el análisis geoquímico e isotópico de una serie de muestras de roca, suelos y agua extraídas de diferentes reservorios de yodo presentes en Atacama. Durante la investigación se realizaron variados procedimientos para la obtención de estos datos, los cuales abarcan desde la toma de diferentes tipos de muestra hasta análisis específicos de laboratorio. En este capítulo se describen en detalle las diferentes etapas metodológicas para la determinación de la composición química e isotópica de yodo y otros elementos en las muestras.

### **III.1 Metodología en terreno**

Se realizaron cuatro campañas de terreno a lo largo del Desierto de Atacama entre las latitudes ( $19^{\circ}20'S$ - $24^{\circ}10'S$ ): Octubre 2010, Mayo 2011, Octubre 2011 y Mayo 2012, abarcando desde el Océano Pacífico hasta el arco volcánico actual (Fig. III.1). Se recolectaron muestras de rocas y suelos correspondientes a depósitos de nitratos (Fig. III.2) y rocas sedimentarias (Fig. III.3). Por otro lado, también se obtuvieron muestras de aguas subterráneas y superficiales, tales como: agua de mar, ríos, lagos, salares, aguas de vertientes, aguas termales y agua de lluvia (Fig. III.4, Fig. III.5).

Se colectaron un total de 90 muestras en un área de aproximadamente 100.000 km<sup>2</sup>, de las cuales 33 corresponden a suelos o depósitos de nitratos, 12 a rocas sedimentarias, 4 a minerales asociados a depósitos supérgenos de cobre y 41 a muestras de agua (Fig. III.1).

A continuación se describen los diferentes tipos de muestras extraídos en las campañas de terreno.

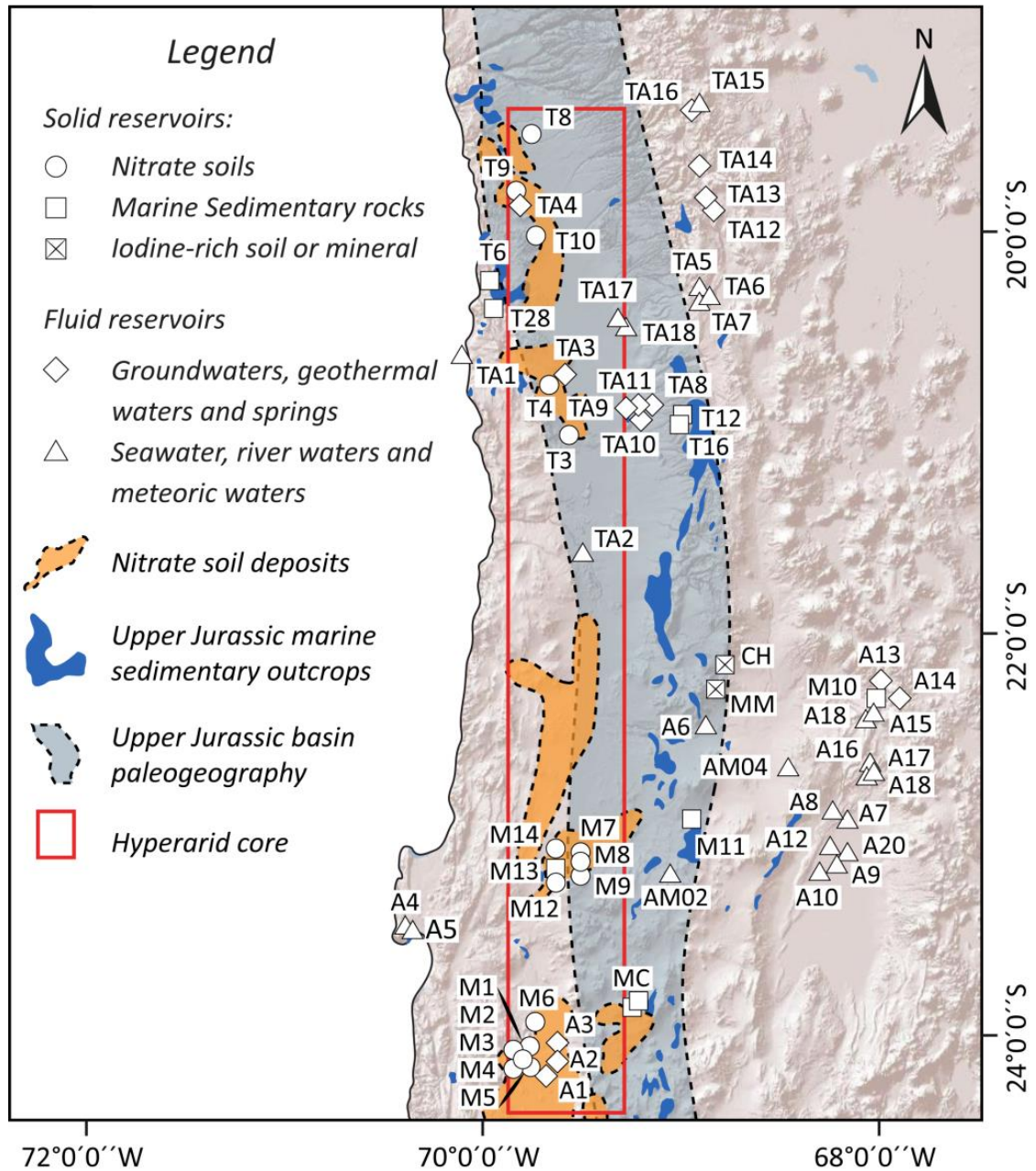


Figura III.1. Mapa del área de estudio con los sitios de muestreo.

### **III.1.1 Muestras de roca y suelo**

#### **Depósitos de nitratos**

Los depósitos de nitratos del Desierto de Atacama, también conocidos como caliche, se ubican principalmente en el borde occidental de la Depresión Central entre los 19°S y 26°S, a los pies de la Cordillera de la Costa, donde forman una franja de ~700 km de largo y 30 km de ancho (Figs. III.1, III.2A). Están compuestos por una compleja mezcla de minerales: nitratos, sulfatos, carbonatos, cloruros, yodatos, cromatos y boratos (Ericksen, 1981; Chong, 1994). Históricamente han sido divididos en cinco distritos: Tarapacá, Tocopilla, Baquedano, Aguas Blancas y Taltal.

Se reconocen dos tipos principales de yacimientos: (1) Nitratos aluviales, donde el caliche se presenta como cemento en gravas e infiltrado dentro de abanicos aluviales (Figs. III.2B, C, D) y (2) Nitratos en roca, en los cuales el caliche se manifiesta como impregnaciones o vetillas en rocas volcánicas o en capas entre rocas estratificadas (Figs. III.2E, F).

Se recolectaron muestras de ambos tipos de nitratos, en el caso de aquéllos de origen aluvial se seleccionaron muestras de los distintos niveles del perfil de suelo (Fig. III.2B), donde se distinguieron zonas de caliche blanco, generalmente cristalino (Fig. III.2C) y zonas de caliche con alto contenido detrítico (Fig. III.2D). Mientras que de los nitratos en roca, se seleccionaron muestras de caliche presentes como cemento entre fragmentos volcánicos (Fig. III.2E) y caliche en capas interestratificadas con rocas sedimentarias (Fig. III.2F).

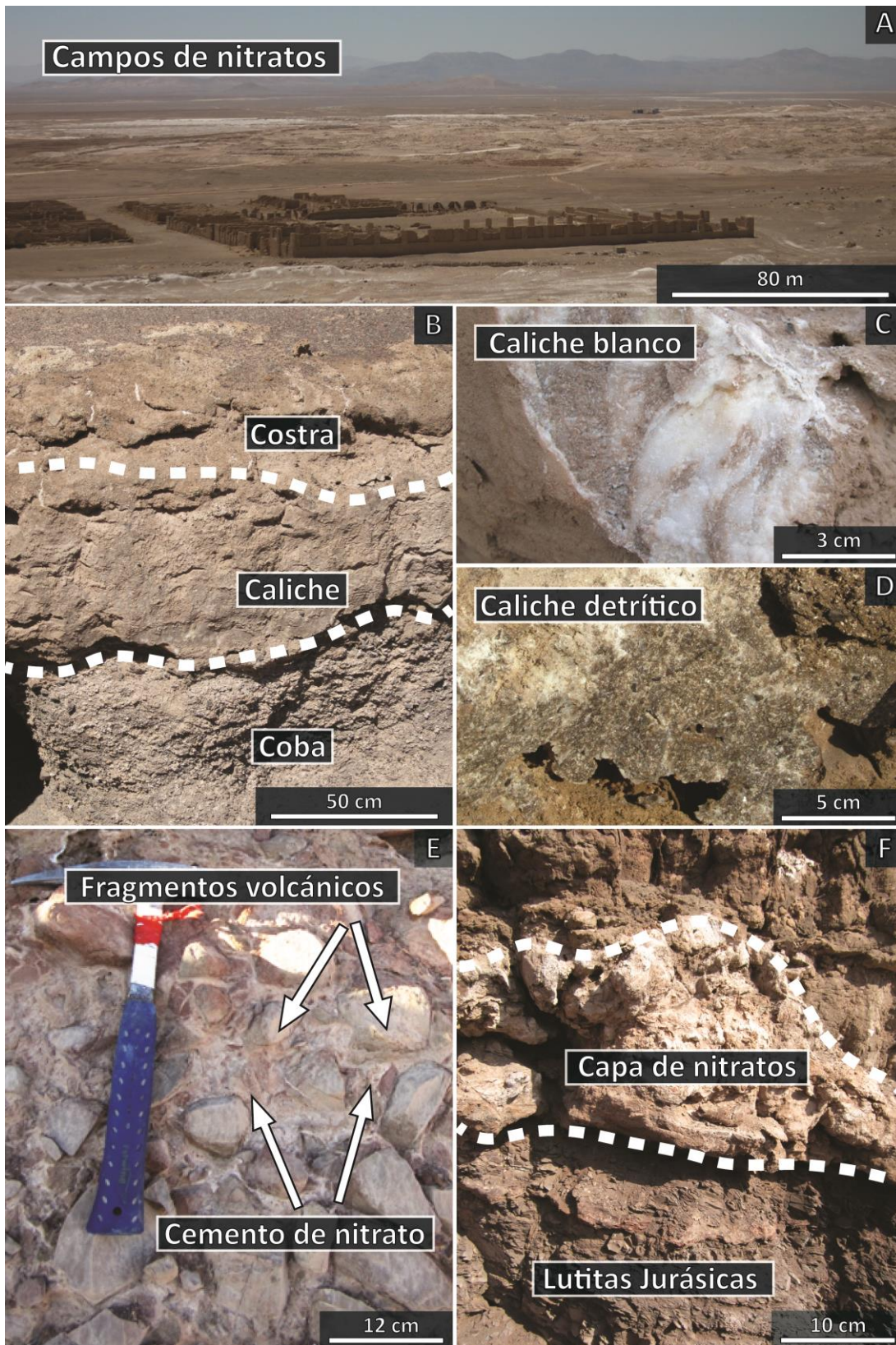


Figura III.2. (A) Campos de nitratos o “Caliche”. (B) Perfil tipo de un depósito de nitrato según Ericksen (1981). (C) Caliche blanco en afloramiento de yacimiento en roca. (D) Caliche detrítico en yacimiento de afloramiento en roca. (E) Caliche cementando fragmentos de rocas volcánicas. (F) Capa de nitrato entre planos de estratificación de rocas sedimentarias.

## Rocas Sedimentarias

En este estudio se muestrearon diferentes facies de rocas sedimentarias con variaciones en el contenido orgánico (Fig. III.3). Los afloramientos de interés en la zona de estudio corresponden a secuencias marinas del Jurásico Superior (Mpodozis *et al.*, 2005; Vicente *et al.*, 2006). En la región de Antofagasta afloran principalmente en la Precordillera, mientras que en la región de Tarapacá éstas se extienden hasta la Depresión Central. Las muestras corresponden a areniscas calcáreas, limolitas calcáreas (Fig. III.3A) y lutitas ricas en contenido orgánico (Fig. III.3B).

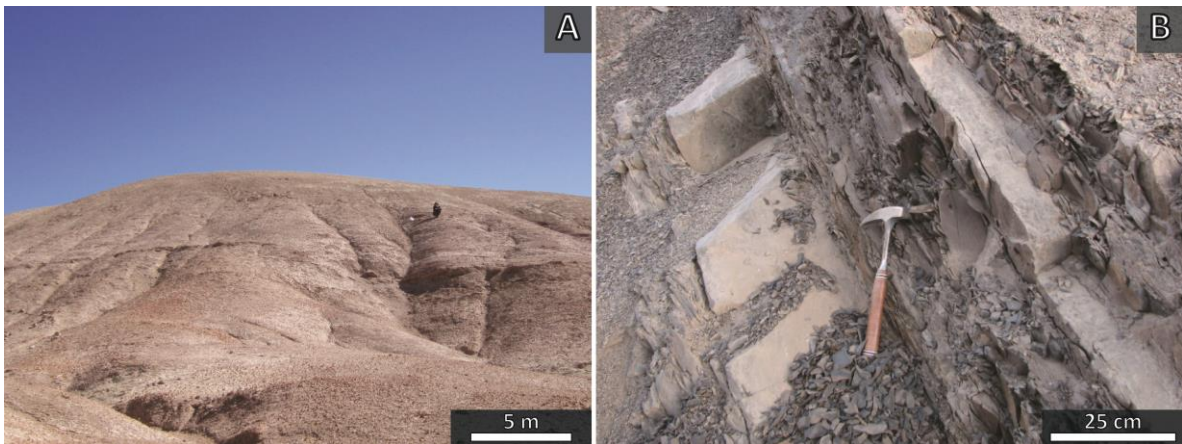


Figura III.3. (A) Secuencias calcáreas y fosilíferas jurásicas del Grupo Caracoles (García, 1967). (B) Lutitas de la Formación Quinchamale (Ladino, 1998).

### III.1.2 Muestras de agua

Se colectaron diferentes tipos de muestra de aguas subterráneas y superficiales, que corresponden a agua de mar, ríos, lagos, salares, aguas de vertientes, aguas termales y agua de lluvia (Fig. III.4).

El procedimiento de muestreo fue el mismo para todas las muestras de agua exceptuando el agua de lluvia. En todos los sitios se midió la temperatura ( $^{\circ}\text{C}$ ), el pH y la conductividad eléctrica ( $\mu\text{S}/\text{cm}$ ) *in situ*. En el caso de aguas termales la temperatura se midió con una termocupla digital de resolución  $0.1^{\circ}\text{C}$ , para el resto de las muestras se utilizó un multiparámetro Hanna, previamente calibrado en laboratorio, con resolución de 0.01 para el pH y de  $0.01 \mu\text{S}/\text{cm}$  para la conductividad (Fig. III.5A).



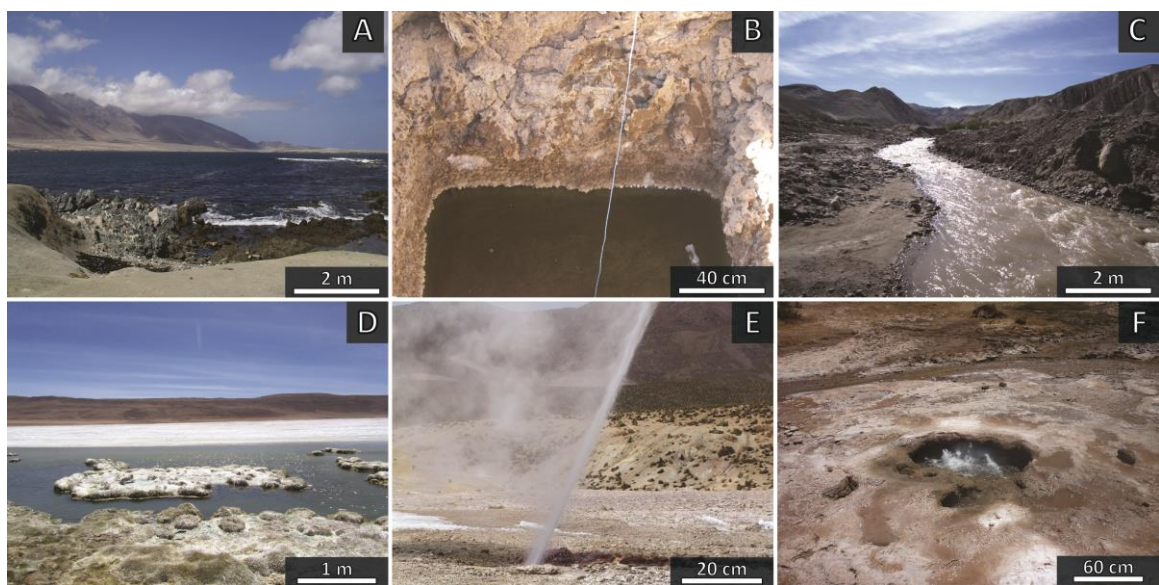


Figura III.4. (A) Agua de mar, región de Antofagasta. (B) Agua subterránea, región de Tarapacá. (C) Río Tarapacá, región de Tarapacá. (D) Salar del Huasco, región de Tarapacá. (E) Campo geotermal Puchuldiza, región de Tarapacá. (F) Campo geotermal El Tatio, región de Antofagasta.

En cada sitio de muestreo se recolectaron tres muestras filtradas en botellas de polietileno de alta densidad, previamente ambientadas. Una para isótopos de yodo (de 1000 a 2000 ml), otra para aniones (200 ml) y otra para cationes (200 ml), ésta última fue acidificada con 2 ml de ácido clorhídrico (HCl) diluido al 4% para evitar la precipitación de cationes. El volumen necesario de muestra colectada para llevar a cabo la medición de razones isotópicas  $^{129}\text{I}/\text{I}$ , depende de la concentración de yodo disuelto, ya sea como yoduro ( $\text{I}_2$ ) o como yodato ( $\text{IO}_3^-$ ). La muestra de agua debiese ser suficiente para producir 1 mg de yoduro de plata (AgI), masa mínima requerida para analizar las razones isotópicas, en caso de que el volumen de muestra sea insuficiente se debe añadir un *carrier* de yodo para incrementar la concentración (Fehn *et al.*, 1992; sección III.2.5.4).

Para filtrar las muestras se utilizó un sistema compuesto por un matraz de Erlenmeyer de 1000 ml, una bomba manual de succión y presión, un porta filtro y filtros Milipore de  $0.45 \mu\text{m}$  (Fig. III.5B). El porta filtro es ambientado tres veces con agua directamente extraída del sitio de muestreo, posteriormente se ambienta el matraz y la botella de almacenamiento con agua filtrada. Una vez que todos los recipientes están ambientados se procede a extraer la muestra hasta llenar la botella, evitando así la presencia de burbujas de aire. Finalmente las muestras son rotuladas y refrigeradas.



Figura III.5. (A) Medición *in situ* de temperatura, pH y conductividad eléctrica en muestras de agua. (B) Procedimiento de filtrado.

### Muestras de agua de lluvia

Se intentó recolectar muestras de precipitaciones de la costa, Depresión Central y Cordillera Principal de la región de Antofagasta y Tarapacá. Para esto se instalaron 8 recipientes, especialmente preparados para muestrear aguas de lluvia (Fig. III.6A). Los recipientes consisten en un balde con tapa a la cual se le realiza un agujero de 15 cm de diámetro, el que está cubierto con una malla delgada en la parte superior. Esta malla se conecta mediante un embudo a un recipiente plástico, más pequeño y gradado (Fig. III.6B). El recipiente gradado contiene vaselina líquida, para evitar la evaporación de la muestra de agua entre el período de precipitación y de recolección. Las muestras fueron recolectadas con una jeringa, en botellas de polietileno de alta densidad de 200 ml.

Debido al clima hiperárido de la zona estudiada y a la intervención de terceros, sólo se obtuvieron dos muestras de agua de lluvia pertenecientes a la Depresión Central y Cordillera Principal de la región de Antofagasta.

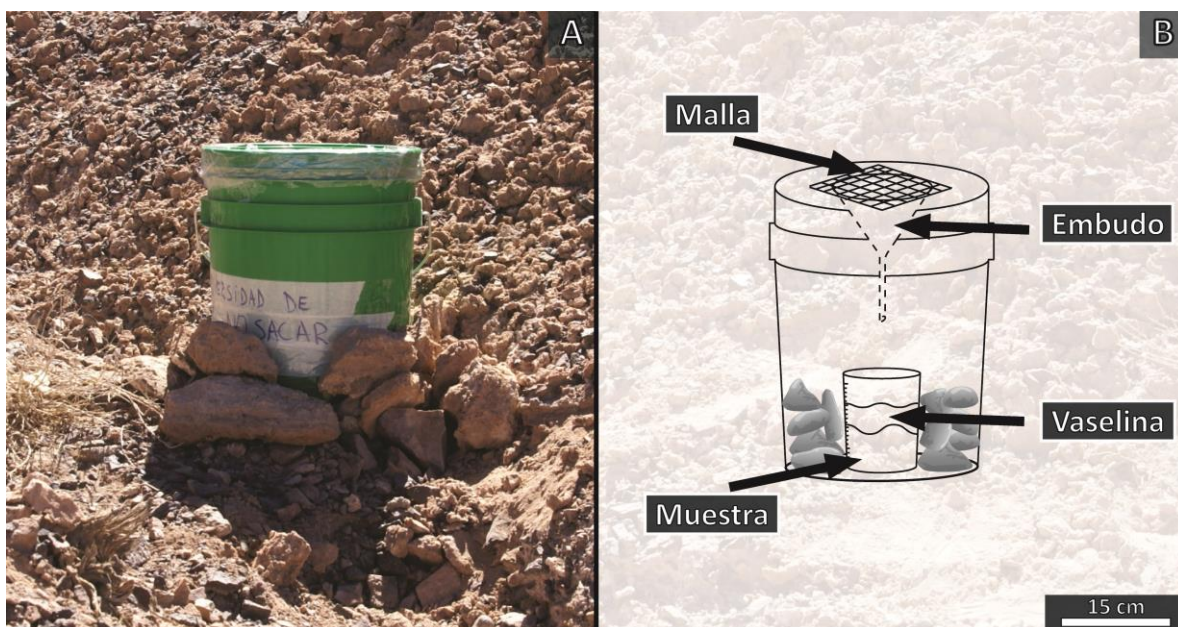


Figura III.6. (A) Colector de agua de lluvia. (B) Sistema en detalle de los colectores.

## III.2 Metodología en laboratorio

Una vez que las muestras son extraídas, éstas requieren ser almacenadas en un laboratorio para su posterior análisis. A continuación se presenta un resumen de los principales procedimientos llevados a cabo y el lugar en que se realizaron:

- (1) Medición de concentraciones de cationes (ICP-AES), procedimiento realizado en el *Marine Geochemistry Laboratory, de Rice University, Texas, E.E.U.U.*
- (2) Medición de concentraciones de yodo y bromo (ICP-MS), procedimiento realizado en el *Chemistry Department, Gakushuin University.*
- (3) Medición de concentraciones de cloro (IC), procedimiento realizado en el Laboratorio de Química, Departamento de Geología, Universidad de Chile.
- (4) Preparación de muestras para calcular la razón isotópica de yodo, procedimiento realizado en el *Marine Geochemistry Laboratory, de Rice University, Texas, E.E.U.U.*
- (5) Medición de las razones isotópicas de yodo (AMS), procedimiento realizado en *PRIME Laboratory, Purdue University* y en *AMS Facility, University of Arizona.*

Previo a la explicación detallada de estos procedimientos y la técnica analítica asociada es necesario realizar una revisión del comportamiento geoquímico y del sistema isotópico del yodo.

### III.2.1 Comportamiento geoquímico

El yodo es un elemento químico fuertemente biofílico por lo que comúnmente se encuentra asociado a material orgánico (Wong, 1991). Al pertenecer al grupo de los halógenos comparte ciertas propiedades con el cloro y el bromo, sin embargo, no puede considerarse un elemento conservativo, ya que éste se concentra preferentemente en fluidos asociados a materia orgánica, además puede ser absorbido con mayor facilidad que los otros halógenos por óxidos e hidróxidos de hierro (Couture y Seitz, 1983; Kodoma *et al.*, 2006).

Debido a su naturaleza geoquímica, la distribución global de yodo es dominada por sistemas marinos, en particular por los sedimentos orgánicos en el fondo del océano que almacenan cerca del 70% del yodo total de la tierra (Muramatsu y Wedepohl, 1998).

Las concentraciones de yodo en fluidos superficiales son generalmente bajas, por ejemplo el agua de mar promedia  $0.4 \mu\text{M}$  y las aguas dulces  $0.05 \mu\text{M}$  (Muramatsu y Wedepohl, 1998). Estos valores son considerablemente mayores en reservorios asociados a material orgánico: las salmueras petrolíferas registran concentraciones de  $80 \mu\text{M}$  (Moran *et al.*, 1995), aguas de poros relacionadas a hidratos de gas y fluidos ricos en metano en zonas de antearco pueden superar los  $1000 \mu\text{M}$  (Fehn *et al.*, 2007a).

#### Ciclo geoquímico del yodo

La interacción aire-agua proporciona los mecanismos por los cuales el yodo es transferido desde el océano a la atmósfera, luego al continente, y finalmente de vuelta al océano, constituyendo el ciclo atmosférico del yodo. A continuación se detallan las etapas de este ciclo (Baker *et al.*, 2001; Leblanc *et al.*, 2006; Figura III.7):

- (1) La forma más estable del yodo en el océano es el yodato ( $\text{IO}_3^-$ ) el cual, por medio de actividad biológica en el océano, es reducido a yoduro ( $\text{I}^-$ ).
- (2) El  $\text{I}^-$  es incorporado a algas y fitoplancton, los que posteriormente liberan el yodo como gases orgánicos al océano ( $\text{CH}_3\text{I}$ ,  $\text{CH}_2\text{I}_2$ ) Luego, éstos ascienden hasta la interfaz agua-aire.
- (3) Al ingresar a la atmósfera, los gases reaccionan con rayos solares y el yodo es liberado. Éste continúa ascendiendo hasta la parte alta de la atmósfera.
- (4) En la atmósfera ocurren distintas reacciones químicas que involucran al yodo, entre ellas la destrucción del ozono produciéndose peryodato ( $\text{IO}^-$ ). Además, en esta zona se presentan otras formas químicas del yodo:  $\text{I}^-$ ,  $\text{IO}_3^-$ , yodo orgánico soluble (RI), yodo inorgánico soluble e insoluble ( $\text{I}'$ ), entre otros compuestos que existen durante cortos períodos.

- (5) El yodo es depositado en el océano y continente por lluvia o deposición seca (aerosol). Generalmente, la concentración de yodo decrece rápidamente a medida que éste se aleja del mar.
- (6) Si el yodo es depositado en el continente permanecerá en algún reservorio superficial hasta que sea removido, generalmente por ríos que finalmente desembocan en el océano.

Por otro lado, existe una porción de yodo que no obedece al ciclo atmosférico previamente descrito. Como se mencionó anteriormente, los sedimentos marinos formados en la parte superior de la placa subductante son el principal reservorio de yodo (Muramatsu y Wedepohl, 1998). Cuando éstos son subducidos, el material orgánico es sometido a un intenso proceso de compactación, liberando parte del yodo almacenado. Así una porción formará parte de fluidos corticales profundos y otra permanecerá almacenada en aguas de poro presentes en formaciones marinas (Fehn et al., 2000, 2007a, 2007b; Tomaru et al., 2007).

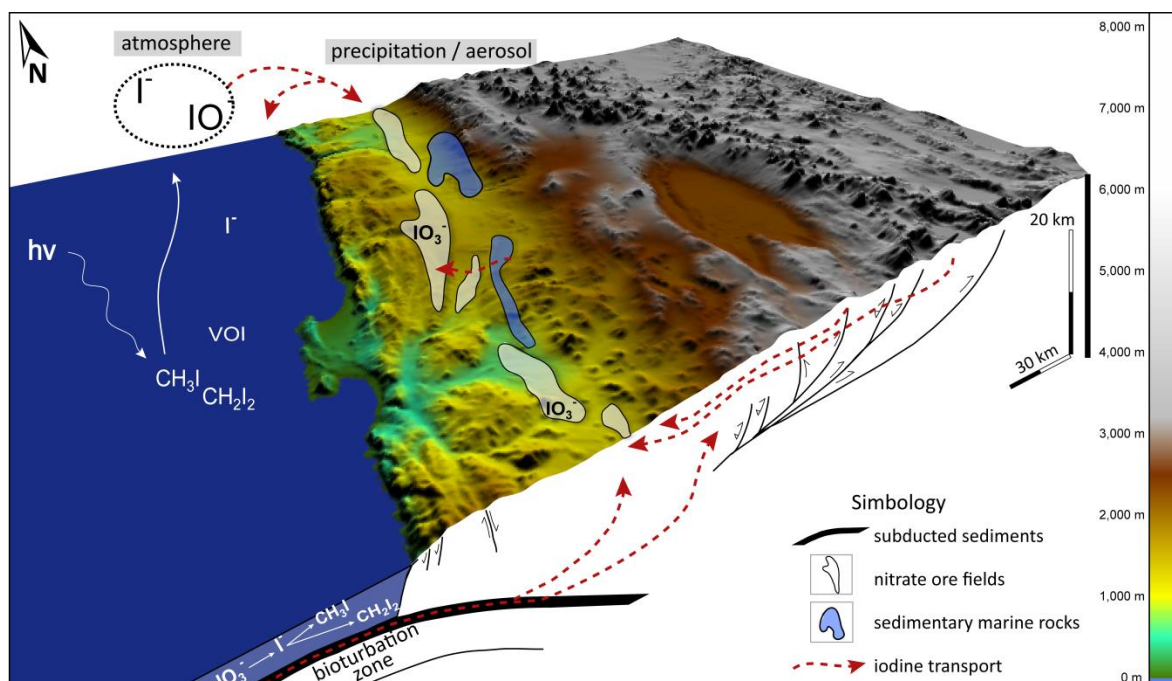


Figura III.7. Ciclo geoquímico del yodo en márgenes convergentes.

### III.2.2 Sistema isotópico del yodo $^{129}\text{I}$

El yodo posee tres isótopos principales, sólo uno de ellos es estable ( $^{127}\text{I}$ ), los otros dos radiogénicos ( $^{131}\text{I}$ ,  $^{129}\text{I}$ ). El  $^{131}\text{I}$  tiene una vida media de unos pocos días, mientras que el  $^{129}\text{I}$  posee una vida media de 15.7 Ma (Fehn et al., 2007b). Debido a las características del yodo y a la larga vida media del  $^{129}\text{I}$ , es posible datar y trazar fluidos desde formaciones ricas en componentes orgánicos.

En sistemas naturales el  $^{129}\text{I}$  se puede generar a partir de dos procesos distintos: el primero corresponde a la interacción de rayos cósmicos con xenón (Xe) en la atmósfera, proceso conocido como espalación de xenón y que constituye la componente cosmogénica del  $^{129}\text{I}$ ; el segundo mecanismo se basa en la fisión espontánea de  $^{238}\text{U}$  en la corteza terrestre, donde uno de los isótopos generados corresponde al  $^{129}\text{I}$  por lo que constituye la componente fisiogénica. Ambos procesos naturales de producción contribuyen cantidades similares de  $^{129}\text{I}$  a los reservorios superficiales (Fabryka-Martin *et al.*, 1985).

Debido al comportamiento geoquímico de yodo, el cual permite el rápido intercambio entre océanos, atmósfera y biósfera, y al largo tiempo de residencia del yodo en los océanos (300.000 años; Broecker y Peng, 1982), la señal isotópica natural de yodo se encuentra en equilibrio en los reservorios superficiales que estén en comunicación con el océano (Moran *et al.*, 1998). Por lo tanto existe una única razón isotópica inicial de:  $^{129}\text{I}/^{127}\text{I} = 1500 \pm 150 \times 10^{-15}$  en sistemas con señales pre-antropogénicas, este valor es constante y se considera como el valor inicial para la datación o trazado de fluidos (Moran *et al.*, 1998; Fehn *et al.*, 2007b). Debido a la existencia de un solo isótopo estable de yodo ( $^{127}\text{I}$ ) y a la extremadamente baja concentración de  $^{129}\text{I}$  en los reservorios (del orden de  $10^{-12}$  a  $10^{-15}$  átomos de yodo 129 sobre yodo total), el sistema isotópico se define por la razón  $^{129}\text{I}/\text{I}$ .

En la actualidad existe una tercera componente de  $^{129}\text{I}$  de origen antropogénico (e.g. Fehn y Snyder, 2005), la cual ha estado presente desde el comienzo de la era nuclear, donde el  $^{129}\text{I}$  es producido por fisión inducida de  $^{235}\text{U}$  en plantas de procesamiento nuclear y en menor medida por la liberación durante ensayos y accidentes nucleares, como por ejemplo los de Chernobyl (1986) y Fukushima (2011). La adición del  $^{129}\text{I}$  antropogénico ha perturbado el equilibrio en reservorios superficiales incrementando las razones isotópicas  $^{129}\text{I}/\text{I}$  en varios ordenes de magnitud (Snyder y Fehn, 2004). Aunque la señal antropogénica ha sido detectada en reservorios superficiales, no está presente en los sedimentos marinos bajo la capa de bioturbación, formaciones rocosas antiguas, fluidos profundos ni aguas subterráneas con edades > 60 años, reservorios que han conservado la razón isotópica inicial  $^{129}\text{I}/\text{I}$  pre-antropogénica:  $R_i = 1500 \times 10^{-15}$ .

En sistemas naturales, cuando el yodo en equilibrio es apartado del reservorio superficial, la razón isotópica inicial cambia en función del tiempo, esto ocurre porque las componentes cosmogénica y fisiogénica son perturbadas, por ejemplo, en los sedimentos marinos enterrados la razón isotópica disminuirá con el transcurso del tiempo ya que no continua produciéndose  $^{129}\text{I}$  cosmogénico, por otro lado si el reservorio de yodo está próximo a una roca con altas concentraciones de U, la razón isotópica aumentará en función del tiempo debido a la producción de  $^{129}\text{I}$  fisiogénico (Fig. III.8).

## <sup>129</sup>I Systematics

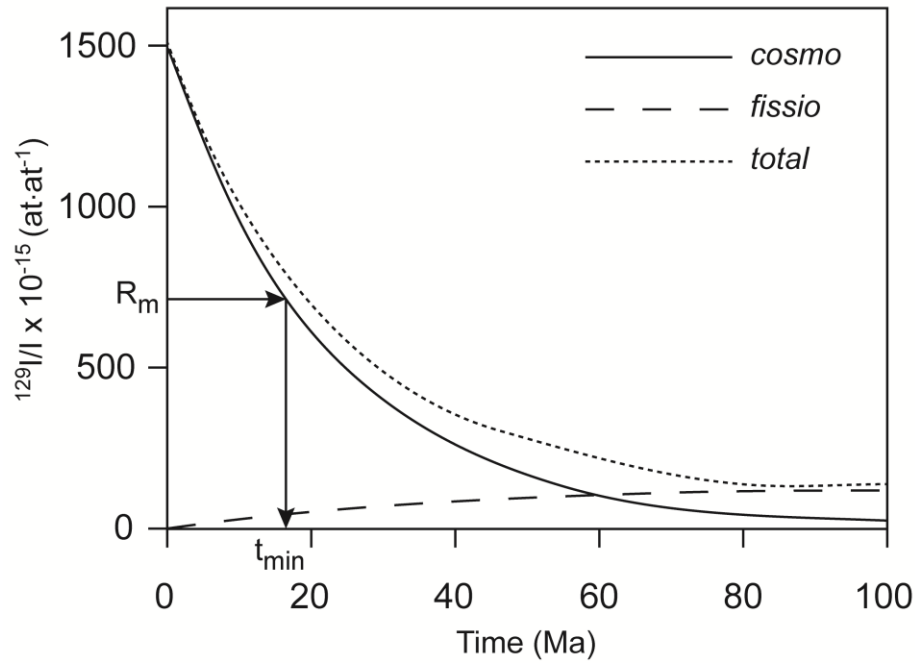


Figura III.8. Datación de yodo: decrecimiento de la razón isotópica <sup>129</sup>I cosmogénica (línea continua) y crecimiento de la fisiogénica (línea segmentada) con respecto al tiempo, ambas componentes se suman (curva punteada) alcanzando el equilibrio secular a los 80 Ma. Las flechas indican la determinación de la edad mínima a partir de una razón medida  $R_m$ , utilizando la curva de decaimiento cosmogénico (Fehn *et al.*, 2007a).

### Cálculo de edad y origen del yodo

Como se mencionó anteriormente la razón isotópica <sup>129</sup>I/I permite calcular el tiempo transcurrido desde que el yodo fue separado del sistema en equilibrio. El cálculo de la edad de separación del I(t), está dado por la siguiente ecuación:

$$\left(\frac{^{129}\text{I}}{\text{I}}\right)_m = \left(\frac{^{129}\text{I}}{\text{I}}\right)_i e^{-\lambda_{129}t} + \frac{N_{238}\lambda_{sf}Y_{129}\varepsilon\rho \left\{\frac{(1-\varphi)}{\varphi}\right\} \left\{\frac{(1-e^{-\lambda_{129}t})}{\lambda_{129}}\right\}}{N_{127}} \quad (\text{Eq. III. 1})$$

Donde  $(^{129}\text{I}/\text{I})_m$  es la razón isotópica de la muestra, la cual fue medida en laboratorio. El primer término de la ecuación corresponde a la componente cosmogénica donde  $(^{129}\text{I}/\text{I})_i$  equivale a la razón isotópica inicial pre-antropogénica ( $1500 \times 10^{-15}$ ),  $\lambda_{129} = 4.41 \times 10^{-8}$  años equivale a la constante de decaimiento del <sup>129</sup>I. El segundo término corresponde a la componente fisiogénica (Fabryka-Martin *et al.*, 1989), donde  $N_{238} = ^{238}\text{U}$  átomos/kg de roca,  $\lambda_{sf}$  = constante de decaimiento de la fisión espontánea de <sup>238</sup>U ( $8.5 \times 10^{-17}$  años<sup>-1</sup>; Decarvalho *et al.*, 1982),  $Y_{129}$  = tasa de fisión espontánea de <sup>238</sup>U a la masa 129 ( $3 \times 10^{-4}$ ; Hebeda *et al.*, 1987),  $\varepsilon$  = eficiencia de escape del <sup>129</sup>I desde la estructura

mineral al fluido,  $\rho$  = densidad de la roca,  $\phi$  = porosidad efectiva, ( $4.41 \times 10^{-8}$  años $^{-1}$ ) y  $N_{127} = {}^{127}\text{I}$  atomos/L fluid. El equilibrio secular se alcanza cuando el término  $e^{-\lambda^{129}}$  tiende a 0.

La razón isotópica medida de yodo, no solo permite calcular la edad de separación, sino que también entrega importante información sobre la fuente de yodo. Fehn *et al.* (2007b) plantea rangos de razones  ${}^{129}\text{I}/\text{I}$  característicos para las diferentes fuentes (Fig. III.9), más aún propone que estos valores están relacionados a la historia geológica de la fuente de yodo: las razones para fluidos de antearco varían entre  $200\text{-}400 \times 10^{-15}$  y dependen de la edad de la roca caja, por otra parte los fluidos volcánicos presentan valores entre  $700\text{-}1000 \times 10^{-15}$ , los cuales se relacionan con la edad de la placa subductante (Fig. III.3). Finalmente, en el caso de fluidos corticales profundos, los valores pueden ser mayores a  $1500 \times 10^{-15}$ , esto debido al aporte de  ${}^{129}\text{I}$  fisiogenico a partir de rocas ricas en uranio.

Los valores isotópicos de yodo se miden mediante espectrometría de aceleración de masa (AMS), técnica que posee un límite de detección de  $2 \times 10^{-14}$  (Sharma *et al.*, 2000) dos órdenes de magnitud menor al valor inicial de  ${}^{129}\text{I} = 1500 \times 10^{-15}$  ( $R_i$ ), esto junto con la vida media del isótopo permite medir edades de hasta 80 Ma (Fehn *et al.*, 2007b).

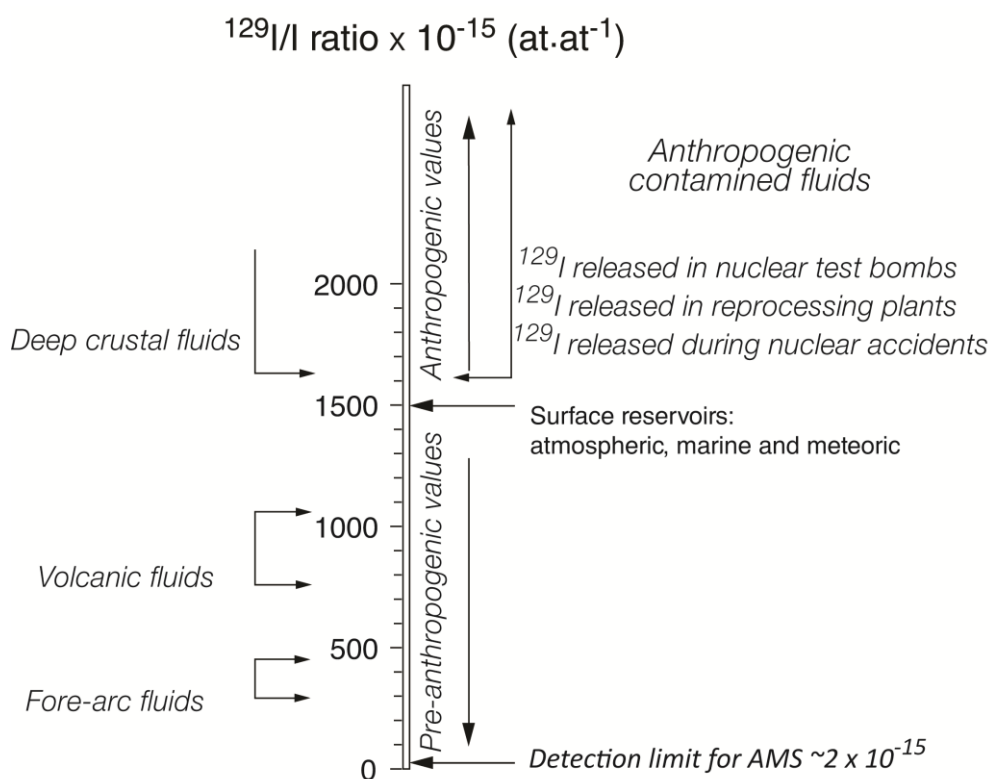


Figura III.9. Rangos de valores para razones isotópicas de yodo en diferentes tipos de fluidos. Modificado de Fehn *et al.* (2007a).



### III.2.3 Procedimientos analíticos: Concentraciones de halógenos

En este estudio se analizó la composición química del agua, con énfasis en el estudio de los halógenos (yodo, bromo y cloro). Se utilizaron diferentes instrumentos para obtener la concentración de estos elementos.

#### Análisis químico de yodo y bromo

En primera instancia se determinó la concentración de yodo mediante espectroscopía óptica por plasma inductivamente acoplado (ICP-AES). Si bien este instrumento no es el más adecuado para medir yodo, se utilizó para determinar el volumen necesario de muestra para precipitar al menos 1 mg de yoduro de plata (AgI), procedimiento detallado en la siguiente sección. Un volumen equivalente a 1 ml de muestra líquida o sólida previamente disuelta (también llamada extracto) es colocado en un tubo plástico de 15 ml (*corning*), luego se agregan 9 ml de agua desionizada de 18 MΩ, es decir, la muestra presenta una dilución de 1:10 (las muestras con concentraciones elevadas de sales deben ser diluidas 1:100 y el agua de lluvia no se diluye). Posteriormente, con el fin de calibrar y evitar que la muestra se adhiera a las paredes del tubo, se añade 0.1 ml de una solución de 100 ppm de escandio (Sc), 0.1 ml de una solución de 100 ppm de itrio (Y) y 0.1 ml de una solución de hidróxido de tetrametilamonio (TMA-H). Luego se deben mezclar el contenido del tubo en un mezclador eléctrico (*Mini Vortexer*). Finalmente, se ubican los tubos en el porta-muestras del ICP-AES para su medición. Junto con esto se preparan y analizan ocho estándares preparados con cantidades variables de agua de mar (IAPSO) y un “*stock*” compuesto por distintos elementos (bario, fósforo, silicio, litio, cromo, estroncio, boro, manganeso, cobre, níquel, y zinc), además se agregan 0.5 ml de solución de escandio, 0.5 ml de solución de itrio y 0.5 ml de ácido nítrico a cada uno de ellos. Este procedimiento fue realizado en el Marine Geochemistry Laboratory, de Rice University, Texas, E.E.U.U.

En una segunda instancia, las concentraciones tanto de yodo como bromo fueron medidas mediante espectrometría de masa por plasma inductivamente acoplado (ICP-MS). Esta vez la medición presenta un menor error analítico ya que este instrumento posee un menor límite de detección que el ICP-AES. Este procedimiento fue realizado en el *Chemistry Department, Gakushuin University*. Antes de la medición las muestras deben ser diluidas con agua desionizada de 18 MΩ. En general, el factor de dilución varía según el tipo de muestra cómo se describe a continuación:

- (1) Aguas de mar y meteórica poseen un factor de dilución 5.
- (2) Aguas dulces de río o vertientes poseen un factor de dilución que varía entre 10 y 20.
- (3) Extractos de rocas sedimentarias marinas poseen un factor de dilución que varía entre 10 y 100.

(4) Extractos de nitratos poseen un factor de dilución que varía entre 200 y 2000.

### **Análisis químico de cloro**

Las concentraciones de cloro, así como de otros aniones mayores (e.g. NO<sub>3</sub>, SO<sub>4</sub>) fueron determinadas mediante cromatografía iónica en el Laboratorio de Química del Departamento de Geología de la Universidad de Chile. Para no saturar el instrumento, antes de la medición las muestras deben ser diluidas con agua desionizada de 18 MΩ, con un factor de dilución que varía entre 1 y 10000 según la salinidad de la muestra.

### **III.2.4 Extracción de yodo y medición de razones isotópicas <sup>129</sup>I/I**

Debido a las bajas concentraciones de yodo en los distintos reservorios de la corteza terrestre y considerando que las razones isotópicas (<sup>129</sup>I/I) se miden en 10<sup>-15</sup> at·at<sup>-1</sup>, orden de magnitud mucho más bajo que el límite de detección de técnicas analíticas convencionales de espectrometría de masa (Fehn *et al.*, 1992), la medición se realiza mediante espectrometría de aceleración de masa (AMS). Sin embargo, antes de realizar este análisis es necesario extraer, purificar y concentrar el yodo de la muestra para que finalmente sea precipitado como AgI. A continuación, se explican los procedimientos necesarios para la preparación de *targets* de AgI: preparación de reactivos, extracción de yodo en muestras de agua, extracción de yodo en muestras sólidas y precipitación de AgI.

Durante el proceso de extracción de yodo se utilizan algunos compuestos orgánicos altamente dañinos para el organismo, por lo que este proceso debe realizarse en una campana de extracción lo más cerrada posible y con elementos de protección personal (gafas de seguridad, mangas y calcetines de Tyvec, delantal de laboratorio, delantal engomado y guantes de Viton). Junto con esto, se debe disponer de los recipientes de desechos apropiados para cada compuesto.

### **Preparación de instrumentos de laboratorio**

En un laboratorio existen diferentes agentes contaminantes (e.g. agua potable, transpiración, material orgánico, polvo en suspensión) que pueden provocar cambios en la concentración de yodo y en la razón isotópica <sup>129</sup>I/I de la muestra, ya sea directamente o mediante los instrumentos utilizados en el proceso de extracción de yodo. Para evitar cualquier tipo de contaminación cruzada, un área de trabajo e instrumental limpios son requisitos esenciales a mantener en un laboratorio. A continuación se enumeran los procedimientos que se deben seguir para el manejo y mantención de instrumental limpio:

- (1) Lavar tres veces con agua potable.
- (2) Lavar tres veces con agua desionizada de 2 MΩ.
- (3) Remojar el material por al menos 15 minutos en una solución preparada con un 1% de Micro-90 (Producto internacional de limpieza) en agua desionizada de 2 MΩ.
- (4) Enjuagar el material tres veces con agua desionizada de 2 MΩ.
- (5) Remojar el material por al menos 4 horas en una solución preparada con 5% de ácido nítrico (HNO<sub>3</sub>) en agua desionizada de 2 MΩ.
- (6) Enjuagar el material tres veces con agua desionizada de 2 MΩ.
- (7) Lavar tres veces con agua desionizada de 18 MΩ contenida.
- (8) Secar el material en una campana de flujo.

### Preparación de reactivos

Los reactivos preparados cumplen un papel fundamental en el proceso de extracción de yodo y en la obtención de resultados confiables, por esta razón sólo deben utilizarse los reactivos mencionados en esta sección u otros de mayor pureza. Para llevar a cabo de forma correcta el proceso se debe verificar que el material a utilizar se encuentre limpio (Sección III.2.5.1). Las soluciones deben estar contenidas en matraces de vidrio volumétricos sellados con *parafilm* y almacenadas en el refrigerador. Cada reactivo debe ser cuidadosamente etiquetado con el nombre, concentración, fecha y nombre del investigador a cargo. A continuación se presenta una lista con los reactivos preparados y utilizados en laboratorio:

- (1) **Solución de bisulfito de sodio (0.1 M NaHSO<sub>3</sub>):** En un matraz volumétrico de 500 ml se deben disolver 5 ml de H<sub>2</sub>SO<sub>4</sub> y 4.75 g de NaHSO<sub>3</sub> en agua desionizada de 18 MΩ (cada matraz volumétrico presenta una línea blanca que indica hasta donde debe ser llenado).
- (2) **Solución de nitrato de plata (1 M AgNO<sub>3</sub>):** En un matraz volumétrico de 50 ml se disuelven 8.5 g de nitrato de plata (Aldrich 99.9999 %, 7761-88-8) en agua desionizada de 18 MΩ.
- (3) **Solución de nitrato de sodio (0.5 M NaNO<sub>3</sub>):** En un matraz volumétrico de 100 ml se disuelve 4.25 g de NaNO<sub>3</sub> en agua desionizada de 18 MΩ.
- (4) **Hidrocloreuro de hidroxilamina (1 M NH<sub>2</sub>OH·HCl):** En un matraz volumétrico de 100 ml se disuelve 6.95 g de NH<sub>2</sub>OH·HCl (EM Sciece HX0770-H) en agua desionizada de 18 MΩ.
- (5) **Carrier de yoduro de sodio (NaI):** La preparación de un *carrier* de yodo es necesaria para incrementar la concentración en muestras líquidas con bajo contenido de yodo (e.g. aguas meteóricas, agua de mar). Para preparar el *carrier* se deben disolver láminas de yodo (I<sub>2</sub>) provenientes del lote “Woodward” en una solución. En este proceso, la razón isotópica medida fue de  $^{129}\text{I}/\text{I} = 78 \pm 8$  (at·at<sup>-1</sup>).

A continuación se describen los pasos a seguir, los cuales deben ser realizados en una campana de extracción con el material de protección adecuado:

- Determinar exactamente la masa de las láminas de yodo utilizadas en el proceso (~0.1 g) en una balanza de precisión.
  - En una campana de extracción, agregar las láminas de yodo en 10 ml de cloroformo ( $\text{CHCl}_3$ ) en un recipiente de precipitados (*beaker*), el cual debe ser cubierto por una tapa de vidrio (*wathglass*) debido a que es un compuesto volátil. Luego se deja en reposo (~10 horas) dentro de una bolsa sellada para prevenir evaporación.
  - Una vez que el yodo ha sido disuelto en el cloroformo, se forma una solución de color morado, la cual debe colocarse en un embudo de separación de 60 ml. Luego se agregan 15 ml de 0.1 M  $\text{NaHSO}_3$  y se agita la solución, ventilando frecuentemente. La capa orgánica inferior debiese comenzar a aclararse en tanto el yodo ( $\text{I}_2$ ) es reducido a yoduro ( $\text{I}^-$ ). En caso de que esto no ocurra se deben agregar 5 ml más de  $\text{NaHSO}_3$  y agitar nuevamente (repetir esto las veces que sea necesario).
  - Remover y eliminar la capa inferior de la solución (que ya no contiene yodo). El resto debe ser separado en un *beaker*. En el caso que gotas de cloroformo se encuentren en el fondo de la solución, éstas deben ser extraídas con una pipeta.
  - Verter la solución en un recipiente gradado de 100 ml y diluir con agua desionizada de 18 M $\Omega$ .
  - Etiquetar el recipiente y asignar un número de lote.
  - Una pequeña porción de *carrier* debe ser diluida para determinar la concentración total de yodo mediante ICP-MS.
  - El recipiente debe ser tapado con parafilm y puesto en una bolsa sellada en el refrigerador. Si la solución empieza a tomar una coloración amarilla, es necesario eliminar este *carrier* y elaborar uno nuevo.
- (6) **La Solución Weeks Island (NaCl):** Durante las etapas de purificación del proceso de extracción, se debe precipitar yoduro de plata ( $\text{AgI}$ ) en conjunto con cloruro de plata ( $\text{AgCl}$ ). Esto requiere la adición de una pequeña cantidad de  $\text{NaCl}$ , la cual no debe tener cantidades detectables de yodo total o  $^{129}\text{I}$ . Se utiliza una solución compuesta de cristales de halita de Weeks Island. A continuación se explican los pasos a seguir durante su preparación:
- Determinar la masa de un cristal de halita (~2 g) en la balanza de precisión.
  - Verter la solución en un matraz volumétrico de 250 ml y diluir con agua desionizada de 18 M $\Omega$ .
  - Calcular la cantidad de solución necesaria para obtener 2 mg de iones cloruro.
  - El recipiente debe ser tapado con parafilm y puesto en una bolsa sellada en el refrigerador.

(7) **Otros reactivos:**

- Cloroformo (CHCl<sub>3</sub>, Mallinckrodt Nanograde #2175)
- Tetracloruro de Carbono (99.9% CCl<sub>4</sub>, Sigma Aldrich 319961).
- Peróxido de Hidrógeno (30% H<sub>2</sub>O<sub>2</sub>, Perhydrol Suprapure, EM Science #2175).
- Ácido nítrico HNO<sub>3</sub> (Seastar Baseline, Ultrex).

**Preparación de muestras sólidas: extractos**

Para llevar a cabo la extracción de yodo en muestras sólidas es necesario obtener el yodo en solución. A la solución generada a partir de la muestra sólida se le denomina extracto. Posterior a esto, se continua con el mismo procedimiento que para las muestras líquidas (sección III.2.5.4).

En este trabajo las muestras sólidas corresponden a rocas sedimentarias marinas y suelos de nitratos (con contenido de yodatos), el yodo en solución debe estar como ion yoduro (I<sup>-</sup>) o yodato (IO<sub>3</sub><sup>-</sup>). A continuación se enumeran los pasos a seguir:

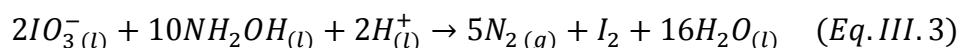
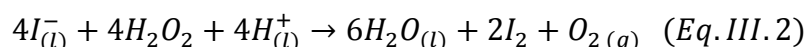
- (1) Se deben pulverizar aproximadamente de ~30 a ~60 mg de muestra sólida, de esta manera es más fácil pasar el yodo a solución.
- (2) Colocar la muestra pulverizada en botellas de polietileno de alta densidad, previamente masadas.
- (3) Determinar la masa exacta de muestra a utilizar en una balanza de precisión.
- (4) Agregar 100 ml de agua desionizada de 18 MΩ. Además, en el caso de las muestras de rocas sedimentarias marinas se deben agregar 10 ml de hipoclorito de sodio (NaClO).
- (5) Determinar la masa de líquido agregada, de esta forma se conoce el factor de dilución de la muestra.
- (6) Las botellas deben ser colocadas en un mezclador eléctrico (*Mini Vortexer*) por algunos segundos (~30 segundos)
- (7) Las botellas deben ser colocadas en un agitador mecánico durante al menos ~ 2 horas, de esta forma pasará el yodo (altamente soluble) a la solución.
- (8) Agregar agua desionizada de 18 MΩ a las muestras con el fin de balancear las botellas para ser puestas en la centrífuga, donde deben ser ubicados en pares opuestos con el peso más similar posible. Centrifugar durante 30 minutos a una velocidad máxima de 1000 rpm.
- (9) Dejar decantar la muestra hasta que no queden partículas suspendidas en la solución (~ 10 minutos) la que posteriormente debe ser separada en una nueva botella. En este punto obtenemos un extracto de muestra sólida.
- (10) Medir la concentración de yodo en solución mediante ICP-OES o ICP-MS, con el fin de estimar el volumen necesario de muestra para precipitar 1 mg de AgI.

Posteriormente se sigue el tratamiento de muestras líquidas según Fehn *et al.* (1992), el cual se describe en la siguiente sección.

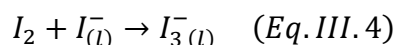
### Preparación de muestras líquidas

Para extraer el yodo de muestras líquidas se siguen los procedimientos establecidos por Fehn *et al.* (1992). El primer paso a realizar es la medición de la concentración de yodo, esto para estimar el volumen necesario para precipitar 1 mg de cloruro de plata (AgCl). Debido a la baja concentración de yodo en algunas muestras de agua (generalmente meteóricas o marinas) no se alcanza a obtener el volumen mínimo requerido para la medición de razones isotópicas (concentraciones de yodo menores a 5 ppm), en estos casos es necesario la adición de *carrier* (sección III.2.5.5).

Debido a su comportamiento biofílico, el yodo en su estado molecular ( $I_2$ ) es altamente soluble en compuestos orgánicos (cloroformo o tetracloruro de carbono), los cuales se utilizan para llevar a cabo la extracción de yodo en la muestra. Sin embargo, en ambientes naturales, el yodo suele estar presente como una especie reducida llamada yoduro ( $I^-$ ) o en un estado oxidado llamado yodato ( $IO_3^-$ ), por lo tanto, para llevar a cabo la extracción de yodo, es necesario oxidarlo si se encuentra como  $I^-$  (generalmente en muestras de agua y extractos de roca sedimentaria) o reducirlo en caso de que esté como  $IO_3^-$  (generalmente en extractos de nitratos y aguas subterráneas). Para lograr el cambio en el estado de oxidación del yodo se utilizan diferentes reactivos (sección III.2.5.2). Tanto el ácido nítrico ( $HNO_3$ ) como el peróxido de hidrógeno ( $H_2O_2$ ) se utilizan como agentes oxidantes y el bisulfito de sodio ( $NaHSO_3$ ) junto al hidrocloreuro de hidroxilamina ( $NH_2OH \cdot HCl$ ) como agentes reductores. A continuación se presentan las ecuaciones de oxidación del  $I^-$  en solución (Eq. III.2) y de reducción del  $IO_3^-$  (Eq. III.3):



Cuando se logra que el yodo esté presente como  $I_2$  en la muestra, el cloroformo (o tetracloruro de carbono) es capaz de disolverlo, adoptando un color que varía de rosado a morado según la concentración de yodo. Por otro lado, el  $I_2$  en la muestra reacciona con  $I^-$  (incolore en solución) formando el ion peryoduro (Eq. III.4):



A medida que ocurre esta reacción, la solución adquiere un color ámbar (indicando que el yodo está en el estado correcto de oxidación para ser extraído). Cuando el cloroformo contiene casi la totalidad del yodo la muestra pierde este color. Si la solución está excesivamente oxidada se formará el ión metaperyodato ( $\text{IO}_4^-$ ), adquiriendo una tonalidad verde clara. A continuación se detallan los pasos a seguir para extraer el yodo de muestras líquidas y sólidas previamente disueltas, procedimiento que debe ser llevado a cabo dentro de una campana de extracción:

- (1) Verter la muestra en un separador de vidrio de 250 o 500 ml (dependiendo del tamaño de la muestra).
- (2) Agregar ~1 ml de  $\text{HNO}_3$  a la muestra (Seastar Baseline o Ultrex). Agitar y ventilar el separador, evitando un aumento de presión.
- (3) Agregar de ~1 a ~2 ml del agente oxidante ( $\text{HNO}_3$ ,  $\text{H}_2\text{O}_2$ ) o reductor ( $\text{NaHSO}_3$ ,  $\text{NH}_2\text{OH}\cdot\text{HCl}$ ) según corresponda. Agitar y ventilar el separador.
- (4) Agregar 5 ml del compuesto orgánico ( $\text{CHCl}_3$ ,  $\text{CCl}_4$ ), agitar y ventilar el separador. Debido a que el compuesto orgánico tiene una densidad mayor a la de la muestra, éste se posiciona en el fondo del separador y adquiere una coloración rosada (o morada, según la concentración de yodo). En caso de que esto no ocurra se debe repetir el paso (3) hasta que el yodo este en el estado correcto de oxidación en la muestra.
- (5) Apartar el compuesto orgánico con el yodo disuelto en un recipiente de precipitados (*beaker*), el cual debe ser cubierto por una tapa de vidrio (*wathglass*). Se debe repetir el paso (4) hasta que el compuesto orgánico no cambie su color al agitar el separador.
- (6) Realizar el proceso opuesto al paso (3), es decir, si la muestra fue oxidada ahora es necesario reducirla y viceversa, con el fin de extraer todo el yodo de ésta. Entonces, se agregan 2 ml del agente correspondiente y 5 ml del compuesto orgánico. Agitar y ventilar el separador.
- (7) Apartar el compuesto orgánico en el recipiente de precipitados (junto con el anterior). Se debe repetir el paso (6) hasta que el compuesto orgánico no cambié su color al agitar el separador.
- (8) Eliminar el líquido que queda en el separador en un contenedor de desechos de polietileno de alta densidad.
- (9) Limpiar el separador con agua desionizada de 18 M $\Omega$ . Verter el compuesto orgánico en el separador.
- (10) Agregar de ~5 a ~10 ml de bisulfito de sodio con el fin de reducir y re-extraer el yodo hacia una solución. Agitar y ventilar el separador. Si el compuesto orgánico continúa de color rosado o morado se debe agregar 1 ml más de bisulfito y repetir el proceso hasta que éste se vuelva incoloro en el fondo del separador.
- (11) Dejar escurrir el compuesto orgánico (ya sin yodo) en un contenedor de desechos propio. Por lo tanto, sólo quedará el bisulfito de sodio con el yodo reducido ( $\text{I}^-$ ) en el separador.
- (12) Apartar el bisulfito de sodio en un tubo de vidrio de 15 ml.

- (13) Con una pipeta de Pasteur se extraen los restos del compuesto orgánico que pudieron quedar en la muestra.

### Preparación de *targets* de yoduro de plata (Agl)

El AgI se forma al agregar iones de plata a la solución de yodo re-extraída. Para obtener los *targets* finales de AgI (compuesto en que debe estar la muestra antes de la medición de razones isotópicas por AMS), estos deben ser purificados. Para evitar que la plata precipite con diferentes especies de azufre se deben agregar iones de cloro ( $\text{Cl}^-$ ) a la muestra, esto provoca que solamente co-precipite  $\text{AgCl}$  y AgI. A continuación se describen los pasos a seguir para la obtención de *targets* purificados de AgI:

- (1) Agregar suficiente solución de cloruro Week Island (~ 0.2 ml) para precipitar 2 mg de  $\text{Cl}^-$  en la solución re-extraída de yodo en el tubo para centrifugar. Para conseguir esto, éste debe ser agitado cuidadosamente.
- (2) Agregar 0.2 ml de solución de nitrato de plata. Tanto el AgI como el  $\text{AgCl}$  serán precipitados.
- (3) Agregar agua desionizada de 18 M $\Omega$  a las muestras con el fin de balancear los tubos para ser puestos en la centrífuga, donde deben ser ubicados en pares opuestos con el peso más similar posible. Posteriormente se centrifugan durante 10 minutos. Se debe dejar decantar la muestra hasta que no queden partículas suspendidas en la solución (~ 10 minutos) la que posteriormente debe ser eliminada en un contenedor de desechos de cloruro.
- (4) Agregar 4 ml de hidróxido de amonio al precipitado restante en el fondo del tubo. Cerrar y agitar. Con este procedimiento el  $\text{AgCl}$  debiera disolverse quedando solamente precipitado AgI. Se debe eliminar el amonio en un contenedor propio.
- (5) Nuevamente se debe agregar agua desionizada de 18 M $\Omega$  a las muestras con el fin de balancear los tubos para ser puestos en la centrífuga durante 10 minutos. Se debe dejar decantar la muestra y eliminar la solución en un contenedor de desechos de cloruro.
- (6) Agregar agua desionizada de 18 M $\Omega$  a la muestra, agitarla hasta que el contenido quede en suspensión. Centrifugar durante 10 minutos.
- (7) Repetir los pasos (5) y (6) al menos dos veces más, hasta que la solución no emita olor a amonio. Finalmente se debe dejar decantar la solución dejando el AgI húmedo en el fondo del tubo.
- (8) Envolver el tubo en papel aluminio dejándolo destapado. Se debe dejar secar bajo una lámpara de calor en una campana de flujo laminar hasta que esté completamente seco (~ 24 horas)
- (9) Con una micro-espátula se debe soltar y extraer la muestra en el fondo del tubo, luego se debe colocar en un trozo de papel encerado (de masa conocida). posteriormente se determina la masa de la muestra al 0.00001 g.



- (10) Sellar la muestra, anotar el nombre y masa obtenida para finalmente embalarla junto a las demás para enviar al laboratorio seleccionado donde se efectuará la medición por AMS.

### **Adición de *carrier***

Algunas veces la concentración de yodo en muestras de agua meteórica es insuficiente para precipitar 1 mg de yoduro de plata (AgI), cantidad mínima requerida para medir la razón isotópica de yodo en la muestra mediante AMS. Para solucionar esto, se requiere la adición de una solución llamada *carrier*, la cual permite aumentar la señal de yodo en la muestra. Cuando se trabaja con *carrier* de yodo, una muestra de éste debe ser apartada con el fin de determinar su concentración y razón isotópica ( $^{129}\text{I}/\text{I}$ ). El detalle de la preparación del *carrier* se explica en la sección III.2.5.3.

La cantidad de *carrier* añadida dependerá de la concentración inicial de la muestra pero debe ser la suficiente como para precipitar 1 mg de AgI. Una vez que la muestra contenga el *carrier* se debe mezclar cuidadosamente dentro de la campana de extracción y continuar el procedimiento de muestras líquidas según Fehn *et al.* (1992), descrito en las secciones previas.

## **III.3 Bibliografía**

- Broecker W. S. y Peng T. H. (1982) Tracers in the Sea. Palisades, NY: Eldigio. pp. 690.
- Chong G. (1994) The Nitrate Deposits of Chile. *In* Tectonics of the Southern Central Andes: Structure and Evolution of an Active Continental Margin (Reutter, K.J.; Scheuber, E.; Wigger, P.J.; editors). *Springer*, 303-316.
- Couture R. A. y Seitz M. G. (1983) Sorption of anions of iodine by iron oxides and kaolinite, *Nucl. Chem. Waste Manag.* **4**, 301-306.
- Ericksen G. E. (1981) Geology and origin of the Chilean nitrate deposits. *U.S. Geol. Surv. Prof. Paper* 1188-B. Unites States Government Printing Office, Washington.
- Fabryka-Martin J., Bentley H., Elmore D. y Airey P. L. (1985) Natural I-129 as an environmental tracer. *Geochim. Cosmochim. Acta* **49**, 337-347.
- Fehn U., Snyder G. T. and Egeberg P. K. (2000) Dating of pore waters with  $^{129}\text{I}$ . Relevance for the origin of marine gas hydrates. *Science* **289**, 2332-2335.
- Fehn U. y Snyder G. T. (2005) Residence times and source ages of deep crustal fluids: interpretation of  $^{129}\text{I}$  and  $^{36}\text{Cl}$  results from the KTB-VB drill site, Germany. *Geofl.* **5**, 42-51.

- Fehn U., Peters E. K., Tullai-Fitzpatrick S., Kubik P. W., Sharma P., Teng R. T. D., Gove H. E. y Elmore D. (1992)  $^{129}\text{I}$  and  $^{36}\text{Cl}$  concentrations in waters of the eastern Clear Lake area, California: residence times and source ages of hydrothermal fluids. *Geochim. Cosmochim. Acta* **56**, 2069-2079.
- Fehn U., Snyder G. T. y Muramatsu Y. (2007a) Iodine as a tracer of organic material:  $^{129}\text{I}$  results from gas hydrate systems and fore arc fluids. *J. Geochem. Explor.* **95**, 66-80.
- Fehn U. Moran J. E., Snyder G. T. y Muramatsu Y. (2007b) The initial  $^{129}\text{I}/\text{I}$  ratio and the presence of "old" iodine in continental margins. *Nucl. Instrum. Meth. B.* **259**, 496-502.
- García F. (1967) Geología del Norte Grande de Chile. In *Simposium sobre Geosinclinal Andino*, pp. 138.
- Kodama S., Takahashi Y., Okumura K. y Uruga, T. (2006) Speciation of iodine in solid environmental samples by iodine K-edge XANES: application to soils and ferromanganese oxides. *Sci. Total Environ.* **363**, 275-284.
- Ladino M. (1998) Geología de la parte oriental de los Cuadrángulos Quebrada Chug-Chug y Cerros de Montecristo, Región de Antofagasta, Chile. Universidad de Chile.
- Moran J. E, Fehn U. y Hanor J. S. (1995) Determination of source ages and migration patterns of brines from the U.S. Gulf Coast basin using  $^{129}\text{I}$ . *Geochim. Cosmochim. Acta* **59**, 5055-5069.
- Moran J. E., Fehn U. y Teng R. T. D. (1998) Variations in  $^{129}\text{I}/^{127}\text{I}$  ratios in recent marine sediments: Evidence for a fossil organic component. *Chem. Geol.* **152**, 193-203.
- Mpodozis C., Arriagada C., Basso M., Roperch P., Cobbold P. y Reich M. (2005) Late Mesozoic to Paleogene stratigraphy of the Salar de Atacama Basin, Antofagasta, Northern Chile: Implications for the tectonic evolution of the Central Andes. *Tectonophysics* **399**, 125-154.
- Muramatsu Y. y Wedepohl K. H. (1998) The distribution of iodine in the earth's crust. *Chem. Geol.* **147**, 201-216.
- Sharma, P., Bourgeois M., Elmore D., Granger D., Lipschutz M. E., Ma X., Miller T., Mueller K., Rickey F., Simms P. y Vogt S. (2000) PRIME lab AMS performance, upgrades and research applications. *Nucl. Instr. Meth. B.* **172**, 112-123.
- Snyder G. T. and Fehn U. (2004) Global distribution of  $^{129}\text{I}$  in rivers and lakes: implications for iodine cycling in surface reservoirs. *Nucl. Instr. Meth. B.* **223/224**, 579-586.
- Tomaru H., Ohsawa S., Amita K., Lu Z. and Fehn U. (2007) Influence of subduction zone settings on the origin of forearc fluids: Halogen concentrations and  $^{129}\text{I}/\text{I}$  ratios in waters from Kyushu, Japan. *Appl. Geochem.* **22**, 676-691.

Vicente J. C. (2006) Dynamic Paleogeography of the Jurassic Andean Basin: pattern of regression and general considerations of main features. *Rev. Asoc. Geol. Argent.* **61**, 408-437.

Wong G. T. F. (1991) The marine geochemistry of iodine. *Rev. Aquatic. Sci.* **4**, 45-73.

# Capítulo IV. Iodine in supergene copper blankets: a case study from the giant Chuquicamata porphyry deposit\*

## IV.1 Abstract

Although iodine is rare in crustal settings, previous studies have documented its occurrence in the supergene zones of base and precious metal ore deposits in arid environments. In this report, we present a novel application of the iodine-129 ( $^{129}\text{I}$ ) isotope tracer to iodine-rich samples from the world's largest supergene copper (Cu) profile at the Chuquicamata deposit in northern Chile, where anomalous concentrations of this element have been reported. All supergene malachite ( $\text{Cu}_2\text{CO}_3(\text{OH})_2$ ) samples from Chuquicamata and iodine-rich soil above the Mansa Mina deposit have  $^{129}\text{I}/\text{I}$  isotope ratios ( $\sim 190\text{-}560 \times 10^{-15}$ ) that are significantly lower than those of surface waters (*i.e.*,  $1500 \times 10^{-15}$ ), indicating that iodine was most likely derived from a reservoir of marine origin rather than a meteoric and/or atmospheric source. Geochemical modeling shows that the long-term dilution of iodine rich deep formation waters by meteoric water during the main stage of supergene alteration ( $\sim 40\text{-}10$  Ma) resulted in fluid  $^{129}\text{I}/\text{I}$  ratios that are within the range of mineral/soil  $^{129}\text{I}/\text{I}$  ratios observed at Chuquicamata, strongly suggesting that iodine was remobilized from the Lower Jurassic to mid Cretaceous marine basement. Results from this study show that iodine isotopes can be successfully applied to trace the origin and nature of supergene fluids in iodine-rich oxide blankets, leach caps, and soils above buried Cu deposits, and also to constrain the timescales of fluid circulation during supergene enrichment.

## IV.2 Introduction

Iodine is commonly overlooked in ore systems and crustal settings in general, since the global iodine distribution is dominated by the marine system, in particular marine sediments, which hold about 70% of the total iodine in the crust at concentrations from 200 to 1300 ppm (Muramatsu and Wedepohl, 1998; Muramatsu *et al.*, 2001; Snyder and Fehn, 2002). A recent survey of the relative proportions of iodides and iodates in metallogenic provinces show that they can be found in the supergene zones of base (Cu, Pb-Zn) and precious (Ag, Au) metal ore deposits in extremely arid environments such as desert areas of Chile, Australia, Arizona, Iran, and Kazakhstan, among other regions (Jarrel, 1939, 1944; Williams, 1963; Srinivasan *et al.*, 1971; Mortimer *et al.*, 1978; Boyle,

\*Una versión completa de este capítulo se encuentra publicada en *Geology*. Apéndice A.

1997; Millstead, 1998; Chouinard *et al.*, 2005; Witzke *et al.*, 2006; Sillitoe, 2007; Reich *et al.*, 2009a; Golebiowska *et al.*, 2010).

In the Atacama Desert of northern Chile, iodide ( $I^-$ ) and iodate ( $IO_3^-$ ) minerals have been reported in the supergene zones of porphyry and Manto-type Cu deposits (e.g., Chuquicamata, Mantos de la Luna), and iodine geochemical anomalies have been recognized in soils above buried porphyry Cu deposits (e.g., Spence, Chimborazo, Tamarugal; Jarrel, 1939, 1944; Mortimer *et al.*, 1978; Kelley *et al.*, 2003; Leybourne and Cameron, 2006a; Reich *et al.*, 2009a; Cameron *et al.*, 2002, 2010). These occurrences remain unexplained, considering the fact that (1) meteoric surface and ground waters have exceedingly low concentrations of iodine, <10 ppb (Muramatsu and Wedepohl, 1998; Moran *et al.*, 1999; Fehn *et al.*, 2007a), and (2) supergene enrichment of Cu in the region was driven by downward circulation of meteoric water from ~44 to 14 to 9 Ma under a semiarid to arid climate, followed by a late stage of oxidation which was dominated by saline ground waters under conditions of progressive aridification (Alpers and Brimhall, 1988; Sillitoe and McKee, 1996; Mote *et al.*, 2001; Hartley and Chong, 2002; Sillitoe, 2005; Arancibia *et al.*, 2006; Leybourne and Cameron, 2006b; Rech *et al.*, 2006; Reich *et al.*, 2008, 2009a, 2009b; Palacios *et al.*, 2011).

### **IV.3 Iodine in the study area and samples**

At Chuquicamata, anomalous concentrations of iodine were reported in the supergene oxide zone, including historic accounts on the observation of small clouds of purplish smoke noted on several occasions during blasting of the oxidation blanket, which was shown to contain significant iodine (Jarrell, 1939, 1944). The Cu iodide marshite ( $CuI$ ) was identified by Jarrell (1939) at the oxidized orebody at Chuquicamata, and in a later study, other Cu iodate minerals such as salesite ( $Cu(IO_3)(OH)$ ) and bellingerite ( $Cu_3(IO_3)_6 \cdot 2H_2O$ ) were documented to occur in the oxide zone (Jarrell, 1944). All known marshite specimens occur between the south end of the Chuquicamata open pit and the Exotica mine (Jarrell, 1939; Mortimer, 1978; Fig. IV.1).

Samples for this study came from the oxide zone of the deposit in the south end of the open pit (Fig. IV.1), and contain fine-grained (<2 mm) marshite crystals ( $CuI$ , pale orange) that occur as associated with atacamite ( $Cu_2Cl(OH)_3$ , green) (Fig. IV.1B). Intergrowth textures between the two minerals suggest that they were deposited more or less contemporaneously, with some atacamite deposited after the marshite. No iodate minerals were observed in the samples.

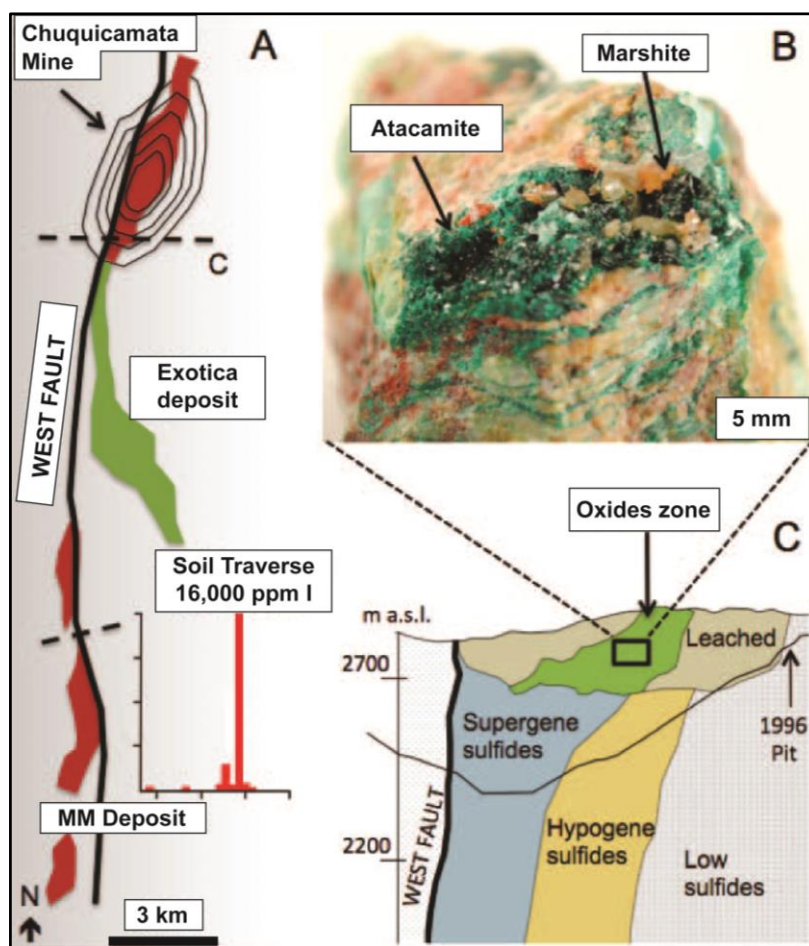


Figure IV.1. (A). Chuquicamata district, showing the location of mines and main structural features. Soil sample was taken above the West fault. (B). Marshite (CuI) sample from Chuquicamata. The fine-grained pale orange crystals occur in association with atacamite (green). (C). Supergene enrichment and oxidation profile at Chuquicamata, showing the leach capping, oxidation zone, and supergene sulfide blanket.

#### IV.4 Iodine geochemistry and the $^{129}\text{I}$ isotopic system

Iodine has the most biophilic nature among the halogens and is commonly associated with organic material (Wong, 1991). As a member of the halogen group, iodine shares characteristics with chlorine (Cl) and bromine (Br), but iodine has the largest ionic radius of the three elements and is much less frequently incorporated into minerals. Thus, iodine remains in the aqueous phase much longer than chlorine, the least biophilic element of these three. While the largest reservoir of chlorine in the Earth's surface is seawater, iodine is concentrated in marine sediments where the total amount of iodine reaches up to  $5.90 \times 10^{12}$  tonnes, corresponding to ~70% of the total iodine inventory in the Earth's crust (Muramatsu and Wedepohl, 1998). Due to its biophilic behavior, iodine in marine particulate organic matter varies from 200 to 1300 ppm while seawater contains approximately 0.05 ppm iodine (Wong, 1991; Muramatsu and Wedepohl, 1998).

Iodine has one stable isotope ( $^{127}\text{I}$ ), and a long-lived radioisotope ( $^{129}\text{I}$ ) with a half-life of 15.7 Ma. In nature,  $^{129}\text{I}$  has two major production modes in nature (Fig. IV.2): (1) a cosmogenic component produced by the spallation of xenon isotopes in the atmosphere, and (2) a fissiogenic component related to the spontaneous fission of  $^{238}\text{U}$  in the crust, and to a much lesser extent, by neutron-induced fission of  $^{235}\text{U}$ . Both production pathways contribute similar amounts of natural  $^{129}\text{I}$  to surface reservoirs (Fabryka-Martin et al., 1985). Since there is only one stable isotope of iodine ( $^{127}\text{I}$ ) and the radiogenic isotope  $^{129}\text{I}$  is present in very small amounts,  $^{129}\text{I}/\text{I}$  ( $^{129}\text{I}$  over total iodine) is for all practical purposes identical to  $^{129}\text{I}/^{127}\text{I}$ . Due to the long residence time of iodine in the oceans (300,000 yr, Broecker and Peng, 1982) and the fact that iodine moves quickly through most surface reservoirs, natural iodine is in isotopic equilibrium in all surface reservoirs, with an initial  $^{129}\text{I}$ -to-stable  $^{127}\text{I}$  isotopic ratio ( $^{129}\text{I}/\text{I}$ ) of  $(1500 \pm 150) \times 10^{-15} \text{ at}\cdot\text{at}^{-1}$  (Moran et al., 1998; Fehn et al., 2007a). This ratio is independent of latitudinal variations in the production of cosmogenic  $^{129}\text{I}$  and is considered as the starting value for  $^{129}\text{I}$  calculations.

The equilibrium in surface reservoirs has been disturbed since ~1945 by the addition of anthropogenic  $^{129}\text{I}$  from nuclear weapons tests and fuel reprocessing (Fig. IV.2), which has increased the  $^{129}\text{I}/\text{I}$  ratio of surficial reservoirs by several orders of magnitude (Snyder and Fehn, 2004). Thus, in most cases the anthropogenic  $^{129}\text{I}$  signal can be detected because of the large difference between anthropogenic and natural values (Fehn et al., 2007a). Although this signal is present in all surface reservoirs which are in rapid exchange with the oceans, anthropogenic  $^{129}\text{I}$  is not affecting marine sediments, deep fluids and aquifers with ages >60 years.

While the initial  $^{129}\text{I}/\text{I}$  ratio in surface reservoirs is  $\sim 1500 \times 10^{-15}$ , different values have been reported in fore-arc, volcanic and deep crustal fluids. The  $^{129}\text{I}/\text{I}$  ratios in fore-arc fluids are significantly lower than surficial reservoirs, ranging between  $\sim 100$  and  $500 \times 10^{-15}$ . These fluids contain “old” cosmogenic iodine that has been derived from organic material, and are hosted in marine sequences that are substantially older (Fehn et al., 2004; Fehn et al., 2007a; Lu et al., 2011). In contrast, volcanic fluids from active continental margins have higher ratios, with values that range between 700 and  $1000 \times 10^{-15}$  (e.g., Snyder et al., 2002). These values reflect the age of the subducted slab, indicating a “young”, slab-derived marine sediment source component for iodine in volcanic fluids (Snyder and Fehn, 2002; Snyder et al., 2003). When iodine is separated from its original source (e.g., marine sediments), the isotopic equilibrium is broken and the cosmogenic signal starts to decrease as a function of time until secular equilibrium with the fissiogenic (in situ) signal is reached (Fehn et al., 2007a). Additionally, deep crustal fluids can show high  $^{129}\text{I}/\text{I}$  ratios ( $>2000 \times 10^{-15}$ ) due to accumulation of  $^{129}\text{I}$  from rock sources that are anomalously enriched in uranium (e.g., Bottomley et al., 2002; Snyder et al., 2003; Fehn and Snyder, 2005).

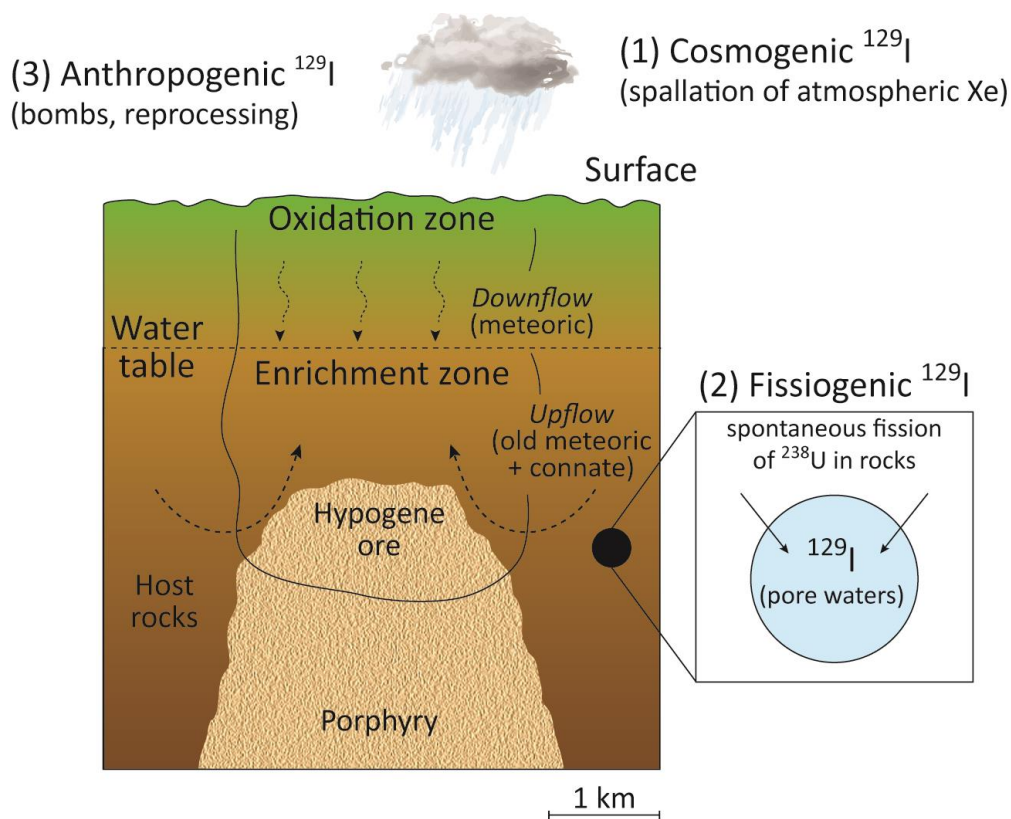


Figure IV.2. Scheme showing the two natural modes of production of  $^{129}\text{I}$  (cosmogenic and fissiogenic components). Also shown is the anthropogenic component of  $^{129}\text{I}$ , produced as a fission product of  $^{235}\text{U}$  and  $^{239}\text{Pu}$  from nuclear tests and nuclear fuel reprocessing.

The iodine isotopic system has received increasing attention because it covers an age range of wide applicability includes, for example: (1) tracing groundwater and geothermal fluid sources (e.g., Fabryka-Martin et al., 1991; Frohlich et al., 1991; Fehn et al., 2000), (2) unraveling the origin and transport history of deep crustal fluids (e.g., Fehn and Snyder 2005), (3) dating oil field brines and coal-bed methane (e.g., Fehn et al., 1990; Snyder and Fabryka-Martin 2007) and (4) investigating sediment recycling in subduction zones (Martin et al., 1993; Lu et al., 2008), where iodine source compartments include subducting marine sediments (e.g., Snyder and Fehn, 2002), organic-rich formations in the overlying plate (e.g., Fehn and Snyder, 2003) and, to a lesser extent, a serpentinized sub-arc mantle wedge (e.g., Snyder et al., 2005).

The different applications are possible due to the existence of the two natural modes of iodine production (i.e., cosmogenic and fissiogenic). Since the cosmogenic signal predominates in fluids related to organic material, the measured  $^{129}\text{I}/\text{I}$  ratios allows to determine the time of separation from surficial reservoirs (Moran et al., 1995; Snyder et al., 2003). Otherwise, the fissiogenic signal is more important in fluids hosted in U-rich rocks in the crust, where the  $^{129}\text{I}/\text{I}$  ratios have been used to calculate the age and residence time of fluids in deep formations (Fabryka-Martin et al., 1989; Fehn et al., 1992; Bottomley et al., 2002).



## IV.5 Results

The  $^{129}\text{I}/\text{I}$  ratios of supergene iodide mineral and soil from Chuquicamata are shown in Figure IV.3. Marshites from Chuquicamata are clustered within a narrow range of  $^{129}\text{I}/\text{I}$  ratios, with values at  $187 \pm 17$ ,  $201 \pm 14$ ,  $218 \pm 72$ , and  $562 \pm 77$  ( $\times 10^{-15}$ ), similar to the ratio reported for the anomalous iodine-rich soil above the Mansa Mina deposit, nearby Chuquicamata ( $473 \pm 75 \times 10^{-15}$ ; Fig. IV.3).

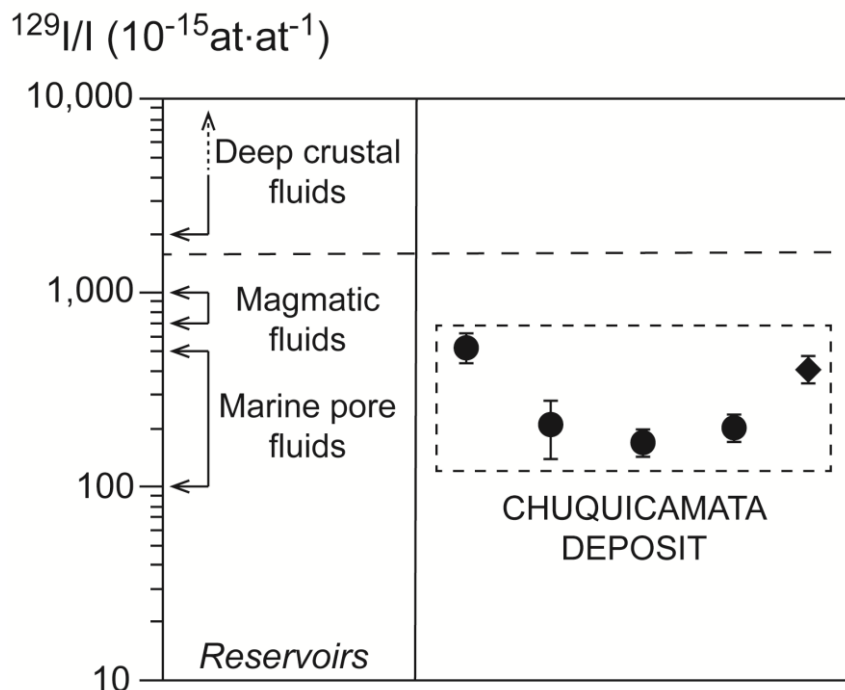


Figure IV.3.  $^{129}\text{I}/\text{I}$  data of marshites (circles) and iodine-rich soil sample (diamond) from Chuquicamata. Error bars are shown for each ratio. The left scale shows the known  $^{129}\text{I}/\text{I}$  ratios of different reservoirs, and the horizontal segmented line represents the pre-anthropogenic  $^{129}\text{I}/\text{I}$  ratio for surface reservoirs.

## IV.6 Discussion

The majority of the Earth's surficial iodine resides in marine sediments along continental margins, intra- and backarc marines basins (Muramatsu and Wedepohl, 1998; Snyder *et al.*, 2010). Therefore, one probable source for the iodine in Chuquicamata could be the Jurassic to mid Cretaceous marine shales that form part of the uplifted Paleozoic-Mesozoic basement outcropping in the Calama basin (Mpodozis *et al.*, 2005). Pore fluids hosted in recent marine sediments on the Peru margin have iodine ratios that decrease asymptotically with depth from seawater values ( $1500 \times 10^{-15}$ ) to values of  $\sim 290 \times 10^{-15}$  at several hundred meters (Fehn *et al.*, 2007b). Assuming similar iodine contents, an initial

$^{129}\text{I}/\text{I}$  ratio of  $290 \times 10^{-15}$  and a uranium content of 9 ppm, Mesozoic shales in the vicinity of Chuquicamata would have reached secular equilibrium ratio values of  $38 \times 10^{-15}$  after 40 m.y.

All marshite samples from Chuquicamata and soil above Mansa Mina have  $^{129}\text{I}/\text{I}$  ratios that are significantly lower than surface waters (*i.e.*,  $<1500 \times 10^{-15}$ ), strongly suggesting that fluids involved in supergene enrichment were not exclusively meteoric in origin (Fig. IV.3). The low  $^{129}\text{I}/\text{I}$  ratios observed at Chuquicamata ( $\sim 200\text{-}600 \times 10^{-15}$ ) indicate that an “old” cosmogenic contribution was present in the supergene fluids that precipitated the Cu iodides in the oxidation blanket of Chuquicamata and imprinted an anomalously rich iodine signature the soil sampled above the Mansa Mina buried body. This cosmogenic iodine component must have been most likely derived from organic material of marine origin (Fehn *et al.*, 2000; Muramatsu *et al.*, 2001).

Assuming that the  $^{129}\text{I}$  budget in the Cu iodides represents the  $^{129}\text{I}$  budget of the water from which they precipitated (*i.e.*, no mineral-fluid isotope fractionation occurred during precipitation), the  $^{129}\text{I}/\text{I}$  ratios can be used as isotopic tracers for iodine. Since the low  $^{129}\text{I}/\text{I}$  ratios observed at Chuquicamata are not consistent with surface and ground water sources of meteoric origin, we calculated the expected  $^{129}\text{I}/\text{I}$  ratios of iodine-rich fluids sourced from the sedimentary rocks of marine origin that form part of the basement in the Calama and/or Chuquicamata area (the Low Jurassic to mid Cretaceous marine sequences, Arcuri and Brimhall, 2003; Mpodozis *et al.*, 2005).

The first modeled scenario is represented by the black curve in Figure IV.4 and considers that the parent fluid source (1) had a typical initial condition found in marine pore fluids during sediment deposition (*i.e.*, an “old” cosmogenic component of  $^{129}\text{I}/\text{I} = 290 \times 10^{-15}$ , and  $\text{I} = 143$  ppm,  $\text{Cl} = 18$  g/L; Fehn *et al.*, 2007b); (2) had a subsurface contribution of  $^{129}\text{I}$  related to spontaneous fission of U in the host rocks (*i.e.*, “fissiogenic” component, calculated considering  $\text{U} = 9$  ppm at Chuquicamata (International Atomic Energy Agency, 1980; porosity = 10% and density =  $2700 \text{ kg} \times \text{m}^{-3}$ ); and (3) did not mix with other fluid sources, including ground water of meteoric origin. The modeled  $^{129}\text{I}/\text{I}$  ratios indicate that secular equilibrium was attained at  $\sim 40$  Ma at  $38 \times 10^{-15}$  ratio (Fig. IV.4). Taking into account the fact that all of the Chuquicamata samples show  $^{129}\text{I}/\text{I}$  ratios greater than the secular equilibrium value (Fig. IV.4), solutions that precipitated the iodides could not have been exclusively undiluted deep pore fluids or formation waters.

The second scenario involves dilution of the deep pore fluids by ground water of meteoric origin, using a mixing model that takes into account the past climatic evolution of the region. The fluid  $^{129}\text{I}/\text{I}$  ratios were modeled assuming that the pore waters mixed with meteoric ground waters during the main supergene enrichment and oxidation stage in the Atacama region between 40 and 10 Ma, under semiarid climate conditions with moderate precipitation ( $>10$  cm/yr) and groundwater recharge (Alpers and Brimhall, 1988; Sillitoe and McKee, 1996; Arancibia *et al.*, 2006). The model considered the dilution of iodine-rich pore fluids in the host formations (using same initial conditions as scenario (1)

by a meteoric water end member (with  $^{129}\text{I}/\text{I} = 1500 \times 10^{-15}$ ,  $\text{I} = 0.013 \text{ ppm}$ ,  $\text{Cl} = 0.35 \text{ ppm}$ , Fehn *et al.*, 2007a). Mixing or dilution steps were taken at 40, 30, 20, and 10 Ma, and the expected  $^{129}\text{I}/\text{I}$  ratios are represented by the black arrowed curves in Figure IV.4. Results indicate that expected  $^{129}\text{I}/\text{I}$  ratios of the fluid overlap the mineral/soil  $^{129}\text{I}/\text{I}$  data at Chuquicamata, considering a pore/meteoric water fluid mixing ratio of  $\sim 0.05$  (5% pore fluids, 95% meteoric water). Therefore, iodine occurrence at Chuquicamata was most likely the result of a three-stage process that involved (1) the deposition of Mesozoic marine sediments, accompanied by decay of  $^{129}\text{I}$  over time to reach secular equilibrium iodine ratios at  $\sim 40 \text{ Ma}$ ; followed by (2) mixing of iodine-rich pore fluids in the marine sequences with downflowing meteoric fluids during the main stage of supergene enrichment ( $\sim 40\text{-}10 \text{ Ma}$ ), diluting the original iodine and allowing higher secular equilibrium ratios; and (3) precipitation of Cu iodides and formation of soil anomalies by interaction of the mixed fluids with the deposit under hyperarid conditions, leading to closure of the iodine system.

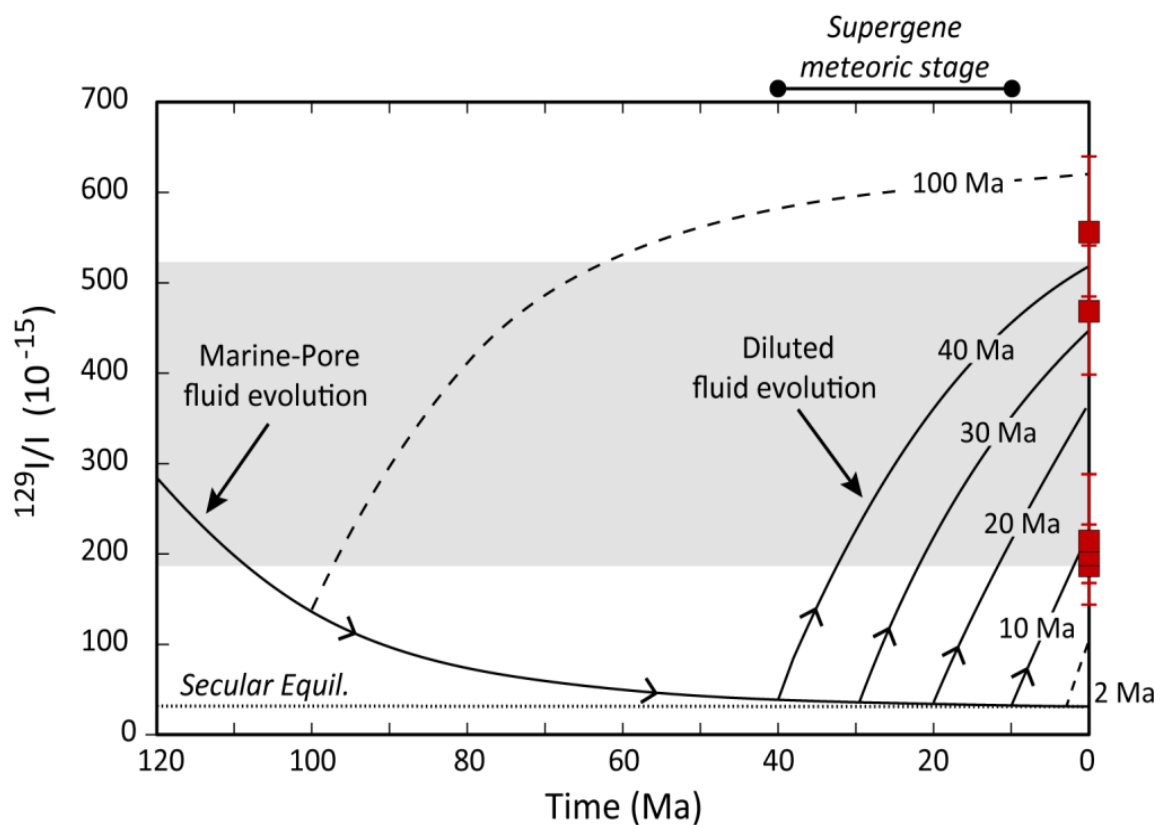


Figure IV.4. Mixing model of progressive dilution between iodine-rich sediment pore fluids (deep formation waters) and meteoric water. The black curve below shows the evolution of pore fluids in the basement rocks, assuming decay of the cosmogenic  $^{129}\text{I}$  component and fissiogenic  $^{129}\text{I}$  build-up conditions found at Chuquicamata. Secular equilibrium is reached at  $\sim 40 \text{ Ma}$  (dotted horizontal line). Modeled fluid trajectories (ascending black curves with arrows) show the effect of dilution of the pore fluids (5%) by sufficient meteoric water (95%) between 40 and 10 Ma (supergene meteoric stage), before desiccation of the Atacama region. The modeled trajectories predict the observed range of  $^{129}\text{I}/\text{I}$  ratios at Chuquicamata (horizontal gray area, and red data points with error bars). Also shown are fluid trajectories resulting from mixing at 100 and 2 Ma that do not reproduce the observed I-129 data (segmented curves).

## IV.7 Conclusion

Results from this study show that the iodine  $^{129}\text{I}/\text{I}$  isotope ratios of mineral and soil samples can be successfully used to trace the origin of supergene fluids in iodine-rich oxidation blankets, leach caps, and soils above buried Cu deposits. For the particular case of the Chuquicamata deposit, the low  $^{129}\text{I}/\text{I}$  ratios ( $\sim 200\text{-}600 \times 10^{-15}$ ) suggest that iodine was most likely derived from the sedimentary rocks that form part of the Low Jurassic to mid Cretaceous marine basement in the Chuquicamata and/or Calama area. These low  $^{129}\text{I}/\text{I}$  ratios observed at Chuquicamata are predicted by geochemical models that involve mixing between  $\sim 5\%$  deep pore fluids and  $\sim 95\%$  meteoric water during the main stage of supergene alteration ( $\sim 40\text{-}10$  Ma), which peaked between  $\sim 19$  to 15 Ma in the Chuquicamata area (Sillitoe and McKee, 1996; Sillitoe, 2005; Arancibia *et al.*, 2006).

## IV.8 References

- Alpers C. N., Brimhall G. H. (1988) Middle Miocene climatic change in the Atacama Desert, northern Chile: Evidence from supergene mineralization at La Escondida. *Geol. Soc. Am. Bull.* 100, 1640-1656.
- Arancibia G, Matthews S. J. and De Arce, C. P. (2006) K-Ar and Ar-40/Ar-39 geochronology of supergene processes in the Atacama Desert, northern Chile: Tectonic and climatic relations. *J. Geol. Soc. London* **163**, 107-118.
- Arcuri T. and Brimhall G. (2003) The chloride source for atacamite mineralization at the Radomiro Tomic porphyry copper deposit, northern Chile. *Econ. Geol.* **98**, 1667-1681.
- Boyle D. R. (1997) Iodargyrite as an indicator of arid climatic conditions and its association with gold-bearing glacial tills of the Chibougamau-Chapais area, Quebec. *Can. Mineral.* **35**, 23-34.
- Cameron E. M., Leybourne M. I. and Kelley, D. L. (2002) Exploring for deeply covered mineral deposits: Formation of geochemical anomalies in northern Chile by earthquake-induced surface flooding of mineralized groundwaters. *Geology* **30**, 1007-1010.
- Cameron E. M., Leybourne M. I., Reich M. and Palacios C. (2010) Geochemical anomalies in northern Chile as a surface expression of the extended supergene metallogenesis of buried copper deposits. *Geochem-Explor. Env.* **10**, 1-14.
- Fehn U., Snyder G. T. and Egeberg P. K. (2000) Dating of pore waters with  $^{129}\text{I}$ . Relevance for the origin of marine gas hydrates. *Science* **289**, 2332-2335.

- Fehn U. Moran J. E., Snyder G. T. and Muramatsu Y. (2007a) The initial  $^{129}\text{I}/\text{I}$  ratio and the presence of “old” iodine in continental margins. *Nucl. Instrum. Meth. B.* **259**, 496-502.
- Fehn U., Snyder G. T. and Muramatsu Y. (2007b) Iodine as a tracer of organic material:  $^{129}\text{I}$  results from gas hydrate systems and fore arc fluids. *J. Geochem. Explor.* **95**, 66-80.
- Fehn U. (2012) Tracing Crustal Fluids: Applications of Natural  $^{129}\text{I}$  and  $^{36}\text{Cl}$ . *Annu. Rev. Earth Pl. Sc.* **40**, 45-67.
- Golebiowska B., Pieczka A., Rzepa G., Matyszkiewicz J. and Krajewski M. (2010) Iodargyrite from Zalas (Cracow area, Poland) as an indicator of Oligocene–Miocene aridity in Central Europe. *Palaeogeogr. Palaeoclimatol. Palaeoecol.* **296**, 130-137.
- Hartley A. J. and Chong G. (2002) Late Pliocene age for the Atacama Desert: Implications for the desertification of western South America. *Geology* **30**, 43-46.
- International Atomic Energy Agency (1980) Nuclear theory for applications: Report IAEA-SMR-68.
- Jarrell O. (1939) Marshite and other minerals from Chuquicamata, Chile. *Am. Miner.* **24**, 629-635.
- Jarrell O. (1944) Oxidation at Chuquicamata, Chile. *Econ. Geol.* **39**, 251-286.
- Kelley D. L., Hall G. E., Closs G., Hamilton I. C. and McEwen R. M. (2003) The use of partial extraction geochemistry for copper exploration in northern Chile. *Geochem.: Explor. Environ., Anal.* **3**, 85-104.
- Leybourne M. I. and Cameron E. M. (2006a) Composition of soils and ground waters at the Pampa del Tamarugal, Chile: Anatomy of a fossil geochemical anomaly derived from a distant porphyry copper deposit. *Econ. Geol.* **101**, 1569-1581.
- Leybourne M. I. and Cameron, E. M. (2006b) Composition of groundwaters associated with porphyry-Cu deposits, Atacama Desert, Chile: Elemental and isotopic constraints on water sources and water-rock reactions. *Geochim. Cosmochim. Acta* **70**, 1616-1635.
- Millsted P. W. (1998) Marshite-miersite solid solution and iodargyrite from Broken Hill, New South Wales, Australia. *Mineral. Mag.* **62**, 471-475.
- Moran J. E., Fehn U. and Teng R. T. D. (1998) Variations in  $^{129}\text{I}/^{127}\text{I}$  ratios in recent marine sediments: Evidence for a fossil organic component. *Chem. Geol.* **152**, 193-203.
- Mortimer C., Munchmeyer C. and Urqueta I. (1978) Emplazamiento del yacimiento Exótica, Chile. *Andean Geol.* **6**, 41-51.

- Mpodozis C., Arriagada C., Basso M., Roperch P., Cobbold P. and Reich M. (2005) Late Mesozoic to Paleogene stratigraphy of the Salar de Atacama Basin, Antofagasta, Northern Chile: Implications for the tectonic evolution of the Central Andes. *Tectonophysics* **399**, 125-154.
- Muramatsu Y. and Wedepohl K. H. (1998) The distribution of iodine in the earth's crust. *Chem. Geol.* **147**, 201-216.
- Muramatsu Y., Fehn U., and Yoshida S. (2001) Recycling of iodine in fore-arc areas: Evidence from the iodine brines in Chiba, Japan. *Earth Planet. Sci. Lett.* **192**, 583–593.
- Palacios C., Rouxel O., Reich M., Cameron E. and Leybourne M. I. (2011) Pleistocene recycling of copper at a porphyry system, Atacama Desert, Chile: Cu isotope evidence. *Miner. Deposita* **46**, 1-7.
- Reich M., Palacios C., Alvear M., Cameron E. M., Leybourne M. I. and Deditius A. (2009a) Iodine-rich waters involved in supergene enrichment of the Mantos de la Luna argentiferous copper deposit, Atacama Desert, Chile. *Miner. Deposita* **44**, 719-722.
- Reich M., Palacios C., Vargas G., Luo S., Cameron E. M., Leybourne M. I., Parada M. A., Zúñiga A. and You C.F. (2009b) Supergene enrichment of copper deposits since the onset of modern hyperaridity in the Atacama Desert, Chile. *Miner. Deposita* **44**, 497-504.
- Sillitoe R. H. and McKee E. H. (1996) Age of supergene oxidation and enrichment in the Chilean porphyry copper province. *Econ. Geol.* **91**, 164-179.
- Sillitoe R. H. (2005) Supergene oxidized and enriched porphyry copper and related deposits. *Econ. Geol. 100<sup>th</sup> Anniversary Volume*, 723-768.
- Sillitoe R. H. (2007) Hypogene reinterpretation of supergene silver enrichment at Chañarcillo, northern Chile. *Econ. Geol.* **102**, 777-781.
- Snyder G. T. and Fehn U. (2002) Origin of iodine in volcanic fluids: <sup>129</sup>I results from the Central American Volcanic Arc. *Geochim. Cosmochim. Acta* **67**, 3827-3838.
- Snyder G., Aldahan A. and Possnert G. (2010) Global distribution and long term fate of anthropogenic I-129 in marine and surface water reservoirs. *Geochem. Geophys. Geosy.* **11(4)**, Q04010.
- Srinivasan B., Alexander E.C. and Manuel O.K. (1971) I-129 in terrestrial ores. *Science* **173**, 327-328.
- Williams S.A. (1963) Oxidation of sulfide ores in the Mildren and Steppe mining districts, Pima County, Arizona. *Econ. Geol.* **58**, 1119-1125.

Witzke T., Kolitsch U., Krause W., Wiechowski A., Medenbach O., Kampf A. R., Steele I. M. and Favreau G, (2006) Guanacoite,  $\text{Cu}_2\text{Mg}_2(\text{Mg}_{0.5}\text{Cu}_{0.5})(\text{OH})_4(\text{H}_2\text{O})_4(\text{AsO}_4)_2$ , a new arsenate mineral species from the El Guanaco mine, near Taltal, Chile: Description and crystal structure. *Eur. J. Mineral.* **18**, 813-821.

# Capítulo V. Iodine in nitrate deposits from the Antofagasta Districts\*

## V.1 Abstract

The giant nitrate deposits of the hyperarid Atacama Desert (Chile) are one of the most extraordinary, yet enigmatic, mineral occurrences on Earth. These deposits are complex assemblages of highly soluble nitrates, chlorides, sulfates, perchlorates, iodates, and chromates, and their preservation is the result of prevalent hyperarid climate conditions in the Atacama Desert since the late Miocene, with average rainfall rates of <10 mm/yr in the past ~3 m.y. Although several hypotheses have been proposed since the mid-1800s, the formation of these extensive deposits still remains highly controversial despite the fact that recent studies have argued toward an atmospheric source for the nitrate, sulfate, and perchlorate components. In this report, we focus on the often overlooked and poorly studied iodine and chromium components of Atacama's nitrates. We present the first cosmogenic iodine ( $^{129}\text{I}$ ) isotope data of nitrates showing that groundwater has played an unforeseen role in the formation of these massive deposits.

The isotopic signature of iodine in the nitrates ( $^{129}\text{I}/\text{I} \sim 150\text{-}600 \times 10^{-15}$ ) share similarities with deep sedimentary (marine) pore waters and shales, deviating significantly from atmospheric iodine ( $^{129}\text{I}/\text{I} \sim 1500 \times 10^{-15}$ ). Our evidence points toward a multi-source genetic model for the Atacama Desert nitrate deposits, where these extensive accumulations were the result of long-lived, near-surface mineral precipitation driven by groundwater (*i.e.*, chromates, iodates) coupled with dry atmospheric deposition (*i.e.*, nitrates, perchlorates) and sea spray inputs (*i.e.*, sulfates, chlorides), triggered by increasing aridity and tectonic uplift.

## V.2 Introduction

Massive nitrate accumulations on Earth's surface are scarce and their existence is restricted to hyperarid environments like the Atacama Desert of northern Chile, although minor amounts of nitrate are present in other desert environments such as Death Valley (western United States), the Gobi Desert (Turpan-Hami area, northwestern China), and the McMurdo Dry Valleys (Antarctica) (Ericksen, 1981; Ericksen *et al.*, 1988; Michalski *et al.*, 2005; Qin *et al.*, 2012).

\*Una versión completa de este capítulo se encuentra publicada en *Geology*. Apéndice A.



The Atacama deposits are unique in terms of their massive extent and diversity in chemical and mineralogical compositions. First, they are the largest nitrate accumulations in the world, making up an almost continuous ~700-km-long by ~20-km-wide belt, and have been the premier source for natural nitrate since the 1800s. The nitrate deposits of Atacama are also singular due to the presence of unusual oxidized components such as iodates, chromates, and perchlorates, hosted by a complex mineral bed ~0.2-3 m thick composed of nitrates, sulfates, and chlorides. The Atacama's nitrates are currently the world's prime source for I, with concentrations in the range of hundreds to thousands of parts per million (ppm), ~3-4 orders of magnitude higher than the average iodine content of the continental crust. Despite these recent advances, available geochemical and isotopic data on nitrate, sulfate, and perchlorate are not sufficiently diagnostic to yield a genetic model that explains the occurrence of all mineral components, including the exotic iodates and chromates. Iodine (I) occurrence is so exceptional that Atacama's nitrates are currently the world's prime source for I, with concentrations in the range of hundreds to thousands of parts per million (ppm), ~3-4 orders of magnitude higher than the average iodine content of the continental crust.

In this report, we propose a multi-source model for the genesis of the nitrate deposits of Atacama that (1) explains the presence of the exotic iodine components, (2) integrates their occurrence to the most common compounds, such as nitrate and sulfate, and (3) incorporates the previously unforeseen role of groundwater, constraining nitrate deposit formation to an outstanding convergence of tectonic, hydrologic, and climatic conditions that favored the long-lived fixation and accumulation of chemical components from the atmosphere and subsurface water.

### **V.3 Results**

The  $^{129}\text{I}/\text{I}$  ratios of nitrate samples from the Aguas Blancas and Baquedano districts in the hyperarid core of the Atacama Desert range between  $148.9 \pm 9.5 \times 10^{-15}$  and  $1580 \pm 244.1 \times 10^{-15}$ , but most of them are clustered within a narrow range, ~100-500  $\times 10^{-15}$  (average  $483.2 \pm 107.9 \times 10^{-15}$ ), deviating significantly from the pre-anthropogenic atmospheric value of  $1500 \pm 150 \times 10^{-15}$  (Fig. V.1).

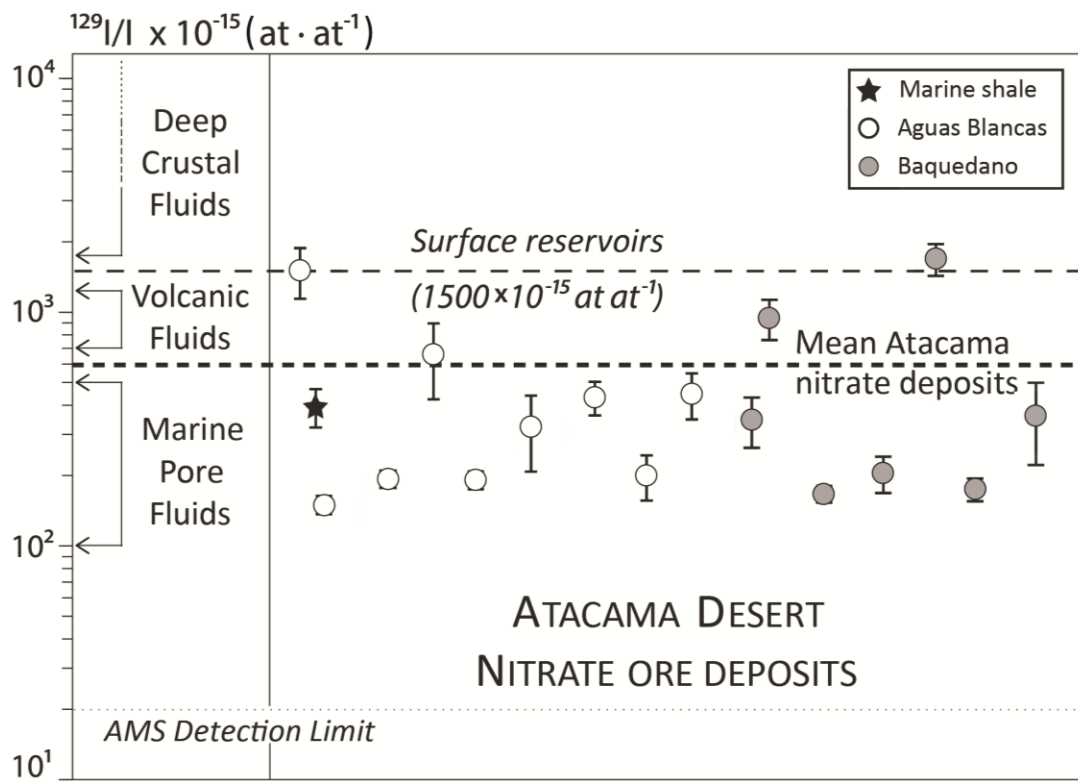


Figure V.1.  $^{129}\text{I}/\text{I}$  ratios of nitrate samples from Atacama Desert (northern Chile) (AMS-accelerator mass spectrometry). Left vertical axis shows  $^{129}\text{I}/\text{I}$  ratios for different Earth reservoirs (Fehn *et al.*, 2007). Error bars are shown for each ratio. Thick horizontal dashed line shows average  $^{129}\text{I}/\text{I}$  ratio of the nitrates ( $483 \times 10^{-15}$ ), while light horizontal dashed line shows pre-anthropogenic surficial/atmospheric iodine ratios ( $1500 \times 10^{-15}$ ). White circles represent Aguas Blancas samples, and gray circles represent Baquedano samples. Black star shows  $^{129}\text{I}/\text{I}$  ratio of Jurassic marine shales from Atacama Desert.

## V.4 Discussion

The significantly low ratios rule out a prevalent atmospheric/eolian source for most of the iodine and point toward an old iodine source (Fehn *et al.*, 2007; Fehn, 2012). Our results are in close agreement with  $^{129}\text{I}$  data from supergene enrichment zones of the giant Chuquicamata porphyry Cu deposit located ~100 km north east of the nitrate ore fields (Chapter IV), strongly suggesting that the anomalous enrichment of iodine in the nitrates and in supergene Cu deposits shares a similar source. Considering that the cosmogenic signal is accumulated in fluids related to organic matter (*e.g.*, marine sediments; Fehn *et al.*, 2007), the low  $^{129}\text{I}/\text{I}$  ratios ( $\sim 100\text{-}500 \times 10^{-15}$ ) reported here indicate that iodine was most likely leached from marine sedimentary rocks that form part of the Jurassic marine basin at the eastern border of the Atacama Desert (Mpodozis *et al.*, 2005; Vicente, 2006), which show a distinct  $^{129}\text{I}/\text{I}$  ratio of  $\sim 393.1 \pm 73.5 \times 10^{-15}$  (Fig. V.1). The higher  $^{129}\text{I}/\text{I}$  ratios ( $\sim 600\text{-}1580 \times 10^{-15}$ ) observed in a few samples are indicative of the influence of meteoric water with high pre-anthropogenic  $^{129}\text{I}/\text{I}$  ratios, most likely related to infrequent moisture

and flooding events associated with increased precipitation in the High Andes, and subsequent groundwater recharge (e.g., 16-10 ka) (Nester *et al.*, 2007).

Our data provide new insights toward the understanding of the genesis of the enigmatic nitrate deposits of Atacama. Iodine isotopic ratios point toward the important and previously unforeseen role played by groundwater during leaching and transport of the exotic iodine in the Atacama nitrates. Based on our results and previously published O, N, and S stable isotope data, we propose an integrated, multi-source genetic model that explains the occurrence of all components found in the nitrate deposits and is consistent with the geological, hydrologic, and climatic evolution of this region (Fig. V.2).

Our model involves leaching of iodine from sedimentary rocks, which was then transported westwards along with other chemical species to the Central Basin by groundwater. Neogene climate change and tectonic uplift resulted in decreased precipitation rates from >200 mm/yr to <20 mm/yr between ca. 20 and 10 Ma, and to <3 mm/yr today in its hyperarid core (Hartley and Chong, 2002; Rech *et al.*, 2006; Reich *et al.*, 2009; Amundson *et al.*, 2012). This led to the development of an exclusively endorheic drainage system recharged in the High Andes (Magaritz *et al.*, 1990), where increase in elevation of the Andean plateau due to uplift in the late Miocene (Allmendinger *et al.*, 1997; Garzzone *et al.*, 2008) would also have increased the hydraulic potential between the wet Altiplano and the dry western slope, creating favorable conditions for increased groundwater flow toward the Central Basin (Hoke *et al.*, 2004). The precipitation of iodate minerals (and probably some sulfate and nitrate) was favored downstream in the Central Basin by an “impermeable” barrier effect of the eastern slope of the Coastal Range (>1000 m above sea level at 10 Ma; Allmendinger and González, 2010) that allowed saline and reduced groundwater to efficiently rise, evaporate, and oxidize in the presence of a continuous dry deposition flux of atmospheric nitrate and perchlorate, and excursions of sulfate and/or chloride-bearing sea spray from the Pacific Ocean (Fig. V.2).

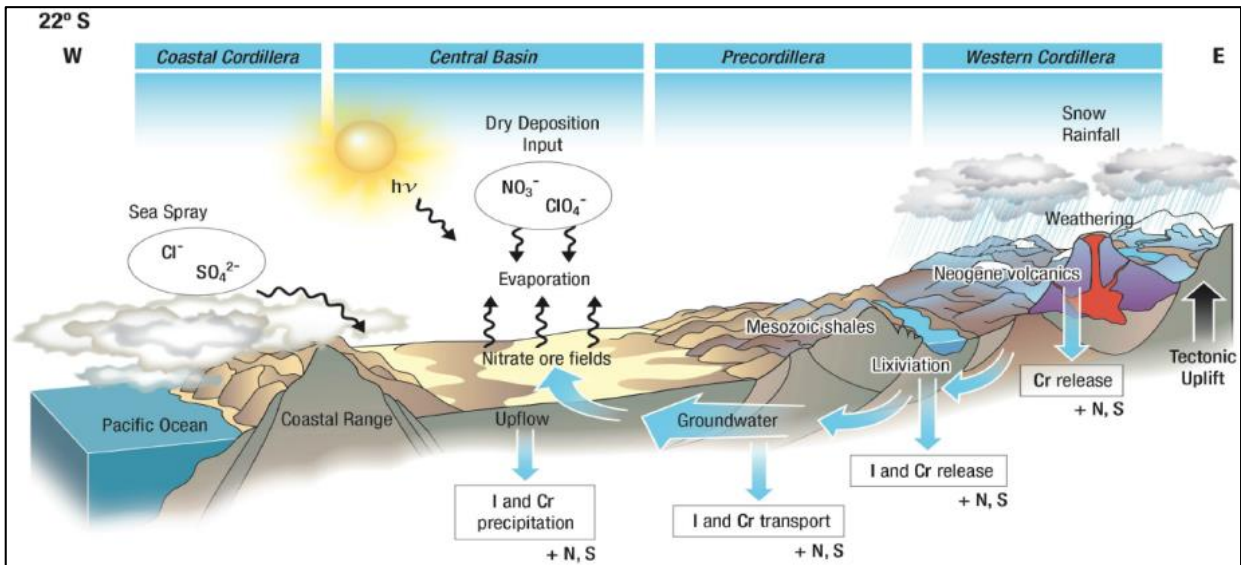


Figure V.2. Multi-source genetic model for the formation of Atacama Desert's nitrate deposits. West-east section at latitude 22°S shows main structural domains. Processes involved in formation of nitrate deposits are shown, *i.e.*, atmospheric dry deposition, groundwater transport and precipitation, sea spray inputs, and evaporation. I-iodine as iodate ( $\text{IO}_3^-$ ) or iodide ( $\text{I}^-$ ); Cr-chromium as chromate ( $\text{CrO}_4^{2-}$ ), dichromate ( $\text{Cr}_2\text{O}_7^{2-}$ ), or Cr(III); S-sulfur as sulfate ( $\text{SO}_4^{2-}$ ); N-nitrogen as nitrate ( $\text{NO}_3^-$ ). Perchlorate ( $\text{ClO}_4^-$ ) and chloride ( $\text{Cl}^-$ ) are also shown.

## V.5 Conclusion

We conclude that the large and almost continuous, ~700-km-long by ~20-km-wide belt of nitrate deposits of Atacama represent an unusual convergence of common physical-chemical processes with an ideal geologic, tectonic, hydrologic, and climatic setting that is specific to Atacama—that is, a convergent margin section undergoing rapid uplift since the late Miocene to elevations sufficient for exhumation and weathering of Jurassic marine sequences, and enhanced large-scale groundwater flow toward the Central Basin. The critical trigger for the formation of Atacama's nitrate deposits was the concomitant increase in tectonic uplift and desiccation that allowed not only the precipitation of transported species from uprising groundwater in the Central Basin due to evaporation, but also the long-term accumulation and preservation of atmospheric nitrate.

## V.6 References

- Allmendinger R. W., Jordan T. E., Kay S. M. and Isacks B. L. (1997) The evolution of the Altiplano-Puna Plateau of the central Andes. *Annu. Rev. Earth Pl. Sc.* **25**, 139-174.
- Allmendinger R. and González G. (2010) Neogene to Quaternary tectonics of the coastal Cordillera, northern Chile. *Tectonophysics* **495**, 93-110.
- Amundson R., Dietrich W., Bellugi D., Ewing S., Nishiizumi K., Chong G., Owen J., Finkel R., Heimsath A. and Stewart B. (2012) Geomorphologic evidence for the late Pliocene onset of hyperaridity in the Atacama Desert. *Geol. Soc. Am. Bull.* **124**, 1048-1070.
- Ericksen G. E. (1981) Geology and origin of the Chilean nitrate deposits. U.S. Geol. Surv. Prof. Paper 1188-B. United States Government Printing Office, Washington.
- Ericksen G. E., Hosterman J. W. and St. Amand P. (1988) Chemistry, mineralogy and origin of the clay-hill nitrate deposits, Amargosa River valley, Death Valley region, California, U.S.A: *Chem. Geol.* **67**, 85-102.
- Fehn U. Moran J. E., Snyder G. T. and Muramatsu Y. (2007) The initial  $^{129}\text{I}/\text{I}$  ratio and the presence of "old" iodine in continental margins. *Nucl. Instrum. Meth. B.* **259**, 496-502.
- Fehn U. (2012) Tracing Crustal Fluids: Applications of Natural  $^{129}\text{I}$  and  $^{36}\text{Cl}$ . *Annu. Rev. Earth Pl. Sc.* **40**, 45-67.
- Garzione C. N., Hoke G. D., Libarkin J. C., Whithers S., MacFadden B., Eiler J., Ghosh P. and Mulch A. (2008) Rise of the Andes. *Science* **320**, 1304-1307.
- Hartley A. J. and Chong G. (2002) Late Pliocene age for the Atacama Desert: Implications for the desertification of western South America. *Geology* **30**, 43-46.
- Hoke G. D., Isacks B. L., Jordan T. E. and Yu J. S. (2004) Groundwater-sapping origin for the giant quebradas of northern Chile. *Geology* **32**, 605-608.
- Magaritz M., Aravena R., Peña H., Suzuki O. and Grilli A. (1990) Source of Ground Water in the Deserts of northern Chile: Evidence of Deep Circulation of Ground Water from the Andes. *Ground Water* **28**, 513-517.
- Michalski G., Böhlke J.K. and Thiemens M. (2004) Long term atmospheric deposition as the source of nitrate and other salts in the Atacama Desert, Chile: New evidence from mass independent oxygen isotopic compositions. *Geochim. Cosmochim. Acta* **68**, 4023-4038.
- Mpodosis C., Arriagada C., Basso M., Roperch P., Cobbold P. and Reich M. (2005) Late Mesozoic to Paleogene stratigraphy of the Salar de Atacama Basin, Antofagasta,

- northern Chile: Implications for the tectonic evolution of the Central Andes. *Tectonophysics* **399**, 125-154.
- Nester P. L., Gayo E., Latorre C., Jordan T. E. and Blanco N (2007) Perennial stream discharge in the hyperarid Atacama Desert of northern Chile during the latest Pleistocene. *P. Natl. Acad. Sci. USA* **104**, 19724-19729.
- Qin Y., Bao H., Liu F., Hou K., Wan D. and Zhang C. (2012) Massive atmospheric nitrate accumulation in a continental interior desert, northwestern China. *Geology* **40**, 623-626.
- Rech J. A., Currie B. S., Michalski G. and Cowan, A. M. (2006) Neogene climate change and uplift in the Atacama Desert, Chile. *Geology* **34**, 761-764.
- Reich M., Palacios C., Vargas G., Luo S., Cameron E. M., Leybourne M. I., Parada M. A., Zúñiga A. and You C.F. (2009) Supergene enrichment of copper deposits since the onset of modern hyperaridity in the Atacama Desert, Chile. *Miner. Deposita* **44**, 497-504.
- Vicente J. C. (2006) Dynamic Paleogeography of the Jurassic Andean Basin: pattern of regression and general considerations of main features. *Rev. Asoc. Geol. Argent.* **61**, 408-437.

# Capítulo VI. Sources of natural and anthropogenic iodine in natural waters from the Atacama Desert, northern Chile\*

## VI.1 Abstract

The compositional data presented in the previous chapters show unique iodine enrichment in nitrate-rich soils, supergene copper deposits and sedimentary marine rocks from the Atacama Desert, suggesting that groundwater has played a key role in the remobilization, transport and deposition of iodine in these deposits. In order to determine the origin of natural and anthropogenic iodine in surficial fluid reservoirs and their association with geological and climatic processes, we investigate the halogen chemistry and iodine isotopic composition of natural waters in Atacama, including shallow seawater, rivers, salt lakes, cold and thermal spring water, rainwater and groundwater. Data reported here show that a combination of halogen concentrations and iodine isotopic ratios are useful to trace meteoric, marine and crustal sources for such waters. Results for halogen concentrations show that iodine values range between 0.35  $\mu\text{M}$  and 26  $\mu\text{M}$  in Tarapacá and between 0.25  $\mu\text{M}$  and 48  $\mu\text{M}$  in Antofagasta, while bromine concentrations vary from 1.28  $\mu\text{M}$  to 45.68  $\mu\text{M}$  and from 1.66  $\mu\text{M}$  to 87.38  $\mu\text{M}$ , respectively. Thus, water samples from the Atacama region in northern Chile show a strong iodine enrichment when compared to seawater concentrations ( $\text{I} = \sim 0.4 \mu\text{M}$ ,  $\text{Br} = \sim 600$ ). In contrast, no bromine enrichment is detected, suggesting the existence of an organic-rich source (or “initial” fluid) with high iodine content that interacted with meteoric water to produce a mixed fluid. On the other hand, the  $^{129}\text{I}/\text{I}$  ratios show influence of different natural and anthropogenic sources of iodine in the studied area. Isotopic results are consistent with halogen chemistry and support the notion that most of the iodine present in natural waters derives from organic-rich deep sources (*i.e.*, Jurassic marine sedimentary rocks) and one or more atmospheric sources. Samples with the lowest isotopic ratios ( $^{129}\text{I}/\text{I}$  from  $\sim 215$  to  $\sim 1000 \times 10^{-15}$ ) strongly suggest mixing between the “initial”, organic-rich and deep fluid and pre-anthropogenic meteoric water, while samples with higher values ( $> 1500 \times 10^{-15}$ ) indicate the input of anthropogenic meteoric water and/or anthropogenic seawater (seaspray). Considering the geological, hydrological and climatic conditions of the Atacama Desert, we propose two different contributions of anthropogenic  $^{129}\text{I}$ . The first is associated with  $^{129}\text{I}$  releases during nuclear weapon tests carried out in the Pacific Ocean ( $^{129}\text{I}/\text{I} = \sim 12000 \times 10^{-15}$ ); and the second contribution is related to  $^{129}\text{I}$  releases in reprocessing nuclear plants in the Northern Hemisphere ( $^{129}\text{I}/\text{I} = \sim 93700 \times 10^{-15}$ ). Both sources reflect rapid redistribution of

\*Una versión adaptada de este capítulo será sometida en una revista ISI *ad-hoc*.

this radioisotope on a global scale. Our results strongly point towards a long-lived continental iodine cycle in the hyperarid margin of western South America, which is driven by local hydrological conditions, producing iodine enrichment and subsequent remobilization and transport in surficial reservoirs.

## VI.2 Introduction

Available data of total iodine concentration and  $^{129}\text{I}/\text{I}$  isotopic ratios in natural waters are quite scarce in the Southern Hemisphere. In general, natural waters have very low iodine concentrations, and therefore, chemical and isotopic measurements involve important difficulties. However, the particular geochemical behavior of iodine makes this isotopic system a powerful methodology to trace surficial and deep fluids. Iodine has the most biophilic nature of the major halogens, and its behavior is considerably different from other halogens (chlorine and bromine). Because of its nature, iodine enrichment is commonly explained by derivation from organic-rich formations. Subducting marine sediments in the slab, as well as organic-rich formations in the continental plate, are potential iodine sources along active continental margins.

The iodine isotopic system covers an important age range of applications in geological settings, especially in systems related to fluids or sediments associated with organic material. These applications include: (1) Groundwater, pore waters and geothermal fluids tracing and dating (*e.g.* Frohlich *et al.*, 1991; Fabryka-Martin *et al.*, 1991; Fehn *et al.*, 2000; Fehn and Snyder, 2003), (2) Origin and migration of the deep crustal fluids (*e.g.* Fehn and Snyder 2005), (3) Oil field brines and coal-bed methane dating (*e.g.* Fehn *et al.*, 1990; Snyder *et al.*, 2003; Snyder and Fabryka-Martin 2007) and (4) Sediment subduction and recycling of marine sediments (Martin *et al.*, 1993; Snyder and Fehn., 2002; Lu *et al.*, 2008). A potential inconvenient in the application of this isotopic system is the recent release of anthropogenic radioisotope from nuclear era, which has increased the  $^{129}\text{I}$  concentration in most surface reservoirs (Moran *et al.*, 1999; Snyder and Fehn, 2004).

The Atacama region, located in the western margin of northern Chile, provides a unique opportunity to study iodine (halogen) cycling in natural waters. This region hosts the driest desert on Earth and is the world's premier iodine production province. In Chapters IV and V, iodine concentration and I-129 isotopic data in rocks, sediments and nitrate soils were reported, pointing to an "old" iodine source in these deposits related to groundwater flow, which has played an unforeseen role in the transport and precipitation of iodine, and probably other components in the region. Despite these recent advances, little is known about the sources, distribution and accumulation of iodine in natural waters from Atacama.



The purpose of this study is to determine the natural and anthropogenic origin of iodine in waters from Atacama and to contribute to the understanding of the  $^{129}\text{I}$  sources and the environmental distribution of this radioisotope in northern Chile. To achieve this purpose, we characterize the chemical and isotopic signature of iodine in natural waters. The following discussions comprise a systematic analysis of iodine, chlorine and bromine concentrations, and  $^{129}\text{I}/\text{I}$  isotopic ratios of selected water samples, including seawater, rainwater, rivers, salt-lakes, and cold and thermal spring waters. By coupling new iodine and other halogen concentration data with  $^{129}\text{I}/\text{I}$  isotopic ratios we show that iodine, as well as in rocks, sediments and soils, is significantly enriched in most natural waters, and its origin can be related to multiple natural and anthropogenic sources.

### **VI.3 Climatic and hydrological setting**

The Atacama Desert of northern Chile is one of the driest environments on Earth and makes up much of the hyperarid margin of western South America (Fig. VI.1). It is located between the central Andes and the Pacific Ocean, in the western margin of northern Chile ( $18^{\circ}$ - $26^{\circ}\text{S}$ ). Many authors have been attributed the current extreme hyperaridity of the Atacama Desert to three major factors (e.g., Houston and Hartley, 2003): (1) subtropical atmospheric subsidence; (2) the coastal temperature inversion related to the upwelling caused by the cold Humboldt current, which prevents precipitation in the coastal regions; and (3) the rain-shadow effect caused by the high altitude of the Andean Cordillera, which prevents the progress of humid air masses from the Atlantic Ocean. Thus, the hyperarid core of the Atacama Desert receives less than 2 mm/yr, and occasional rainfalls occur only once every decade (Houston and Hartley, 2003; Garreaud *et al.*, 2010). Despite the absence of precipitation, the western margin of the Atacama Desert receives consistent moisture in the form of coastal fog or sea spray from the Pacific Ocean, at elevations between 300 and 1000 m.a.s.l. (Rundel *et al.*, 1991). Along the eastern margin of the Atacama Desert, at the base of the Andes ( $\sim 2500$  m), precipitation is  $> 20$  mm/yr, and grades to a semiarid desert between 2700 to 3000 m.a.s.l. Occasional precipitation events in the central Atacama Desert generally result from Pacific air masses that migrate northward from the westerly precipitation well. On the other hand, precipitation in the eastern margin of the Atacama Desert reaches 20 mm/yr at the base of the Andes ( $\sim 2500$  m), which is associated with the South American Summer Monsoon, causing rain fall between December and March (e.g., Garreaud and Aceituno, 2001).

The precipitation pattern previously described is the main control of the hydrology in the region. Due to the extreme hyperaridity of the Atacama Desert, an almost exclusively endorheic drainage system has been developed. The only river in the study area with perennial stream is the Loa River, which flows from the Andes across the desert to the ocean (Fig. VI.1). Thus, the main source of water is precipitation in the High Andes (recharge areas), originating a base flow that goes from northeast to southwest (Magaritz *et al.*, 1990; Aravena *et al.*, 1995). Groundwater is frequently stored in aquifers that are

part of a sedimentary sequence, which was deposited during the Neogene and the Quaternary (Magaritz *et al.*, 1990). Discharge occurs as fracture flow through the volcanic units situated at the foothills of the Andes and in the Atacama Desert, generally in *salar*s located at the terminus of the groundwater flow system (Magaritz *et al.*, 1990; Aravena *et al.*, 1999).

## VI.4 Sampling materials

Water samples were collected in an area of ~100,000 square kilometers, including waters from the Pacific Ocean to the high Andes (Fig. VI.1). These samples are representative of the different iodine-bearing geochemical reservoirs in Atacama, and include: seawater, groundwater from the Central Depression; cold and thermal spring water from Precordillera, and the Puchuldiza and El Tatio geothermal fields, both located in the Western Cordillera; fresh water from surface streams in the Central Depression and Western Cordillera; and rainwater in the High Andes. Groundwater samples were taken from wells in the Central Depression, below nitrate iodine-rich deposits, salt lake ("*salar*"). Temperature, conductivity and pH were measured in situ and particulate matter was removed using 0.45  $\mu\text{m}$  filter. At each location 250 ml of water were collected for concentration measurements and 1000 ml for isotopic determinations. Dissolved chlorine concentrations were determined by ion chromatography at Universidad de Chile in Santiago (5% error, 1  $\sigma$ ). The total iodine and bromine content was determined using inductively-coupled plasma mass spectrometry (3% error, 1  $\sigma$ ) at Gakushuin University in Tokyo, water samples were diluted 200-5000 times and tetramethyl ammonium hydroxide (1%) and  $\text{Na}_2\text{SO}_3$  (100 ppm) were added to avoid loss of iodine from the solution.

Extraction of iodine and preparation of silver iodide (AgI) targets for accelerator mass spectrometry (AMS) determinations followed previously established methods (Fehn *et al.*, 1992), *i.e.*, extraction into carbon tetrachloride ( $\text{CCl}_4$ ) followed by back extraction using sodium bisulfite ( $\text{NaHSO}_3$ ) or hydroxylamine hydrochloride ( $\text{NH}_2\text{OH}\cdot\text{HCl}$ ). Finally, approximately 1 mg of iodine was precipitated as AgI targets. The AMS measurements were performed at Prime Lab, Purdue University (Indiana), following established procedures (Sharma *et al.*, 2000). Due to the small size of the targets, the results have larger error margins than typical for AMS determinations (5-10%). Uncertainties in samples where carrier was added reflect errors in isotopic determinations of the carrier material as well as of the actual samples.

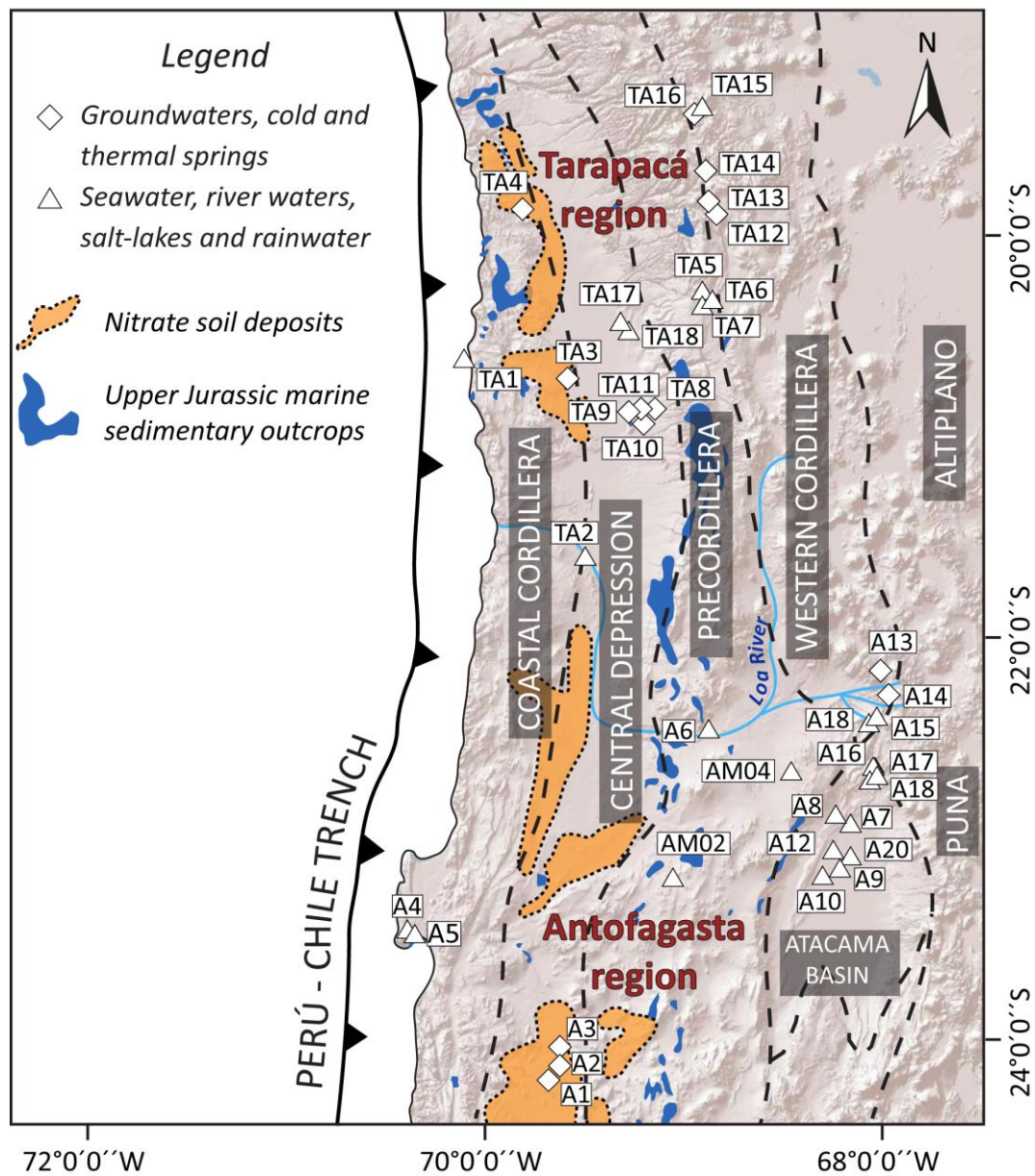


Figure VI.1. Map of the studied area showing the main morphological units and the distribution of samples.

## VI.5 Results

The water samples analyzed in this study complement the reported data in Chapters IV and V. We measured iodine, bromine and chlorine concentrations of 18 water samples from the Tarapacá and 17 from Antofagasta region. Also, we determine  $^{129}\text{I}/\text{I}$  ratios for 20 samples. Results for concentrations, as well as for  $^{129}\text{I}/\text{I}$  ratios, are listed in Table VI.1. Of a total of 35 samples, 3 correspond to seawater from the South Pacific Ocean, 4 are groundwater from the Central Depression, 8 are cold spring water from the Precordillera, 7 correspond to cold and thermal springs from the Western Cordillera (from El Tatio and Puchuldiza geothermal fields), 5 samples were taken from salt lakes, 7 samples were taken from rivers and lakes, and one sample correspond to rainwater in the Western Cordillera.

Iodine concentrations range between 0.35  $\mu\text{M}$  and 26  $\mu\text{M}$  in Tarapacá and between 0.25  $\mu\text{M}$  and 48  $\mu\text{M}$  in Antofagasta. The highest concentrations of iodine were measured in groundwater below the nitrate ore deposits with values between 0.5  $\mu\text{M}$  and 48  $\mu\text{M}$ , averaging  $\sim 12$   $\mu\text{M}$ . These high iodine concentrations are followed by water samples from the Puchuldiza ( $\sim 21$   $\mu\text{M}$ ) and El Tatio ( $\sim 7$   $\mu\text{M}$ ) geothermal fields in the Western Cordillera. Spring waters from the Precordillera present values between  $\sim 1$  and 12  $\mu\text{M}$  (averaging  $\sim 5$   $\mu\text{M}$ ). Finally, the lowest iodine contents were measured in seawater, surface waters and waters from salt lakes ("*salars*") with concentrations from 0,25 to 8  $\mu\text{M}$ , with an average of  $\sim 0,7$   $\mu\text{M}$ .

Chlorine concentrations of samples range from 0.61 mM to 69.21 mM in Tarapacá region and from 1.43 mM to 202.58 mM in Antofagasta region (Table VI.1). Finally, bromine concentrations vary from 1.28  $\mu\text{M}$  to 45.68  $\mu\text{M}$  in Tarapacá and from 1.66  $\mu\text{M}$  to 87.38  $\mu\text{M}$  in Antofagasta. These ranges of values exclude water samples expose to high evaporation rates and sample with evidence of dissolution of the bedrock. The measured halogen concentrations for meteoric water and seawater in two regions present very similar values, in the case of meteoric water halogen concentrations average Cl = 0.08 mM, I = 0.30  $\mu\text{M}$  and Br = 0.44  $\mu\text{M}$ , while in seawater the values average Cl = 549 mM, I = 0.40  $\mu\text{M}$  and Br = 610  $\mu\text{M}$ .

Concentrations of radiogenic iodine and  $^{129}\text{I}/\text{I}$  isotopic ratio measurements in 13 water samples from Tarapacá and 8 samples from Antofagasta are reported in Table VI.1. Figure VI.2 shows the isotopic ratios for each liquid reservoir in Atacama. A significant number of samples have  $^{129}\text{I}/\text{I}$  ratios substantially above the pre-anthropogenic threshold value of  $1500 \times 10^{-15}$  (Fehn *et al.*, 2007a), indicating the likely presence of anthropogenic  $^{129}\text{I}$ .

Table VI.1. Analytical results of halogen concentrations and <sup>129</sup>I/I ratios in water samples

Sample	Type	Location		pH*	T* (°C)*	EC (μS/cm)*	I(μM)*	Br (μM)	Cl (mM)	<sup>129</sup> I/I (10 <sup>-15</sup> at-at <sup>-1</sup> )	1σ (10 <sup>-15</sup> at-at <sup>-1</sup> )	<sup>129</sup> I (10 <sup>7</sup> at/L)
		Latitude (°S)	Longitude (°W)									
Tarapaca												
TA1	Seawater	20° 39' 36"	70° 11' 06"	8.1	17.2	ND	0.37	594.86	543.83	ND		
TA2	River	21° 37' 31"	69° 33' 17"	7.7	17.9	5870	1.56	19.76	ND	803.45	179.62	0.08
TA4	Groundwater	19° 53' 05"	69° 51' 54"	7.5	31.7	2780	7.25	8.18	11.84	9417.13	2319.71	4.11
TA5	Salt lake	20° 18' 23"	68° 52' 33"	6.1	14.5	8600	7.99	126.66	292.61	268.89	33.61	0.13
TA6	Salt lake	20° 18' 23"	68° 52' 33"	ND	ND	ND	1.00	5.72	8.80	ND		
TA7	Spring	20° 18' 32"	68° 52' 21"	6.7	15.6	940	0.35	3.98	7.68	ND		
TA8	Spring	20° 57' 50"	69° 10' 23"	7.3	22.1	2290	3.85	15.28	21.13	4742.53	911.62	1.10
TA9	Spring	20° 57' 50"	69° 10' 23"	7.4	22.1	2240	10.36	26.28	32.30	1551.97	334.48	0.97
TA10	Spring	20° 57' 50"	69° 10' 23"	7.3	21.8	2250	12.00	29.61	42.27	ND		
TA11	Spring	20° 55' 45"	69° 05' 48"	8.1	14.4	1950	3.76	13.91	18.69	14461.37	2345.45	3.28
TA12	Geothermal	19° 24' 38"	68° 58' 17"	8.4	19.2	3800	18.35	48.34	766.87	2148.90	947.14	2.37
TA13	Geothermal	19° 24' 51"	68° 57' 45"	6.8	50.0	4300	15.23	44.14	725.17	4570.49	1299.96	4.19
TA14	Geothermal	19° 24' 44"	68° 57' 33"	8.0	84.0	4600	26.24	45.68	69.21	2851.72	1298.04	4.51
TA15	River	19° 40' 49"	69° 10' 53"	7.9	16.5	390	0.36	2.98	1.20	12483.82	5021.79	0.27
TA16	Geothermal	19° 40' 59"	69° 10' 36"	8.4	40.0	450	0.54	1.89	1.53	ND		
TA17	Spring	20° 29' 14"	69° 19' 06"	8.2	30.3	170	1.25	1.28	0.61	1015.52	266.71	0.08
TA18	Spring	20° 29' 14"	69° 19' 06"	8.5	10.0	ND	2.29	2.26	1.65	ND		
TA25	Geothermal	19° 24' 30"	68° 57' 25"	8.1	33.0	ND	15.88	55.60	74.74	313.92	58.30	0.30
Antofagasta												
A1	Groundwater	24° 10' 31"	69° 52' 07"	7.2	22.8	1570	48.12	20.02	3.22	217.00**	15.00	0.63
A4	Seawater	23° 28' 10"	70° 30' 46"	7.8	16.8	ND	0.40	610.34	548.32	9982.27	2127.67	0.24
A5	Seawater	22° 28' 35"	68° 54' 51"	7.9	16.5	ND	0.44	623.15	554.74	11971.56	2626.68	0.32
A6	River	22° 55' 20"	68° 09' 59"	7.8	15.3	7235	0.93	10.32	61.33	2728.54	720.19	0.15
A7	Groundwater	22° 53' 25"	68° 12' 50"	6.4	28.6	3670	2.64	14.91	26.35	ND		
A9	Salt lake	23° 03' 32"	68° 12' 49"	7.8	16.0	ND	6.18	108.77	831.86	8471.03	1058.88	3.15
A10	Groundwater	23° 03' 32"	68° 12' 49"	ND	ND	ND	0.46	6.85	38.15	ND		
A12	Salt lake	23° 07' 40"	68° 14' 39"	7.0	23.5	ND	0.25	2.09	29.34	ND		
A13	Geothermal	22° 19' 48"	68° 00' 36"	6.8	81.0	ND	7.92	87.38	202.58	2081.52	429.20	0.99
A14	Geothermal	22° 24' 24"	68° 00' 41"	6.4	85.5	ND	6.29	60.18	145.32	ND		
A15	Lake	22° 25' 58"	68° 02' 57"	7.7	16.9	1020	0.51	2.61	3.86	ND		
A16	Spring	22° 43' 12"	68° 02' 37"	ND	ND	ND	1.78	8.40	1.43	ND		
A17	River	22° 46' 09"	68° 04' 07"	8.4	11.0	2240	1.49	9.89	20.16	ND		
A18	Lake	22° 25' 58"	68° 02' 57"	7.7	13.9	1360	0.37	1.88	3.80	ND		
A19	River	22° 46' 09"	68° 04' 07"	8.8	20.2	2120	1.51	8.30	15.90	ND		
A20	Salt lake	23° 03' 54"	68° 12' 52"	8.2	19.7	ND	3.59	100.23	7262.06	1301.14	162.64	0.28
AM-02	Rainwater	22° 25' 59"	68° 02' 57"	7.7	ND	1180	0.29	0.47	0.10	93721.56	6383.51	2.82

ND: Not determined.

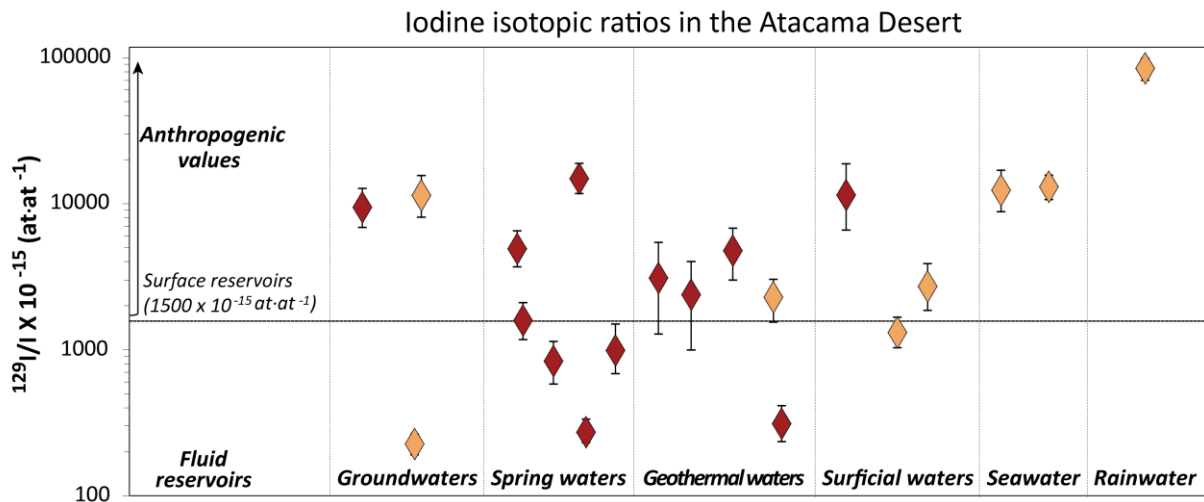


Figure VI.2. Iodine isotopic ratios ( $^{129}\text{I}/\text{I}$ ) of fluid samples from the Atacama Desert. Most of the  $^{129}\text{I}/\text{I}$  ratios are above  $1500 \times 10^{-15}$  (initial isotopic ratio of surface reservoirs; Fehn *et al.*, 2007a). Detailed information about samples is presented in Table VI.1.

## VI.6 Discussion

### VI.6.1 Halogen concentrations

Most of the iodine concentration values in the studied samples are elevated compared to natural iodine reservoirs. For example, freshwater and rainwater from Atacama have iodine concentrations one order of magnitude above the crustal average, while groundwater present concentrations in the same order of magnitude of fluids related to organic material (Fehn *et al.*, 2007b). Iodine enrichment in Atacama has also been reported in nitrate soils, supergene enrichment zones of copper deposits and Mesozoic shales (Chapters IV, V). Thus, rocks, soils, sediments and natural waters from Atacama present enrichment of iodine, which can be caused by the presence of an enriched source and/or due to a later concentration process. In order to identify which of these factors is predominant in the region, we use halogen diagrams between chlorine and the other two halogens (Figs. VI.3, VI.4). Water samples exposed to high evaporation rates and/or with evidence of dissolution of the bedrock were not considered for this analysis.

Chlorine, the most conservative halogen, is biophilically and petrologically incompatible (You and Gieskes, 2001). Lower Cl concentrations in deep fluids from seawater values are explained by freshening due to water of meteoric and/or diagenetic origin (*e.g.* Kastner *et al.*, 1991; Brown *et al.*, 2001). Thus, Cl preserves best the mixing behavior of the fluids between paleo-seawater and fresh waters. Assuming that all the chlorine is of seawater origin (*i.e.*, Cl = 549 mM, Table VI.1) and diluted by fresh water, initial iodine and bromine concentrations representatives of the primitive endmembers can

then be estimated using regression lines in the halogen diagrams (Tomaru *et al.*, 2007, 2009).

Iodine concentrations were plotted versus chlorine concentrations (Fig. VI.3), where two trends can be distinguished. These trends are distinctly different for each region; samples from Tarapacá follow the higher trend line, while samples from Antofagasta follow the lower trend line. Iodine concentrations of the initial fluids were estimated for each region resulting in two different endmembers with iodine concentrations of  $\sim 150 \mu\text{M}$  in Tarapacá ( $I/\text{Cl} = 0.34 \times 10^{-3}$ ) and  $\sim 20$  in Antofagasta ( $I/\text{Cl} = 0.04 \times 10^{-3}$ ). These estimated values are much higher than that of seawater ( $0.4 \mu\text{M}$  in the studied area; black star in Fig. VI.3), but are different in one order of magnitude between themselves. Due to the high iodine concentration estimated for the initial fluids, we suggest that these correspond to organic-rich fluids.

Regression lines in Figure VI.3 indicate mixing processes between the organic-rich fluids and fresh waters. In both cases, the extrapolation of each group of samples intersects the x-axis ( $I = 0 \mu\text{M}$ ) at  $\text{Cl} = 0 \text{ mM}$ , which indicates that these fluids are more efficiently diluted by a low Cl-low I fluid, such as meteoric water (white star in Fig. VI.3), than seawater.

A similar diagram from bromine versus chlorine concentrations is shown in Figure VI.4, but in this case no level of bromine enrichment is observed in Tarapacá or Antofagasta regions compared to seawater. The diagram shows two different trends that represent mixing between the initial fluids and meteoric water (white star in Fig. VI.4). Similar to iodine, we calculated bromine concentrations of the initial fluids for Tarapacá and Antofagasta resulting in  $\sim 380 \mu\text{M}$  ( $\text{Br}/\text{Cl} = 0.41 \times 10^{-3}$ ) and  $\sim 225 \mu\text{M}$  ( $\text{Br}/\text{Cl} = 0.67 \times 10^{-3}$ ), respectively. These values are in the same order of magnitude indicating a slight difference between two groups; both calculated values are lower than the seawater value (black star in Fig. VI.4), and higher than the meteoric water.

Halogen diagrams also show an important difference between iodine and bromine concentrations, a comparison between  $I/\text{Cl}$  and  $\text{Br}/\text{Cl}$  ratios (Fig. VI.5) and the calculated initial concentrations indicate that the variation observed between fluids is mainly associated with iodine concentrations. While the  $I/\text{Cl}$  ratios vary over more than four orders of magnitude between the two regions,  $\text{Br}/\text{Cl}$  ratios vary in only two orders of magnitude (with the exception of one sample, Fig. VI.5). The highest  $I/\text{Cl}$  ratios occur in the samples from Tarapacá reflecting major iodine enrichment in this region respect to samples from Antofagasta. The difference between ratios suggests that iodine has a substantially distinctive geochemical history compared to the chlorine and bromine. Because iodine has the strongest affinity to organic material of the three halogens, the variation between initial estimated concentrations probably reflects the existence of an organic-rich source, which is essential to obtain the current iodine enrichment in fluids from Atacama. Without this source a concentration process is not capable to concentrate preferentially iodine over other halogens.

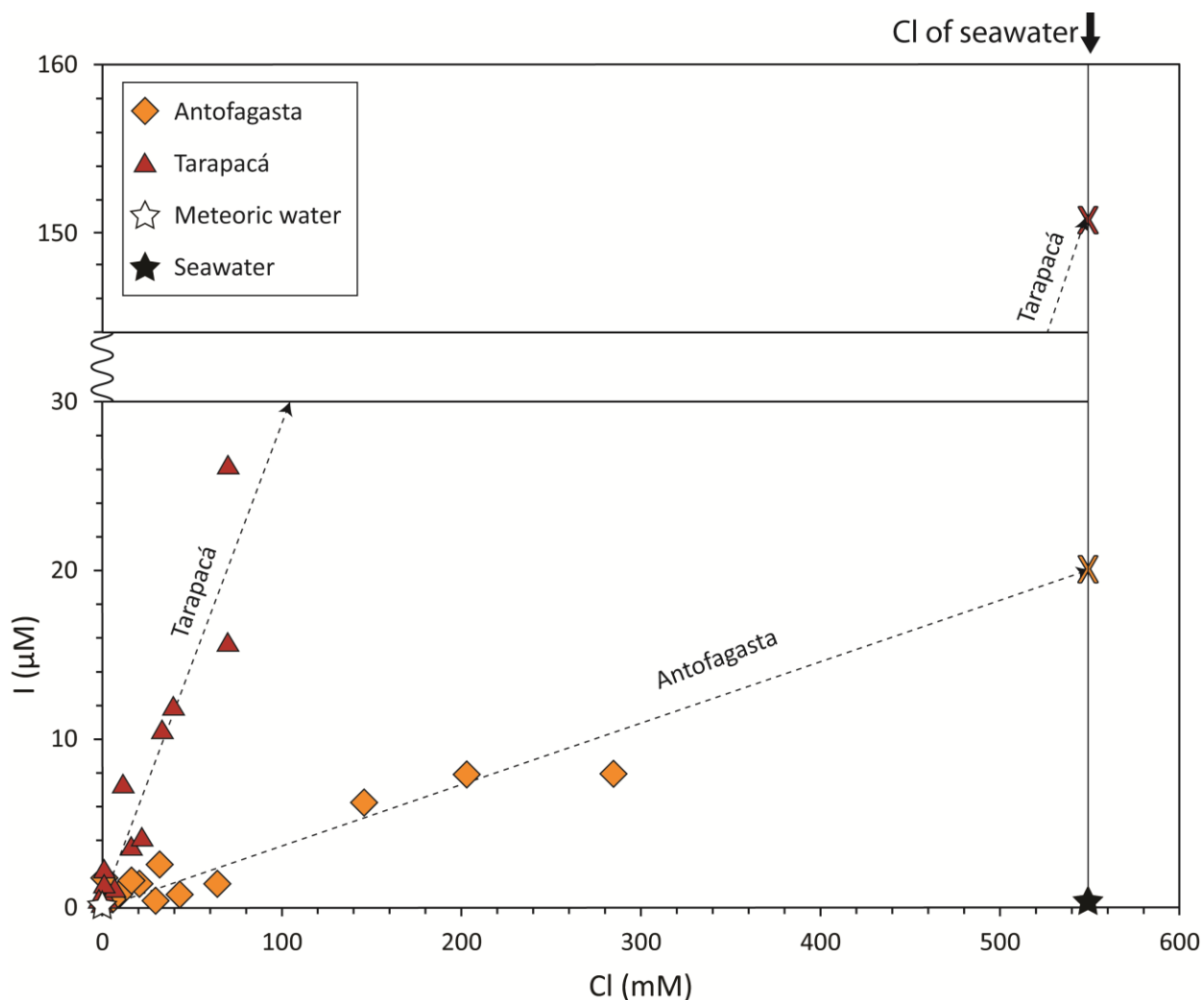


Figure VI.3. Iodine vs. chlorine concentrations of fluids from the Atacama Desert. Segmented regression lines indicate mixing of meteoric water with enriched iodine fluids. The “X” symbols at the right ends of these lines indicate the initial iodine concentration: 150  $\mu\text{M}$  for Tarapacá fluids and 20  $\mu\text{M}$  for Antofagasta fluids.

As mentioned early, the estimated initial iodine concentrations for each region are different in one order of magnitude; this difference indicates that the mixing processes occur from the Cordillera to the sea. Possible causes of this are: (1) The existence of two organic-rich sources, (2) Differences in the organic content in only one organic source, and (3) Differences in the remobilization or transport processes. Based on previous data reported in Chapters IV and V the organic source of iodine would correspond to pore water stored in Jurassic marine sedimentary sequences and/or deep and old groundwater that has strongly-interacted with such rocks over a protracted period, which mainly extend along the Precordillera from Tarapacá and Antofagasta regions. The Jurassic sequences are the only source with considerable organic content to explain the high levels of iodine enrichment. Moreover, these sequences do not present important variation in the facies or extension (Marinovic et al., 1995; Vicente, 2006; Oliveros et al., 2012). Thus, we suggest that the difference between initial iodine concentrations would be more related to



a process (e.g., remobilization, transport) rather than variations in the initial organic content of the source.

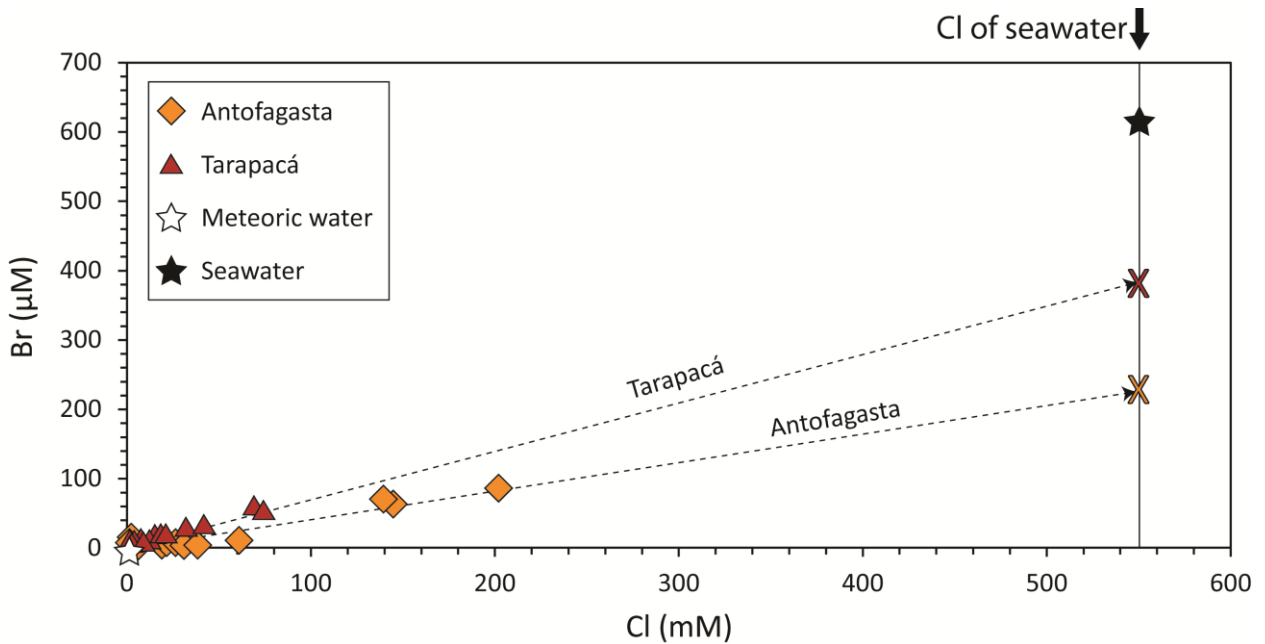


Figure VI.4. Bromine vs. chlorine concentrations of fluids from the Atacama Desert. Segmented regression lines indicate mixing of meteoric water with enriched iodine fluids. The “X” symbols at the right ends of these lines indicate the initial bromine concentration: 380  $\mu\text{M}$  for Tarapacá fluids and 225  $\mu\text{M}$  for Antofagasta fluids.

This analysis suggests the presence of an “old” iodine component in natural waters from Atacama, which is related to organic-rich fluid. Based on previously reported data (Chapters IV, V), iodine would be leached from Jurassic sequences, and then transported westwards by groundwater flow. Halogen diagrams also indicate dilution of the organic-rich fluid with meteoric water, which, due to the hyperarid conditions in Atacama, probably corresponds to rainwater in the High Andes. On the other hand, this meteoric water interacts with geothermal and hydrothermal fluids associated with the magmatic arc (e.g. Giggenbach, 1978; Snyder and Fehn, 2002). Thus, groundwater flow is composed by variable contributions from: (i) meteoric/surficial inputs and (ii) magmatic waters; which then interact with the organic formations.

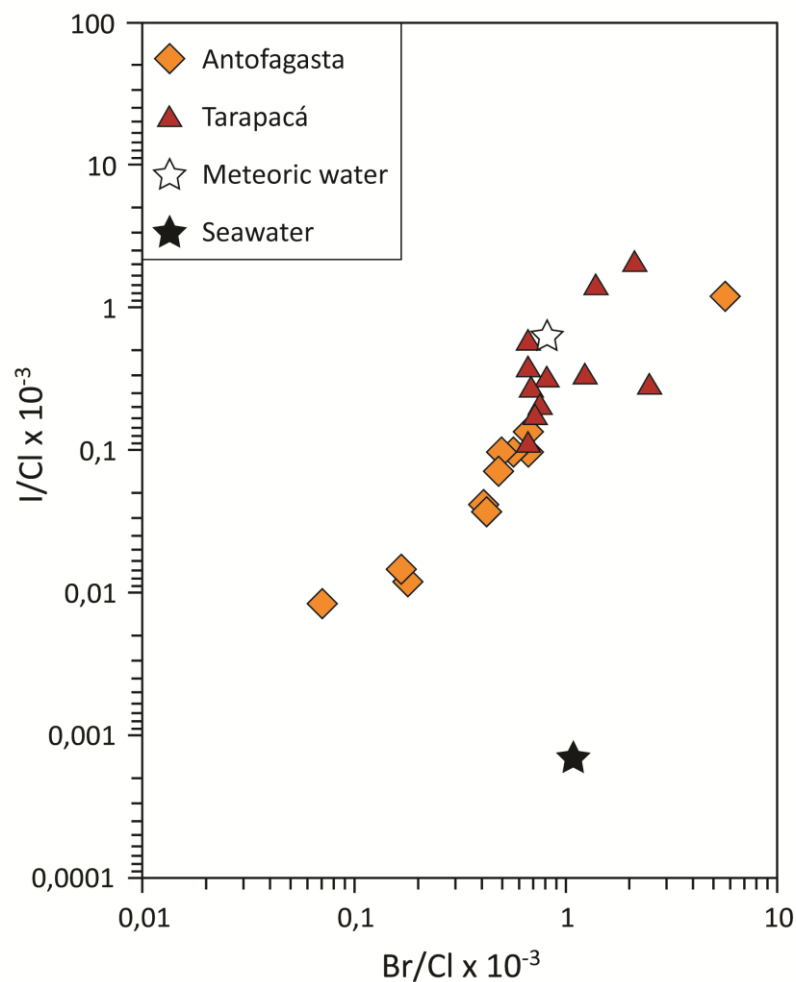


Figure VI.5. I/Cl vs. Br/Cl diagram. Seawater (black star) and meteoric (rain) water (white star) are shown in the diagram.

## VI.6.2 $^{129}\text{I}$ concentrations and $^{129}\text{I}/\text{I}$ isotopic ratios

Results of  $^{129}\text{I}$  concentrations and  $^{129}\text{I}/\text{I}$  isotopic ratios in Tarapacá and Antofagasta regions as a function of latitude are shown in Figure VI.6, these values are compared to the mean natural and anthropogenic limits of the system and worldwide data on shallow seawater (<3 m), river water, lake water, snowmelt, and rainfall (data compiled by Snyder *et al.*, 2010). As mentioned earlier, an important number of samples have ratios of one to two orders of magnitude above the pre-anthropogenic value of  $1500 \times 10^{-15}$  (Fig. VI.2).

Potential sources for anthropogenic iodine include: (1) Nuclear weapon tests, where  $^{129}\text{I}$  was released to the atmosphere, where the main period of testing occurred from the late 1940s to the 1960s (UNSCEAR, 2008). Some important test sites correspond to Novaya Zemlya in the Arctic Ocean (URSS), Bikini atoll (USA) and Mururoa atoll (France) in the central Pacific Ocean. (2) Nuclear fuel reprocessing plants in the Northern Hemisphere, where reprocessing facilities Sellafield (U.K.); and La Hague (France) are the main contributors to the European  $^{129}\text{I}$  releases (Reithmeier *et al.*, 2006). (3) Nuclear

accidents, for example, the explosion of the Chernobyl reactor in 1986 (Michel et al., 2005) and Fukushima accident during March 2011 (Muramatsu et al., 2015).

Because virtual absence of any history of nearby releases from nuclear activity in South America, the isotopic ratios measured in natural waters from Atacama are most likely related to transport and/or removal processes of anthropogenic iodine from the original source. Fehn and Snyder (2000) propose that the most likely sources of anthropogenic  $^{129}\text{I}$  in the Southern Hemisphere are releases from reprocessing plants located in the Northern Hemisphere. However, most samples studied there are from Australia and New Zealand. On the other hand, Reithmeier *et al.* (2010), through model predictions and measured  $^{129}\text{I}$  concentrations, suggest that the fallout from the atmospheric weapons tests is the dominant source of  $^{129}\text{I}$  on the Southern Hemisphere and the contribution to the present  $^{129}\text{I}$  deposition fluxes by the gaseous releases from reprocessing facilities on the Northern Hemisphere is still very low. Recently, Negri *et al.* (2013) report  $^{129}\text{I}/\text{I}$  isotopic ratios in surface and seawater samples from Argentina, also associating the measured values to levels related to nuclear weapon tests.

In our study area,  $^{129}\text{I}$  concentrations have values above nuclear testing, but below the modern average limit (Fig. VI.6A). Although the data presented here generally show  $^{129}\text{I}$  concentrations lower than values measured in freshwater and shallow seawater from Europe, a significant number of samples present roughly similar values to the  $^{129}\text{I}$  concentrations reported in North America (Fig. VI.6A). In addition, it is noteworthy to mention that  $^{129}\text{I}$  concentrations in Atacama are higher than values measured in rivers and lakes from Argentina (Negri *et al.*, 2013), where the latter do not exceed the nuclear testing limit (Fig. VI.6A).

On the other hand, most of the  $^{129}\text{I}/\text{I}$  ratios are above the pre-anthropogenic background, but unlike the  $^{129}\text{I}$  concentrations, the isotopic ratios are below nuclear testing and are significantly lower than isotopic ratios reported in the Northern Hemisphere (*e.g.*, Rucklidge *et al.*, 1994, Rao and Fehn, 1999, Snyder *et al.*, 2010). Moreover,  $^{129}\text{I}/\text{I}$  ratios from Argentina (Negri *et al.*, 2013) are slightly higher than values reported here. Therefore, a clear difference is observed between the  $^{129}\text{I}$  concentrations and  $^{129}\text{I}/\text{I}$  isotopic ratios when these values are compared to worldwide data.

We suggest that the strong iodine enrichment in natural waters from Atacama is the cause of the difference between  $^{129}\text{I}$  concentrations and  $^{129}\text{I}/\text{I}$  ratios, thus, the high  $^{129}\text{I}$  concentrations would be affected by this enrichment, reaching values of the same order of magnitude than in the Northern Hemisphere. However, when  $^{129}\text{I}$  concentrations are normalized with respect to the local background (*i.e.*, total iodine concentration), the effect of iodine enrichment is suppressed. A comparison between Figures VI.6A and VI.6B shows that, except for the values from Atacama, all other worldwide data remain in the same  $^{129}\text{I}$  anthropogenic origin range. Therefore, surface waters from Tarapacá and Antofagasta regions would be reflecting the unique iodine enrichment in the Atacama

Desert. According to this analysis, in order to trace the sources of natural and anthropogenic iodine, isotopic ratios must be used in Atacama region.

Our data show that most of the  $^{129}\text{I}/\text{I}$  ratios have similar levels to the values associated with nuclear tests (Fig. VI.6B), suggesting that the  $^{129}\text{I}$  released to the atmosphere during these tests is founded in natural waters from Atacama. The nearest site where nuclear tests were carried out corresponds to Mururoa atoll in the central Pacific Ocean. Given the geographical location of the Atacama Desert, we propose that this anthropogenic iodine would have been transported eastwards from the central Pacific to the South American margin through the prevailing westerlies winds developed at subtropical latitudes (Garreaud, 2009)., where marine currents and wind patterns are responsible for the rapid redistribution of this radioisotope across the Pacific Ocean.

On the other hand, a small but significant group of samples have with lower ratios ( $<1500 \times 10^{-15}$ ) is observed. In addition, there is one sample from Antofagasta with an isotopic ratio remarkably higher ( $^{129}\text{I}/\text{I} = \sim 93700 \times 10^{-15}$ ), comparable to ratios from the Northern Hemisphere. Precisely, this sample corresponds to rainwater in the High Andes, which is associated to the Atlantic Ocean, suggesting the presence of more than one anthropogenic source in Atacama. In the next section we evaluate the participation of atmospheric and deep sources of iodine in the Atacama region.

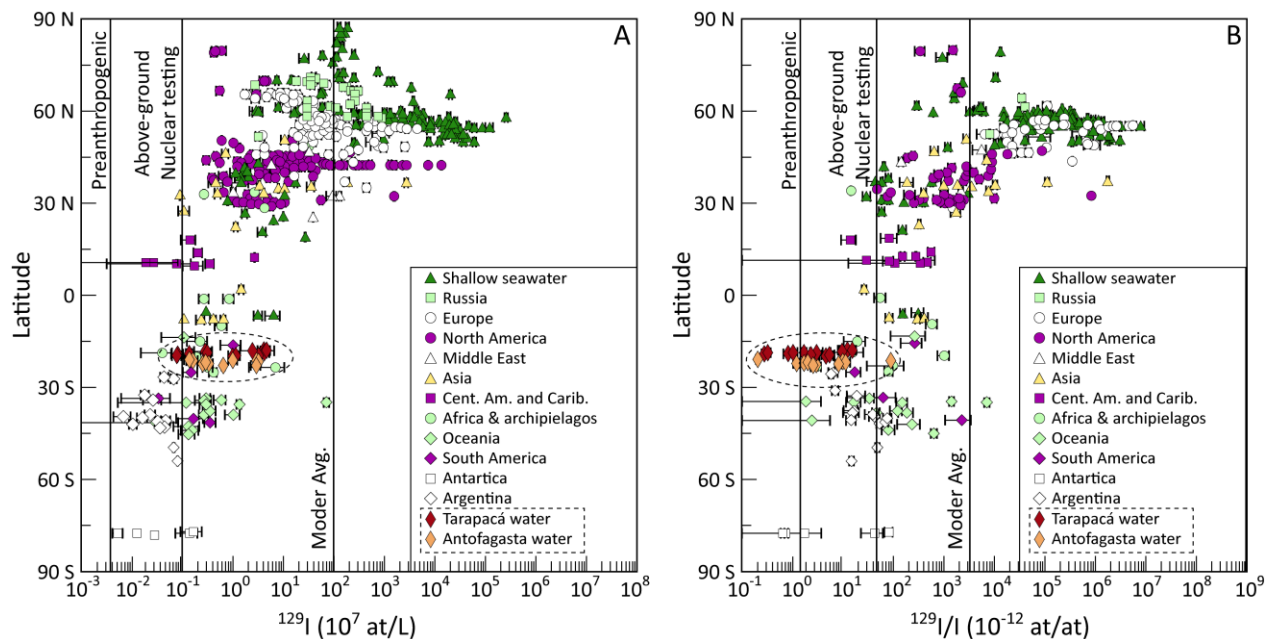


Figure VI.6. (A) Concentrations of  $^{129}\text{I}$  as a function of latitude show values in Tarapacá and Antofagasta are comparable with data from the Northern Hemisphere. (B) Ratios of  $^{129}\text{I}/\text{I}$  indicate difference between the Northern Hemisphere and samples from Tarapacá and Antofagasta.

### VI.6.3 Relative contributions of pre-anthropogenic vs. anthropogenic sources for iodine in Atacama waters

Summarizing the previous discussions, halogen concentration analysis indicate that the main source of total iodine is an organic-rich fluid, which is diluted by meteoric water, probably rainwaters in the High Andes, which is related to Atlantic Ocean. On the other hand, isotopic data suggest that an important source of anthropogenic  $^{129}\text{I}$  is related to an atmospheric-marine source, presumably associated with nuclear bomb tests carried out in the Pacific Ocean. However, this last component is not reflected in iodine vs. chlorine diagram (Fig. VI.3), which shows no dilution with a saline fluid (e.g., seawater). A possible explanation for this phenomenon is that the transport mechanism for “marine” iodine would be associated with coastal fog, where aerosol particles are generated, and then incorporated by sea spray (Böhlke et al., 1997; Rech et al., 2003; Michalski et al., 2004; Ewing et al., 2006; Ewing et al., 2007; Ewing et al., 2008). Supporting this hypothesis is the fact that the ratio of I/Cl in sea spray is much greater than the same ratio in seawater, owing to efficient injection of seawater iodine to the atmosphere (Rahn et al., 1976). In agreement with this observation several authors have reported solutes (i.e., sulfates, chlorides) deposition through coastal fog, which can penetrate up to 50-90 km in land, depending of the elevation of the Coastal Cordillera (Rech et al., 2002, 2006; Michalski et al., 2004; Ewing et al., 2006; 2007).

In addition to the meteoric and anthropogenic influence of  $^{129}\text{I}$  in most waters in the studied region, the lower  $^{129}\text{I}/\text{I}$  ratios ( $< 1500 \times 10^{-15}$ ) and halogen chemistry are reflective of mixing between meteoric waters and deeper and older organic-rich fluid source for iodine (see section VI.6.1). In order to determine the effect of atmospheric  $^{129}\text{I}$  on isotopic ratios, as well as the effect of other potential (deeper) sources for iodine, we plotted the  $^{129}\text{I}/\text{I}$  isotopic ratios versus the reciprocal of iodine concentration (Fig. VI.7). As a first approximation, we propose a fluid mixing model between the organic-rich (“initial”) fluid (IF), which represent the highest estimated iodine concentration of the organic-rich fluid found through I/Cl diagram (i.e.,  $150 \mu\text{M}$ ) and the lowest isotopic ratio ( $217 \times 10^{-15}$ , sample A1), and three surficial endmembers: (1) Anthropogenic meteoric water (AMW, white star in Fig. VI.7); (2) Anthropogenic seawater (ASW, black star in Fig. VI.7); and (3) Pre-anthropogenic meteoric water (PMW, grey star in Fig. VI.7). The composition of all endmembers is shown in the Figure VI.7, where AMW and ASW correspond to rainwater and seawater collected samples (AM02 and A4, respectively), and the PMW endmember was defined with the surficial isotopic ratio ( $1500 \times 10^{-15}$ ) and the same measured iodine concentration in AM02 (Table VI.1).

Most of the samples fall into the area bounded by IF-AMW and IF-PMW mixing lines, suggesting that observed isotopic ratios correspond to a mixing between the organic-rich fluid and one or more surficial endmembers. Moreover, the samples with the lowest isotopic ratios (from 217 to  $1015 \times 10^{-15}$ ) show a strong correlation with the IF-PMW

mixing line, discarding the influence of an anthropogenic contaminated source in these samples. On the other hand, another group of samples are slightly shifted from the IF-AMW mixing line; we attribute this displacement to evaporation processes, which can increase the total iodine concentration without affect the isotopic ratios. Among these, previous works have been suggested significant evaporation of groundwater related to soil anomalies in the Central Depression (Leybourne and Cameron, 2006; Leybourne et al., 2013). Some samples that show this behavior correspond to thermal springs from Puchuldiza and El Tatio geothermal fields. Both sites are located 4200 m above sea level, where extreme climatic conditions related to high evaporation rates occur (Nicolau *et al.*, 2014).

Thus, mixing diagram analysis confirms the presence of more than one anthropogenic source in the Atacama Desert, these surficial components correspond to (1) coastal fog from the Pacific Ocean ( $^{129}\text{I}/\text{I} = \sim 12000 \times 10^{-15}$ ) and (2) rainwater related to an Atlantic Ocean signature of iodine ( $^{129}\text{I}/\text{I} = \sim 93700 \times 10^{-15}$ ).

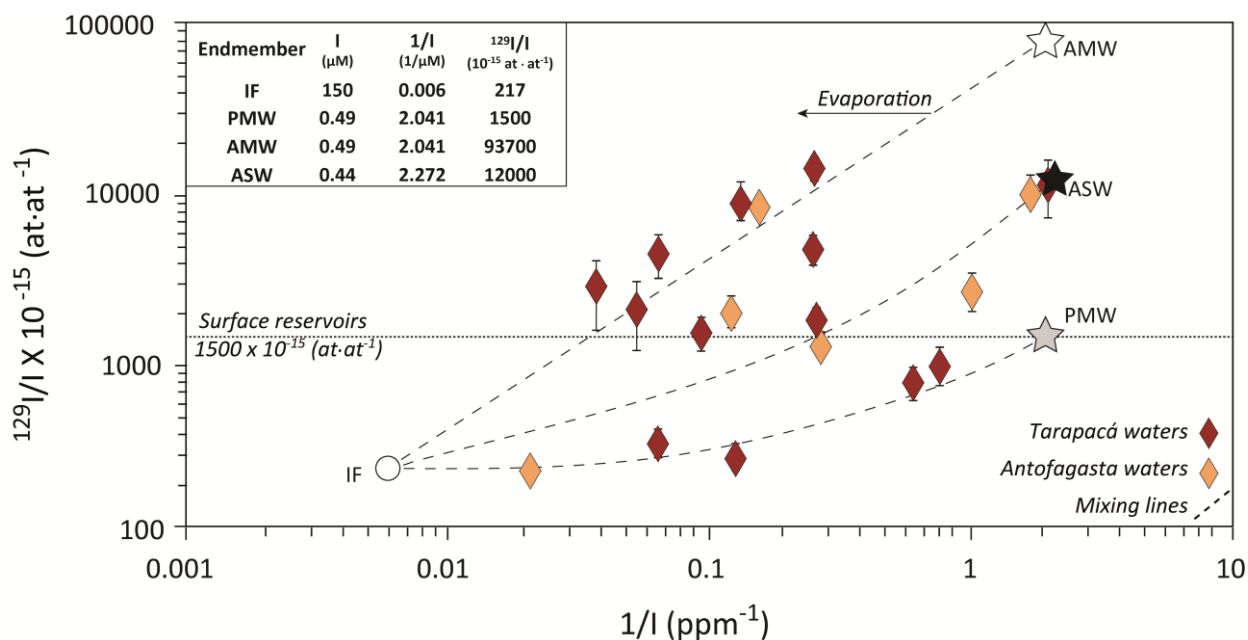


Figure VI.7.  $^{129}\text{I}/\text{I}$  ratios vs. reciprocal iodine concentrations. Mixing lines are indicated between the primitive endmember (IF) and surficial endmembers: AMW (anthropogenic meteoric water), ASW (anthropogenic seawater) and PMW (pre-anthropogenic meteoric water).

#### VI.6.4 Hydrological cycle of iodine in Atacama

Based on the previous analysis, we propose a modern hydrological cycle for iodine, which is capable to explain the high occurrence of iodine in fluid surficial reservoirs (*i.e.*, freshwater, rainwater and groundwater). The model presented here implies the presence of previous discussed sources of iodine and consequently different isotopic signatures, besides is consistent with the climate and hydrology of this region (Fig. VI.8). Our model

involves evaporation of iodine from salt-lakes and thermal springs located in the High Andes (Houston and Hartley, 2003; Nicolau *et al.*, 2014). The evaporation process increases the available iodine in the atmosphere, causing the subsequent pre-enrichment detected in rainwaters from Atacama. Thus, the iodine introduced in the atmosphere is re-deposited in surficial reservoirs by rain-out or dry deposition of aerosol (Baker *et al.*, 2001).

Precipitation in the High Andes is associated with the South American Summer Monsoon, where air masses spill over the central Andes and generate precipitation at elevations above ~2800 m a.s.l. (Houston and Hartley, 2003), being the Atlantic Ocean the main source of precipitation in this region. Therefore, iodine isotopic signature in rainwater reflects a mixing between the local reservoirs (*i.e.*, groundwater with variable inputs of meteoric and volcanic fluids) and iodine coming from the Atlantic Ocean, (*i.e.*, anthropogenic  $^{129}\text{I}$  released from reprocessing plants located in the Northern Hemisphere), which then is redistributed by marine currents and wind patterns to the Southern Hemisphere. This hypothesis is supported by estimated residence times of groundwater in some aquifers from Atacama, which ranges between 18 and 44 a (Houston 2007, 2009). Therefore, groundwater flow would have enough time to transport iodine with the anthropogenic signal of Northern Hemisphere.

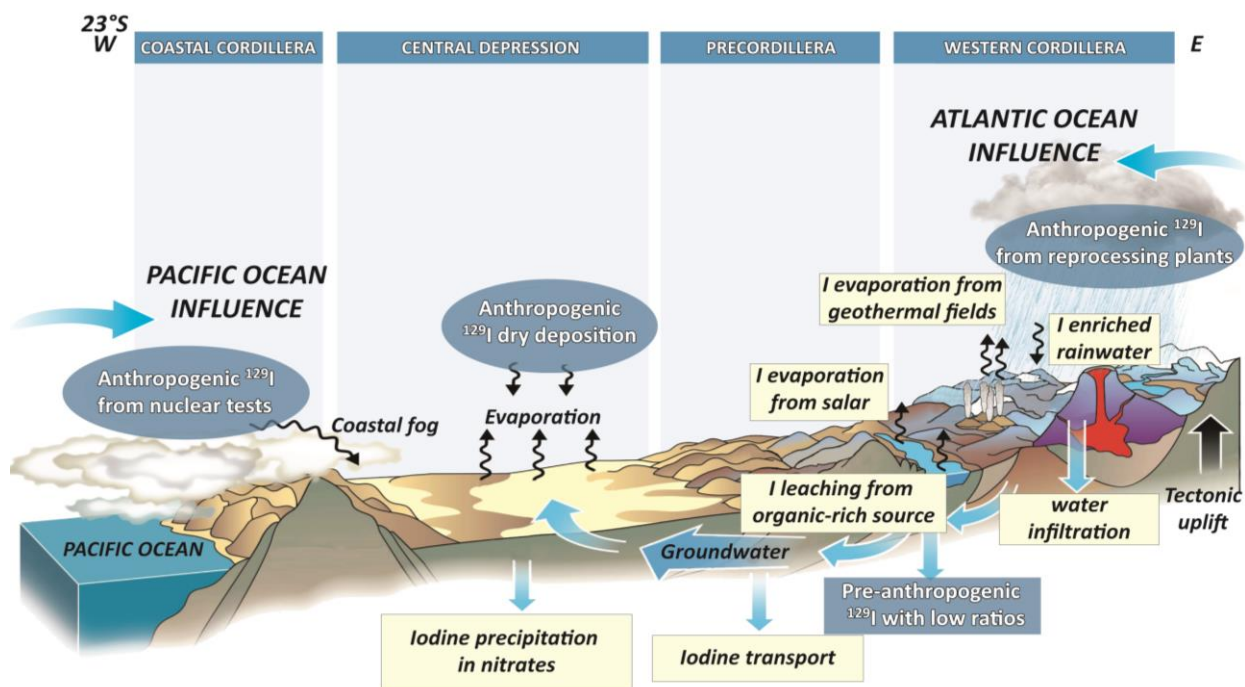


Figure VI.8. Hydrological cycle of natural and anthropogenic iodine in the Atacama Desert.

Precipitation over the High Andes generates surface water runoff and infiltration to aquifers (Magaritz *et al.*, 1990). Thus, iodine is transported westwards along with other chemical species by groundwater flow, which leach “old” iodine from sedimentary rocks located in the Precordillera (Chapter V). The isotopic signature of iodine stored in these sequences reflects an old component related to the Jurassic marine basin. Then, groundwater continues westwards to the Central Depression, where iodine precipitation is favored by an “impermeable” barrier effect at the eastern slope of the Coastal Cordillera.

The Atacama Desert also receives iodine inputs from the west, specifically from the Pacific Ocean. Contribution from the ocean occurs through coastal fog input, which advances up to 90 km eastward (Rech *et al.*, 2002, 2006; Michalski *et al.*, 2004). This component also reflects an anthropogenic signal related to anthropogenic  $^{129}\text{I}$  that comes from nuclear weapon tests carried out in the Pacific Ocean. This signature has elevated isotopic ratios (from 1500 to  $\sim 15000 \times 10^{-15}$ , Snyder *et al.*, 2010; Fig. VI.6), but are lower than values from the Atlantic Ocean source, where anthropogenic  $^{129}\text{I}$  is released by reprocessing nuclear plants in the Northern Hemisphere. The residence time of iodine in the atmosphere (about 14 days; Rahn *et al.*, 1976), the mode of transport and its high level of reactivity in atmosphere allow its widespread dispersal.

## VI.7 Conclusions

This work is the first one to characterize the chemical and isotopic signature of iodine in natural waters from Chile. Based on iodine and other halogens concentration analysis, we show that natural waters in the Atacama Desert are enriched in iodine relative to seawater, but not in the other halogens. In particular, estimated iodine concentrations of the “initial” organic-rich fluids in Tarapacá and Antofagasta regions are three and two orders of magnitude, respectively, higher than those of seawater. Although I/Cl ratios in Tarapacá and Antofagasta are different in one order of magnitude, they are all derived from the same organic-rich source. Halogens diagrams also indicate dilution of the organic-rich fluid with meteoric water. Due to the current hyperarid conditions in Atacama, which result nearly absent precipitation, rainwater in the High Andes is the more probable meteoric endmember.

The  $^{129}\text{I}/\text{I}$  ratios show influence of different natural and anthropogenic sources of iodine. The results indicate that iodine in natural waters derives from one organic-rich (deep) source (*i.e.*, marine Jurassic rocks in the Precordillera and Central Depression) and three atmospheric sources. While samples with lowest isotopic ratios reflect mixing between the organic-rich fluid and pre-anthropogenic meteoric water, samples with higher values indicate the input of two anthropogenic sources. Thus, there is an older contaminated source related to  $^{129}\text{I}$  released during nuclear weapon tests carried out in the central Pacific Ocean, where  $^{129}\text{I}$  was transported eastwards and then deposited inland as marine fog. In addition, there is a younger contaminated source, which is



associated with  $^{129}\text{I}$  released from nuclear fuel reprocessing plants in the Northern Hemisphere. Both sources point to a rapid redistribution of this radioisotope on a global scale. The presence of unique climatic, geologic and hydrological factors allows the development of a local hydrological iodine cycle in Atacama where natural and anthropogenic sources converge.

## VI.8 References

- Amilibia A., Sàbat F., McClay K. R., Muñoz J. A., Roca E. and Chong G. (2008) The role of inherited tectono-sedimentary architecture in the development of the central Andean mountain belt: Insights from the Cordillera de Domeyko. *J. Struct. Geol.* **30** (12), 1520-1539.
- Aravena R. (1995) Isotope hydrology and geochemistry of northern Chile groundwaters. *Bull. Inst. Fr. Etudes Andin.* **24**, 495–503.
- Aravena R., Suzuki O., Peña H., Pollastri A., Fuenzalida H. and Grilli A. (1999) Isotopic composition and origin of the precipitation in northern Chile. *Appl. Geochem.* **14**, 411-422.
- Böhlke J. K., Ericksen G. E. and Revesz K. (1997) Stable isotope evidence for an atmospheric origin of desert nitrate deposits in northern Chile and southern California, USA. *Chem. Geol.* **136**, 135-152.
- Broecker W. S. and Peng T. H. (1982) Tracers in the Sea. Palisades, NY: Eldigio. pp. 690.
- Brown K. M., Saffer D. M. and Bekins B. A. (2001) Smectite diagenesis, pore-water freshening, and fluid flow at the toe of the Nankai wedge. *Earth Planet. Sci. Lett.* **194**, 97-109.
- Carson B., Suess E. and Strasser J.C. (1990) Fluid flow and mass flux determinations at vent sites on the Cascadia margin accretionary prism. *J. Geophys. Res. B, Solid Earth Planets* **95**, 8891-8897.
- Cortés J. (2000) Hoja Palestina, Región de Antofagasta. Servicio Nacional de Geología y Minería, Mapas Geológicos 19, 1 mapa escala 1:100.000. Santiago.
- Edmonds H. N., Zhou Z. Q., Raisbeck G. M., Yiou F., Kilius L. and Edmond J. M. (2001) Distribution and behaviour of anthropogenic  $^{129}\text{I}$  in water masses ventilating the North Atlantic Ocean. *J. Geophys. Res.* **106**, 6881-6894.
- Ericksen G. E. (1981) Geology and origin of the Chilean nitrate deposits. *U.S. Geol. Surv. Prof. Paper* 1188-B. Unites States Government Printing Office, Washington.

- Ewing S. A., Sutter B., Amundson R., Owen J., Nishiizumi K., Sharp W., Cliff S. S., Perry K., Dietrich W. E. and McKay C. P. (2006) A threshold in soil formation at Earth's arid-hyperarid transition. *Geochim. Cosmochim. Acta* **70**, 5293-5322.
- Ewing S. A., Michalski G., Thiemens M., Quinn R. C., Macalady J. L., Kohl S., Wankel S.D., Kendall C., Mackay C. P. and Amundson, R. (2007) Rainfall limit of the N cycle on Earth. *Global Biogeoche. Cy.* **21**, GB3009.
- Ewing S. A., Yang W., DePaolo D. J., Michalski G., Kendall C., Stewart B., Thiemans M. and Amundson, R. (2008) Non-biological fractionation of Ca isotopes in soils of the Atacama Desert, Chile. *Geochim. Cosmochim. Acta* **72**, 1096-1110.
- Fabryka-Martin J., Bentley H., Elmore D. y Airey P. L. (1985) Natural I-129 as an environmental tracer. *Geochim. Cosmochim. Acta* **49**, 337-347.
- Fabryka-Martin J., Whittemore D. O., Davis S. N., Kubik P. W. and Sharma P. (1991) Geochemistry of halogens in the Milk River aquifer, Alberta, Canada. *Appl. Geochem.* **6**, 447-464.
- Fehn U., Tullai-Fitzpatrick S., Teng R. T. D., Gove H. E., Kubik P. W., Sharma P. and Elmore D. (1990) Dating of oil field brines using  $^{129}\text{I}$ . *Nucl. Instrum. Methods Phys. Res.* **52**, 446-50.
- Fehn U., Peters E. K., Tullai-Fitzpatrick S., Kubik P. W., Sharma P., Teng R. T. D., Gove H. E. and Elmore D. (1992)  $^{129}\text{I}$  and  $^{36}\text{Cl}$  concentrations in waters of the eastern Clear Lake area, California: residence times and source ages of hydrothermal fluids. *Geochim. Cosmochim. Acta* **56**, 2069-2079.
- Fehn U. and Snyder G. (2000)  $^{129}\text{I}$  in the Southern Hemisphere: Global redistribution of an anthropogenic isotope. *Nucl. Instr. Meth. Phys. Res.* **172**, 366-371.
- Fehn U., Snyder G. T. and Egeberg P. K. (2000) Dating of pore waters with  $^{129}\text{I}$ . Relevance for the origin of marine gas hydrates. *Science* **289**, 2332-2335.
- Fehn U. and Snyder G. T. (2003) Origin of iodine and  $^{129}\text{I}$  in volcanic and geothermal fluids from the North Island of New Zealand: implications for subduction zone processes. *Soc. Econ. Geol. Spec. Publ.* **10**, 159-170.
- Fehn U. and Snyder G. T. (2005) Residence times and source ages of deep crustal fluids: interpretation of  $^{129}\text{I}$  and  $^{36}\text{Cl}$  results from the KTB-VB drill site, Germany. *Geofl.* **5**, 42-51.
- Fehn U. Moran J. E., Snyder G. T. and Muramatsu Y. (2007a) The initial  $^{129}\text{I}/\text{I}$  ratio and the presence of "old" iodine in continental margins. *Nucl. Instrum. Meth. B.* **259**, 496-502.

- Fehn U., Snyder G. T. and Muramatsu Y. (2007b) Iodine as a tracer of organic material:  $^{129}\text{I}$  results from gas hydrate systems and fore arc fluids. *J. Geochem. Explor.* **95**, 66-80.
- Frohlich K, Ivanovich M, Hendry M. J., Andrews J. N, Davis S. N., Drimmie, R. J., Fabryka-Martin, J., Florkowski, T., Fritz, P., Lehmann, B., Loosli, H. H. and Nolte, E. (1991) Application of isotopic methods to dating of very old groundwaters: Milk River aquifer, Alberta, Canada. *Appl. Geochem.* **6**, 465-72.
- Garreaud R. and Aceituno P. (2001) Interannual rainfall variability over the South American Altiplano, *J. Climate* **14**, 2779-2789.
- Garreaud R. (2009) The Andes climate and weather. *Adv. Geosci.* **22**, 3-11.
- Garreaud R., Molina A. and Farias M. (2010) Andean Uplift and Atacama Hyperaridity: A Climate Modeling Perspective. *Earth Planet. Sc. Lett.* **292**, 39-50.
- Giggenbach W. (1978) The isotope composition of waters from the El Tatio geothermal field, northern Chile. *Geochim. Cosmochim. Acta* **42**, 979-988.
- Hervé M., Marinovic N., Mpodozis C. and Smoje I. (1991) Mapa Geológico de la Hoja Sierra de Varas (1:100.000), Región de Antofagasta. Servicio Nacional de Geología y Minería, Documento de Trabajo 2.
- Hartley A. J. and Chong G. (2002) Late Pliocene age for the Atacama Desert: Implications for the desertification of western South America. *Geology* **30**, 43-46.
- Houston J. and Hartley A.J. (2003) The Central Andean west-slope rainshadow and its potential contribution to the origin of hyper-aridity in the Atacama Desert. *Int. J. Climatol.* **23**, 1453-1464.
- Houston J. (2007) Recharge to groundwater in the Turi Basin, northern Chile: An evaluation based on tritium and chloride mass balance techniques. *J. Hydrol.* **334**, 534-544.
- Houston J. (2009) A recharge model for high altitude, arid, Andean aquifers. *Hydrol. Process.* **23**, 2383-2393.
- Kastner M., Elderfield H. and Martin J. B. (1991) Fluids in convergent margins: what do we know about their composition, origin, role in diagenesis and importance for oceanic chemical fluxes. *Philos. Trans. Roy. Soc. Lond.* **335**, 243-259.
- Kastner M., Elderfield H., Jenkins W. J., Gieskes J. M., Gamo T. (1993) Geochemical and isotopic evidence for fluid flow in the western Nankai subduction zone, Japan. *Proc. Ocean Drill. Program Sci. Results* **131**, 397-413.

- Leybourne M. I. and Cameron E. M. (2006) Composition of soils and ground waters at the Pampa del Tamarugal, Chile: Anatomy of a fossil geochemical anomaly derived from a distant porphyry copper deposit. *Econ. Geol.* **101**, 1569-1581.
- Leybourne M. I., Cameron E. M., Reich M., Palacios C., Faure K. and Johannesson, K. H. (2013) Stable isotopic composition of soil calcite (O, C) and gypsum (S) overlying Cu deposits in the Atacama Desert, Chile: implications for mineral exploration, salt sources, and paleoenvironmental reconstruction. *Appl. Geochem.* **29**, 55-72
- Lu Z., Hensen C., Fehn U. and Wallmann K. (2008) Halogen and  $^{129}\text{I}$  systematics in gas hydrate fields at the northern Cascadia margin (IODP Expedition 311): insights from numerical modeling. *Geochem. Geophys. Geosyst.* **9**, Q10006.
- Magaritz M., Aravena R., Peña H., Suzuki O. and Grilli A. (1990) Source of Ground Water in the Deserts of northern Chile: Evidence of Deep Circulation of Ground Water from the Andes. *Ground Water* **28**, 513-517.
- Marinovic N., Smoje, L. MaksaeV, V., Hervé M. and Mpodozis C. (1995) Hoja Aguas Blancas, Región de Antofagasta. Servicio Nacional de Geología y Minería, Carta Geológica de Chile, No. **70**, pp. 150.
- Marinovic N. and García M. (1999) Hoja Pampa Unión, Región de Antofagasta. Servicio Nacional de Geología y Minería, Mapas Geológicos 9 (escala 1:100.000), Santiago
- Martin J. B., Gieskes J. M., Torres M. and Kastner M. (1993) Bromine and iodine in Peru margin sediments and pore fluids: implications for fluid origins. *Geochim. Cosmochim. Acta* **57**, 4377-4389.
- Martin S., Ducker R. and Fort M. (1995) A laboratory study of frost flower growth on the surface of young sea ice. *J. Geophys. Res.* **100**, 7027-7036.
- McDonough W. F. and Sun S. S. (1995) The composition of the Earth, *Chem. Geol.* **120**, 223-253.
- Michalski G., Bohlke J. K. and Thiemens M. (2004) Long term atmospheric deposition as the source of nitrate and other salts in the Atacama Desert, Chile: New evidence from mass independent oxygen isotopic compositions. *Geochim. Cosmochim. Acta* **68**, 4023-4038.
- Michel R., Handl J., Ernst T., Botsch W., Szidat S., Schmidt A., Jakob D., Beltz D., Romantschuk L. D., Synal H. A., Schnabel C. and López-Gutiérrez J. M. (2005) Iodine-129 in soils from Northern Ukraine and the retrospective dosimetry of the iodine-131 exposure after the Chernobyl accident. *Sci Total Environ.* **340**, 35-55.

- Moran J. E., Fehn U. and Hanor J. S. (1995) Determination of source ages and migration patterns of brines from the U.S. Gulf Coast basin using  $^{129}\text{I}$ . *Geochim. Cosmochim. Acta* **59**, 5055-5069.
- Moran J. E., Fehn U. and Teng R. T. D. (1998) Variations in  $^{129}\text{I}/^{127}\text{I}$  ratios in recent marine sediments: Evidence for a fossil organic component. *Chem. Geol.* **152**, 193-203.
- Moran J. E., Oktay S. D., Santschi P. H., and Schink D. R. (1999a) Atmospheric dispersal of  $^{129}\text{I}$  from European nuclear fuel reprocessing facilities. *Environ. Sci. Technol.* **33**, 2536-2542.
- Moran, J. E., Oktay S. D., Santschi P. H., and Schink D. R., Fehn U., and Snyder G. (1999b) World-wide redistribution of  $^{129}\text{I}$  from nuclear fuel reprocessing facilities: Results from meteoric, river, and seawater tracer studies. IAEA-SM-354/101.
- Mpodozis C., Arriagada C., Basso M., Roperch P., Cobbold P. and Reich M. (2005) Late Mesozoic to Paleogene stratigraphy of the Salar de Atacama Basin, Antofagasta, Northern Chile: Implications for the tectonic evolution of the Central Andes. *Tectonophysics* **399**, 125-154.
- Muramatsu Y. and Wedepohl K. H. (1998) The distribution of iodine in the earth's crust. *Chem. Geol.* **147**, 201-216.
- Muramatsu Y., Matsuzaki H., Toyama C. and Ohno T. (2015) Analysis of  $^{129}\text{I}$  in the soils of Fukushima Prefecture: preliminary reconstruction of  $^{131}\text{I}$  deposition related to the accident at Fukushima Daiichi Nuclear Power Plant (FDNPP). *J. Environ. Radioactiv.* **139**, 344-350.
- Negri A., Fernandez J., Wallner A., Arazi A., Fifield L. and Tims S. (2013)  $^{129}\text{I}$  Dispersion in Argentina: Concentrations in fresh and marine water and deposition fluences in Patagonia. *Environ. Sci. Technol.* **47**, 9693-9688.
- Nicolau C., Reich M. and Lynne B. (2014) Physico-chemical and environmental controls on siliceous sinter formation at the high-altitude El Tatio geothermal field, Chile. *J. Volcanol. Geotherm. Res.* **282**, 60-76.
- Oliveros V., Labbé M., Rossel P., Charrier R. and Encinas A. (2012) Late Jurassic paleogeographic evolution of the Andean back-arc basin: New constrains from the Lagunillas Formation, northern Chile ( $27^{\circ}30'-28^{\circ}30'S$ ). *J. S. Am. Earth Sci.* **37**, 25-40.
- Rahn K. A., Borys R. D. and Duce R. A. (1976) Tropospheric halogen gases: Inorganic and organic components. *Science* **192** 549-550.
- Raisbeck G. M., Yiou F., Zhou Z. Q. and Kilius L. R. (1995)  $^{129}\text{I}$  from nuclear fuel reprocessing facilities at Sellafield (UK) and La Hague (France): potential as an oceanographic tracer. *J. Mar. Syst.* **6**, 561-570.

- Rao U. and Fehn U. (1999) Sources and reservoirs of anthropogenic  $^{129}\text{I}$  in western New York. *Geochim. Cosmochim. Acta* **63**, 1927-1938.
- Rech J. A., Quade J. and Betancourt J. L. (2002) Late Quaternary paleohydrology of the central Atacama Desert (lat 22 degrees-24 degrees S), Chile. *Geol. Soc. Am. Bull.* **114**, 334–348.
- Rech J. A., Quade J. and Hart W.S. (2003) Isotopic evidence for the source of Ca and S in soul gypsum, anhydrite and calcite in the Atacama Desert, Chile. *Geochim. Cosmochim. Acta* **67**, 575-586.
- Rech J. A., Currie B. S., Michalski G. and Cowan, A. M. (2006) Neogene climate change and uplift in the Atacama Desert, Chile. *Geology* **34**, 761-764.
- Reithmeier H., Lazarev V., Rühm W., Schwikowski M., Gäggeler H. W. and Nolte E. (2006) Estimate of European  $^{129}\text{I}$  releases supported by  $^{129}\text{I}$  analysis in an Alpine Ice Core. *Environ. Sci. Technol.* **40(19)**, 5891-5896.
- Reithmeier H., Lazarev V., Rühm W. and Nolte E. (2010) Anthropogenic  $^{129}\text{I}$  in the atmosphere: Overview over major sources, transport processes and deposition pattern. *Sci. Total Environ.* **408**, 5052-5064.
- Rucklidge J., Kilius L. and Fuge R. (1994)  $^{129}\text{I}$  in moss down-wind from the Sellafield nuclear reprocessing plant. *Nucl. Instr. Meth. Phys. Res.* **92**, 417-420.
- Rundel P. W., Dillon M. O., Palma B. Mooney H. A., Gulmon S. L. and Ehleringer J. R. (1991) The phytogeography and ecology of the coastal Atacama and Peruvian deserts. *ALISO* **13**, 1-49.
- Santschi P. H., Roberts K. A., Guo L. D. (2002) Organic mature of colloidal actinides transported in surface water environments. *Environ. Sci. Technol.* **36**, 3711-3719.
- SERNAGEOMIN (2003) Geologic map of Chile, digital version, scale 1:1000000.
- Sharma, P., Bourgeois M., Elmore D., Granger D., Lipschutz M. E., Ma X., Miller T., Mueller K., Rickey F., Simms P. and Vogt S. (2000) PRIME lab AMS performance, upgrades and research applications. *Nucl. Instr. Meth. B.* **172**, 112-123.
- Spivack A. J., Kastner M. and Ransom, B. (2002) Elemental and isotopic chloride geochemistry and fluid flow in the Nankai Trough. *Geophys. Res. Lett.* **29**, 1-4.
- Snyder G. T. and Fehn U. (2002) Origin of iodine in volcanic fluids:  $^{129}\text{I}$  results from the Central American Volcanic Arc. *Geochim. Cosmochim. Acta* **67**, 3827-3838.
- Snyder G. T, Fehn U. and Goff F. (2002) Iodine isotope ratios and halide concentrations of the Satsuma-Iwojima volcano, Japan. *Earth Planets Space* **54**, 265-273.

- Snyder G.T., Riese R.C., Franks S., Fehn U., Pelzmann W. L., Gorody A. W. and Moran J. E. (2003) Origin and history of waters associated with coalbed methane:  $^{129}\text{I}$ ,  $^{36}\text{Cl}$ , and stable isotope results from the Fruitland Formation, CO and NM. *Geochim. Cosmochim. Acta* **67**, 4529-4544.
- Snyder G. T. and Fehn U. (2004) Global distribution of  $^{129}\text{I}$  in rivers and lakes: implications for iodine cycling in surface reservoirs. *Nucl. Instr. Meth. B.* **223/224**, 579-586.
- Snyder G. T. and Fabryka-Martin J. T. (2007)  $^{129}\text{I}$  and  $^{36}\text{Cl}$  in dilute hydrocarbon waters: marine-cosmogenic, in situ, and anthropogenic sources. *Appl. Geochem.* **22**. 692-714.
- Snyder G., Aldahan A. and Possnert G. (2010) Global distribution and long-term fate of anthropogenic  $^{129}\text{I}$  in marine and surface water reservoirs. *Geochem. Geophys. Geosyst.* **11**, 1-19.
- Taran Y. M., Hedenquist J. A., Korzhinsky M. A., Tkachenko S. I. and Schmulovich K.I. (1995) Geochemistry of magmatic gases from Kudryavy Volcano, Iturup, Kuril Islands. *Geochim. Cosmochim. Acta* **59**, 1749-1761.
- Tomaru H., Ohsawa S., Amita K., Lu Z. and Fehn U. (2007) Influence of subduction zone settings on the origin of forearc fluids: Halogen concentrations and  $^{129}\text{I}/\text{I}$  ratios in waters from Kyushu, Japan. *Appl. Geochem.* **22**, 676-691.
- Tomaru H., Lu Z., Fehn U. and Muramatsu Y. (2009) Origin of hydrocarbons in the Green Tuff region of Japan:  $^{129}\text{I}$  results from oil field brines and hot springs in the Akita and Niigata basins. *Chem. Geol.* **264**, 221-31.
- UNSCEAR, United Nations Scientific Committee on the Effects of Atomic Radiation. (2008) Sources and Effects of Ionizing Radiation. Report to the General Assembly, United Nations, New York, USA.
- Vicente J. C. (2006) Dynamic Paleogeography of the Jurassic Andean Basin: pattern of regression and general considerations of main features. *Rev. Asoc. Geol. Argent.* **61**, 408-437.
- Wagner M. J. M., Dittrich-Hannen B., Synal H. A., Suter M. and Schotterer U. (1996) Increase of  $^{129}\text{I}$  in the environment. *Nucl. Instr. Meth. Phys. Res.* **113**, 490-494.
- Wong G. T. F. (1991) The marine geochemistry of iodine. *Rev. Aquatic. Sci.* **4**, 45-73.
- Yiou F., Raisbeck G. M., Christensen G. C. and Holm E. (2002) I-129/I-127, I-129/Cs-137 and I-129/Tc-99 in the Norwegian coastal current from 1980 to 1998. *J. Env. Radioact.* **60**, 61-71.
- You C. F. and Gieskes J. M. Hydrothermal alteration of hemi-pelagic sediments: experimental evaluation of geochemical processes in shallow subduction zones. *Appl. Geochem.* **16**, 1055-1066.

# Capítulo VII. Sources, sinks and long-term cycling of iodine in the hyperarid Atacama continental margin\*

## VII.1 Abstract

The Atacama region in northern Chile hosts the driest desert on Earth and is the world's premier iodine production province. The origin of iodine enrichment in Atacama is controversial and fundamentally different processes have been invoked over the years that involve marine, aeolian and more recently deep sedimentary fluid and groundwater sources. As a result of the very limited geochemical iodine data in Atacama and the western South American margin, the origin of iodine enrichment in this region still remains elusive. In this study, we present a comprehensive survey of iodine concentrations and isotopic ratios ( $^{129}\text{I}/\text{I}$ ) of different reservoirs in the Atacama Desert of northern Chile, including nitrate soils, supergene copper deposits, marine sedimentary rocks, geothermal fluids, groundwater and meteoric water. Nitrate soils along the eastern slope of the Coastal Cordillera are found to have mean iodine concentrations of at least three orders of magnitude higher than the mean crustal abundances of  $\sim 120$  ppb, with a mean concentration of  $\sim 700$  ppm. Soils above giant copper deposits in the Central Depression are also highly enriched in iodine (100's of ppm range), and Cu-iodide and iodate minerals occur in the supergene enrichment zones of some of these deposits. Further east in the Precordillera, Jurassic sedimentary shales and limestones show above-background iodine concentrations, the latter averaging  $\sim 50$  ppm in the southern portion of the study area.

The highest iodine concentrations in fluids were measured in groundwater below nitrate soils in the Coastal Range ( $\sim 3.5$ -10 ppm) and in geothermal waters (1-3 ppm) along the volcanic arc. Although highly variable, the iodine isotopic ratios ( $^{129}\text{I}/\text{I}$ ) of Jurassic marine sedimentary rocks ( $\sim 300$  to  $600 \times 10^{-15}$ ), nitrate soils ( $\sim 150$ -1500  $\times 10^{-15}$ ) and waters ( $\sim 215 \times 10^{-15}$ ) are consistently low ( $< 1500 \times 10^{-15}$ ), indicating that recent anthropogenic additions are almost negligible in most surficial and deeper reservoirs. Geochemical mixing models reveal that the measured  $^{129}\text{I}/\text{I}$  ratios in Atacama are in agreement with multiple sources of iodine that include variable contributions from old organic iodine sources (*i.e.*, marine sedimentary rocks) and younger fluids such as pore waters, geothermal fluids and meteoric waters. Our results show that the large variation observed in the iodine isotopic ratios of different reservoirs ( $^{129}\text{I}/\text{I}$  from 150 to  $1580 \times 10^{-15}$ ) is indicative of significant mixing and circulation of fluids of meteoric, sedimentary and

\*Una versión completa de este capítulo se encuentra aceptada en *Geochimica et Cosmochimica Acta*.



volcanic origin along the Chilean continental margin in the last 30 million years. We conclude that this protracted and large-scale fluid flow was driven by tectonic uplift and highly influenced by the climatic history of the Atacama Desert. The combination of such factors has played an unforeseen role in transporting and accumulating iodine and other soluble components in the Atacama region, and is evidence that elemental remobilization is a key process in the overall crustal cycle of iodine over scales of millions of years.

## VII.2 Introduction

The global distribution of iodine (I) is dominated by the marine system, in particular marine sediments, which hold about 70% of the total iodine in the crust at concentrations from 1600 to 10000  $\mu\text{M}$  (Wong, 1991; Muramatsu and Wedepohl, 1998). In contrast, seawater contains only 0.4  $\mu\text{M}$  due to extensive iodine partition into marine phytoplankton and algae, and subsequent accumulation in marine sediments (Broecker and Peng, 1982; Ullman and Aller, 1983; Ullman and Aller, 1985; Küpper *et al.*, 2008).

Although the global iodine budget and its distribution in marine settings is well constrained (Fehn *et al.*, 1986; Fehn *et al.*, 2007a), naturally elevated iodine concentrations in rocks, soils and waters are rarely reported, with iodine mineral occurrences being restricted to hyper-arid desert environments. Among these, the Atacama Desert in northern Chile hosts mineral deposits with some of the highest iodine concentrations known in continental settings (Ericksen, 1981). In Atacama, iodine is highly concentrated in the nitrate soils, a ~1 meter thick layer that covers an almost continuous 700 km long by 20 km wide area along the western margin of the Central Depression. Iodine in the nitrates exceed 3-4 orders of magnitude the average crustal concentrations and form iodate ( $\text{IO}_3^-$ ) minerals that occur along with nitrates, sulfates, chlorides and rare perchlorates and chromates (Muramatsu and Wedepohl, 1998; Ericksen, 1981; Chapter V). In addition, recent studies suggest that iodine enrichment in the region is more widespread than previously thought. For example, high iodine occurrences have been reported in copper deposits from the Coastal Range (*e.g.*, Mantos de la Luna) to the Central Depression (*e.g.*, Spence) and the Precordillera (*e.g.*, Chuquicamata and Escondida). These anomalous iodine concentrations are restricted to supergene zones and soils above copper deposits, forming fine-grained iodides and iodates that coexist with Cu-chlorides and sulfates, among other oxidized Cu phases (Jarrell, 1939; Jarrell 1944; Cameron *et al.*, 2010; Reich *et al.*, 2009a).

In the Chapter V reported  $^{129}\text{I}/\text{I}$  isotopic ratios of iodine-rich nitrate soils from Atacama ( $\sim 150 - 600 \times 10^{-15}$ ) revealing signatures similar to marine sedimentary pore waters ( $\sim 200 - 500 \times 10^{-15}$ ; Fehn *et al.*, 2007b). These surprisingly low  $^{129}\text{I}/\text{I}$  ratios are strong evidence for a non-atmospheric source for the iodine component of nitrates and point towards a significant role of groundwater and deep sedimentary fluids in the formation of iodine-bearing nitrate soils in Atacama.

Despite these recent advances, little is known about the regional setting and distribution of iodine in the Atacama Desert. In fact, a survey of previously published studies suggest that iodine enrichment is not exclusively restricted to discrete reservoirs (e.g., nitrate soils and supergene copper deposits), but is rather wide-spread in most surficial reservoirs in Atacama such as surface and ground water, spring and thermal water, and marine sedimentary rocks outcropping between the Central Depression and the Precordillera. Considering the fact that the cycling of iodine is still poorly understood in continental settings, the convergence of anomalous iodine occurrences with unique geologic, tectonic and climatic factors in Atacama offers an intriguing opportunity to investigate iodine enrichment over long timescales in an active continental margin.

In this study, we present a comprehensive survey of iodine concentrations and isotopic ratios ( $^{129}\text{I}/\text{I}$ ) of selected reservoirs in the Atacama Desert of northern Chile, including nitrate soils, supergene copper ores, sedimentary rocks, geothermal fluids, groundwater and surface water. By coupling new iodine concentration data and  $^{129}\text{I}/\text{I}$  ratios with previously published data, we show that iodine is significantly enriched in most surface reservoirs, and its origin can be related to multiple sources that include marine sedimentary rocks, geothermal/volcanic fluids and meteoric water. We also explore the role of groundwater as a transport agent in the region, and by using geochemical mixing models, we show that the iodine  $^{129}\text{I}/\text{I}$  ratios can be used not only to trace the origin of iodine, but also to constrain the timescales of groundwater circulation over scales of millions of years.

## **VII.3 Background**

### **VII.3.1 Geological setting**

The study area is located in the central Atacama region of northern Chile ( $19^{\circ}20'$  S- $24^{\circ}10'$  S), and covers an important portion of the Tarapacá and Antofagasta regions (Fig. VII.1A). The present tectonic configuration of the Chilean active margin is characterized by the subduction of the Nazca Plate beneath the South American Plate (Fig. VII.1A). This configuration was acquired after the breakup of the Farallon Plate into the Nazca and the Cocos Plates around 25 Ma ago (Pardo-Casas and Molnar, 1987). Currently, the convergence rate between Nazca and South American plates is 7.8 cm/yr in this region, and the sediment column undergoing subduction includes the entire range from the oldest sediments to sediments of recent age at the top (DeMets *et al.*, 1994; Angermann *et al.*, 1999).

The uplift history of the northern Chilean Andes has been subject of debate, with two opposing end member models: a rapid rise in elevation in the past 10 Ma (of  $\sim 2.5$  km at  $\sim 10$ -6 Ma, Garzzone *et al.*, 2008) and a slow and steady rise to present elevations since  $\sim 60$  or 40 Ma (e.g., Barnes and Ehlers, 2009; Charrier *et al.*, 2013 and references within).

However, both views are in agreement with the fact that the Central Andean Cordillera is the result of protracted shortening and thickening over the past ~50 Ma.

In the central Atacama region, four different morphostructural units are identified from west to east: Coastal Cordillera, Central Depression, Precordillera (Domeyko Range) and Western Cordillera (Fig. VII.1A). The Coastal Cordillera is mainly composed of Jurassic andesitic and Cretaceous sedimentary rocks that are intruded by Jurassic and Lower Cretaceous plutonic rocks (Coira *et al.*, 1982; Marinovic *et al.*, 1995). The Central Depression is mostly covered by Neogene alluvial fan deposits with scattered outcrops of the Jurassic – Early Cretaceous marine/continental sediments and Cretaceous volcanic units. The Precordillera is composed by some of the oldest rocks in the region that correspond to stratified volcanic and sedimentary sequences of Paleozoic to Mesozoic age, intruded by Paleozoic to Triassic and Paleocene-Eocene plutonic rocks (Hervé *et al.*, 1991). The Western Cordillera is composed mostly of Tertiary andesitic volcanic rocks (Marinovic and García, 1999; Cortes, 2000; SERNAGEOMIN, 2003). The major structural features in the area are the strike-slip Atacama Fault System (AFS), the Antofagasta-Calama Lineament (ACL) and the Domeyko Fault System (DFZ) (Fig. VII.1B).

### **VII.3.2 Climatic and hydrologic setting**

The Atacama Desert of northern Chile is the driest desert on Earth and makes up much of the hyperarid margin of western South America (Fig. VII.1B). The hyperarid core of the Atacama Desert receives virtually no precipitation, with less than 2 mm/yr (Figs. VII.1B, VII.2), and scattered rainfall events occur only once every decade (Houston and Hartley, 2003; McKay *et al.*, 2003; Garreaud *et al.*, 2010). The western margin of the Atacama Desert receives consistent moisture in the form of coastal fog or sea spray, at elevations between 300 and 1000 m a.s.l. (Rundel *et al.*, 1991). Along the eastern margin of the Atacama Desert, at the base of the Andes (~2500 m), precipitation is > 20 mm/yr, and grades to a semiarid desert between 2700 to 3000 m a.s.l. (Fig. VII.1B). Occasional precipitation events in the central Atacama Desert generally result from Pacific air masses that migrate northward from the westerly precipitation. On the other hand, precipitation in the eastern margin of the Atacama Desert is associated with the South American Summer Monsoon (roughly 80% of annual rainfall occurs during the austral summer), where air masses spill over the central Andes and generate precipitation at elevations above ~2800 m a.s.l. (Houston and Hartley., 2003), but do not cause rainfall in the central Atacama (Zhou and Lau, 1998; Rech *et al.*, 2006). Therefore, the main source of precipitation in this region is the Atlantic Ocean and most of the rain falls between December and March (Garreaud and Aceituno, 2001).

The extreme lack of precipitation is a feature that has remained stable over millions of years because of major coupled atmospheric and tectonic feedbacks (Rech et al, 2006). However, short-lived times of increased precipitation exist in paleohydrological and

pedological records (e.g., late Quaternary, Betancourt *et al.*, 2000; Ewing *et al.*, 2006; Nester *et al.*, 2011; Amundson *et al.*, 2012).

Groundwater resources in the Atacama Desert are frequently stored in aquifers that are part of sedimentary sequences that were deposited during the Neogene and the Quaternary (e.g., alluvial fan deposits), and have thicknesses of up to 900 m (Magaritz *et al.*, 1990). Although there is limited hydrologic information in the south portion of the studied area (Antofagasta region), several investigations have studied the groundwater system to the north, where the main aquifers are located in the Pampa del Tamarugal (19°30'-22°S), corresponding to a terminal basin of an endorheic drainage system (e.g., Magaritz *et al.*, 1990, Aravena *et al.*, 1995, Gayo *et al.*, 2012; Dorsaz *et al.*, 2013).

Isotopic, chemical and geological evidence support the hypothesis that a regional primary inflow to the aquifers in the hyperarid Atacama Desert occurs via groundwater associated with recharge areas located in the higher part of the Andes region (Magaritz *et al.*, 1990; Aravena, 1995; Aravena *et al.*, 1999). The most important recharge areas are located along the Western Cordillera and Sierra Moreno (Nester *et al.*, 2007; Gayo *et al.*, 2012). The recharge of the aquifers is strongly related to annual atmospheric conditions and the high topography of the Andes where annual rainfall increases from <10 mm/yr below 2,000 m to 120 mm/yr at 4,000 m elevation (Houston, 2002; Houston, 2006). Thus, precipitation over the High Andes generates surface water runoff and infiltration to aquifers, where discharge occurs as fracture flow through the volcanic units situated at the foothills of the Andes and in the Atacama Desert along the Central Depression (Magaritz *et al.*, 1990).

The hydrologic environment in Atacama has exerted strong controls on the different types of sedimentary facies deposited. In the eastern canyons, alluvial fan deposits triggered by mass wasting due to the rare storms at high elevations are dominant (Houston, 2002; Houston, 2006). On the other hand, the regional groundwater flow goes from northeast to southwest feeding aquifers in the western part of the Central Depression. Here, the water table nearly intersects with the land surface allowing the generation of salt lakes or salars (Magaritz *et al.*, 1990; Aravena *et al.*, 1999). Shallow aquifers and desert oases in the hyperarid zone have been known since pre-Colombian times, and were used by the communities surrounding nitrate mines over a century ago (Latorre *et al.*, 2013). Despite the documented presence of the near-surface water table, the influence of groundwater on the accumulation of nitrate and iodine in the caliche deposits has often been ignored in previous studies.

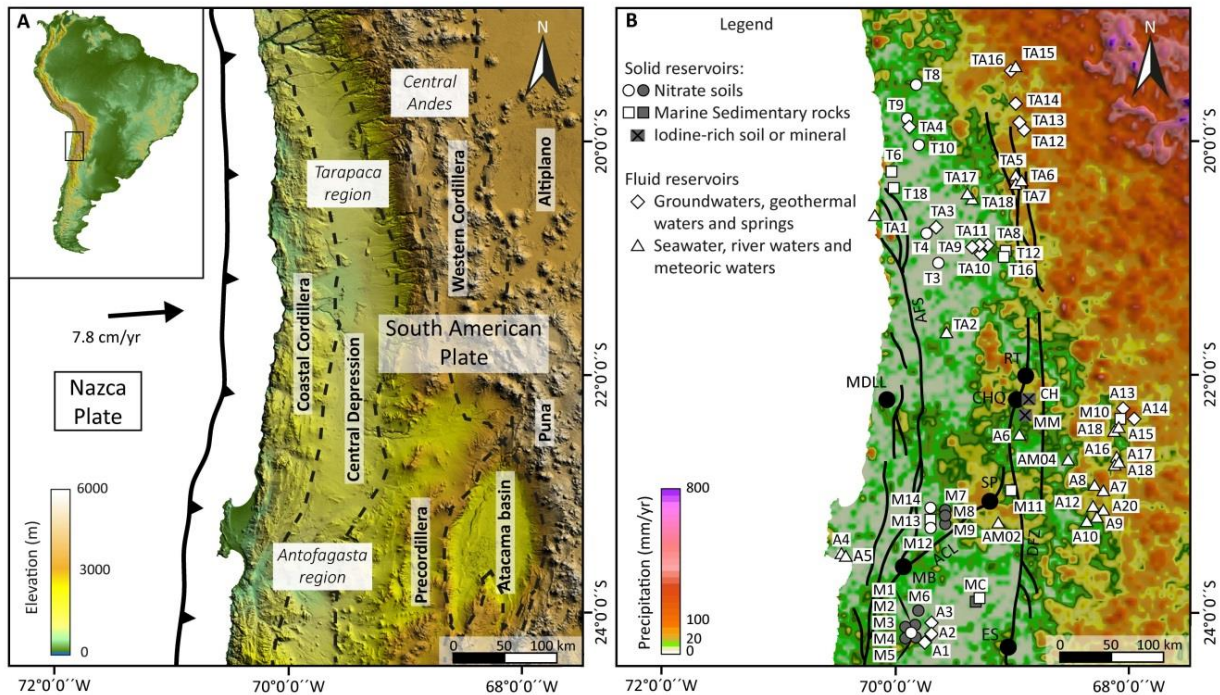


Figure VII.1. Map of the studied area: (A) Digital elevation map of northern Chile showing the main morphological units. (B) Mean-annual precipitation map of northern Chile, Puna and Altiplano, showing the distribution of sampling sites used for this study, data points in grey were sampled in previous works (Table VII.1). The major structural features shown are the Atacama Fault System (AFS), the Antofagasta-Calama Lineament (ACL) and the Domeyko Fault Zone (DFZ). Solid black circles show the location of supergene Cu deposits where high-iodine concentrations have been reported (MDLL: Mantos de la Luna, RT: Radomiro Tomic, CHQ: Chuquicamata, SP: Spence, MB: Mantos Blancos, ES: Escondida).

Currently, the water table levels in the Central Depression vary from near-surface in salars and wetlands (Rech *et al.*, 2002) to 33-55 m (below surface) at the Pampa del Tamarugal (Leybourne and Cameron, 2006a). Other studies set the water table level at 30-90 m (below surface) near the Spence copper mine in the Central Depression (Leybourne and Cameron, 2006b) and 27 m (below surface) near the Salar de Imilac in Precordillera (Quade *et al.*, 2008).

### VII.3.3 Iodine-rich nitrate soils and supergene copper deposits

The Atacama Desert is the premier source of natural iodine, which is highly concentrated in the nitrate-rich "saltpeter" soils or "caliche" deposits located between 19°S and 26°S (Fig. VII.2). These deposits are unique due to their mineralogical features and extension, and are composed of a complex mixture of nitrates (~7-15% NO<sub>3</sub>), iodates, perchlorates, chromates and even borates (Ericksen, 1981; Chong, 1994). They are significantly enriched in iodine, with concentrations in excess of 500 ppm. Virtually all the iodine in the nitrates occurs as iodate minerals such as lautarite (Ca(IO<sub>3</sub>)<sub>2</sub>), fuenzalidite

( $K_6(Na,K)_4Na_6Mg_{10}(SO_4)_{12}(IO_3)_{12}\cdot 12H_2O$ ) and hectorfloresite ( $Na_9(IO_3)(SO_4)_4$ ) (Pueyo *et al.*, 1998).

This almost continuous belt is only interrupted by salars (e.g., Salar Grande and Salar de Llamara) and the Loa River. The iodine-rich nitrate deposits have a longitudinal extension that vary from a few kilometers to up to 30 km wide, and have been geographically separated in two distinctive domains in the Tarapacá and Antofagasta regions (Fig. VII.1A). Five historic districts are recognized from north to south: Tarapacá, Tocopilla, Baquedano, Aguas Blancas and Taltal. The nitrate deposits occur within alluvial fans cementing gravels, and also interstratified as vetiform and lenticular bodies (Ewing *et al.*, 2006; Ewing *et al.*, 2007). Neogene alluvial fans along the eastern margin of Coastal Cordillera host large amounts of nitrates and display a narrow, NS-trending, ~700 km long belt with an average altitude of ~1000 m a.s.l (Fig. VII.2). Typically, nitrate rich-soils gently cover the landscape and their maximum concentrations are found near the salars, also exhibiting east-west variations in their chemistry that are a function of the distance from marine aerosol sources (Rech *et al.*, 2003; Ewing *et al.*, 2006).

Nitrate soils vary between 3 and 13 m in thickness and consist of several horizons (Ericksen, 1981): (i) chusca: surface horizon (~30 cm) of powdery gypsum and anhydrite; (ii) costra: thick horizon below the chusca that ranges between ~50 cm to 2 m, and is composed of cemented gypsum and anhydrite; (iii) caliche: corresponds to a firmly-cemented horizon below the costra that varies from 1 to 5 m in thickness, and contains nitrate and other soluble salts; (iv) conjelo: is a horizon up to 2 m thick of salt-cemented regolith; and (v) coba: a loose, unconsolidated soil. A representative iodine-rich nitrate soil profile from the Aguas Blancas mine is shown in Figure VII.5.

Several theories about the origin of nitrate deposits have been proposed since the 19th century. These hypotheses have pointed to biologic sources (Forbes, 1860; Noellner, 1867; Penrose, 1910; Gale, 1912; Brüggén, 1938), atmospheric/meteoric factors (Pissis, 1878; Singewald and Miller, 1916; Wetzel, 1924; Mueller, 1968; Ericksen 1983; Böhlke *et al.*, 1997; Michalski *et al.*, 2004; Ewing *et al.*, 2006; Ewing *et al.*, 2007; Ewing *et al.*, 2008), and volcanic inputs (Ericksen, 1961; Fiesta, 1966; Oyarzún and Oyarzún, 2007), to name a few. Even though the debate about the origin of nitrate deposits is still open, recent studies show robust evidence towards a multi-source origin for the principal components of nitrate deposits. These cover dominant atmospheric sources, including marine aerosol, for the nitrate, sulphate and calcium components (Böhlke *et al.*, 1997; Rech *et al.*, 2003; Michalski *et al.*, 2004; Ewing *et al.*, 2006; Ewing *et al.*, 2007; Ewing *et al.*, 2008). The oxygene-17 data in perchlorate present in the Atacama nitrate soils are also consistent with a natural atmospheric origin for this component (Bao and Gu, 2004). On the other hand, a groundwater source model has been proposed to explain the presence of chromate and iodate components in the nitrates (Chapter V).

Apart from nitrate deposits, iodine mineral occurrences in Atacama have been documented in the supergene zones of porphyry and Manto-type copper deposits (Fig. VII.1B). The copper-iodide marshite (CuI) and other copper-iodate minerals such as salesite [Cu(IO<sub>3</sub>)(OH)] and bellingerite [Cu<sub>3</sub>(IO<sub>3</sub>)<sub>6</sub>•2H<sub>2</sub>O] were reported to occur in the oxide zone of the giant Chuquicamata Cu deposit (Jarrell 1939; Jarrel 1944), while the silver iodide iodargyrite (AgI) was documented more recently at the Mantos de la Luna Cu-Ag deposit (Reich *et al.*, 2009a). Geochemical surveys have also shown high iodine concentrations in soils above giant Cu deposits (e.g., Spence, Chimborazo; Cameron *et al.*, 2010 and Kelley *et al.*, 2003; Fig. VII.1B), and fossil soil anomalies have been reported at the Pampa del Tamarugal (Leybourne and Cameron, 2006a). Almost all of these geochemical anomalies occur above fracture zones in the gravels that can be correlated to deeper structural features of the hypogene deposits (Cameron *et al.*, 2002). At the Spence porphyry Cu deposit, Leybourne and Cameron (2006b) have reported high iodine concentrations (>65 ppm) along with high Cu concentrations (2 ppm) in saline groundwaters. Thus, recent studies have related the occurrence of Cu-(halogen) soil anomalies to the uprise of deep and saline groundwaters that have been pumped to the surface along active faults and/or fractures during seismic events (Cameron *et al.*, 2002; Cameron *et al.*, 2007; Cameron *et al.*, 2008; Reich *et al.*, 2008; Reich *et al.*, 2009b; Leybourne *et al.*, 2013).

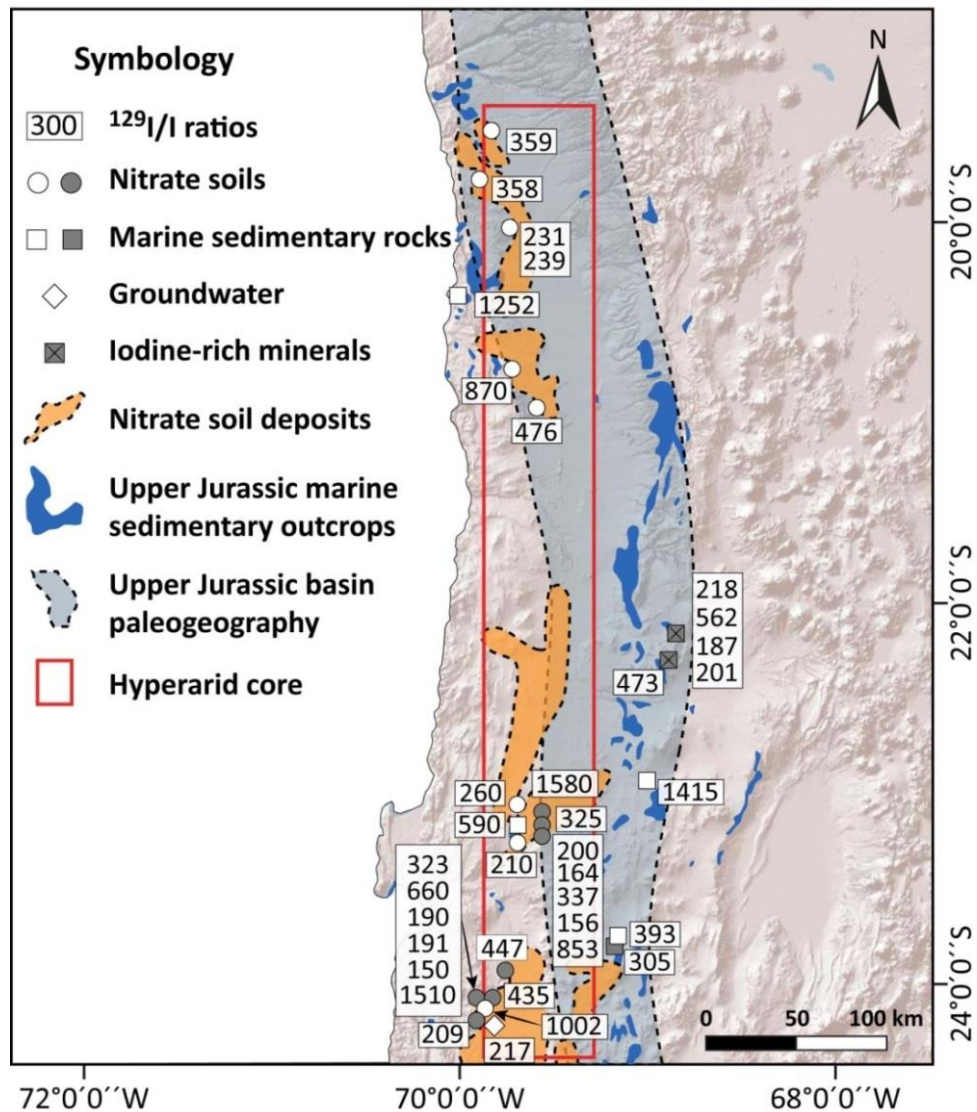


Figure VII.2. Nitrate-rich soils in northern Chile and iodine isotopic ratios ( $^{129}\text{I}/\text{I}$ ) distribution. Data points in grey correspond to results of other authors listed in Table VII.1.

## VII.4 Sample material and analytical methods

Rock, nitrate soils and water samples were collected in the study area (~100,000 square kilometers), including the Coastal Range, Central Depression, Precordillera and Western Cordillera in northern Chile (Fig. VII.1B). These selected samples are representative of different reservoirs in the Atacama region, and include nitrate deposits from the Tarapacá and Antofagasta districts in the Central Depression (Tarapacá, Baquedano and Aguas Blancas districts), Jurassic marine sedimentary rocks outcropping in the Central Depression and Precordillera, and geothermal fluids from the Puchuldiza and El Tatio geothermal fields in the High Andes (Figs. VII.1, VII.2). In addition, groundwater samples were collected from wells in the Central Depression and below nitrate deposits, and from salt lakes or "salars" in the Precordillera. Meteoric water



samples were collected from surface streams in the Central Depression, Precordillera and Western Cordillera, including the Loa, San Pedro and Purifica rivers. Rainwater samples were collected during the 2010-2012 period. Custom-made stations were placed in selected areas in the Western Cordillera and Central Depression, and samples were retrieved after rainfall events. Light paraffin oil was placed at the bottom of the collector to seal the sample and prevent evaporation. The thickness of the paraffin oil layer floating on the water was ~0.5 cm. Finally, seawater samples were taken along the coast, near the cities of Iquique and Antofagasta.

For water samples, temperature, conductivity and pH were measured in situ (Table VII.2) and 250 ml were collected and filtered (0.45  $\mu\text{m}$  Millipore filter) for chemical and isotopic analysis. Previous to iodine extraction for Accelerator Mass Spectrometry (AMS)  $^{129}\text{I}/\text{I}$  isotopic determinations, all water, rock and soil samples were analyzed for iodine concentrations using inductively-coupled plasma mass spectrometry (ICP-MS) at Rice University in Houston and Gakushuin University in Tokyo. Water samples were diluted 200-5000 times and tetramethyl ammonium hydroxide (1%), and 100 ppm  $\text{Na}_2\text{SO}_3$  were added to avoid loss of iodine from the solution prior to the ICP-MS determination. For rocks and soils, approximately 50 g of sample material were grounded and combined with 100 ml of purified 18 M $\Omega$  water and placed in 250 ml high-density polyethylene container. In order to enhance iodate dissolution, samples were agitated during 8 hours and centrifuged for 30 minutes at 1000 rpm. Iodine was extracted from water and solid samples following established methods, *i.e.*, extraction into chloroform or carbon tetrachloride followed by back extraction using sodium bisulfite or hydroxylamine hydrochloride (Fehn *et al.*, 1992). Finally, approximately 1 mg of iodine was precipitated as silver iodide (AgI) targets for AMS isotopic determinations. The AMS measurements were performed at Prime Lab, Purdue University (Indiana), following established procedures (Sharma *et al.*, 2000). The analytical error ( $1\sigma$ ) for each analyzed sample is included in Table VII.1. Due to the small size of the targets, ratios generally have errors between 5 and 25%. Because the  $^{129}\text{I}$  abundance depends on the total amount of iodine in samples, values are expressed as  $^{129}\text{I}/\text{I}$  ratios. The theoretical AMS detection limit is on the order of  $2 \times 10^{-15}$   $^{129}\text{I}$  atoms per total iodine atoms, estimated based on counting statistics and measurement times. However, the practical detection limit is somewhat higher because of the lack of suitable blank materials with ratios below  $\sim 20 \times 10^{-15}$  (Fehn *et al.*, 2007a).

## VII.5 Results

### VII.5.1 Iodine concentrations

Iodine concentrations of nitrate soils and rocks samples from the Atacama Desert are listed in Table VII.1. The nitrate samples of the Tarapacá and Antofagasta districts

contain the highest iodine concentrations of all reservoirs in the Atacama region, with a mean concentration of ~700 ppm, with maximum and minimum values of ~4000 ppm and 2 ppm, respectively (Table VII.1). Soils above the Spence and Mina Sur copper deposits in the Central Depression and Precordillera show iodine concentrations in excess of 100 ppm above fracture zones crosscutting supergene copper mineralization (Cameron *et al.*, 2010). Mesozoic shales and limestones are also enriched in iodine, averaging ~50 ppm in the Antofagasta region (*i.e.*, Caracoles Group), with a maximum iodine concentration of ~130 ppm (Table VII.1). These values are significantly higher than Mesozoic sedimentary marine rocks (shales and calcareous siltstones) in the northern portion of the studied area (Tarapacá, iodine concentrations <1 ppm). Additionally, iodine concentrations above crustal averages are found in selected continental sedimentary rocks, siliceous sinter deposits and lacustrine evaporite samples in the study area, with iodine concentrations varying between ~1 and 6 ppm (Table VII.1).

Iodine concentrations of water samples are reported in Table VII.2. The highest concentrations of iodine were measured in groundwater below nitrate deposits with values between 0.5  $\mu\text{M}$  and 48  $\mu\text{M}$ , averaging ~12  $\mu\text{M}$ , and the highest concentrations are found in the Antofagasta region (sample A1; Table VII.2). These high iodine concentrations are followed by water samples from the Puchuldiza (~21  $\mu\text{M}$ ) and El Tatio (~7  $\mu\text{M}$ ) geothermal springs in the Western Cordillera. Spring waters from the Precordillera present values between ~1 and 12  $\mu\text{M}$  (average of ~5  $\mu\text{M}$ ), and waters from salt lakes ("salars") have concentrations from 0.25 to 8  $\mu\text{M}$  (average of ~3 M). Finally, the lowest iodine contents were measured in seawater (near Antofagasta), surface water and rain water with an average of ~0.7  $\mu\text{M}$ , although surficial (river) water from the Western Cordillera present slightly higher values.

### VII.5.2 $^{129}\text{I}/\text{I}$ isotopic ratios

The  $^{129}\text{I}/\text{I}$  ratios (at  $1\sigma$  error) of soil/rock and water samples are listed in Tables VII.1 and VII.2, and sample distribution is shown in Figure VII.2. The results for each reservoir are plotted schematically in Figure VII.3. The  $^{129}\text{I}/\text{I}$  ratios of the high-iodine nitrates from the Tarapacá district in the northern part of the study area are low and range from 230 to  $\sim 870 \times 10^{-15}$ , while the  $^{129}\text{I}/\text{I}$  ratios of nitrate soils in the Antofagasta region, show a larger dispersion and range from ~150 to  $\sim 1500 \times 10^{-15}$  (Chapter V). The iodine isotopic ratios for Mesozoic marine sedimentary rocks could only be obtained for two shales and one calcareous sandstone (Antofagasta samples), and vary from ~300 to  $\sim 600 \times 10^{-15}$ . Because of the relatively low concentrations of iodine in the water samples, an isotope ratio could only be determined in one groundwater sample. This sample from the Central Depression below nitrate soils in the Aguas Blancas district yielded a  $^{129}\text{I}/\text{I}$  ratio of  $217 \times 10^{-15}$  (Table VII.2; Figs. VII.2, VII.3).

Table VII.1. Analytical results of iodine concentrations and  $^{129}\text{I}/\text{I}$  ratios in soils, sediments and rocks

Site	Sample	Type	Location (UTM)		Elevation (masl)	Soil depth (m)	I concentration (ppm)	$^{129}\text{I}/\text{I}$ ( $10^{-15}\text{at-at}^{-1}$ )	$1\sigma$ ( $10^{-15}\text{at-at}^{-1}$ )	$^{129}\text{I}$ concentration ( $10^7\text{at/Kg}$ )
			Latitude ( $^{\circ}\text{S}$ )	Longitude ( $^{\circ}\text{W}$ )						
Tarapacá										
T3	T3A-A	Nitrate soil			889	0.50	2.00	ND		
	T3E-A	Nitrate soil	21° 2' 25"	69° 37' 30"	889	0.60	28.57	476	30	6.45
	T3C-A	Nitrate soil			889	0.80	4.78	LCV		
	T3D-A	Nitrate soil			889	1.05	38.50	ND		
T4	T4A-A	Nitrate soil			20° 50' 15"	69° 43' 15"	960	0.25	24.81	ND
T4	T4B-A	Nitrate soil			960	0.30	17.39	870	112	7.18
	T6	T6B-A	20° 15' 43"	70° 02' 04"	802	-	0.74	AV		
T6	T6C-A	802			-	0.39	ND			
T8	T8B-A	Nitrate soil	19° 52' 20"	69° 49' 20"	1176	0.30	46.45	LCV		
	T8A-A	Nitrate soil			1176	0.80	74.58	359	46	12.71
T9	T9A-A	Nitrate soil	20° 03' 04"	69° 45' 58"	1114	0.20	61.70	358	83	10.48
T10	T10B-A	Nitrate soil	20° 02' 48"	69° 45' 53"	1123	0.40	120.75	239	39	13.70
	T10A-A	Nitrate soil			1123	0.50	839.94	231	33	92.08
T12	T12A-A	Shale	20° 55' 41"	69° 03' 37"	2263	-	0.60	LCV		
T16	T16A-A	Siltstone	20° 55' 41"	69° 03' 37"	2263	-	0.75	ND		
Antofagasta										
M1	M1G-A*	Nitrate soil			1048	0.10	101.98	323	115	15.63
	M1E-A*	Nitrate soil			1048	0.40	817.90	660	236	256.17
	M1D-A*	Nitrate soil			1048	0.70	2439.27	190	15	219.94
	M1F-A*	Nitrate soil	24° 09' 25"	69° 51' 40"	1048	1.10	1003.46	191	14	90.95
	M1C-A*	Nitrate soil			1048	1.40	912.36	150	10	64.95
	M1B-A	Nitrate soil			1048	1.70	24.70	ND		
	M1A-A*	Nitrate soil			1048	2.15	59.60	1510	371	42.71
M2	M2A-A*	Nitrate soil	24° 09' 25"	69° 51' 40"	1048	1.30	237.11	435	74	48.95
M3	M3A-A	Nitrate soil	24° 09' 25"	69° 51' 40"	1048	1.10	168.75	1002	460	80.24
M4	M4A-A	Nitrate soil	24° 09' 14"	69° 52' 27"	1049	0.80	96.37	LCV		
M5	M5B-A*	Nitrate soil	24° 10' 01"	69° 51' 12"	1068	1.05	152.39	209	49	15.11
M6	M6B-A*	Nitrate soil	24° 08' 39"	69° 53' 54"	1038	1.30	846.67	447	99	179.60
M7	M7B-A*	Nitrate soil	23° 12' 28"	69° 41' 32"	1274	0.70	75.76	1580	244	56.80
M8	M8A-A	Nitrate soil	23° 11' 58"	69° 41' 13"	1299	0.30	4.39	ND		
	M8B-A*	Nitrate soil			1299	1.10	3978.63	325	79	613.63
M9	M9B-A*	Nitrate soil			1295	0.40	475.87	200	31	45.17
	M9E-A*	Nitrate soil			1295	1.05	261.05	164	18	20.32
	M9D-A*	Nitrate soil	23° 12' 05"	69° 41' 24"	1295	1.20	519.44	338	130	83.32
	M9A-A*	Nitrate soil			1295	1.35	476.67	156	13	35.29
	M9C-A*	Nitrate soil			1295	1.80	92.35	853	229	37.38
	M10	M10A-A	Sinter	22° 19' 48"	68° 00' 36"	4281	0.00	6.08	ND	
M11	M11A-A	Evaporite rock	23° 03' 54"	68° 12' 52"	2337	0.00	32.00	1415	72	21.49
M12	M12A-A	Nitrate soil	23° 11' 58"	69° 41' 13"	1305	1.10	824.51	210	30	82.17
M13	M13A-A	Shale	23° 11' 58"	69° 41' 13"	1305	-	37.58	590	60	10.52
M14	M14A-A	Nitrate soil	23° 11' 11"	69° 39' 22"	1336	0.50	896.78	260	50	110.65
MC	MC3A-A	Calcareous siltstone			2494	-	9.08	ND		
	MC3B-A*	Shale			2494	-	128.46	393	74	23.96
	MC3D-A	Calcareous sandstone	22° 55' 52"	68° 58' 19"	2494	-	2.30	305	76	0.33
	MC4A-A	Shale			2494	-	3.64	ND		
	MC5A-A	Calcareous sandstone			2494	-	4.15	ND		
CH	C103579**	Marshite			2260	-	ND	218	72	
	105768**	Marshite	22° 17' 12"	68° 54' 03"	2260	-	ND	562	77	
	Atac-Ch**	Marshite			2260	-	1704.09	187	17	151.22
	Mshxx-B**	Marshite			2260	-	11415.66	207	14	1121.40
MM	EMC107**	Iodine-rich soil	22° 23' 56"	68° 55' 28"	2343	ND	ND	473	75	

ND: Not determined; LCV: Low current values.

Table VII.2. Analytical results of iodine concentrations in water samples

Sample	Morphostructural unit	Type	Location		pH	T° (°C)	EC (μS/cm)	I concentration (μM)
			Latitude (°S)	Longitude (°W)				
Tarapacá								
TA1	Tarapaca Coast	Seawater	20° 39' 36"	70° 11' 06"	8.1	17.2	ND	0.37
TA2	Central depression	River	21° 37' 31"	69° 33' 17"	7.7	17.9	5870	1.56
TA3	Central depression	Groundwater	20° 50' 21"	69° 42' 49"	ND	ND	ND	22.29
TA4	Central depression	Groundwater	19° 53' 05"	69° 51' 54"	7.5	31.7	2780	7.25
TA5	Western Cordillera	Salt lake	20° 18' 23"	68° 52' 33"	6.1	14.5	8600	7.99
TA6	Western Cordillera	Salt lake	20° 18' 23"	68° 52' 33"	ND	ND	ND	1.00
TA7	Western Cordillera	Spring	20° 18' 32"	68° 52' 21"	6.7	15.6	940	0.35
TA8	Precordillera	Spring	20° 57' 50"	69° 10' 23"	7.3	22.1	2290	3.85
TA9	Precordillera	Spring	20° 57' 50"	69° 10' 23"	7.4	22.1	2240	10.36
TA10	Precordillera	Spring	20° 57' 50"	69° 10' 23"	7.3	21.8	2250	12.00
TA11	Precordillera	Spring	20° 55' 45"	69° 05' 48"	8.1	14.4	1950	3.76
TA12	Western Cordillera	Geothermal	19° 24' 38"	68° 58' 17"	8.4	19.2	3800	18.35
TA13	Western Cordillera	Geothermal	19° 24' 51"	68° 57' 45"	6.8	50.0	4300	15.23
TA14	Western Cordillera	Geothermal	19° 24' 44"	68° 57' 33"	8.0	84.0	4600	26.24
TA15	Western Cordillera	River	19° 40' 49"	69° 10' 53"	7.9	16.5	390	0.36
TA16	Western Cordillera	Geothermal	19° 40' 59"	69° 10' 36"	8.4	40.0	450	0.54
TA17	Precordillera	Spring	20° 29' 14"	69° 19' 06"	8.2	30.3	170	1.25
TA18	Precordillera	Spring	20° 29' 14"	69° 19' 06"	8.5	10.0	ND	2.29
Antofagasta								
A1*	Central Depression	Groundwater	24° 10' 31"	69° 52' 07"	7.2	22.8	1570	48.12
A2	Central Depression	Groundwater	24° 10' 38"	69° 52' 06"	6.9	18.4	1010	1.17
A3	Central Depression	Groundwater	24° 03' 29"	69° 49' 31"	7.7	22.7	3570	4.26
A4	Antofagasta Coast	Seawater	23° 28' 10"	70° 30' 46"	7.8	16.8	ND	0.40
A5	Antofagasta Coast	Seawater	22° 28' 35"	68° 54' 51"	7.9	16.5	ND	0.44
A6	Central Depression	River	22° 55' 20"	68° 09' 59"	7.8	15.3	7235	0.93
A7	Central Depression	Groundwater	22° 53' 25"	68° 12' 50"	6.4	28.6	3670	2.64
A8	Central Depression	River	23° 03' 54"	68° 12' 52"	7.3	22.4	5510	0.25
A9	Atacama Basin	Salt lake	23° 03' 32"	68° 12' 49"	7.8	16.0	ND	6.18
A10	Atacama Basin	Groundwater	23° 03' 32"	68° 12' 49"	ND	ND	ND	0.46
A12	Atacama Basin	Salt lake	23° 07' 40"	68° 14' 39"	7.0	23.5	ND	0.25
A13	Western Cordillera	Geothermal	22° 19' 48"	68° 00' 36"	6.8	81.0	ND	7.92
A14	Western Cordillera	Geothermal	22° 24' 24"	68° 00' 41"	6.4	85.5	ND	6.29
A15	Western Cordillera	Lake	22° 25' 58"	68° 02' 57"	7.7	16.9	1020	0.51
A16	Western Cordillera	Spring	22° 43' 12"	68° 02' 37"	ND	ND	ND	1.78
A17	Western Cordillera	River	22° 46' 09"	68° 04' 07"	8.4	11.0	2240	1.49
A18	Western Cordillera	Lake	22° 25' 58"	68° 02' 57"	7.7	13.9	1360	0.37
A19	Western Cordillera	River	22° 46' 09"	68° 04' 07"	8.8	20.2	2120	1.51
A20	Western Cordillera	Salt lake	23° 03' 54"	68° 12' 52"	8.2	19.7	ND	3.59
AM-02	Western Cordillera	Rainwater	22° 25' 59"	68° 02' 57"	7.7	ND	1180	0.29
AM-04	Central Depression	Rainwater	22° 42' 06"	68° 26' 44"	7.8	ND	1175	0.50

ND: Not determined.

\* This sample yielded a  $^{129}\text{I}/\text{I}$  ratio of  $217 \pm 18$  and  $^{129}\text{I}$  concentration of  $0.63 \times 10^7$  at/L

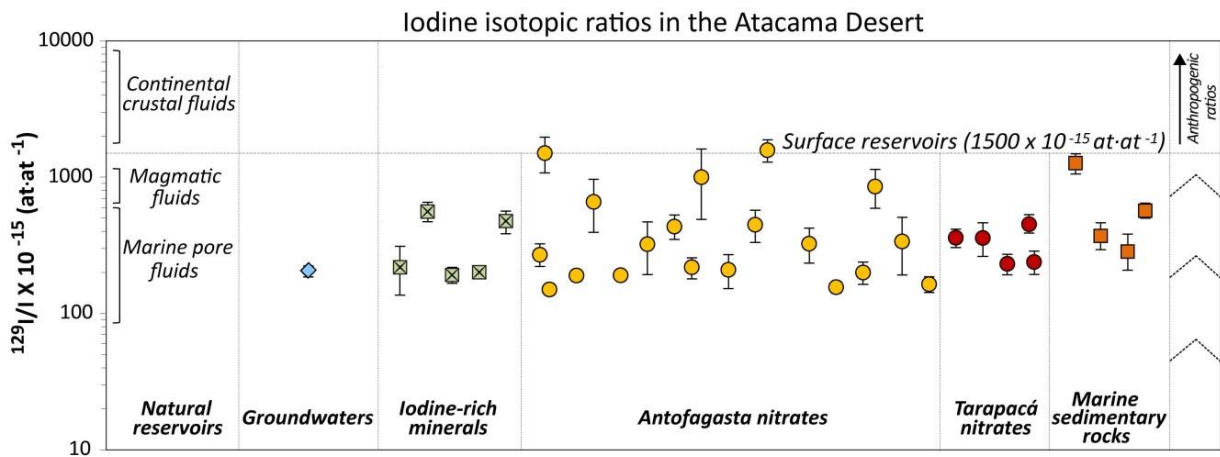


Figure VII.3. Iodine isotopic ratios ( $^{129}\text{I}/\text{I}$ ) of water, rock and soil samples from the Atacama Desert. Most of the  $^{129}\text{I}/\text{I}$  ratios range between  $\sim 150$  to  $450 \times 10^{-15}$  and all values are at or below  $1500 \times 10^{-15}$  (initial isotopic ratio of surface reservoirs; Fehn *et al.*, 2007a). Detailed information about samples is presented in Table VII.1.

## VII.6 Discussion

### VII.6.1 Distribution of iodine in Atacama

Iodine concentrations in nitrate soils, soils above Cu deposits and selected rock samples from the Atacama region (Table VII.1) are considerably higher than the average crustal value of  $\sim 120$  ppb (Muramatsu and Wedepohl., 1998). Iodine concentrations in the studied samples are plotted in Figure VII.4 and compared to natural iodine reservoirs (Fehn, 2012). Figure VII.4 shows that selected soils and Mesozoic marine sedimentary rocks from Atacama are strongly enriched in iodine compared to most natural reservoirs (rocks and organic-rich sediments). On the other hand, water samples (groundwater, geothermal waters and spring waters) also show elevated iodine concentrations, within the range of pore waters in marine formations and volcanic fluids. In the case of freshwaters from Atacama, iodine concentrations are one order of magnitude higher than the average in continental meteoric waters. Concerning iodine distribution in the Atacama region, concentrations reach maximum values in the nitrate belt of Antofagasta (1000's ppm range; Table VII.1), although high iodine values in soils and groundwater are distributed over a much wider area (Fig. VII.2). No other significant relations are observed between latitude or longitude and iodine concentrations, although soils and groundwater in the Central Depression generally contain higher iodine concentrations than in the other morphostructural units shown in Figure VII.1A.

In general, the iodine isotopic ratio of soils, rocks and waters show no significant longitudinal or latitudinal variations. However, nitrate deposits are characterized by variations in  $^{129}\text{I}/\text{I}$  ratios and iodine concentrations along soil profiles. In order to better

understand how iodine is distributed in these soils, we studied a depth profile of a representative iodine-rich nitrate soil hosted in an alluvial fan deposit in the Aguas Blancas iodine mine (site M1, Fig. VII.1B). Figure VII.5 shows the iodine concentrations and isotopic ratios for each sample in a profile of 2.3 meters thickness. Iodine concentrations show a sharp increase from the top layer (102 ppm in chusca; Fig. VII.5) to the nitrate-rich core of the soil profile. Within this portion (~1.3-1.8 m), iodine is significantly high and ranges from 912 to 2439 ppm in the conjelo and caliche, respectively (Fig. VII.5). Iodine concentrations decrease below the caliche by almost two orders of magnitude to 25-60 ppm in coba. The highest iodine concentrations observed in the soil profile are closely related with the highly cemented horizon, *i.e.*, the caliche layer that contain low detritic components, while the lowest concentrations are associated with the unconsolidated regolith (coba) below the caliche horizon. The highest iodine concentrations along the soil profile strongly correlate with the lowest  $^{129}\text{I}/\text{I}$  ratios (between 150 and 191  $\times 10^{-15}$ ) observed in the more cemented horizons, *i.e.*, the caliche and conjelo. In the upper non-consolidated soil horizons (chusca), the isotopic ratios are higher (323 and 660  $\times 10^{-15}$ ) but still substantially lower than the pre-anthropogenic ratio of 1500  $\times 10^{-15}$ , typical of surface (meteoric) reservoirs. It is noteworthy that the highest  $^{129}\text{I}/\text{I}$  ratio (1510  $\times 10^{-15}$ ), located at the bottom of the soil profile, is associated with the lowest iodine concentrations (Fig. VII.5).

The observation that samples with lower iodine concentrations have higher isotopic ratios points to the input of pre-anthropogenic meteoric water, because this “surficial” signal is more easily detectable in samples with low iodine concentrations. Based on these observations, we suggest that iodine distribution and isotopic ratios variations in nitrate soils may be related to changes in climate such as increased surface precipitation (meteoric water addition) and/or inputs of groundwater with “older” signatures. Previous studies have suggested that vertical variation in nitrate soil chemistry in the Atacama Desert may be related to events of downward water movement (Ewing *et al.*, 2006; Ewing *et al.*, 2008).

Based on nitrate and chloride distribution in soils from Atacama, in the southern boundary of our study area, Ewing *et al.* (2006) related the increased concentrations within a ~1.5 m layer to rare rainfall events on a centennial to millennial scale. This interpretation is consistent with our new iodine data, since recent downward flow in nitrate soils would shift the originally low  $^{129}\text{I}/\text{I}$  ratios of caliche to higher, more meteoric values by isotopic mixing within the less cemented horizons (*e.g.*, chusca and coba, Fig. VII.5). As a first approximation, if we consider a mean iodine concentration and thicknesses of the chusca, caliche, conjelo and coba in Figure 5, and an average density of 1900 kg/m<sup>3</sup> (Ewing *et al.*, 2006) the total iodine content in these deposits corresponds to 4.4 kg/m<sup>2</sup>. Assuming a steady state precipitation rate of 10mm/yr and a meteoric iodine concentration of approximately 30 nmol/L (Golfedder *et al.*, 2008), It would take ~120 Myr to accumulate this amount of iodine through a cycle of precipitation and drying, clearly much longer than the period of hyperaridity in the region.

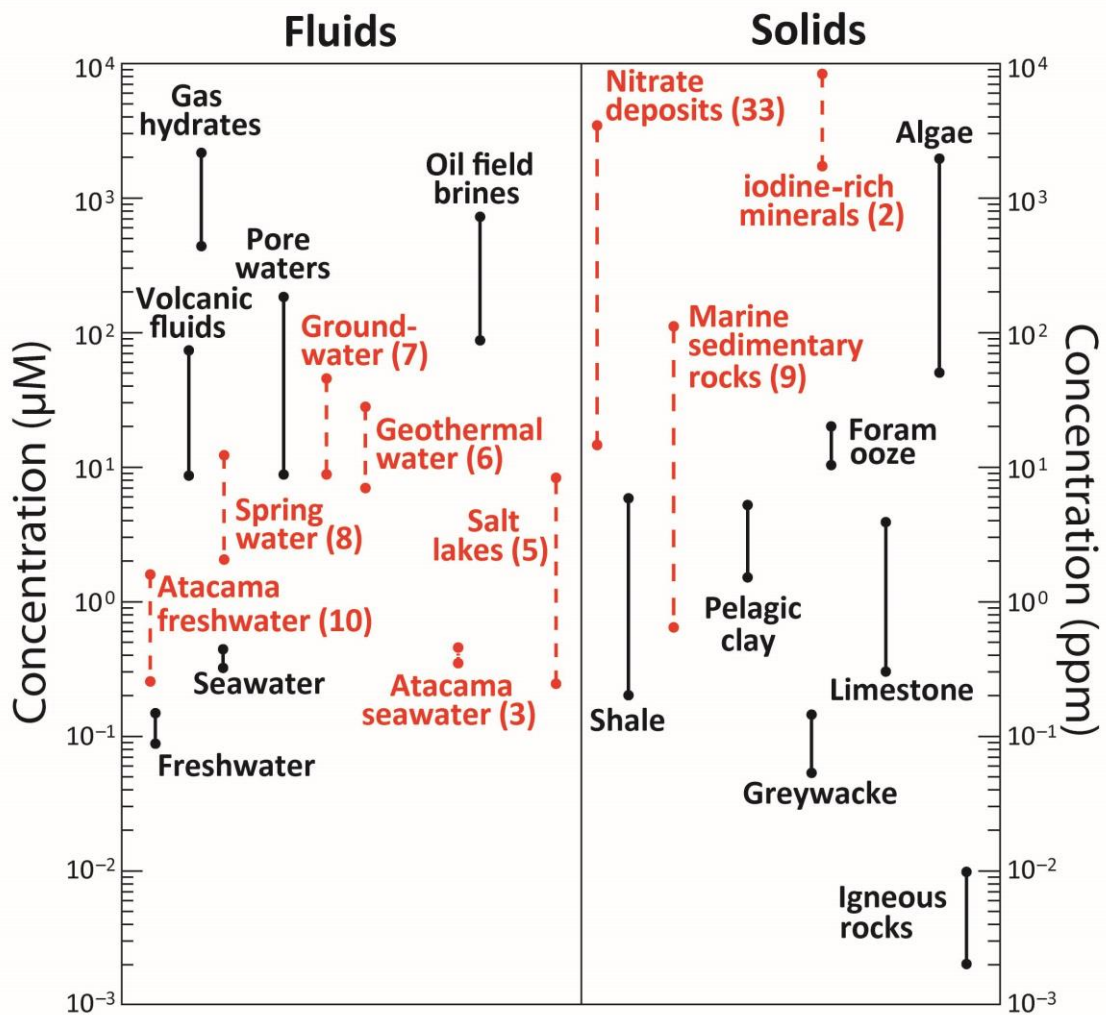


Figure VII.4. Concentration ranges of iodine in rock, soils and water in the Atacama region (red segmented lines). The concentration ranges of fluids and solids in natural reservoirs are shown after Fehn (2012) (solid black lines). Numbers in parenthesis show the number of samples analyzed for each material.

Dry deposition is another possibility that has been used to explain the presence of nitrate deposits. Using a molar ratio  $\text{IO}_3^-/\text{NO}_3^-$  of 0.0034 (or 0.0096 in weight; Grossling and Ericksen, 1971), and a total estimated wet and dry deposition flux of  $16.5 \text{ mg N m}^{-2} \text{ yr}^{-1}$  (Michalski et al., 2004), the estimated time for reach the current iodine content of  $4.4 \text{ kg/m}^2$  (and assuming 100% of retention) is  $\sim 26.5 \text{ Ma}$ . This period of atmospheric deposition of iodine is more than twice the estimated age of nitrate deposits, which is related to the onset of hyper-arid conditions of the Atacama Desert (at least 6 Ma and perhaps as long as 15 Ma; Alpers and Brimhall, 1988; Hartley and Chong, 2002). Even though mass balance calculations indicate that atmospheric deposition cannot explain the high contents of iodine and low isotopic ratios reported in the nitrates, we would like to stress the importance of the atmospheric input for most components of the nitrate. The atmospheric signature is indeed recorded in the nitrates and is included in our analysis and model but – it does not explain by itself the massive occurrence of iodine in Atacama.

The iodine concentrations are most concentrated in the caliche layer and do not suggest steady-state deposition. In addition, the ratios of  $^{129}\text{I}/\text{I}$ , do not display a clear trend from a young iodine isotopic signature in shallow sediments to an old iodine isotopic signature in deep sediments which should have been preserved through steady-state accumulation if this were the case. However, it is important to mention that a model that exclusively considers iodine contribution to nitrate soils from liquid or dry precipitation sources does not fully explain the lower isotopic values that correlate with the significantly high iodine concentrations in the caliche horizons. In the next sections we evaluate the participation of a deep and “old” organic source with low  $^{129}\text{I}/\text{I}$  ratios and high iodine concentrations as an additional source of iodine in the Atacama region.

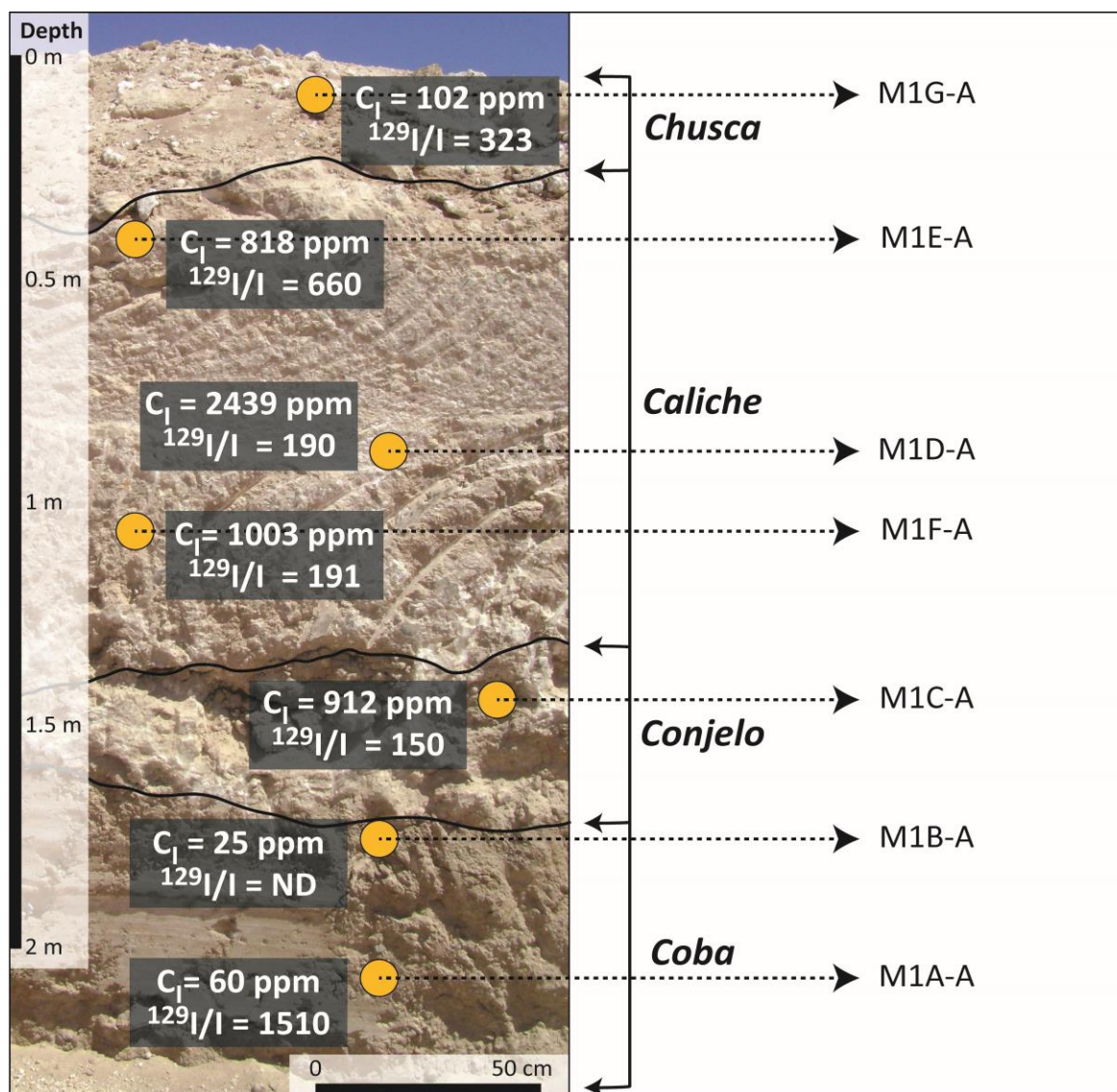


Figure VII.5. Representative soil profile at the Aguas Blancas iodine mine near Antofagasta. Iodine concentrations (ppm) and isotopic ratios ( $^{129}\text{I}/\text{I}$ ) of selected samples are shown in each soil horizon.



## VII.6.2 Sources of iodine

Most of the Earth's surficial iodine resides in marine sediments along continental margins, intra and back-arc marine basins, and nearly 98.8% of the total atmospheric iodine is contributed by oceans due to air-sea exchange, where iodine is transferred from the oceans to the atmosphere and land (Muramatsu and Wedepohl, 1998; Snyder *et al.*, 2010). For this reason and because of its high mobility, iodine is strongly depleted in continental environments. Thus, any model proposed to explain the anomalously high iodine concentrations in Atacama region requires an enriched iodine source and/or enrichment process. In both cases, a process that removes iodine from its original source to its final sink is necessary. Finally, and in order to preserve an originally "old" signature, strong iodine fixation and long-term preservation are needed.

Iodine enrichment in terrestrial environments can be related to the following sources: (i) Atmospheric "young" iodine derived from seawater, rivers, lakes and other surficial reservoirs, deposited by liquid, solid or dry (aerosol) precipitation. This source will present a pre-anthropogenic isotopic signal of  $\sim 1500 \times 10^{-15}$  (initial ratio, Moran *et al.*, 1998; Fehn *et al.*, 2007a), or in certain cases higher ratios caused by anthropogenic iodine contamination (Schink *et al.*, 1995; Rao and Fehn, 1999; Snyder and Fehn, 2004); (ii) "Old" cosmogenic iodine stored in rocks and weathered soils, in particular from marine sedimentary formations that have low ratios usually between  $100\text{-}500 \times 10^{-15}$  (Fehn *et al.*, 2004; Fehn *et al.*, 2007a; Lu *et al.*, 2011); (iii) Iodine from volcanic fluids that have variable ratios between  $500\text{-}800 \times 10^{-15}$  (Snyder and Fehn, 2002; Snyder *et al.*, 2002).

Figure VII.3 shows that the isotopic signature of iodine in most nitrate soils from Atacama, supergene Cu-iodine minerals, Mesozoic marine sedimentary rocks and groundwater are in agreement with previously reported  $^{129}\text{I}/\text{I}$  ratios of marine pore fluids derived from organic material ( $200\text{-}500 \times 10^{-15}$ ; Fehn *et al.*, 2007b; Fehn, 2012). Despite the fact that some higher, surface-like values were measured in the nitrates (see previous section and Figure VII.5), iodine ratios in Atacama average  $\sim 430 \times 10^{-15}$ . Marine sedimentary rocks present a somewhat similar isotopic signature, with shales and calcareous sandstones showing low ratios ( $\sim 300\text{-}600 \times 10^{-15}$ ), and one evaporitic rock sample showing a surface-like ratio of  $1415 \times 10^{-15}$ . One groundwater from Antofagasta has an isotopic ratio of  $217 \times 10^{-15}$  (Fig. VII.3). Most of these data are significantly lower than surficial values represented by the pre-anthropogenic marine input ratio of  $1500 \times 10^{-15}$ , and point towards one or more old and deep organic sources for iodine. Potential sources for organic iodine within an active continental margin include marine sediments (*e.g.*, Snyder and Fehn, 2002) and organic-rich formations in the overlying plate (*e.g.*, Fehn and Snyder, 2003). The Jurassic marine basement, outcropping in the Central Depression and Precordillera of the Atacama region, is formed by a thick,  $\sim 1.5$  km thick marine sedimentary sequence containing organic rich deposits as shales, richly fossiliferous limestones and calcareous sandstones, and has been proposed as a viable source of organic iodine (Arcuri and Brimhall, 2003; Amilibia

*et al.*, 2008; Chapters IV, V and VI). On the other hand, sources of pre-anthropogenic atmospheric iodine could correspond to aerosol deposition or meteoric water addition before the onset of nuclear age (Chapter VI).

Therefore, the large variation observed in the isotopic ratios in Atacama is most likely the result of fluid mixing from different organic and non-organic sources. Figure VII.6 shows a mixing diagram where the  $^{129}\text{I}/\text{I}$  ratios in soil and rock samples were plotted vs. the reciprocal of iodine concentration. Datapoints in Figure VII.6 display an inverse relation between isotopic ratios and iodine concentrations, which provides additional evidence that there is more than one source of iodine in Atacama (Fehn *et al.*, 2007b). Most of the isotopic data range between  $\sim 150$  and  $450 \times 10^{-15}$ , although a small but significant group with higher ratios is observed. This, together with the wide variation in iodine concentrations suggests that iodine in these reservoirs could have different mixing histories (Lu *et al.*, 2008). In Figure VII.6, we identify two different mixing trends and three endmembers (A, B, and C). The “A” endmember corresponds to the point with the lowest isotopic ratio and the highest iodine concentration (nitrate soils and supergene Cu deposits), and is indicative of significant inputs of old organic iodine sources from, for example, the Jurassic marine sequences. It is possible that high iodine concentrations of this endmember reflect a concentration process. However, if we shift the “A” endmember to a lower concentration in the x-axis (Fig. 6), the trend lines practically not change, and moreover, this endmember remains the highest iodine concentration and lowest isotopic ratio respect to the other ones. The “B” endmember corresponds to the highest isotopic ratio showing the lowest concentration (in this case sample M1A-A; Table VII.1). Finally, the “C” endmember is characterized by the lowest iodine concentration (sample T4B-A; Table VII.1). The A-B trend indicates mixing of iodine in nitrate soils/supergene Cu deposits (A) with a largely atmospheric source of  $^{129}\text{I}/\text{I} \sim 1500 \times 10^{-15}$  (B). In contrast, the A-C trend represents interaction between the nitrates/Cu deposits (A) and a possible volcanic source (C) with an isotopic ratio of  $\sim 800 \times 10^{-15}$  (Snyder and Fehn, 2002). A large number of datapoints plot in the lower part of the diagram and have isotopic ratios  $< 450 \times 10^{-15}$ , reflecting a stronger influence of the “A” endmember. Although most of the samples do not show any significant preference for a particular trend, five of the six samples from the Tarapacá nitrate soils are in agreement with the A-C trend (Fig. VII.6).

This analysis suggests that organic-rich (marine sedimentary rocks), volcanic (arc-related) and meteoric (atmospheric) sources are most likely involved in iodine enrichment in Atacama. Of all these sources, the Jurassic marine-sedimentary sequences (e.g., shales, limestones and sandstones) are the most probable source of “old” organic iodine since they have low  $^{129}\text{I}/\text{I}$  ratios (Table VII.1, Fig. VII.2), high organic content, and a widespread regional occurrence upstream in the drainage basin (Mpodozis *et al.*, 2005; Vicente, 2006). Marine Jurassic rocks in the Precordillera and Central Depression are interpreted as a series of back-arc basins associated with a magmatic arc located westwards along the present-day Coastal Cordillera. In the study area ( $19^{\circ}\text{S}$ - $25^{\circ}\text{S}$ ), the Jurassic geological record to the east is characterized by a thick succession of marine

sedimentary deposits composed of fossiliferous limestones, calcareous sandstones and shales, the result of an important marine regression that occurred in the Andean Basin (Marinovic *et al.*, 1995; Vicente, 2006; Oliveros *et al.*, 2012).

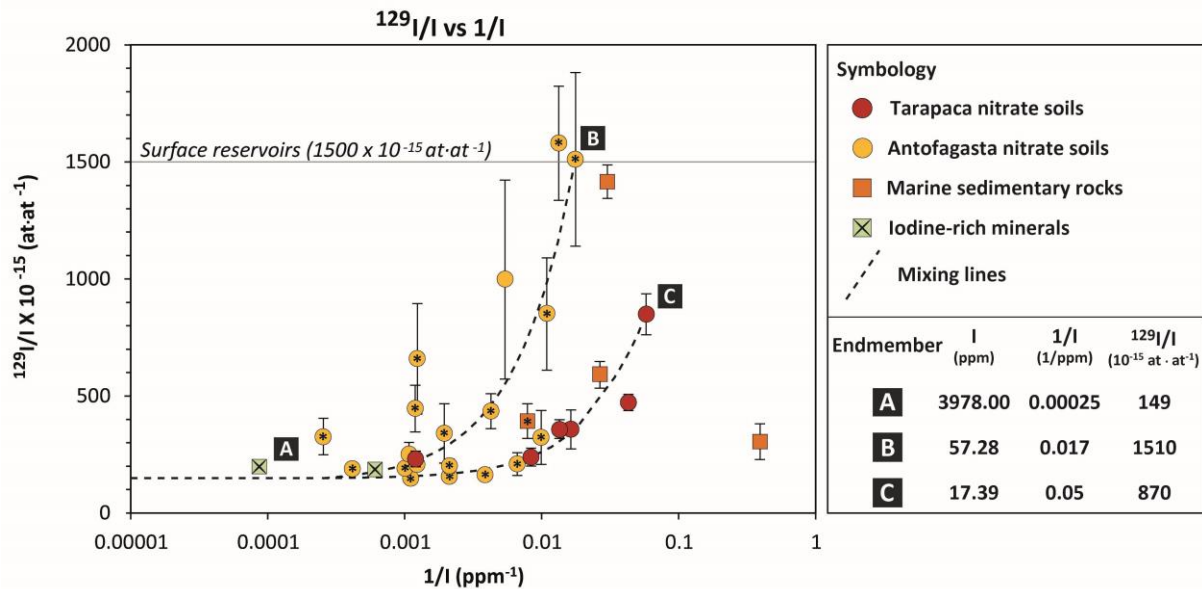


Figure VII.6. Iodine mixing diagram. Three endmembers are shown (A, B and C) and two mixing trends (A-B and A-C). See section 5.2 for detailed discussion. Samples from Chuquicamata were reported in Chapter IV and selected nitrate soil and marine sedimentary data were reported in Chapter V.

### VII.6.3 Fluid mixing and timescales of groundwater flow

Despite the fact that large-scale groundwater flow has been recognized to play a fundamental role in leaching halogens from the aforementioned Jurassic marine sequences (*e.g.*, Cameron *et al.*, 2002; Cameron *et al.*, 2010; Arcuri and Brimhall, 2003; Chapters IV, V and VI), the extent, amount of mixing and timescales of circulation in the Atacama region still remain unconstrained.

In this section we evaluate the iodine contributions from additional sources such as meteoric water and volcanic fluids, considering also the effects of fissiogenic or "*in situ*" iodine production, which can have a significant impact within the "old" isotopic signal of deep marine fluids hosted by rock formations with significant concentrations of uranium (usually U > 1 ppm, ratios > 1500 x 10<sup>-15</sup>, Fabryka-Martin *et al.*, 1989; Snyder *et al.*, 2003). By combining the isotopic data with a geochemical model of fluid mixing, we estimate the timescales of groundwater circulation and mixing trajectories for the sample dataset.

In our conceptual model, iodine formerly resides in the pore waters of the marine sediments in the Jurassic basin. During or after compaction and diagenesis, a fraction of this "old" and organically derived iodine of low <sup>129</sup>I/I ratio was progressively released from

the sediment column and migrated with the fluid. The remaining iodine in the sedimentary rock, measured today in our rock samples from the Jurassic formations was incorporated into the solid fraction, most likely in the carbonate or clay portions. Thus, it is likely that iodine has been subjected to multiple episodes of remobilization from its original sedimentary source by the effect of fluid migration (e.g., deep formation waters), direct leaching, or both.

In order to explore fluid mixing scenarios, we evaluated the evolution of iodine isotopic ratios as a function of time starting with an analogue deep pore fluid that represents the "old" iodine source with initial  $^{129}\text{I}/\text{I} = 290 \times 10^{-15}$  and iodine concentration of  $\sim 1130 \mu\text{M}$  (pore fluids hosted in recent marine sediments on the Peru fore-arc, Fehn *et al.*, 2007b). These starting values are used in the absence of  $^{129}\text{I}/\text{I}$  data in marine sediments from the Chilean fore-arc, and are considered representative of marine sediments in a continental margin setting. The black curve in Figure VII.7 shows the evolution of  $^{129}\text{I}/\text{I}$  ratios in the marine sediment source as a function of time:

$$\frac{^{129}\text{I}}{\text{I}} = \left( \frac{^{129}\text{I}}{\text{I}} \right)_i e^{-\lambda_{129}t} + \frac{N_{238}\lambda_{sf}Y_{129}\varepsilon\rho \left\{ \frac{(1-\varphi)}{\varphi} \right\} \left\{ \frac{(1-e^{-\lambda_{129}t})}{\lambda_{129}} \right\}}{N_{127}} \quad (\text{VII.1})$$

The first term on the right-hand side of Equation VII.1 corresponds to the cosmogenic decay component, where  $(^{129}\text{I}/\text{I})_i$  is the initial value ( $1500 \times 10^{-15}$ ),  $\lambda_{129}$  is the decay constant ( $4.41 \times 10^{-8} \text{ yr}^{-1}$ ), and  $t$  is the time elapsed since burial of organic matter. The second term corresponds to the fissiogenic or "*in situ*" component, which was included in the model, where  $N_{238} = ^{238}\text{U}$  atoms/kg rock,  $\lambda_{sf}$  = spontaneous fission decay constant for  $^{238}\text{U}$  ( $8.5 \times 10^{-17} \text{ yr}^{-1}$ ; Decarvalho *et al.*, 1982),  $Y_{129}$  = spontaneous fission yield of  $^{238}\text{U}$  at mass 129 ( $3 \times 10^{-4}$ ; Hebeda *et al.*, 1987),  $\varepsilon$  = escape efficiency of  $^{129}\text{I}$  from the mineral lattice into the fluid,  $\rho$  = rock density,  $\varphi$  = effective porosity,  $\lambda_{129}$  = decay constant for  $^{129}\text{I}$  ( $4.41 \times 10^{-8} \text{ yr}^{-1}$ ),  $t$  = residence time of fluids in contact with the rocks and  $N_{127}$  = stable  $^{127}\text{I}$  atoms/L fluid. When the term  $e^{-\lambda_{129}t}$  goes to zero, secular equilibrium value for  $^{129}\text{I}$  is reached. For our model, we considered a shale density of  $2.7 \text{ g/cm}^3$  and effective porosity of 0.01 (Young *et al.*, 1991; International Atomic Energy Agency, 1980b), if  $\varphi \ll 1$ , the term  $\{(1-\varphi)/\varphi\}$  in Eq. 1 reduces to  $(1/\varphi)$ . Taken into consideration recent studies in Atacama (Lacassie *et al.*, 2012), a uranium concentration in the host rocks of 9 ppm was used, and a value for  $\varepsilon$  of 0.006 was assumed (Fabryka-Martin *et al.*, 1991; Snyder and Fabryka-Martin, 2007).

Considering a minimum age of formation of marine sequences at 160 Ma in the Atacama region (Amilibia, 2008; Blanco *et al.*, 2013) and all previous conditions, the secular equilibrium for the iodine isotopic system was reached at  $\sim 80 \text{ Ma}$  with a ratio of  $\sim 35 \times 10^{-15}$  (Fig. VII.7, dotted horizontal line). Within this scenario, an organically-derived

fluid separated from the Jurassic marine basement would have had a  $^{129}\text{I}/\text{I}$  ratio too low ( $35 \times 10^{-15}$ ) to explain the whole range of  $^{129}\text{I}/\text{I}$  ratios measured in the studied samples (Fig. VII.7, horizontal grey area and data points for each reservoir), and thus seems unlikely as a sole fluid source for iodine enrichment in Atacama.

The second scenario involved fluid mixing, considering the evidence presented in the section VII.6.2 (Fig. VII.6). Figure VII.7 shows segmented lines that represent the evolution of the starting iodine source that, instead of having evolved in a closed system as in the previous scenario, mixed with iodine inputs from additional sources (*i.e.*, meteoric and volcanic sources) at specific times (Fig. VII.7, white stars). We considered the same deep pore fluid source containing an “old” iodine component ( $X_{fw} = 5\%$ ;  $(^{129}\text{I}/\text{I})_{fw} = 290 \times 10^{-15}$ ,  $\text{I} = 1130 \mu\text{M}$ ; Fehn *et al.*, 2007b), that was diluted with a younger fluid (*e.g.*, groundwater) composed of meteoric water ( $X_{mw} = 90\%$ ;  $(^{129}\text{I}/\text{I})_{mw} = 1500 \times 10^{-15}$ ; Fehn *et al.*, 2007a,  $\text{I} = 0.4 \mu\text{M}$ ; Table VII.2) and volcanic fluid ( $X_{vw} = 5\%$ ; Giggenbach, 1992,  $(^{129}\text{I}/\text{I})_{vw} = 500 \times 10^{-15}$ ,  $\text{I} = 35 \mu\text{M}$ ; Snyder and Fehn, 2002):

$$\left(\frac{^{129}\text{I}}{\text{I}}\right)_{mix} = \frac{X_{fw} \left(\frac{^{129}\text{I}}{\text{I}}\right)_{fw} N_{fw}^{127} + X_{mw} \left(\frac{^{129}\text{I}}{\text{I}}\right)_{mw} N_{mw}^{127} + X_{vw} \left(\frac{^{129}\text{I}}{\text{I}}\right)_{vw} N_{vw}^{127}}{X_{fw} N_{fw}^{127} + X_{mw} N_{mw}^{127} + X_{vw} N_{vw}^{127}} \quad (\text{VII. 2})$$

and

$$N_{127mix} = X_{fw}N_{fw} + X_{vw}N_{vw} + X_{mw}N_{mw} \quad (\text{VII. 3})$$

The isotopic evolution of the diluted fluids was modeled using Equation 1, substituting  $(^{129}\text{I}/\text{I})_{mix}$  for  $(^{129}\text{I}/\text{I})_i$  and  $N_{127mix}$  for  $N_{127}$  (Fig. VII.7, segmented curves). It is noteworthy to mention that most of the total iodine concentration ( $\sim 96.8\%$ ) is provided by the deep pore fluid source (first term in Eq. 3), while the volcanic fluid provides about 3% (second term in Eq. VII.3), and meteoric water only  $\sim 0.2\%$  (third term in Eq. VII.3). Therefore, the number of atoms of  $^{129}\text{I}$  in the deep pore fluid ( $\sim 94.7\%$ ) is much larger than the number of atoms of  $^{129}\text{I}$  in the volcanic fluid ( $\sim 5\%$ ) and meteoric water ( $\sim 0.3\%$ ). Therefore, even though the ratios for meteoric water and volcanic fluids are higher than the ratio for the deep formation waters, the latter will not be seriously affected at the time of mixing.

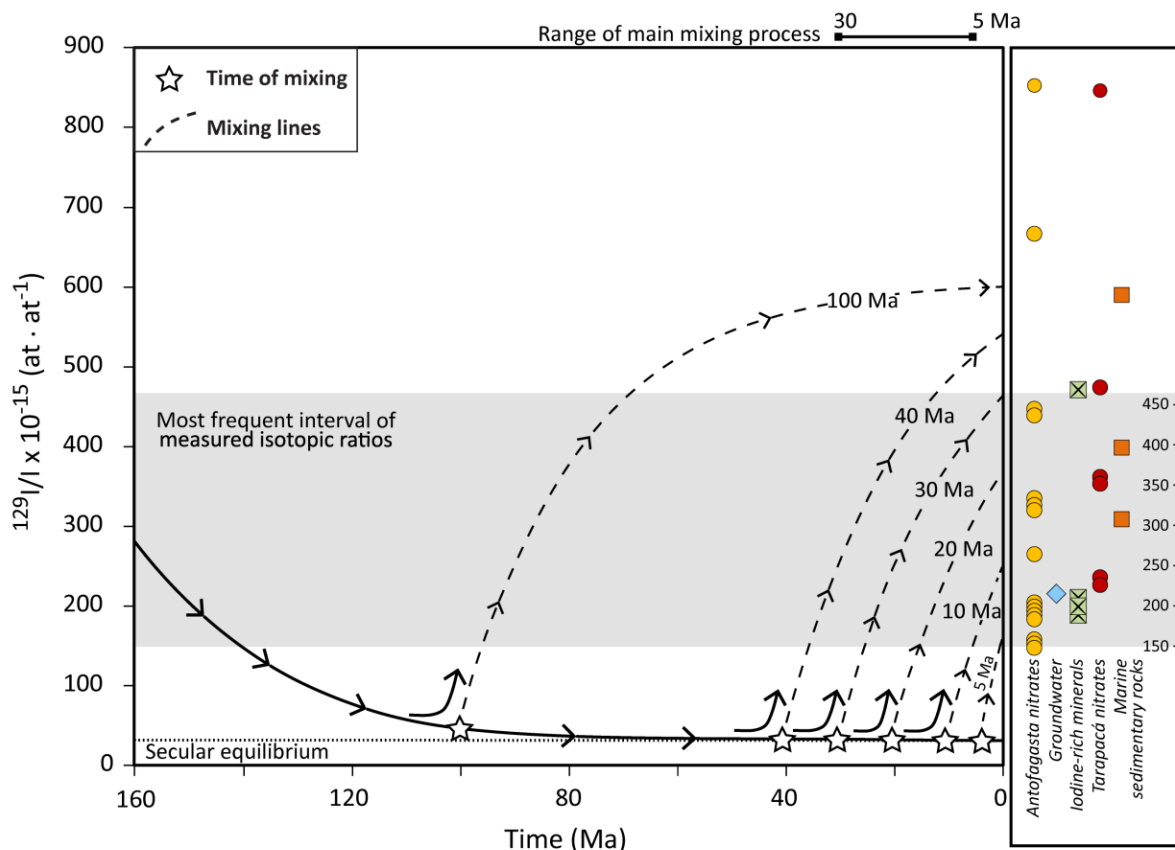


Figure VII.7. Geochemical mixing model showing the secular variation of the iodine isotopic ratio of an organically derived deep pore fluid (solid black curve). This source fluid undergoes mixing with volcanic fluids and meteoric water at selected times (stars), and arrows indicate the fluid evolution. Modeled fluid trajectories (dotted curves and arrows) show that fluid mixing episodes (stars) occurring between ~30 and 5 Ma increase the  $^{129}\text{I}/\text{I}$  ratios of the source fluid, explaining the range of present  $^{129}\text{I}/\text{I}$  ratios measured in the Atacama samples (horizontal grey area). Individual samples are shown on the right-hand side. Secular equilibrium is reached at ~80 Ma (dotted horizontal line).

Thus, the modeled fluid  $^{129}\text{I}/\text{I}$  ratios are in agreement with the measured  $^{129}\text{I}/\text{I}$  ratios in nitrate soils, rock and groundwater samples (~150 to 450  $\times 10^{-15}$ ; horizontal grey area in Fig. VII.7) when mixing or dilution events between the old organic source and the younger groundwater occurred between 30 and 5 Ma ago.

#### VII.6.4 Tectonic, climatic and metallogenic implications

The calculated range of mixing time above (30-5 Ma) is consistent with the climatic, tectonic and hydrologic evolution of the Atacama region during the last 30 million years. Although there is no consensus about the onset of hyperaridity, different authors have reported semiarid climate conditions with rates of precipitation that have decreased progressively from >10 cm/yr (45 – 15 Ma) to less than 10 mm/yr in the last 10 Ma (Arancibia *et al.*, 2006; Rech *et al.*, 2006; Reich *et al.*, 2009b; Amundson *et al.*, 2012).

Regarding tectonic evolution, a relationship between the Andean uplift during the Miocene and the desiccation of the western margin of the Atacama region has been proposed, where tectonic uplift blocked moisture from the South American summer monsoon from entering the Atacama Desert (e.g., Hartley, 2003; Rech *et al.*, 2006). Regardless of the uplift model invoked, there is consensus that progressive deformation events developed since the late Oligocene-early Miocene (~30 Ma, Charrier *et al.*, 2013) would have caused uplift in the central Andes (Hartley, 2003; Garzzone *et al.*, 2008; Barnes and Ehlers, 2009). Our calculated mixing times are consistent with a protracted groundwater flow phase between ~30 and 5 Ma, most likely triggered by an increase in the hydraulic potential between the Andes and the Central Depression creating favorable conditions for the development of the groundwater system (Hoke *et al.*, 2004). These results are also in agreement with the significant isotopic fractionation of chromium reported by Pérez-Fodich *et al.* (2014), indicative of intense Cr redox cycling due to groundwater transport from a source in the High Andes to a final sink in the chromium-bearing nitrate soils in the Central Depression. Even though detailed geochemical models are still needed to better constrain the extent of groundwater contribution in terms of dissolved salt species, published data sources (Bale *et al.*, 2002) indicate that reduced species of iodine, chromium, nitrogen and sulfur can be stable in groundwater at near-neutral to slightly alkaline pH conditions that are consistent with those measured in the field (Table VII.2).

The calculated mixing period reported in this study (30-5 Ma) overlaps with the peak of supergene enrichment of copper in northern Chile, as determined by Ar-Ar dating of supergene minerals giving ages between ~33 to 9 Ma (Alpers and Brimhall, 1988; Sillitoe and McKee, 1996). However, our data suggest the involvement of groundwater flow until ~5 Ma, in agreement with more recent studies that constrain the age span of supergene enrichment in Atacama. Radiometric data compiled by Hartley and Rice (2005) show an increase in the frequency of supergene ages until ~6 Ma, while Arancibia *et al.* (2006) proposed that supergene oxidation of copper deposits ceased ca. 5 Ma as result of climate desiccation in the southern Atacama Desert. Along the same line, Reich *et al.* (2009) suggest that the “meteoric” supergene enrichment of copper, driven by downward penetration of surficial waters, waned after 9 Ma and ceased at ~5 Ma. As a result of desiccation, the meteoric supergene stage was followed by an atacamite-forming supergene stage, driven by the interaction of old and saline brines with copper minerals under conditions of increasing aridity (Reich *et al.*, 2008). Therefore, during this interval (30-5 Ma), large-scale circulation of groundwater and deep fluids existed in the Atacama region, which would have allowed continuous mixing for at least 25 Ma (Fig. VII.7).

The analysis presented here focus mostly in samples showing low iodine isotopic ratios (from ~150 to  $450 \times 10^{-15}$ ), which are in fact the most abundant. However, the presence of a few datapoints with higher isotopic ratios ( $> 1000 \times 10^{-15}$ ; Fig. VII.3) cannot be explained exclusively by an “old” meteoric water influence, because this would imply mixing episodes before the deposition of the Jurassic organic source ( $> 160$  Ma) to achieve such high ratios. Therefore, “young” meteoric inputs seem more likely to explain

the higher, near-surface isotopic ratios. Such ratios are indicative of recent fluid mixing events between an organic source (e.g., marine sedimentary rocks) and meteoric water younger than 5 Ma, probably in a lesser extent than previously described. This interpretation is in agreement with studies proposing that modern hyperarid conditions would have settled since late Pliocene to early Pleistocene (e.g., Hartley and Chong, 2002; Ewing *et al.*, 2006). Pedological evidence of salt distribution in Pliocene soils near Aguas Blancas suggests large and infrequent storms that infiltrated gentle alluvial fans (Ewing *et al.*, 2006; Amundson *et al.*, 2012). The most recent Atacama's landform ages of ~2 Ma, determined using cosmogenic and Ar-Ar dating, point towards a cessation of fluvial features that are related to an arid-hyperarid rainfall transition (Ewing *et al.*, 2006; Amundson *et al.*, 2012). Even though surface run-off in the last ~2 Ma was infrequent, and most likely related to flooding events associated with increased precipitation in the High Andes, there is geological evidence of subsequent groundwater recharge episodes in the Atacama Desert (e.g., >15.4-9 ka, Rech *et al.*, 2002; ~16-13 ka, Nester *et al.*, 2007; ~16-10, Quade *et al.*, 2008). The presence of recent groundwater flow is also supported by chlorine-36 data in atacamite ( $\text{Cu}_2\text{Cl}(\text{OH})_3$ ) from copper deposits in the region. Atacamite samples from supergene assemblages in Cu deposits from the Precordillera to the Coastal Range show very low  $^{36}\text{Cl}$ -to-Cl ratios ( $11 \times 10^{-15}$  to  $28 \times 10^{-15}$  at-at<sup>-1</sup>), comparable to previously reported  $^{36}\text{Cl}$ -to-Cl ratios of deep formation waters and old groundwaters (Reich *et al.*, 2008). Chlorine-36 data in atacamite indicate that the chlorine in saline waters related to atacamite formation is old (>1.5 Ma) but that atacamite formation occurred more recently (<1.5 Ma). This strongly suggests that significant groundwater mixing and circulation events have occurred intermittently since the onset of hyperaridity (Nester *et al.*, 2007; Reich *et al.*, 2009; Sáez *et al.*, 2012).

Results from this study show that the anomalous iodine enrichment in Atacama is evidence of extensive and protracted fluid flow within an active continental margin. The extent of fluid circulation is reflected by the remobilization of iodine from volcanic fluids and marine sedimentary rocks in the Precordillera and volcanic arc. This groundwater, originally composed of low salinity regional fluids of meteoric origin and fluids of volcanic origin, diluted the "old" organic iodine in marine sequences along its flow path and increased the  $^{129}\text{I}/\text{I}$  ratios during a significant period of time (between ~30-5 Ma). Iodine fixation in soils/sediments and precipitation of supergene Cu minerals was possible due to the interaction between these mixed fluids and preexisting deposits under increasing tectonic uplift and desiccation conditions, with significant (and highly variable) inputs of atmospheric, eolian and seapray contributions (Hoke *et al.*, 2004; Chapters V and VI). Even though increased aridity resulted in the preservation of iodine and other soluble components, detailed analyses of soil profiles suggest subsequent in situ mixing processes with pre-anthropogenic meteoric water, which have increased the isotopic ratios to values around  $1500 \times 10^{-15}$  after 5 Ma.

It is noteworthy that old and deep groundwater has played an essential role not only in the continental cycle of iodine in Atacama, but also has had an impact on metal



speciation, transport and mineral precipitation in supergene zones, and on the development of geochemical soil anomalies above copper deposits. This has been documented by several authors, including Cameron *et al.* (2002, 2004, 2007, 2008, 2010), Cameron and Leybourne (2005), Palacios *et al.* (2005), Leybourne and Cameron (2008), and Reich *et al.* (2008, 2009b, 2013). The involvement of a persistent regional groundwater flow in Atacama, supported by stable isotope studies (e.g.,  $\delta^{37}\text{Cl}$  in atacamite at Radomiro Tomic, Arcuri and Brimhall 2003;  $\delta\text{D}$  and  $\delta^{18}\text{O}$  in groundwaters at Spence, Leybourne and Cameron 2006b), strongly suggests that the regional-scale iodine (and supergene copper) enrichment in Atacama is tied to large-scale groundwater circulation over a scale of millions-of-years.

## VII.7 Conclusion

The results reported in this study show that iodine enrichment in the Atacama Desert of northern Chile is widespread and varies significantly between reservoirs. Most iodine isotopic ratios of soils, rocks and waters reported in this study ( $\sim 150$  to  $1580 \times 10^{-15}$ ) are lower than the pre-anthropogenic surface ratio of  $1500 \times 10^{-15}$ , strongly suggesting that iodine in the studied reservoirs is derived from different sources undergoing different mixing histories. Our geochemical mixing models confirm that the most significant organic source for the widespread iodine enrichment in the Atacama region is the Jurassic marine basement, with variable degrees of meteoric water and volcanic fluid inputs that have occurred extensively over a protracted period ( $\sim 30$ -5 Ma).

Our data show that the iodine isotopic system ( $^{129}\text{I}/\text{I}$ ) can be successfully used in continental settings as a paleotracer of water circulation over tens-of-million year timescales. Since large-scale fluid migration is now recognized as playing a major role in virtually all geologic processes (Garven *et al.*, 2010) including metal transport and deposition (e.g., Leybourne and Cameron, 2006b; Leybourne and Cameron, 2008), landscape evolution (e.g., Hoke *et al.*, 2004), geothermal and hydrothermal recharge (e.g., Giggenbach, 1978; Snyder *et al.*, 2002) and halogen recycling through subduction zones (e.g., Kendrick *et al.*, 2011, 2012), the results presented in this study shed new lights on timescales of fluid flow and its relations with the climatic, hydrologic and geodynamic history of active continental margins.

## VII.8 References

- Allmendinger R. W., Jordan T. E., Kay S. M. and Isacks B. L. (1997) The evolution of the Altiplano-Puna Plateau of the central Andes. *Annu. Rev. Earth Pl. Sc.* **25**, 139-174.
- Allmendinger R. and González G. (2010) Invited review paper: Neogene to Quaternary tectonics of the coastal Cordillera, northern Chile. *Tectonophysics* **495**, 93-110.
- Alpers C. N. and Brimhall G. H. (1988) Middle Miocene climatic change in the Atacama Desert, northern Chile: Evidence from supergene mineralization at La Escondida. *Geol. Soc. Am. Bull.* **100**, 1640-1656.
- Amilibia A., Sàbat F., McClay K. R., Muñoz J. A., Roca E. and Chong G. (2008) The role of inherited tectono-sedimentary architecture in the development of the central Andean mountain belt: Insights from the Cordillera de Domeyko. *J. Struct. Geol.* **30**, 1520-1539.
- Amundson R., Dietrich W., Bellugi D., Ewing S., Nishiizumi K., Chong G., Owen J., Finkel R., Heimsath A. and Stewart B. (2012) Geomorphologic evidence for the late Pliocene onset of hyperaridity in the Atacama Desert. *Geol. Soc. Am. Bull.* **124**, 1048-1070.
- Angermann D., Klotz J. and Reigber C. (1999) Space-geodetic estimation of the Nazca-South America Euler vector. *Earth Planet. Sci. Lett.* **171**, 329-334.
- Arancibia G, Matthews S. J. and De Arce, C. P. (2006) K-Ar and Ar-40/Ar-39 geochronology of supergene processes in the Atacama Desert, northern Chile: Tectonic and climatic relations. *J. Geol. Soc. London* **163**, 107-118.
- Aravena R. (1995) Isotope hydrology and geochemistry of northern Chile groundwaters. *Bull. Inst. Fr. Etudes Andin.* **24**, 495-503.
- Aravena R., Suzuki O., Peña H., Pollastri A., Fuenzalida H. and Grilli A. (1999) Isotopic composition and origin of the precipitation in northern Chile. *Appl. Geochem.* **14**, 411-422.
- Arcuri T. and Brimhall G. (2003) The chloride source for atacamite mineralization at the Radomiro Tomic porphyry copper deposit, northern Chile. *Econ. Geol.* **98**, 1667-1681.
- Bale C. W., Chartrand P., Degtrev S. A., Eriksson G., Hack K., Ben Mahfoud R., Melancon J., Pelton A. D. and Petersen S. (2002) FactSage thermochemical software and databases. *Calphad* **26**, 189-228.
- Bao H. M. and Gu, B. (2004) Natural perchlorate has a unique oxygen isotope signature. *Environ. Sci. Technol.* **38**, 5073-5077.

- Barnes J. B. and Ehlers, T. A. (2009) End member models for Andean Plateau uplift. *Earth Sci. Rev.* **97**, 105-132.
- Betancourt J. L., Latorre C., Rech J. A., Rylander K. A. and Quade J. (2000) A 22,000-year record of monsoonal precipitation from northern Chile's Atacama Desert. *Science* **289**, 1542-1546.
- Blanco N., Vásquez P., Sepúlveda F., Tomlinson A., Quezada A. and Ladino M. (2013) Levantamiento geológico para el fomento de la exploración de recursos minerales e hídricos de la Cordillera de la Costa, Depresión Central y Precordillera de la región de Tarapacá (20°-21°S). Servicio Nacional de Geología y Minería, Santiago.
- Böhlke J. K., Ericksen G. E. and Revesz K. (1997) Stable isotope evidence for an atmospheric origin of desert nitrate deposits in northern Chile and southern California, USA. *Chem. Geol.* **136**, 135-152.
- Bottomley D. J., Renaud R., Kotzer T. and Clark I. D. (2002) Iodine-129 constraints on residence times of deep marine brines in the Canadian Shield. *Geology* **30**, 587-590.
- Broecker W. S. and Peng T. H. (1982) Tracers in the Sea. Palisades, NY: Eldigio. pp. 690.
- Muramatsu Y. and Wedepohl K. H. (1998) The distribution of iodine in the earth's crust. *Chem. Geol.* **147**, 201-16.
- Brüggen J. (1938) El salitre. Sociedad Nacional de minería, *Boletín Minero* **50**, 737-754.
- Cameron E. M., Leybourne M. I. and Kelley, D. L. (2002) Exploring for deeply covered mineral deposits: Formation of geochemical anomalies in northern Chile by earthquake-induced surface flooding of mineralized groundwaters. *Geology* **30**, 1007-1010.
- Cameron E. M., Hamilton S. M., Leybourne M. I., Hall, G. E. M. and McClenaghan, M. B. (2004) Finding deeply buried deposits using geochemistry. *Geochem-Explor. Env. A.* **4**, 7-32.
- Cameron E. M. and Leybourne, M. I. (2005) Relationship between groundwater chemistry and soil geochemical anomalies at the Spence copper porphyry deposit, Chile. *Geochem-Explor. Env.* **5**, 135-145.
- Cameron E. M., Leybourne M. I. and Palacios C. (2007) Atacamite in the oxide zone of copper deposits in northern Chile: involvement of deep formation waters? *Miner. Deposita* **42**, 205-218.
- Cameron E. M., Leybourne M. I., Palacios C. and Reich M. (2008) Geochemical Exploration and Metallogenic Studies, Northern Chile. *Geosci. Can.* **35**, 97-107.

- Cameron E. M., Leybourne M. I., Reich M. and Palacios C. (2010) Geochemical anomalies in northern Chile as a surface expression of the extended supergene metallogenesis of buried copper deposits. *Geochem-Explor. Env.* **10**, 1-14.
- Carpenter L. J., Sturgen W. T., Penkett S. A. and Liss P. S. (1999) Short-lived alkyl iodides and bromides at Mace Head, Ireland: Links to biogenic sources and halogen oxide production. *J. Geophys. Res.* **104**, 1679-1689.
- Charrier R., Hérail G., Pinto L., García M., Riquelme R., Farías M., and Muñoz N. (2013) Cenozoic tectonic evolution in the Central Andes in northern Chile and west central Bolivia: implications for paleogeographic, magmatic and mountain building evolution. *Int. J. Earth. Sci.* **102**, 235-264.
- Chong G. (1994) The Nitrate Deposits of Chile. *In* Tectonics of the Southern Central Andes: Structure and Evolution of an Active Continental Margin (Reutter, K.J.; Scheuber, E.; Wigger, P.J.; editors). *Springer*, 303-316.
- Coira B., Davidson J., Mpodozis C. and Ramos V. A. (1982) Tectonic and magmatic evolution of the Andes of northern Argentina and Chile, in: Magmatic evolution of the Andes (Linares, E., editor). *Earth-Science Review, Special Issue* **18**, 303-332.
- Cortés J. (2000) Hoja Palestina, Región de Antofagasta. Servicio Nacional de Geología y Minería, Mapas Geológicos 19, 1 mapa escala 1:100.000. Santiago.
- Decarvalho H. G., Martins J. B., Medeiros E. L. and Tavares O. A. P. (1982) Decay constant for the spontaneous-fission process in  $^{238}\text{U}$ . *Nucl. Instrum. Methods* **197**, 417-426.
- DeMets C., Gordon R. G., Argus D. F. and Stein S. (1994) Effect of recent revisions to the geomagnetic reversal timescale, *Geophys. Res. Lett.* **21**, 2191-2194.
- Dorsaz J., Gironás J., Escauriaza C. and Rinaldo A. (2013) The geomorphometry of endorheic drainage basins: implications for interpreting and modelling their evolution. *Earth Surf. Proc. Land.* **38**, 1881-1896.
- Ericksen G. E. (1961) Rhyolite tuff, a source of the salts of northern Chile. U.S. *Geol. Surv. Prof. Paper* 424-C.
- Ericksen G. E. (1981) Geology and origin of the Chilean nitrate deposits. U.S. *Geol. Surv. Prof. Paper* 1188-B. United States Government Printing Office, Washington.
- Ericksen G. E. (1983) The Chilean nitrate deposits. *American Science* **71**, 366-374.
- Ewing S. A., Sutter B., Amundson R., Owen J., Nishiizumi K., Sharp W., Cliff S. S., Perry K., Dietrich W. E. and McKay C. P. (2006) A threshold in soil formation at Earth's arid-hyperarid transition. *Geochim. Cosmochim. Acta* **70**, 5293-5322.

- Ewing S. A., Michalski G., Thiemens M., Quinn R. C., Macalady J. L., Kohl S., Wankel S.D., Kendall C., MacKay C. P. and Amundson, R. (2007) Rainfall limit of the N cycle on Earth. *Global Biogeochem. Cy.* **21**, GB3009.
- Ewing S. A., Yang W., DePaolo D. J., Michalski G., Kendall C., Stewart B., Thiemans M. and Amundson, R. (2008) Non-biological fractionation of Ca isotopes in soils of the Atacama Desert, Chile. *Geochim. Cosmochim. Acta* **72**, 1096-1110.
- Fabryka-Martin J., Bentley H., Elmore D. and Airey P. L. (1985) Natural I-129 as an environmental tracer. *Geochim. Cosmochim. Acta* **49**, 337-347.
- Fabryka-Martin J. T, Davis S. N., Elmore D. and Kubik P. W. (1989) In situ production and migration of  $^{129}\text{I}$  in the Stripa granite, Sweden. *Geochim. Cosmochim. Acta* **53**, 1817-1823
- Fabryka-Martin J., Whittemore D. O., Davis S. N., Kubik P. W. and Sharma P. (1991) Geochemistry of halogens in the Milk River aquifer, Alberta, Canada. *Appl. Geochem.* **6**, 447-464.
- Fehn U., Holdren G. R., Elmore D., Brunelle T., Teng R., and Kubik P. W. (1986) Determination of natural and anthropogenic I-129 in marine sediments. *Geophys. Res. Lett.* **13**, 137-139.
- Fehn U., Tullai-Fitzpatrick S., Teng R. T. D., Gove H. E., Kubik P. W., Sharma P. and Elmore D. (1990) Dating of oil field brines using  $^{129}\text{I}$ . *Nucl. Instrum. Methods Phys. Res.* **52**, 446-50.
- Fehn U., Peters E. K., Tullai-Fitzpatrick S., Kubik P. W., Sharma P., Teng R. T. D., Gove H. E. and Elmore D. (1992)  $^{129}\text{I}$  and  $^{36}\text{Cl}$  concentrations in waters of the eastern Clear Lake area, California: residence times and source ages of hydrothermal fluids. *Geochim. Cosmochim. Acta* **56**, 2069-2079.
- Fehn U., Snyder G. T. and Egeberg P. K. (2000) Dating of pore waters with  $^{129}\text{I}$ . Relevance for the origin of marine gas hydrates. *Science* **289**, 2332-2335.
- Fehn U., Snyder G. T., and Varekamp J. (2002) Detection of recycled marine sediment components in crater lake fluids using  $^{129}\text{I}$ . *J. Volcanol. Geotherm. Res.* **115**, 451-460.
- Fehn U. and Snyder G. T. (2003) Origin of iodine and  $^{129}\text{I}$  in volcanic and geothermal fluids from the North Island of New Zealand: implications for subduction zone processes. *Soc. Econ. Geol. Spec. Publ.* **10**, 159-170.
- Fehn U., Snyder G. T., Wallmann K., Hensen C. and Lu Z. (2004) Fluid Flow in the Main and Fore Arc of Central America:  $^{129}\text{I}$  as Tracer of subduction processes. AGU Fall Meeting, San Francisco, December 2004. EOS Trans. AGU, **85 (47)** F1851.

- Fehn U. and Snyder G. T. (2005) Residence times and source ages of deep crustal fluids: interpretation of  $^{129}\text{I}$  and  $^{36}\text{Cl}$  results from the KTB-VB drill site, Germany. *Geofl.* **5**, 42-51.
- Fehn U. Moran J. E., Snyder G. T. and Muramatsu Y. (2007a) The initial  $^{129}\text{I}/\text{I}$  ratio and the presence of “old” iodine in continental margins. *Nucl. Instrum. Meth. B.* **259**, 496-502.
- Fehn U., Snyder G. T. and Muramatsu Y. (2007b) Iodine as a tracer of organic material:  $^{129}\text{I}$  results from gas hydrate systems and fore arc fluids. *J. Geochem. Explor.* **95**, 66-80.
- Fehn U. (2012) Tracing Crustal Fluids: Applications of Natural  $^{129}\text{I}$  and  $^{36}\text{Cl}$ . *Annu. Rev. Earth Pl. Sc.* **40**, 45-67.
- Fiesta B. (1966) El origen del salitre de Chile. *Bol. Soc. Esp. Hist. Nat. Geol.* **64**, 47-56.
- Forbes D. (1861) On the geology of Bolivia and southern Perú. *Q. J. Geol. Soc. London.* **17**, 7-62.
- Frohlich K, Ivanovich M, Hendry M. J., Andrews J. N, Davis S. N., Drimmie, R. J., Fabryka-Martin, J., Florkowski, T., Fritz, P., Lehmann, B., Loosli, H. H. and Nolte, E. (1991) Application of isotopic methods to dating of very old groundwaters: Milk River aquifer, Alberta, Canada. *Appl. Geochem.* **6**, 465-72.
- Gale H. S. (1912) Nitrate deposits. *U.S. Geological Survey Bull.* **523**, 19-23.
- Garzione C. N., Hoke G. D., Libarkin J. C., Whithers S., MacFadden B., Eiler J., Ghosh P. and Mulch A. (2008) Rise of the Andes. *Science* **320**, 1304-1307.
- Garreaud R. and Aceituno P. (2001) Interannual rainfall variability over the South American Altiplano, *J. Climate* **14**, 2779-2789.
- Garreaud R., Molina A. and Farias M. (2010) Andean Uplift and Atacama Hyperaridity: A Climate Modeling Perspective. *Earth Planet. Sc. Lett.* **292**, 39-50.
- Garven G., Manning C. E. and Yardley B. W. D. (2010) Frontiers in geofluids: editorial. *Geofluids* **10**, 1-2.
- Gayó E. M., Latorre C., Jordan T. E., Nester P.L., Estay S. A., Ojeda K. F. and Santoro C. M. (2012) Late Quaternary Hydrological and Ecological Change in the Hyperarid Core of the Northern Atacama Desert (~21° S). *Earth Sci. Rev.* **113**, 120-140.
- Giggenbach W. (1978). The isotope composition of waters from the El Tatio geothermal field, northern Chile. *Geochim. Cosmochim. Acta* **42**, 979-988.

- Giggenbach W. F. (1992) Isotopic shifts in waters from geothermal and volcanic systems along convergent plate boundaries and their origin. *Earth Planet. Sci. Lett.* **113**, 495-510.
- Grossling B. F. and Ericksen G. E. (1971) Computer studies of the composition of Chilean nitrate ores: data reduction, basic statistics, and correlation analysis. *U.S. Geol. Surv. Open File Rep.* 1519.
- Hartley A. J. and Chong G. (2002) Late Pliocene age for the Atacama Desert: Implications for the desertification of western South America. *Geology* **30**, 43-46.
- Hartley, A.J. (2003) Andean uplift and climate change. *J. Geol. Soc. Lond.* **160**, 7-10.
- Hartley A. J. and Rice C. M. (2005) Controls on supergene enrichment of porphyry copper deposits in the Central Andes: a review and discussion. *Miner. Deposita* **40**, 515-525.
- Hebeda E. H., Schulz L. and Freundel M. (1987) Radiogenic, fissiogenic, and nucleogenic noble-gases in zircons. *Earth Planet. Sc. Lett.* **85**, 79-90.
- Hervé M., Marinovic N., Mpodozis C. and Smoje I. (1991) Mapa Geológico de la Hoja Sierra de Varas (1:100.000), Región de Antofagasta. Servicio Nacional de Geología y Minería, Documento de Trabajo 2.
- Hoke G. D., Isacks B. L., Jordan T. E. and Yu J. S. (2004) Groundwater-sapping origin for the giant quebradas of northern Chile. *Geology* **32**, 605-608.
- Houston J. (2002) Groundwater recharge through an alluvial fan in the Atacama Desert, northern Chile: mechanisms, magnitudes and causes. *Hydrol. Proc.* **16**, 3019-3035.
- Houston J. and Hartley A.J. (2003) The Central Andean west-slope rainshadow and its potential contribution to the origin of hyper-aridity in the Atacama Desert. *Int. J. Climatol.* **23**, 1453-1464.
- Houston J. (2006) The great Atacama flood of 2001 and implications for Andean hydrology. *Hydrol. Proc.* **20**, 591-610.
- Jarrell O. (1939) Marshite and other minerals from Chuquicamata, Chile. *Am. Miner.* **24**, 629-635.
- Jarrell O. (1944) Oxidation at Chuquicamata, Chile. *Econ. Geol.* **39**, 251-286.
- Kendrick M. A., Scambelluri M., Honda M. and Phillips D. (2011) High abundances of noble gas and chlorine delivered to the mantle by serpentinite subduction. *Nat. Geosci.* **4**, 807-812.

- Kendrick M. A., Woodhead J. D. and Kamenetsky V. S. (2012) Tracking halogens through the subduction cycle. *Geology* **40**, 1075-1078.
- Küpper F. C., Carpenter L. J., McFiggans G. B., Palmer C. J., Waite T. J., Boneberg E. M., Woitsch S., Weiller M., Abela R., Grolimundi D., Potin P., Butler A., Luther III G. W., Kroneck P. M. H., Meyer-Klaucke W. and Feiters M. C. (2008) Iodide accumulation provides kelp with an inorganic antioxidant impacting atmospheric chemistry. *P. Natl. Acad. Sci. USA* **105(19)**, 6954-6958.
- Lacassie J. P., Astudillo F., Baeza L., Castillo P., Figueroa M., Muñoz N. and Ramírez C. (2012) Geoquímica de sedimentos de la Hoja Iquique, Región de Tarapacá. Servicio Nacional de Geología y Minería, Carta Geológica de Chile, Serie Geoquímica 1, 1 DVD versión 1.0, que contiene 1 mapa interactivo para 59 elementos químicos escala 1:250.000, 1 texto (41 p.) y 2 anexos. Santiago.
- Latorre C., Santoro C., Ugalde P., Gayo E., Osorio D., Salas-Egaña C., De Pol-Holz R., Joly D. and Rech J. (2013) Late Pleistocene human occupation of the hyperarid core in the Atacama Desert, northern Chile. *Quaternary Sci. Rev.* **77**, 19-30.
- Leybourne M. I. and Cameron E. M. (2006a) Composition of soils and ground waters at the Pampa del Tamarugal, Chile: Anatomy of a fossil geochemical anomaly derived from a distant porphyry copper deposit. *Econ. Geol.* **101**, 1569-1581.
- Leybourne M. I. and Cameron, E. M. (2006b) Composition of groundwaters associated with porphyry-Cu deposits, Atacama Desert, Chile: Elemental and isotopic constraints on water sources and water-rock reactions. *Geochim. Cosmochim. Acta* **70**, 1616-1635.
- Leybourne M. I. and Cameron E. M. (2008) Source, transport, and fate of rhenium, selenium, molybdenum, arsenic, and copper in groundwater associated with porphyry-Cu deposits, Atacama Desert, Chile. *Chem Geol.* **247**, 208-228.
- Leybourne M. I., Cameron E. M., Reich M., Palacios C., Faure K. and Johannesson, K. H. (2013) Stable isotopic composition of soil calcite (O, C) and gypsum (S) overlying Cu deposits in the Atacama Desert, Chile: implications for mineral exploration, salt sources, and paleoenvironmental reconstruction. *Appl. Geochem.* **29**, 55-72.
- Lu Z., Hensen C., Fehn U. and Wallmann K. (2008) Halogen and  $^{129}\text{I}$  systematics in gas hydrate fields at the northern Cascadia margin (IODP Expedition 311): insights from numerical modeling. *Geochem. Geophys. Geosyst.* **9**, Q10006.
- Lu Z., Tomaru H. and Fehn U (2011) Comparison of iodine dates from mud volcanoes and gas hydrate occurrences: Relevance for the movement of fluids and methane in active margins. *Am. J. Sci.* **311**, 632-650.



- Luther G. W., Wu J. and Cullen J. B. (1995) Redox chemistry of iodine in seawater: Frontier molecular orbital theory considerations. In *Aquatic Chemistry: Interfacial and Interspecies Processes* (eds. C. P. Huang, C. R. O'Melia, and J. J. Morgan). 135-155. *Advances in Chemistry Series 244*. ACS.
- Magaritz M., Aravena R., Peña H., Suzuki O. and Grilli A. (1990) Source of Ground Water in the Deserts of northern Chile: Evidence of Deep Circulation of Ground Water from the Andes. *Ground Water* **28**, 513-517.
- Marinovic N., Smoje, L. Maksaev, V., Hervé M. and Mpodozis C. (1995) Hoja Aguas Blancas, Región de Antofagasta. Servicio Nacional de Geología y Minería, Carta Geológica de Chile, No. 70, pp. 150.
- Marinovic N. and García M. (1999) Hoja Pampa Unión, Región de Antofagasta. Servicio Nacional de Geología y Minería, Mapas Geológicos 9 (escala 1:100.000), Santiago
- Martin J. B., Gieskes J. M., Torres M. and Kastner M. (1993) Bromine and iodine in Peru margin sediments and pore fluids: implications for fluid origins. *Geochim. Cosmochim. Acta* **57**, 4377-4389.
- McKay C.P., Friedmann E.I., Gomez-Silva B., Caceres-Villanueva L., Andersen D.T. and Landheim, R. (2003) Temperature and moisture conditions for life in the extreme arid region of the Atacama Desert: four years of observations including the El Niño of 1997–1998. *Astrobiology* **3**, 393-406.
- Michalski G., Bohlke J. K. and Thiemens M. (2004) Long term atmospheric deposition as the source of nitrate and other salts in the Atacama Desert, Chile: New evidence from mass independent oxygen isotopic compositions. *Geochim. Cosmochim. Acta* **68**, 4023-4038.
- Moran J. E, Fehn U. and Hanor J. S. (1995) Determination of source ages and migration patterns of brines from the U.S. Gulf Coast basin using  $^{129}\text{I}$ . *Geochim. Cosmochim. Acta* **59**, 5055-5069.
- Moran J. E., Fehn U. and Teng R. T. D. (1998) Variations in  $^{129}\text{I}/^{127}\text{I}$  ratios in recent marine sediments: Evidence for a fossil organic component. *Chem. Geol.* **152**, 193-203.
- Mpodozis C., Arriagada C., Basso M., Roperch P., Cobbold P. and Reich M. (2005) Late Mesozoic to Paleogene stratigraphy of the Salar de Atacama Basin, Antofagasta, Northern Chile: Implications for the tectonic evolution of the Central Andes. *Tectonophysics* **399**, 125-154.

- Mueller G. (1960) The theory of formation of north Chilean nitrate deposits through (capillary concentration). International Geological Congress, 21st, Copenhagen 1960, Report 1, 76-86.
- Muramatsu Y. and Wedepohl K. H. (1998) The distribution of iodine in the earth's crust. *Chem. Geol.* **147**, 201-216.
- Muramatsu Y., Fehn U. and Yoshida S. (2001) Recycling of iodine in fore-arc areas: Evidence from the iodine brines in Chiba, Japan. *Earth Planet. Sci. Lett.* **192**, 583-593.
- Nester P. L., Gayo E., Latorre C., Jordan T. E. and Blanco N (2007) Perennial stream discharge in the hyperarid Atacama Desert of northern Chile during the latest Pleistocene. *P. Natl. Acad. Sci. USA* **104**, 19724-19729.
- Noellner C. N. (1867) Über die Entstehung der Salpeter-und Boraxlager in Peru. *J. Prakt. Chem.* **102**, 459-464.
- Oliveros V., Labbé M., Rossel P., Charrier R. and Encinas A. (2012) Late Jurassic paleogeographic evolution of the Andean back-arc basin: New constraints from the Lagunillas Formation, northern Chile (27°30'-28°30'S). *J. S. Am. Earth Sci.* **37**, 25-40.
- Oyarzún J. and Oyarzún R. (2007) Massive volcanism in the Altiplano-Puna Volcanic Plateau and formation of the huge Atacama Desert Nitrate Deposits: A case for thermal and electric fixation of atmospheric nitrogen. *Int. Geol. Rev.* **49**, 962-968.
- Palacios C., Guerra N., Townley B., Lahsen A. and Parada M. (2005) Copper geochemistry in salt from evaporite soils, coastal range of the Atacama Desert, northern Chile: an exploration tool for blind Cu deposits. *Geochem. Explor. Environ. m Analysis A* **5**, 371-378.
- Pardo-Casas F. and Molnar P. (1987) Relative motion of the Nazca (Farallon) and South American Plate since Late Cretaceous time. *Tectonics* **6**, 233-248.
- Penrose R. A.F. Jr. (1910) The nitrate deposits of Chile. *J. Geol.* **18**, 1-32.
- Pérez-Fodich A., Reich M., Álvarez F., Snyder G.T., Schoenberg R., Vargas G., Muramatsu Y. and Fehn U. (2014) Climate change and tectonic uplift triggered the formation of the Atacama Desert's giant nitrate deposits. *Geology* **42**, 251-254.
- Pissis A. (1878) Report upon the Desert of Atacama, its geology and mineral products. In London, Taylor and Francis (eds) Nitrate and guano deposits in the Desert of Atacama, 1-30.
- Pueyo J. C., Chong G. and Vega M. (1998) Mineralogy and parental brine evolution in the Pedro de Valdivia nitrate deposit, Antofagasta, Chile. *Andean Geol.* **25**, 3-15.

- Quade J., Rech J. A., Betancourt J. L., Latorre C., Quade B., Rylander K. A. and Fisher T. (2008) Paleowetlands and regional climate change in the central Atacama Desert, northern Chile. *Quat. Res.* **69**, 343–360.
- Rao U. and Fehn U. (1999) Sources and reservoirs of anthropogenic iodine-129 in western New York. *Geochim. Cosmochim. Acta* **63**, 1927-1938.
- Rech J. A., Quade J. and Betancourt J. L. (2002) Late Quaternary paleohydrology of the central Atacama Desert (lat 22 degrees-24 degrees S), Chile. *Geol. Soc. Am. Bull.* **114**, 334–348.
- Rech J. A., Quade J. and Hart W. S. (2003) Isotopic evidence for the source of Ca and S in soul gypsum, anhydrite and calcite in the Atacama Desert, Chile. *Geochim. Cosmochim. Acta* **67**, 575-586.
- Rech J. A., Currie B. S., Michalski G. and Cowan, A. M. (2006) Neogene climate change and uplift in the Atacama Desert, Chile. *Geology* **34**, 761-764.
- Reich M., Palacios C., Parada M. A., Fehn U., Cameron E. M., Leybourne M. I. and Zúñiga A. (2008) Atacamite formation by deep saline waters in copper deposits from the Atacama Desert, Chile: Evidence from fluid inclusions, groundwater geochemistry, TEM, and <sup>36</sup>Cl data. *Miner. Deposita* **43**, 663-675.
- Reich M., Palacios C., Alvear M., Cameron E. M., Leybourne M. I. and Deditius A. (2009a) Iodine-rich waters involved in supergene enrichment of the Mantos de la Luna argentiferous copper deposit, Atacama Desert, Chile. *Miner. Deposita* **44**, 719-722.
- Reich M., Palacios C., Vargas G., Luo S., Cameron E. M., Leybourne M. I., Parada M. A., Zúñiga A. and You C.F. (2009b) Supergene enrichment of copper deposits since the onset of modern hyperaridity in the Atacama Desert, Chile. *Miner. Deposita* **44**, 497-504.
- Rundel P. W., Dillon M. O., Palma B. Mooney H. A., Gulmon S. L. and Ehleringer J. R. (1991) The phytogeography and ecology of the coastal Atacama and Peruvian deserts. *ALISO* **13**, 1-49.
- SERNAGEOMIN (2003) Geologic map of Chile, digital version, scale 1:1000000.
- Sharma P., Bourgeois M., Elmore D., Granger D., Lipschutz M. E., Ma X., Miller T., Mueller K., Rickey F., Simms P. and Vogt S. (2000) PRIME lab AMS performance, upgrades and research applications. *Nucl. Instr. Meth. B.* **172**, 112-123.
- Sáez A. Cabrera L. I. Garcés M. Bogaard P. Jensen A. and Gimeno G. (2012) The stratigraphic record of changing hyperaridity in the Atacama desert over the last 10 Ma. *Earth Planet. Sci. Lett.* **355**, 32-38.

- Shetaya W. H., Young S. D., Watts M. J., Ander E. L and Bailey E. H. (2012) Iodine dynamics in soils. *Geochim. Cosmochim. Acta* **77**, 457-473.
- Schink D. R., Santschi P. H., Corapcioglu P., Sharma P. and Fehn U. (1995)  $^{129}\text{I}$  in Gulf of Mexico waters. *Earth Planet. Sci. Lett.* **135**, 131-138.
- Snoke J. A., Sacks I. S. and Okada H. (1977) Determination of subducting lithosphere boundary by use of converted phases. *Bull. Seismol. Soc. Am.* **67**, 1051-1060.
- Snyder G. T. and Fehn U. (2002) Origin of iodine in volcanic fluids:  $^{129}\text{I}$  results from the Central American Volcanic Arc. *Geochim. Cosmochim. Acta* **67**, 3827-3838.
- Snyder G. T, Fehn U. and Goff F. (2002) Iodine isotope ratios and halide concentrations of the Satsuma-Iwojima volcano, Japan. *Earth Planets Space* **54**, 265-273.
- Snyder G. T., Riese R. C., Franks S., Fehn U., Pelzmann W. L., Gorody A. W. and Moran J. E. (2003) Origin and history of waters associated with coalbed methane:  $^{129}\text{I}$ ,  $^{36}\text{Cl}$ , and stable isotope results from the Fruitland Formation, CO and NM. *Geochim. Cosmochim. Acta* **67**, 4529-4544.
- Snyder G. T. and Fehn U. (2004) Global distribution of  $^{129}\text{I}$  in rivers and lakes: implications for iodine cycling in surface reservoirs. *Nucl. Instr. Meth. B.* **223/224**, 579-586.
- Snyder G. T., Savov I. P. and Muramatsu Y. (2005) Iodine and boron in Mariana serpentinite mud volcanoes (ODP Legs 125 and 195): implications for forearc processes and subduction recycling. In: Shinohara, M., Salisbury, M.H. and Richter, C. (Eds.), Proc. Ocean Drilling Program, Scientific Results. Ocean Drilling Program, College Station, Texas. 1-18.
- Snyder G. T. and Fabryka-Martin J. T. (2007)  $^{129}\text{I}$  and  $^{36}\text{Cl}$  in dilute hydrocarbon waters: marine-cosmogenic, in situ, and anthropogenic sources. *Appl. Geochem.* **22**. 692-714.
- Snyder G., Aldahan A. and Possnert G. (2010) Global distribution and long term fate of anthropogenic I-129 in marine and surface water reservoirs. *Geochem. Geophys. Geosy.* **11(4)**, Q04010.
- Sillitoe R. H. and McKee, E. H. (1996) Age of supergene oxidation and enrichment in the Chilean porphyry copper province. *Econ. Geol.* **91**, 164-179.
- Singewald J.T. Jr. and Miller B.L. (1916) The genesis of the Chilean nitrate deposits. *Econ. Geol.* **11**, 103-114.
- Tomaru H., Lu Z., Fehn U. and Muramatsu Y. (2009) Origin of hydrocarbons in the Green Tuff region of Japan:  $^{129}\text{I}$  results from oil field brines and hot springs in the Akita and Niigata basins. *Chem. Geol.* **264**, 221-31.

- Ullman W. J. and Aller R. C. (1983) Rates of iodine remineralization in terrigenous near-shore sediments. *Geochim. Cosmochim. Acta* **47**, 1423-1432.
- Ullman W. J. and Aller R. C. (1985) The Geochemistry of iodine in near-shore carbonate sediments. *Geochim. Cosmochim. Acta* **49**, 967-978.
- Vicente J. C. (2006) Dynamic Paleogeography of the Jurassic Andean Basin: pattern of regression and general considerations of main features. *Rev. Asoc. Geol. Argent.* **61**, 408-437.
- Wetzel W. (1924) Petrographische Untersuchungen an chilenischen Salpetergesteinen. *Zeitschrift für praktische Geologie, Jahrg.* **32**, 113-120, 132-142.
- Wong G. T. F. (1991) The marine geochemistry of iodine. *Rev. Aquatic. Sci.* **4**, 45-73.
- Zhou J. and Lau K. M. (1998) Does a monsoon climate exist over South America. *J. Clim.* **11**, 1020-1040.

La región de Atacama, ubicada en el margen occidental del norte de Chile, alberga el desierto más árido del planeta: el Desierto de Atacama. Esta región constituye la principal provincia productora de yodo a nivel mundial y alberga las mayores reservas de este elemento. Con el fin de determinar cuáles son las fuentes de yodo y cómo actúan los procesos que dieron origen a las altas concentraciones en la región, se recolectaron muestras de distintos reservorios: (1) Rocas y suelos correspondientes a diferentes niveles de depósitos de nitratos, minerales de yodo y rocas sedimentarias con variable contenido orgánico; y (2) Aguas subterráneas y superficiales que incluyen agua de mar, vertientes, ríos, salares, agua de lluvia, manantiales fríos y termales.

A través de metodologías químicas e isotópicas, con especial énfasis en el sistema del  $^{129}\text{I}$ , se estudiaron las muestras de los distintos reservorios. Los análisis realizados en esta investigación han demostrado la eficacia del sistema isotópico del yodo como trazador de fluidos en márgenes de subducción.

Se determinaron las concentraciones de yodo en los distintos reservorios del Desierto de Atacama. Los resultados obtenidos muestran que existe un fuerte enriquecimiento de yodo en la zona, el cual se extiende desde la Depresión Central hasta la Cordillera Occidental. Los depósitos de nitratos presentan las concentraciones más altas promediando  $\sim 700$  ppm, seguidos por las rocas sedimentarias con alto contenido orgánico que promedian  $\sim 50$  ppm. Por otro lado, se ha detectado un enriquecimiento en aguas naturales, destacando las aguas subterráneas ( $\sim 12 \mu\text{M}$ ), manantiales termales de Puchuldiza ( $\sim 21 \mu\text{M}$ ) y El Tatio ( $\sim 7 \mu\text{M}$ ). Es importante destacar que las aguas superficiales y de lluvia superan en un orden de magnitud los rangos promedios reportados en reservorios naturales.

En cuanto a las razones isotópicas  $^{129}\text{I}/\text{I}$  obtenidas en los distintos reservorios, prácticamente todas las muestras de rocas y suelos arrojan valores menores a la razón inicial en reservorios superficiales ( $1500 \pm 150 \times 10^{-15} \text{ at}\cdot\text{at}^{-1}$ ), mientras que gran parte de las muestras de agua presentan razones sobre este valor, sugiriendo la presencia de una componente antropogénica. Las bajas razones isotópicas medidas en suelos y rocas de Atacama, junto con las variaciones de la concentración de yodo, sugieren que éste deriva de un proceso de mezcla de diferentes fuentes. A través de modelos de mezcla se determinó que la principal fuente de yodo corresponde a fluidos profundos enriquecidos en contenido orgánico con aportes variables de fluidos volcánicos y meteóricos pre-antropogénicos. Las razones isotópicas medidas en diferentes tipos de agua, junto con las concentraciones de halógenos también indican la presencia de un fluido inicial enriquecido en yodo, el cual habría sido diluido por agua meteórica. Sin embargo, a diferencia de rocas y suelos, en las aguas superficiales se identifica además una componente antropogénica.

De esta forma, se proponen las siguientes fuentes naturales de yodo: (1) Secuencias sedimentarias marinas del Jurásico, donde el yodo proviene del agua de poros o desde facies carbonatadas; (2) Fluidos meteóricos superficiales que infiltran en la Cordillera de los Andes; (3) Fluidos volcánicos, los cuales se mezclan con el flujo de agua subterránea hacia el oeste; y (4) Fluidos corticales profundos de origen fisiogénico asociados al contenido de uranio en las rocas. Por otro lado, la componente antropogénica provendría de dos fuentes distintas: (1)  $^{129}\text{I}$  liberado por ensayos nucleares en el Océano Pacífico Central ( $^{129}\text{I}/\text{I} = 12000 \times 10^{-15}$ ); y (2)  $^{129}\text{I}$  liberado por plantas de reprocesamiento nuclear ubicadas en el hemisferio norte ( $^{129}\text{I}/\text{I} = 97000 \times 10^{-15}$ ). Considerando la ausencia de fuentes antropogénicas de yodo en Sudamérica, la señal reportada en Atacama sugiere una rápida redistribución de este radioisótopo a escala global. De esta manera, se concluye la existencia de múltiples fuentes de yodo en el Desierto de Atacama, descartando que provenga exclusivamente de una fuente atmosférica y reafirmando la importancia del drenaje subterráneo en los procesos de transporte y depositación de elementos en márgenes continentales.

A partir de las fuentes establecidas y en conjunto con modelación geoquímica, se identifica un período de gran actividad de mezcla y circulación de fluidos de origen volcánico, sedimentario y de aguas meteóricas a lo largo del margen continental chileno aproximadamente durante los últimos 30 Ma. Este flujo de larga duración estaría controlado por el alzamiento tectónico y la historia climática desarrollada en el Desierto de Atacama durante este período. La combinación de estos factores tiene un rol fundamental en el transporte y la acumulación del yodo junto con otros componentes solubles en la región de Atacama.

Se propone realizar nuevos estudios geoquímicos que permitan caracterizar muestras de condensados volcánicos, de pozos geotermales y de sedimentos de fondo oceánico. Es necesario conocer la concentración y razón isotópica de yodo en estos reservorios para caracterizar mejor el transporte de fluidos en márgenes activos. Además, se sugiere analizar en detalle muestras de aguas subterráneas pertenecientes a la Depresión Subandina, lo cual permitiría estudiar un probable efecto de la Precordillera en la circulación de estas aguas. Por otro lado, se propone realizar análisis isotópicos de  $^{36}\text{Cl}$  en conjunto con nuevas mediciones de  $^{129}\text{I}$  y  $\delta^{15}\text{N}$  en aguas subterráneas y suelos con el fin de datar y trazar las principales componentes químicas presentes en el Desierto de Atacama.

## **Apéndice A. Publicaciones**

- A.1 Using iodine isotopes to constrain supergene fluid sources in arid regions: insights from the Chuquicamata oxide blanket**
  
- A.2 Climate change and tectonic uplift triggered the formation of the Atacama Desert's giant nitrate deposits**



## SCIENTIFIC COMMUNICATIONS

### USING IODINE ISOTOPES TO CONSTRAIN SUPERGENE FLUID SOURCES IN ARID REGIONS: INSIGHTS FROM THE CHUQUICAMATA OXIDE BLANKET

MARTIN REICH,<sup>1,2,†</sup> GLEN T. SNYDER,<sup>3</sup> FERNANDA ÁLVAREZ,<sup>1</sup> ALIDA PÉREZ,<sup>1</sup> CARLOS PALACIOS,<sup>1</sup> GABRIEL VARGAS,<sup>1,2</sup>  
EION M. CAMERON,<sup>4</sup> YASUYUKI MURAMATSU,<sup>5</sup> AND UDO FEHN<sup>6</sup>

<sup>1</sup> *Departamento de Geología, Universidad de Chile, Santiago, Chile*

<sup>2</sup> *Andean Geothermal Center of Excellence (CEGA), Universidad de Chile, Santiago, Chile*

<sup>3</sup> *Department of Earth Sciences, Rice University, Houston, Texas*

<sup>4</sup> *Eion Cameron Geochemical Inc., Carp, Ontario, Canada*

<sup>5</sup> *Department of Chemistry, Gakushuin University, Tokyo, Japan*

<sup>6</sup> *Department of Earth and Environmental Sciences, University of Rochester, Rochester, New York*

#### Abstract

Although iodine is rare in crustal settings, previous studies have documented its occurrence in the supergene zones of base and precious metal ore deposits in arid environments. In this report, we present a novel application of the iodine-129 (<sup>129</sup>I) isotope tracer to iodine-rich samples from the world's largest supergene Cu profile at the Chuquicamata deposit in northern Chile, where anomalous concentrations of this element have been reported. All supergene marshite (CuI) samples from Chuquicamata and iodine-rich soil above the Mansa Mina deposit have <sup>129</sup>I/I isotope ratios ( $\sim 190\text{--}560 \times 10^{-15}$ ) that are significantly lower than those of surface waters (i.e.,  $1,500 \times 10^{-15}$ ), indicating that iodine was most likely derived from a reservoir of marine origin rather than a meteoric and/or atmospheric source. Geochemical modeling shows that the long-term dilution of iodine-rich deep formation waters by meteoric water during the main stage of supergene alteration ( $\sim 40\text{--}10$  Ma) resulted in fluid <sup>129</sup>I/I ratios that are within the range of mineral/soil <sup>129</sup>I/I ratios observed at Chuquicamata, strongly suggesting that iodine was remobilized from the Lower Jurassic to mid Cretaceous marine basement. Results from this study show that iodine isotopes can be successfully applied to trace the origin and nature of supergene fluids in iodine-rich oxide blankets, leach caps, and soils above buried Cu deposits, and also to constrain the timescales of fluid circulation during supergene enrichment.

#### Introduction

Iodine is commonly overlooked in ore systems and crustal settings in general, since the global iodine distribution is dominated by the marine system, in particular marine sediments, which hold about 70% of the total iodine in the crust at concentrations from 200 to 1,300 ppm (Muramatsu and Wedepohl, 1998; Muramatsu et al., 2001; Snyder and Fehn, 2002). Nevertheless, a survey of the occurrences of iodine minerals in metallogenic provinces show that they can be found in the supergene zones of base (Cu, Pb-Zn) and precious (Ag, Au) metal ore deposits in extremely arid environments such as desert areas of Chile, Australia, Arizona, Iran, and Kazakhstan, among other regions (Jarrel, 1939, 1944; Williams, 1963; Srinivasan et al., 1971; Mortimer et al., 1978; Boyle, 1997; Millstead, 1998; Chouinard et al., 2005; Fard et al., 2006; Witzke et al., 2006; Sillitoe, 2007; Reich et al., 2009a; Golebiowska et al., 2010).

In the Atacama Desert of northern Chile, iodide (I<sup>-</sup>) and iodate (IO<sub>3</sub><sup>-</sup>) minerals have been reported in the supergene zones of porphyry and Manto-type Cu deposits (e.g., Chuquicamata, Mantos de la Luna), and iodine geochemical anomalies have been recognized in soils above buried porphyry Cu

deposits (e.g., Spence, Chimborazo, Tamarugal; Jarrel, 1939, 1944; Mortimer et al., 1978; Kelley et al., 2003; Leybourne and Cameron, 2006a; Reich et al., 2009a; Cameron et al., 2002, 2010). These occurrences remain unexplained, considering the fact that (1) meteoric surface and ground waters have exceedingly low concentrations of iodine, <10 ppb (Muramatsu and Wedepohl, 1998; Moran et al., 1999; Fehn et al., 2007a), and (2) supergene enrichment of Cu in the region was driven by downward circulation of meteoric water from  $\sim 44$  to 14 to 9 Ma under a semiarid to arid climate, followed by a late stage of oxidation which was dominated by saline ground waters under conditions of progressive aridification (Alpers and Brimhall, 1988; Sillitoe and McKee, 1996; Mote et al., 2001; Hartley and Chong, 2002; Sillitoe, 2005; Arancibia et al., 2006; Leybourne and Cameron, 2006b; Rech et al., 2006; Reich et al., 2008, 2009a, b; Palacios et al., 2011).

Here we present an isotopic analysis of radiogenic (<sup>129</sup>I) and stable (<sup>127</sup>I) iodine in supergene iodide minerals and iodine-rich soil from the Chuquicamata porphyry Cu deposit, where notable occurrences of this element have been reported in the supergene oxidation blanket (Jarrel, 1939, 1944; Mortimer et al., 1978). We show that the <sup>129</sup>I/<sup>127</sup>I ratios (by convention expressed as <sup>129</sup>I/I ratios) in iodine-rich minerals and soils can be used to trace the source(s) of iodine in supergene

<sup>†</sup> Corresponding author: e-mail, mreich@ing.uchile.cl

fluids, and when coupled to geochemical mixing models, provide additional constraints about the timescales of fluid circulation during supergene enrichment and oxidation.

### Geologic Background and Samples

The late Eocene-early Oligocene Chuquicamata porphyry Cu deposit is the world's largest Cu orebody (>60 Mt of Cu) and forms part of a cluster of porphyry Cu deposits including Radomiro Tomic and Mansa Mina whose origins are intimately related to active regional faulting during hypogene mineralization (~34–31 Ma; Fig. 1). This included the introduction of Cu related to an early stage of potassic alteration, followed by a structurally controlled phyllic overprint, and a later stage of supergene enrichment and alteration that peaked between 19 to 15 Ma and continued intermittently until the Pleistocene (Sillitoe and McKee, 1996; Ossandón et al., 2001; Reich et al., 2009b). The Chuquicamata pit is separated in two halves by the West fault (formerly known as West Fissure; Fig. 2A), a major strand of the West fault system, as the portion of the Domeyko fault system is called north of Calama (Ossandón et al., 2001; Tomlinson et al., 2001; Fig. 1).

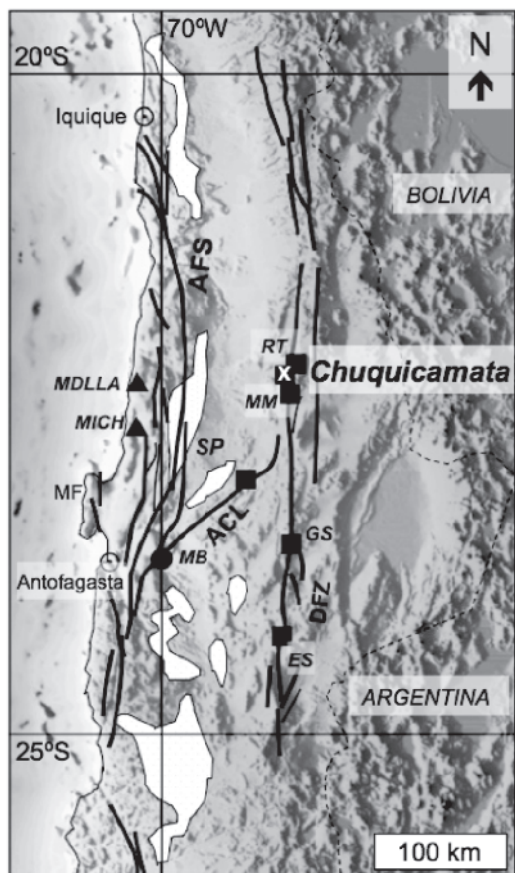


FIG. 1. Location map of the study area, showing Cu deposits with well-developed supergene oxidation zones. Squares are porphyry Cu deposits (GS = Gaby Sur, ES = Escondida, MM = Mansa Mina, RT = Radomiro Tomic), triangles are strata-bound Cu deposits (MDLLA = Mantos de la Luna, MICH = Michilla), and the circle is the porphyry-like Cu deposit Mantos Blancos (MB). Major regional faults and structural trends are shown (ACL = Antofagasta-Calama lineament, AFS = Atacama fault system, DFZ = Domeyko fault zone, MF = Mejillones fault), as well as the extensive nitrate (and iodine) soils of Atacama (in white).

Weathering and Cu recycling produced the world's largest supergene Cu profile at Chuquicamata, which is composed of a partially preserved leached capping and Cu oxide ore that replaced an upper chalcocite blanket, overlying a high-grade supergene chalcocite body that extended up to 800 m in depth (Fig. 2C). Oxide ore assemblages contain a large variety of minerals but primarily antlerite, brochantite, atacamite, chrysocolla, and Cu pitch. Wall-rock alteration mineralogy of the oxide ores is not well documented but was mostly quartz-sericite with increasing kaolinitic clay and residual K-feldspar to the east and at depth (Ossandón et al., 2001). Large quantities of the leached Cu migrated laterally to form exotic Cu oxides and silicates in adjacent gravels, i.e., the 300 Mt Exotica Cu deposit (Fig. 2A; Mortimer et al., 1978; Ossandón et al., 2001). This orebody contained flat high-grade veins of chrysocolla and Cu pitch, within variably altered gravels cemented by chrysocolla, with minor atacamite, Cu wad, and Cu pitch (Munchmeyer, 1996).

At Chuquicamata, anomalous concentrations of iodine were reported in the supergene oxide zone, including historic accounts on the observation of small clouds of purplish smoke noted on several occasions during blasting of the (now mined-out) oxidation blanket, which was shown to contain significant iodine (Jarrell, 1939, 1944). The Cu iodide marshite (CuI) was identified by Jarrell (1939) at the oxidized orebody at Chuquicamata, and in a later study, other Cu iodate minerals such as salesite ( $\text{Cu}(\text{IO}_3)(\text{OH})$ ) and bellingrite ( $\text{Cu}_3(\text{IO}_3)_6 \cdot 2\text{H}_2\text{O}$ ) were documented to occur in the oxide zone (Jarrell, 1944). All known marshite specimens occur between the south end of the Chuquicamata open pit and the Exotica mine (Jarrell, 1939; Mortimer, 1978; Fig. 2C).

Samples for this study came from the oxide zone of the deposit in the south end of the open pit (Fig. 2C), and contain fine-grained (<2 mm) marshite crystals (CuI, pale orange) that occur as associated with atacamite ( $\text{Cu}_2\text{Cl}(\text{OH})_3$ , green) (Fig. 2B). Intergrowth textures between the two minerals suggest that they were deposited more or less contemporaneously, with some atacamite deposited after the marshite. No iodate minerals were observed in the samples. It is important to note that the selection of marshite samples was limited by (1) the small amount of sample or core material remaining from the oxide zone at Chuquicamata, (2) the difficulty in obtaining pristine marshite specimens with no visible (optical) signs of corrosion and/or dissolution suitable for I-129 analysis. In addition to the mineral samples, an anomalously iodine-rich soil sample above the Mansa Mina deposit 10 km south of Chuquicamata was analyzed (Fig. 2A). Sample EMC107 (16,000 ppm I), retrieved just from above the fault trace, was the only one of a set of soil samples that contained the required iodine yield for I-129 determination. The samples were recovered in a transect above the deposit fracture zone during Camiro's Cu exploration program in the early 2000s (Fig. 2A) and have an anomalous element assemblage reflecting saline formation water (high Cl, Br, I) and elements indicating interaction with porphyry mineralization (e.g., high Se, Mo, Re, and Au; Cameron et al., 2010).

### The I-129 Isotope System

Iodine has one stable isotope,  $^{127}\text{I}$ , and one long-lived radioisotope,  $^{129}\text{I}$ , with a half-life of 15.7 Ma (Fehn et al., 2007a).

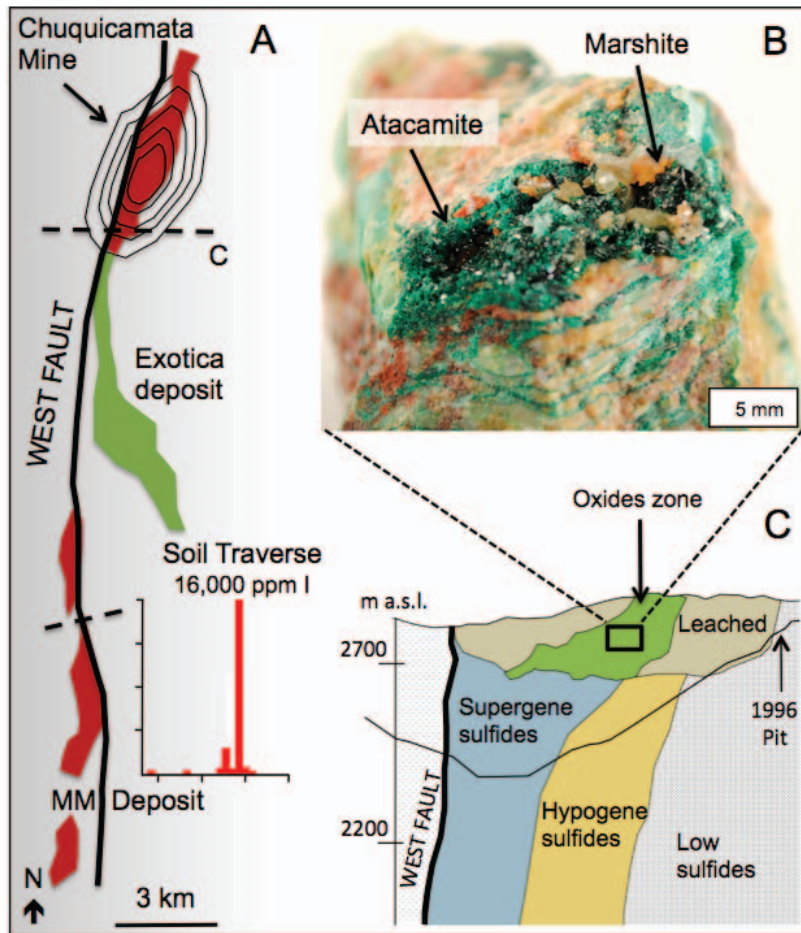


FIG. 2. (A). Chuquicamata district, showing the location of mines and main structural features. Soil sample was taken above the West fault (soil traverse). (B). Marshite (CuI) sample from Chuquicamata. The fine-grained pale orange crystals occur in association with atacamite (green). (C). Supergene enrichment and oxidation profile at Chuquicamata, showing the leach capping, oxidation zone, and supergene sulfide blanket.

The radioisotope  $^{129}\text{I}$  has two major production modes in nature (Fig. 3): (1) a cosmogenic component produced by the spallation of xenon isotopes in the atmosphere, and (2) a fissiogenic component related to the spontaneous fission of  $^{238}\text{U}$  in the crust, and to a much lesser extent, by neutron-induced fission of  $^{235}\text{U}$ . A third and more recent source of  $^{129}\text{I}$  in surface reservoirs is the anthropogenic component, produced from nuclear tests in the 1960s as well as ongoing releases from nuclear reprocessing plants (Fig. 3). Current contributions of anthropogenic  $^{129}\text{I}$  have led to a global increase in concentrations of this isotope by several orders of magnitude (Snyder and Fehn, 2002; Aldahan et al., 2007; Snyder et al., 2010). Although anthropogenic  $^{129}\text{I}$  is present in all surface reservoirs which are in rapid exchange with the marine surface waters, it is not present in deep sediments or in ground waters with ages  $>60$  years. Therefore, in most cases, the anthropogenic  $^{129}\text{I}$  signal can be detected because of the large difference between anthropogenic and natural values (Fehn et al., 2007a; Snyder et al., 2010).

The  $^{129}\text{I}$  system has potentially useful applications for the characterization of fluid sources and evolution of supergene ore systems (Fig. 3). For example, the cosmogenic signal is accumulated in fluids associated with organic matter (e.g.,

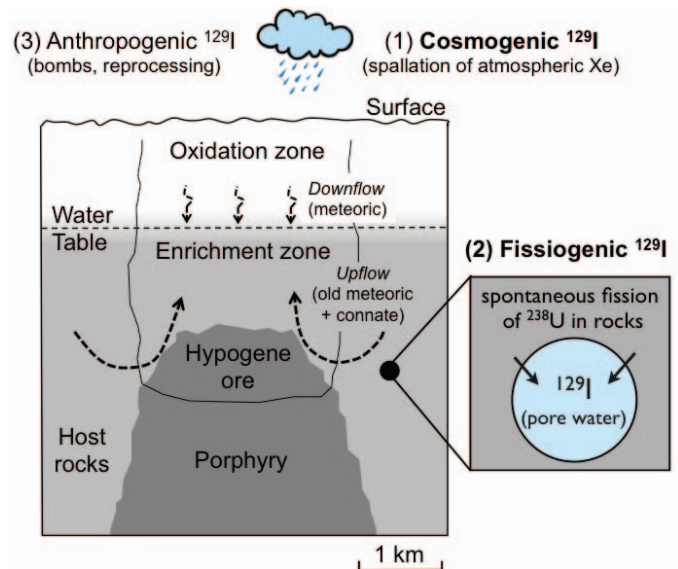


FIG. 3. Scheme showing the two natural modes of production of  $^{129}\text{I}$  (cosmogenic and fissiogenic components). Also shown is the anthropogenic component of  $^{129}\text{I}$ , produced as a fission product of  $^{235}\text{U}$  and  $^{239}\text{Pu}$  from nuclear tests and nuclear fuel reprocessing.

sedimentary rocks of marine origin), where the measured isotopic composition of iodine is used to determine the iodine source and time of separation from surface reservoirs (Moran et al., 1995; Fehn et al., 2000; Snyder et al., 2003). On the other hand, contributions of the fissionogenic component can be used to evaluate the crustal build-up of  $^{129}\text{I}$  and calculate the age and residence time of fluids in host rocks with  $>1$  ppm U (Fabryka-Martin et al., 1985; Fehn et al., 1992; Bottomley et al., 2002).

### Analytical Method

After careful optical inspection, marshite crystals were hand-picked from rock chips and the iodine contents were determined using hydrolysis according to procedures by Schnetger and Muramatsu (1996). Approximately 500 mg of powdered mineral sample was placed in a porcelain boat and heated to  $900^\circ\text{C}$  in a tube furnace using a quartz process tube while being exposed to a steady stream of wet oxygen gas. Vapors formed were passed through a reducing solution of 0.1% tetramethylammonium hydroxide trap solution. For the iodine-rich sediment (where more than 500 mg of sample was required to yield 1 mg iodine), powdered sample was combined with 18M $\Omega$  water and placed in 50 mL centrifuge tubes, then agitated for 8 h. The mixture was then centrifuged and the leachate was separated from the sediment. In both cases, either the trap solution or the leachate was then extracted using ion exchange resin (Hou et al., 2001) and precipitation as purified silver iodide (Fehn et al., 1992).  $^{129}\text{I}/\text{I}$  ratios were determined by accelerator mass spectrometry (AMS) at PRIME lab, Purdue University (Indiana, United States), following established routines (Sharma et al., 2000). Because the  $^{129}\text{I}$  abundance is subject to the total amount of iodine in samples, amounts are expressed as  $^{129}\text{I}/\text{I}$  ratios. Since there is only one stable isotope of iodine ( $^{127}\text{I}$ ) and the long-lived isotope  $^{129}\text{I}$  is present in very small amounts, the  $^{129}\text{I}/\text{I}$  ratio ( $^{129}\text{I}$  over total iodine) is for all practical purposes identical to  $^{129}\text{I}/^{127}\text{I}$ . The theoretical detection limit of the AMS system is on the order of  $2 \times 10^{-15}$   $^{129}\text{I}$  atoms per total I atoms, estimated based on counting statistics and measurement times, although the practical detection limit is, however, somewhat higher since suitable blank materials with ratios below  $\sim 20 \times 10^{-15}$  are not available (Fehn et al., 2007a).

### Results and Discussion

#### $^{129}\text{I}/\text{I}$ ratios of marshite and soil from Chuquicamata

The  $^{129}\text{I}/\text{I}$  ratios of supergene iodide minerals and soil from Chuquicamata are reported in Table 1. Individual precision of the AMS determinations ( $1\sigma$ ) is listed together with the ratios. Marshites from Chuquicamata are clustered within a narrow range of  $^{129}\text{I}/\text{I}$  ratios, with values at  $187 \pm 17$ ,  $201 \pm 14$ ,

$218 \pm 72$ , and  $562 \pm 77$  ( $\times 10^{-15}$ ), similar to the ratio reported for the anomalous iodine-rich soil above the Mansa Mina deposit, nearby Chuquicamata ( $473 \pm 75 \times 10^{-15}$ ; Fig. 4A).

#### Sources of iodine at Chuquicamata

The ratios of individual samples are compared to representative reservoirs for the  $^{129}\text{I}$  system in the Atacama Desert, as illustrated in Figure 4B. The global geochemical cycle of iodine is dominated by the marine system, and because of the long residence time of iodine in the oceans (0.3 Ma), seawater acts as a well-mixed isotopic reservoir for iodine, with a preanthropogenic marine input  $^{129}\text{I}/\text{I}$  ratio of  $1,500 \pm 150 \times 10^{-15}$  (Moran et al. 1998; Fehn et al., 2007a). Considering that oceans alone contribute nearly 98.8% of the total atmospheric iodine by volatilization from seawater, the isotopic composition of iodine in terrestrial surface reservoirs (e.g., meteoric surface and ground waters) is expected to be in isotopic equilibrium with marine iodine (Fabryka-Martin et al., 1985). The majority of the Earth's surficial iodine, however, resides in marine sediments along continental margins, intra- and back-arc basins (Muramatsu and Wedepohl, 1998; Snyder et al., 2010). Therefore, one probable source for the iodine in Chuquicamata could be the Jurassic to mid Cretaceous marine shales that form part of the uplifted Paleozoic-Mesozoic basement outcropping in the Calama basin (Mpodozis et al., 2005). Pore fluids hosted in recent marine sediments on the Peru margin have iodine ratios that decrease asymptotically with depth from seawater values ( $1,500 \times 10^{-15}$ ) to values of  $\sim 290 \times 10^{-15}$  at several hundred meters (Fehn et al., 2007b). Assuming similar iodine contents, an initial  $^{129}\text{I}/\text{I}$  ratio of  $290 \times 10^{-15}$  and a uranium content of 9 ppm, Mesozoic shales in the vicinity of Chuquicamata would have reached secular equilibrium ratio values of  $38 \times 10^{-15}$  after 40 m.y. (Fig. 4B, see Appendix for details).

Alternative sources of iodine in the region include deep crustal fluids and volcanic fluids (Fig. 4A, B). Deep crustal fluids show  $^{129}\text{I}/\text{I}$  ratios  $>2,000 \times 10^{-15}$  due to accumulation of  $^{129}\text{I}$  from sources more enriched in uranium and thorium and are significantly higher than the ratios observed at Chuquicamata. The deepest fluids sampled to date (4,000 m) from the KTB drill site in the Bohemian Massif, Germany, have an average  $^{129}\text{I}/\text{I}$  ratio of  $3460 \times 10^{-15}$  (Fehn and Snyder, 2005). On the other hand, high-temperature magmatic sources also typically have higher  $^{129}\text{I}/\text{I}$  ratios than those observed in marine sediments and in the Chuquicamata samples (Fig. 4A, B). The hottest fumaroles measured for iodine ( $874^\circ\text{C}$ ) at Satsuma-Iwojima, Japan, presented an  $^{129}\text{I}/\text{I}$  ratio of  $754 \times 10^{-15}$  (Snyder et al., 2002) while most fumaroles measured for  $^{129}\text{I}$  generally show an admixture of shallow ground-water and magmatic sources.

TABLE 1.  $^{129}\text{I}/\text{I}$  Ratios in Supergene Iodide Minerals (CuI, marshite) and Soil from the Chuquicamata Area

Material	Sample	Deposit	Location	$^{129}\text{I}/\text{I}$ ( $\times 10^{-15}$ at-at $^{-1}$ )	$\pm 1\sigma$ ( $\times 10^{-15}$ at-at $^{-1}$ )
CuI	C103579	Chuquicamata	South end (pit)	218	72
CuI	105768	Chuquicamata	South end (pit)	562	77
CuI	Atac-CH	Chuquicamata	South end (pit)	187	17
CuI	Mshxx-B	Chuquicamata	South end (pit)	201	14
Soil	EMC107	Mansa Mina	Surface	473	75

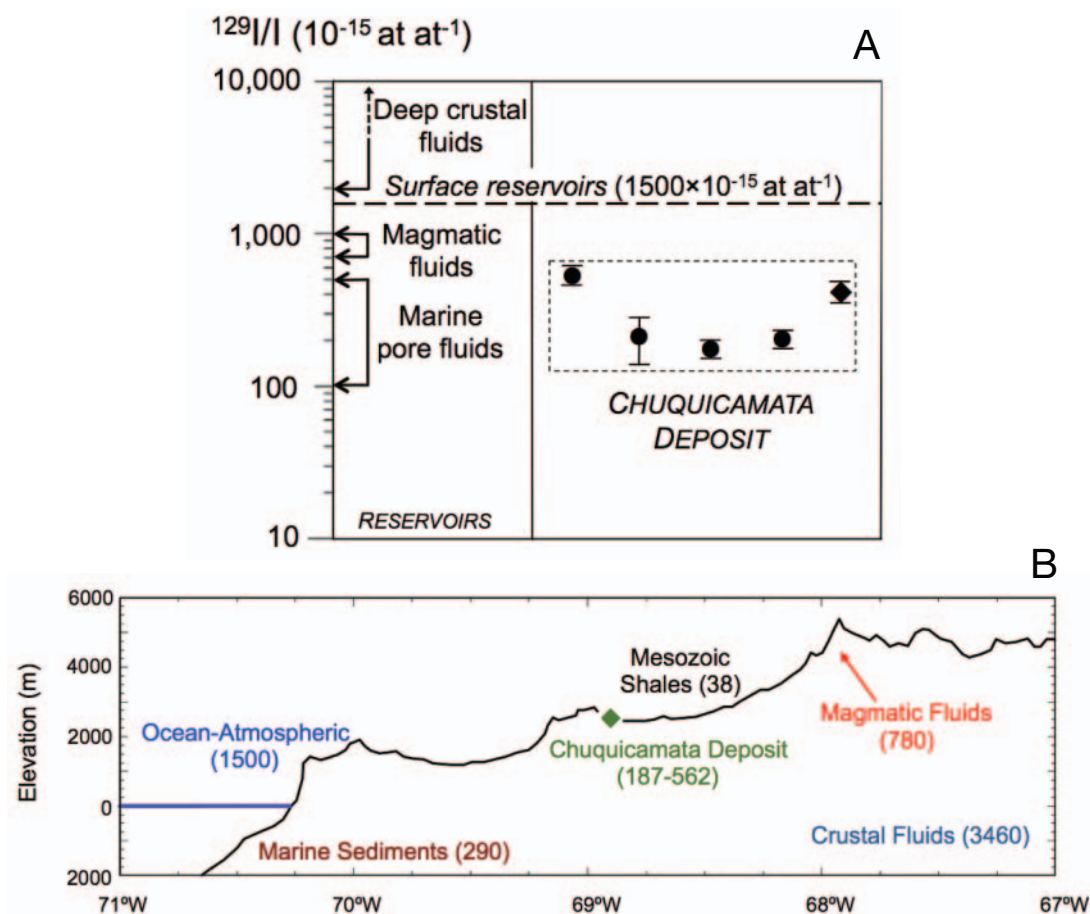


FIG. 4. (A). I-129 isotope data of marshites (circles) and iodine-rich soil sample (diamond) from Chuquicamata. Error bars are shown for each ratio. The left scale shows the known  $^{129}\text{I}/\text{I}$  ratios of different reservoirs, and the horizontal segmented line represents the preanthropogenic  $^{129}\text{I}/\text{I}$  ratio for surface reservoirs. (B). East-west profile at the latitude of Chuquicamata, showing different iodine reservoirs ( $^{129}\text{I}/\text{I}$  isotope ratio ranges in parentheses).

All marshite samples from Chuquicamata and soil above Mansa Mina have  $^{129}\text{I}/\text{I}$  ratios that are significantly lower than surface waters (i.e.,  $<1,500 \times 10^{-15}$ ), strongly suggesting that fluids involved in supergene enrichment were not exclusively meteoric in origin (Fig. 4A, B). The low  $^{129}\text{I}/\text{I}$  ratios observed at Chuquicamata ( $\sim 200\text{--}600 \times 10^{-15}$ ) indicate that an “old” cosmogenic contribution was present in the supergene fluids that precipitated the Cu iodides in the oxidation blanket of Chuquicamata and imprinted an anomalously rich iodine signature the soil sampled above the Mansa Mina buried body. This cosmogenic iodine component must have been most likely derived from organic material of marine origin (Fehn et al., 2000; Muramatsu et al., 2001).

A marine source for iodine is consistent with previous studies that have focused on chloride at the Radomiro Tomic and Chuquicamata supergene oxidation zones (Arcuri and Brimhall et al., 2003; Reich et al., 2008, 2009b). At Radomiro Tomic, located 5 km north of Chuquicamata, chlorine stable isotope data ( $\delta^{37}\text{Cl}$ ) indicate that the chlorine found in the supergene zone was derived from the Upper Jurassic marine sediments (Arcuri and Brimhall, 2003). Atacamite mineralization at Radomiro Tomic, Chuquicamata and Mina Sur share nonmagmatic, near 0.0‰  $\delta^{37}\text{Cl}$  values ( $-0.1$  to  $+0.1$ ‰) and

elevated Br contents (22–180 ppm), indicating a similar source for the introduction of chlorine (Upper Jurassic marine sediments: 22–24 ppm Br,  $-0.8$  to  $+0.5$ ‰  $\delta^{37}\text{Cl}$ ). These results argue against a meteoric source for chloride and are consistent with fissiogenic  $^{36}\text{Cl}$  data in atacamite from Radomiro Tomic and Chuquicamata, which suggest that deep saline formation waters were involved in atacamite formation (Reich et al., 2008, 2009b).

#### *The potential of $^{129}\text{I}$ as a geochemical tracer for supergene processes*

The I-129 system has been successfully used in geochemical studies as a tracer for determining ages and migration of iodine-rich brines related to methane hydrates in active continental margins (Muramatsu et al., 2001; Snyder et al., 2003; Fehn et al., 2007a). Isolated systems (i.e., without anthropogenic contamination) usually contain lower or close to the estimated pre-nuclear  $^{129}\text{I}/\text{I}$  ratios of  $1,500 \times 10^{-15}$ , so for a correct interpretation of results one must consider the effect of possible fissiogenic production and initial concentration on isotopic ratios.

Assuming that the  $^{129}\text{I}$  budget in the Cu iodides represents the  $^{129}\text{I}$  budget of the water from which they precipitated (i.e.,

no mineral-fluid isotope fractionation occurred during precipitation), the  $^{129}\text{I}/\text{I}$  ratios can be used as isotopic tracers for iodine. Since the low  $^{129}\text{I}/\text{I}$  ratios observed at Chuquicamata are not consistent with surface and ground water sources of meteoric origin, we calculated the expected  $^{129}\text{I}/\text{I}$  ratios of iodine-rich fluids sourced from the sedimentary rocks of marine origin that form part of the basement in the Calama and/or Chuquicamata area (the Low Jurassic to mid Cretaceous marine sequences, Arcuri and Brimhall, 2003; Mpodozis et al., 2005). A detailed explanation of the geochemical models used can be found in the Appendix.

The first modeled scenario is represented by the black curve in Figure 5 and considers that the parent fluid source (1) had a typical initial condition found in marine pore fluids during sediment deposition (i.e., an “old” cosmogenic component of  $^{129}\text{I}/\text{I} = 290 \times 10^{-15}$ , and  $\text{I} = 143 \text{ ppm}$ ,  $\text{Cl} = 18 \text{ g/L}$ ; Fehn et al., 2007b); (2) had a subsurface contribution of  $^{129}\text{I}$  related to spontaneous fission of U in the host rocks (i.e., “fisiogenic” component, calculated considering  $\text{U} = 9 \text{ ppm}$  at Chuquicamata (International Atomic Energy Agency, 1980a; porosity = 10% and density =  $2,700 \text{ kg} \times \text{m}^{-3}$ ); and (3) did not mix with other fluid sources, including ground water of meteoric origin. The modeled  $^{129}\text{I}/\text{I}$  ratios indicate that secular equilibrium was attained at  $\sim 40 \text{ Ma}$  at  $38 \times 10^{-15}$  ratio (Fig. 5, see Appendix for details). Taking into account the fact that all of the Chuquicamata samples show  $^{129}\text{I}/\text{I}$  ratios greater than the secular equilibrium value (Fig. 5), solutions that precipitated the iodides could not have been exclusively undiluted deep pore fluids or formation waters.

The second scenario involves dilution of the deep pore fluids by ground water of meteoric origin, using a mixing model

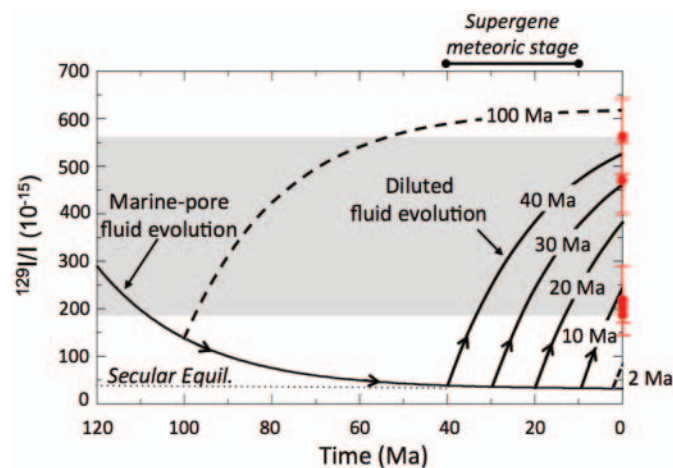


FIG. 5. Mixing model of progressive dilution between iodine-rich sediment pore fluids (deep formation waters) and meteoric water. The black curve below shows the evolution of pore fluids in the basement rocks, assuming decay of the cosmogenic  $^{129}\text{I}$  component and fissiogenic  $^{129}\text{I}$  build-up conditions found at Chuquicamata. Secular equilibrium is reached at  $\sim 40 \text{ Ma}$  (dotted horizontal line). Modeled fluid trajectories (black curves with arrows) show the effect of dilution of the pore fluids (5%) by sufficient meteoric water (95%) between 40 and 10 Ma (supergene meteoric stage), before desiccation of the Atacama region. The modeled trajectories predict the observed range of  $^{129}\text{I}/\text{I}$  ratios at Chuquicamata (horizontal gray area, and red data points with error bars). Also shown are fluid trajectories resulting from mixing at 100 and 2 Ma that do not reproduce the observed I-129 data (segmented curves).

that takes into account the past climatic evolution of the region (see Appendix). The fluid  $^{129}\text{I}/\text{I}$  ratios were modeled assuming that the pore waters mixed with meteoric ground waters during the main supergene enrichment and oxidation stage in the Atacama region between 40 and 10 Ma, under semiarid climate conditions with moderate precipitation ( $>10 \text{ cm/yr}$ ) and ground-water recharge (Alpers and Brimhall, 1988; Sillitoe and McKee, 1996; Arancibia et al., 2006). The model considered the dilution of iodine-rich pore fluids in the host formations (using same initial conditions as scenario (1) by a meteoric water end member (with  $^{129}\text{I}/\text{I} = 1500 \times 10^{-15}$ ,  $\text{I} = 0.013 \text{ ppm}$ ,  $\text{Cl} = 0.35 \text{ ppm}$ , Fehn et al., 2007a). Mixing or dilution steps were taken at 40, 30, 20, and 10 Ma, and the expected  $^{129}\text{I}/\text{I}$  ratios are represented by the black arrowed curves in Figure 5. Results indicate that expected  $^{129}\text{I}/\text{I}$  ratios of the fluid overlap the mineral/soil  $^{129}\text{I}/\text{I}$  data at Chuquicamata, considering a pore/meteoric water fluid mixing ratio of  $\sim 0.05$  (5% pore fluids, 95% meteoric water). Therefore, iodine occurrence at Chuquicamata was most likely the result of a three-stage process that involved (1) the deposition of Mesozoic marine sediments, accompanied by decay of  $^{129}\text{I}$  over time to reach secular equilibrium iodine ratios at  $\sim 40 \text{ Ma}$ ; followed by (2) mixing of iodine-rich pore fluids in the marine sequences with downflowing meteoric fluids during the main stage of supergene enrichment ( $\sim 40\text{--}10 \text{ Ma}$ ), diluting the original iodine and allowing higher secular equilibrium ratios; and (3) precipitation of Cu iodides and formation of soil anomalies by interaction of the mixed fluids with the deposit under hyperarid conditions, leading to closure of the iodine system.

## Conclusions

Results from this study show that the iodine  $^{129}\text{I}/\text{I}$  isotope ratios of mineral and soil samples can be successfully used to trace the origin of supergene fluids in iodine-rich oxidation blankets, leach caps, and soils above buried Cu deposits. For the particular case of the Chuquicamata deposit, the low  $^{129}\text{I}/\text{I}$  ratios ( $\sim 200\text{--}600 \times 10^{-15}$ ) suggest that iodine was most likely derived from the sedimentary rocks that form part of the Low Jurassic to mid Cretaceous marine basement in the Chuquicamata and/or Calama area. These low  $^{129}\text{I}/\text{I}$  ratios observed at Chuquicamata are predicted by geochemical models that involve mixing between  $\sim 5\%$  deep pore fluids and  $\sim 95\%$  meteoric water during the main stage of supergene alteration ( $\sim 40\text{--}10 \text{ Ma}$ ), which peaked between  $\sim 19$  to  $15 \text{ Ma}$  in the Chuquicamata area (Sillitoe and McKee, 1996; Sillitoe, 2005; Arancibia et al., 2006).

Although the exact age of precipitation of the supergene iodides cannot be constrained from the  $^{129}\text{I}/\text{I}$  ratios, they do provide valuable information regarding the supergene history of the region. The nonmeteoric iodine signature reported here, when coupled with previous  $^{36}\text{Cl}$  and U-Th disequilibrium data in atacamite from Chuquicamata and other Cu deposits nearby indicating young ages ( $<2 \text{ Ma}$ ) and marine sources for chlorine (Arcuri and Brimhall, 2003; Reich et al., 2008, 2009b), strongly suggests that iodides precipitated from saline ground waters under well-established hyperarid conditions. Therefore, the presence of iodine minerals in supergene zones of ore deposits, together with other indicators of aridity, can provide cogent evidence of past hyperarid climate

conditions, as originally suggested by Boyle (1997) and more recently by Golebiowska et al. (2010).

It is noteworthy to mention that the close spatial association between major Cu deposits with anomalous supergene iodine concentrations (e.g., Spence, Mantos de la Luna) and the location of the extensive nitrate, iodine-bearing caliche soils in the central depression westward of Chuquicamata (Fig. 1, Ericksen, 1981) suggest a common genetic link for iodine in the region. Although more studies are needed, these features indicate that saline ground-water alteration in the Atacama Desert may have been more extensive than previously thought.

### Acknowledgments

Support for this study was provided by FONDECYT grant 1100014 to Martin Reich and by FONDAP project 15090013 “Centro de Excelencia en Geotermia de los Andes, CEGA.” We thank Paul Pohwat at the Smithsonian Institution, Robert Lavinsky (the Arkenstone), and Álvaro Puig at Codelec for providing samples and logistical support. M. Caffee and the AMS group at PrimeLab, Purdue University, are acknowledged for carrying out the I-129 measurements. Finally, we acknowledge Larry Meinert for handling the manuscript and two anonymous reviewers for their helpful comments and suggestions.

### REFERENCES

- Aldahan, A., Alfimov, V., and Possnert, G., 2007, I-129 anthropogenic budget: Major sources and sinks: *Applied Geochemistry*, v. 22, p. 606–618.
- Alpers, C.N., Brimhall, G.H., 1988, Middle Miocene climatic change in the Atacama Desert, northern Chile: Evidence from supergene mineralization at La Escondida: *Geological Society of America Bulletin*, v. 100, p. 1640–1656.
- Andrews, J.N., Davis, S.N., Fabryka-Martin, J., Fontes, J.-Ch., Lehmann, B.E., Loosli, H., Michelot, J.L., Moser, H., Smith, B., and Wolf, M., 1989, The *in situ* production of radioisotopes in rock matrices with particular reference to the Stripa granite: *Geochimica et Cosmochimica Acta*, v. 53, p. 1803–1815.
- Arancibia, G., Matthews, S.J., and De Arce, C.P., 2006, K-Ar and Ar-40/Ar-39 geochronology of supergene processes in the Atacama Desert, northern Chile: Tectonic and climatic relations: *Journal of the Geological Society of London*, v. 163, p. 107–118.
- Arcuri, T., and Brimhall, G., 2003, The chloride source for atacamite mineralization at the Radomiro Tomic porphyry copper deposit, northern Chile: *ECONOMIC GEOLOGY*, v. 98, 1667–1681.
- Bottomley, D.J., Renaud, R., Kotzer, T., and Clark, I.D., 2002, Iodine-129 constraints on residence times of deep marine brines in the Canadian Shield: *Geology*, v. 30, p. 587–590.
- Boyle, D.R., 1997, Iodargyrite as an indicator of arid climatic conditions and its association with gold-bearing glacial tills of the Chibougamau-Chapais area, Quebec: *Canadian Mineralogist*, v. 35, p. 23–34.
- Cameron, E.M., Leybourne, M.I., and Kelley, D.L., 2002, Exploring for deeply covered mineral deposits: Formation of geochemical anomalies in northern Chile by earthquake-induced surface flooding of mineralized groundwaters: *Geology*, v. 30, p. 1007–1010.
- Cameron, E.M., Leybourne, M.I., Reich, M., and Palacios, C., 2010, Geochemical anomalies in northern Chile as a surface expression of the extended supergene metallogenesis of buried copper deposits: *Geochemistry: Exploration, Environment Analysis*, v. 10, p. 1–14.
- Chouinard, A., Williams-Jones, A.E., Leonardson, R.W., Hodgson, C.J., Silva, P., Tellez, C., Vega, J., and Rojas, F., 2005, Geology and genesis of the multistage high-sulfidation epithermal Pascua Au-Ag-Cu deposit, Chile and Argentina: *ECONOMIC GEOLOGY*, v. 100, p. 463–490.
- Decarvalho, H.G., Martins, J.B., Medeiros, E.L., and Tavares, O.A.P., 1982, Decay constant for the spontaneous fission process in <sup>238</sup>U: *Nuclear Instruments and Methods in Physics Research B*, v. 197, p. 417–426.
- Ericksen, G.E., 1981, Geology and origin of the Chilean nitrate deposits: U.S. Geological Survey Professional Paper 1188, 37 p.
- Fabryka-Martin, J., Bentley, H., Elmore, D., and Airey, P.L., 1985, Natural I-129 as an environmental tracer: *Geochimica et Cosmochimica Acta*, v. 49, p. 337–347.
- Fabryka-Martin, J., Whittemore, D.O., Davis, S.N., Kubik, P.W., and Sharma, P., 1991, Geochemistry of halogens in the Milk River aquifer, Alberta, Canada: *Applied Geochemistry*, v. 6, p. 447–464.
- Fard, M., Rastad, E., and Ghaderi, M., 2006, Epithermal gold and base metal mineralization at Gandy deposit, north of Central Iran and the role of rhyolitic intrusions: *Journal of Sciences, Islamic Republic of Iran*, v. 17, p. 327–335.
- Fehn, U., and Snyder, G.T., 2005, Residence times and source ages of deep crustal fluids: interpretation of I-129 and Cl-36 results from the KTB-VB drill site, Germany: *Geofluids*, v. 5, p. 42–51.
- Fehn, U., Peters, E.K., Tullai-Fitzpatrick, S., Kubik, P.W., Sharma, P., Teng, R.T.D., Gove, H.E., and Elmore, D., 1992, I-129 and Cl-36 concentrations in waters of the eastern Clear Lake area, California—residence times and source ages of hydrothermal fluids: *Geochimica et Cosmochimica Acta*, v. 56, p. 2069–2079.
- Fehn, U., Snyder, G., and Egeberg, P.K., 2000, Dating of pore waters with I-129: Relevance for the origin of marine gas hydrates: *Science*, v. 289, p. 2332–2335.
- Fehn, U., Moran, J.E., Snyder, G.T., and Muramatsu, Y., 2007a, The initial I-129/I ratio and the presence of “old” iodine in continental margins: *Nuclear Instruments and Methods in Physics Research Section B-Beam Interactions with Materials and Atoms*, v. 259, p. 496–502.
- Fehn, U., Snyder, G.T., and Muramatsu, Y., 2007b, Iodine as a tracer of organic material: 129I results from gas hydrate systems and fore arc fluids: *Journal of Geochemical Exploration*, v. 95, p. 66–80.
- Golebiowska, B., Pieczka, A., Rzepa, G., Matyszkiewicz, J., and Krajewski, M., 2010, Iodargyrite from Zalas (Cracow area, Poland) as an indicator of Oligocene–Miocene aridity in Central Europe: *Palaeogeography, Palaeoclimatology, Palaeoecology*, v. 296, p. 130–137.
- Hartley, A.J., and Chong, G., 2002, Late Pliocene age for the Atacama Desert: Implications for the desertification of western South America: *Geology*, v. 30, p. 43–46.
- Hebeda, E.H., Schulz, L., and Freundel, M., 1987, Radiogenic, fissiogenic, and nucleogenic noble-gases in zircons: *Earth and Planetary Science Letters*, v. 85, p. 79–90.
- Hou X., Dahlgard H., and Nielsen S.P., 2001, Chemical speciation analysis of I-129 in seawater and a preliminary investigation to use it as a tracer for geochemical cycle study of stable iodine: *Marine Chemistry*, v. 74, p. 145–155.
- International Atomic Energy Agency, 1980a, Nuclear theory for applications: Report IAEA-SMR-68.
- International Atomic Energy Agency, 1980b, Production of yellow cake and uranium fluorides: Advisory Group Meeting, 5–8 June 1979, Vienna, Proceedings, 368 p.
- Jarrell, O., 1939, Marshite and other minerals from Chuquicamata, Chile: *American Mineralogist*, v. 24, p. 629–635.
- 1944, Oxidation at Chuquicamata, Chile: *ECONOMIC GEOLOGY*, v. 39, p. 251–286.
- Kelley, D.L., Hall, G.E., Closs, G., Hamilton, I.C., and McEwen, R.M., 2003, The use of partial extraction geochemistry for copper exploration in northern Chile: *Geochemistry: Exploration, Environment, Analysis*, v. 3, p. 85–104.
- Leybourne, M.I., and Cameron, E.M., 2006a, Composition of soils and ground waters at the Pampa del Tamarugal, Chile: Anatomy of a fossil geochemical anomaly derived from a distant porphyry copper deposit: *ECONOMIC GEOLOGY*, v. 101, p. 1569–1581.
- 2006b, Composition of groundwaters associated with porphyry-Cu deposits, Atacama Desert, Chile: Elemental and isotopic constraints on water sources and water-rock reactions: *Geochimica et Cosmochimica Acta*, v. 70, 1616–1635.
- Millsted, P.W., 1998, Marshite-miersite solid solution and iodargyrite from Broken Hill, New South Wales, Australia: *Mineralogical Magazine*, v. 62, p. 471–475.
- Moran, J.E., Fehn, U., and Hanor, J.S., 1995, Determination of source ages and migration patterns of brines from the US Gulf Coast basin using I-129: *Geochimica et Cosmochimica Acta*, v. 59, p. 5055–5069.
- Moran, J.E., Fehn, U., and Teng, R.T.D., 1998, Variations in <sup>129</sup>I/<sup>127</sup>I ratios in recent marine sediments: Evidence for a fossil organic component: *Chemical Geology*, v. 152, p. 193–203.
- Moran, J.E., Oktay, S., Santschi, P.H., and Schink, D.R., 1999, Atmospheric dispersal of <sup>129</sup>I from nuclear fuel reprocessing facilities: *Environmental Science and Technology*, v. 33, p. 2536–2542.

- Mortimer, C., Munchmeyer, C., and Urqueta, I., 1978, Emplazamiento del yacimiento Exótica, Chile: *Revista Geológica de Chile*, v. 6, p. 41–51.
- Mote, T.I., Brimhall, G.H., Tidy-Finch, E., Muller, G., and Carrasco, P., 2001, Application of mass-balance modeling of sources, pathways, and sinks of supergene enrichment to exploration and discovery of the Quebrada Turquesa exotic copper orebody, El Salvador district, Chile: *ECONOMIC GEOLOGY*, v. 96, p. 367–386.
- Mpodozis, C., Arriagada, C., Basso, M., Roperch, P., Cobbold, P., and Reich, M., 2005, Late Mesozoic to Paleogene stratigraphy of the Salar de Atacama basin, Antofagasta, northern Chile: Implications for the tectonic evolution of the Central Andes: *Tectonophysics*, v. 399, p. 125–154.
- Munchmeyer, C., 1996, Exotic deposits: Products of lateral migration of supergene solutions from porphyry copper deposits: *Society of Economic Geologists Special Publication 5*, p. 43–58.
- Muramatsu, Y., and Wedepohl, K.H., 1998, The distribution of iodine in the earth's crust: *Chemical Geology*, v. 147, p. 201–216.
- Muramatsu, Y., Fehn, U., and Yoshida, S., 2001, Recycling of iodine in fore-arc areas: Evidence from the iodine brines in Chiba, Japan: *Earth and Planetary Science Letters*, v. 192, p. 583–593.
- Ossandón, G., Freraut, C. R., Gustafson, L.B., Lindsay, D.D., and Zentilli, M., 2001, Geology of the Chuquicamata mine: A progress report: *ECONOMIC GEOLOGY*, v. 96, p. 249–270.
- Palacios, C., Rouxel, O., Reich, M., Cameron, E., and Leybourne, M.I., 2011, Pleistocene recycling of copper at a porphyry system, Atacama Desert, Chile: Cu isotope evidence: *Mineralium Deposita*, v. 46, p. 1–7.
- Rech, J.A., Currie, B.S., Michalski, G., and Cowan, A.M., 2006, Neogene climate change and uplift in the Atacama Desert, Chile: *Geology*, v. 34, p. 761–764.
- Reich, M., Palacios, C., Parada, M.A., Fehn, U., Cameron, E.M., Leybourne, M.I., and Zúñiga, A., 2008, Atacamite formation by deep saline waters in copper deposits from the Atacama Desert, Chile: Evidence from fluid inclusions, groundwater geochemistry, TEM, and  $^{36}\text{Cl}$  data: *Mineralium Deposita*, v. 43, p. 663–675.
- Reich, M., Palacios, C., Alvear, M., Cameron, E.M., Leybourne, M.I., and Deditius, A., 2009a, Iodine-rich waters involved in supergene enrichment of the Mantos de la Luna argentiferous copper deposit, Atacama Desert, Chile: *Mineralium Deposita*, v. 44, p. 719–722.
- Reich, M., Palacios, C., Vargas, G., Luo, S., Cameron, E.M., Leybourne, M.I., Parada, M.A., Zúñiga, A., and You, C.F., 2009b, Supergene enrichment of copper deposits since the onset of modern hyperaridity in the Atacama Desert, Chile: *Mineralium Deposita*, v. 44, p. 497–504.
- Schnetger, B., and Muramatsu, Y., 1996, Determination of the halogens, with special reference to iodine, in geological and biological samples using pyrohydrolysis for preparation of inductively coupled plasma mass spectrometry and ion chromatography for measurement: *Analyst*, v. 121, p. 1627–1631.
- Sharma, P., Bourgeois, M., Elmore, D., Granger, D., Lipschutz, M.E., Ma, X., Miller, T., Mueller, K., Rickey, G., Simms, P., and Vogt, S., 2000, PRIME Lab AMS performance, upgrades and research applications: *Nuclear Instruments and Methods in Physics Research B*, v. 172, p. 112–123.
- Sillitoe, R.H., 2005, Supergene oxidized and enriched porphyry copper and related deposits: *ECONOMIC GEOLOGY 100<sup>TH</sup> ANNIVERSARY VOLUME*, p. 723–768.
- 2007, Hypogene reinterpretation of supergene silver enrichment at Chañarcillo, northern Chile: *ECONOMIC GEOLOGY*, v. 102, p. 777–781.
- Sillitoe, R.H., and McKee, E.H., 1996, Age of supergene oxidation and enrichment in the Chilean porphyry copper province: *ECONOMIC GEOLOGY*, v. 91, p. 164–179.
- Snyder, G.T. and Fabryka-Martin, J.T., 2007,  $^{129}\text{I}$  and  $^{36}\text{Cl}$  in dilute hydrocarbon waters: Marine-cosmogenic, in situ, and anthropogenic sources: *Applied Geochemistry*, v. 22, p. 692–714.
- Snyder, G.T., and Fehn, U., 2002, Origin of iodine in volcanic fluids: I-129 results from the Central American volcanic arc: *Geochimica et Cosmochimica Acta*, v. 66, p. 3827–3838.
- Snyder, G.T., Fehn, U. and Goff, F., 2002, Iodine isotope ratios and halide concentrations of the Satsuma-Iwojima volcano, Japan: *Earth, Planets and Space*, v. 54, p. 265–273.
- Snyder, G.T., Riese, W.C., Franks, S., Fehn, U., Pelzmann, W.L., Gorody, A.W., and Moran, J.E., 2003, Origin and history of waters associated with coalbed methane: I-129, Cl-36, and stable isotope results from the Fruitland Formation, CO and NM: *Geochimica et Cosmochimica Acta*, v. 67, p. 4529–4544.
- Snyder, G., Aldahan, A., and Possnert, G., 2010, Global distribution and long term fate of anthropogenic I-129 in marine and surface water reservoirs: *Geochemistry, Geophysics, Geosystems*, v. 11, 19 p.
- Srinivasan, B., Alexander, E.C., Jr., and Manuel, O.K., 1971, I-129 in terrestrial ores: *Science*, v. 173, p. 327–328.
- Tomlinson, A.J., Dilles, J.H., and Maksiav, V., 2001, Application of apatite (U-Th)/He thermochronometry to the determination of the sense and amount of vertical fault Displacement at the Chuquicamata porphyry copper deposit, Chile—a discussion: *ECONOMIC GEOLOGY*, v. 96, p. 1307–1309.
- Williams, S.A., 1963, Oxidation of sulfide ores in the Mildren and Steppe mining districts, Pima County, Arizona: *ECONOMIC GEOLOGY*, v. 58, p. 1119–1125.
- Witzke, T., Kolitsch, U., Krause, W., Wiechowski, A., Medenbach, O., Kampf, A.R., Steele, I.M., and Favreau, G., 2006, Guanacoite,  $\text{Cu}_2\text{Mg}_2(\text{Mg}_{0.5}\text{Cu}_{0.5})(\text{OH})_4(\text{H}_2\text{O})_4(\text{AsO}_4)_2$ , a new arsenate mineral species from the El Guanaco mine, near Taltal, Chile: Description and crystal structure: *European Journal of Mineralogy*, v. 18, p. 813–821.
- Young, G.B.C., McElhiney, J.E., and Paul, G.W., 1991, An analysis of Fruitland coalbed methane production, Cedar Hill Field, northern San Juan basin: *Society of Petroleum Engineering Publication SPE22913*, p. 263–276.
- Zhou, Z., and Ballentine, C.J., 2006,  $^4\text{He}$  dating of groundwater associated with hydrocarbon reservoirs: *Chemical Geology*, v. 226, p. 309–327.



## APPENDIX

## Geochemical Modeling

In a closed system, where there is no effect of mixing, and also ignoring in situ production of  $^{129}\text{I}$ , the observed iodine isotope ratio is a function of the burial time and can be expressed by the simple decay equation:

$$R_{obs} = R_i e^{-\lambda_{129} t}, \quad (1)$$

where  $R_{obs}$  is the present observed  $^{129}\text{I}/\text{I}$  ratio,  $R_i$  is the initial value ( $1500 \times 10^{-15}$ ), the decay constant  $\lambda_{129}$  is  $4.41 \times 10^{-8} \text{yr}^{-1}$ , and  $t$  is the time elapsed since burial of organic matter. In the case of iodine in the Chuquicamata, one might assume that iodine-bearing marine sediments (shales) accumulated during the Mesozoic are then uplifted. We assume that at the time of uplift, the initial  $R_i$  is lower, at  $290 \times 10^{-15}$ , as is presently observed along the Peru margin (Fehn and Snyder, 2007b) and therefore calculate  $t$  as the time following uplift.

Fissiogenic  $^{129}\text{I}$  can manifest itself by significantly increasing the  $^{129}\text{I}/\text{I}$  ratio, particularly if the concentration of  $^{127}\text{I}$  in the associated pore waters is also low. This has been well documented in the fracture fluids of granites and other uranium-rich host rocks (Andrews et al., 1989; Fabryka-Martin et al., 1985; Bottomley et al., 2002; Fehn and Snyder, 2005). Therefore, amount of fissiogenic  $^{129}\text{I}$  accumulated in ground water as a function of time may be expressed as (Fabryka-Martin et al., 1985):

$$N_{129fis} = N_{238} \lambda_{sf} Y_{129} \varepsilon \rho \{(1 - \varphi)/\varphi\} (1 - e^{-\lambda t}) / \lambda_{129}, \quad (2)$$

where  $N_{129fis}$  = fissiogenic  $^{129}\text{I}$  atoms/L fluid,  $N_{238}$  =  $^{238}\text{U}$  atoms/kg rock,  $\lambda_{sf}$  = spontaneous fission decay constant for  $^{238}\text{U}$  ( $8.5 \times 10^{-17} \text{yr}^{-1}$ ; Decarvalho et al., 1982),  $Y_{129}$  = spontaneous fission yield of  $^{238}\text{U}$  at mass 129 ( $3 \times 10^{-4}$ ; Hebeda et al., 1987),  $\varepsilon$  = escape efficiency of  $^{129}\text{I}$  from the mineral lattice into the fluid,  $\rho$  = rock density,  $\varphi$  = effective porosity,  $\lambda_{129}$  = decay constant for  $^{129}\text{I}$  ( $4.41 \times 10^{-8} \text{yr}^{-1}$ ),  $t$  = residence time of fluids in contact with the rocks. Therefore, secular equilibrium value for  $^{129}\text{I}$  is expressed in equation (2), if one assumes that the term  $e^{-\lambda_{129} t}$  goes to zero.

For the purposes of this investigation, we assume shale density to be  $2.7 \text{g/cm}^3$  and effective porosity to be 0.01

(Young et al., 1991; International Atomic Energy Agency, 1980b). In such cases, where the effective porosity is  $\ll 1$ , the term  $\{(1 - \varphi)/\varphi\}$  in equation (2) reduces to  $(1/\varphi)$ . We assume a mean uranium concentration in the shales to be 9 ppm or  $2.28 \times 10^{13} \text{atom/kg}$  (Zhou and Ballentine, 2006; International Atomic Energy Agency report, 1980b), consistent with U concentrations in the area (Reich et al., 2008). The escape efficiency ( $\varepsilon$ ) is an expression of the fractional release of a given radio isotope produced within a mineral and transferred into the fluid phase. We assume a value of  $\varepsilon$  consistent with shales at 0.006 (Fabryka-Martin et al., 1991; Snyder and Fabryka-Martin, 2007). Equations (1) and (2) may be combined, incorporating the fissiogenic component:

$$R_{obs} = (R_i e^{-\lambda_{129} t} N_{127} + N_{129fis}) / N_{127}, \quad (3)$$

where  $N_{127}$  = stable  $^{127}\text{I}$  atoms/L fluid. We assume the starting concentration of stable iodine in the pores of the shale to be similar to pore waters on the Peru Margin (Fehn and Snyder, 2007b), which are typical of sediments in continental margin settings, where  $N_{127} = 143 \text{ppm}$  or  $6.8 \times 10^{20} \text{atoms/L}$ . Under these conditions, the observed  $^{129}\text{I}/\text{I}$  ratios should reach secular equilibrium at  $\sim 40 \text{Ma}$  at  $38 \times 10^{-15}$ .

For binary mixing, we assume a molar fraction of the original formation waters ( $X_{fw}$ ) with an initial  $^{129}\text{I}/\text{I}$  ratio ( $R_{fw}$ ) and concentration of stable iodine  $N_{127fw}$  as described above. We assume that this is mixed with preanthropogenic meteoric waters ( $X_{mw} = 1 - X_{fw}$ ) where  $R_{mw} = 1500 \times 10^{-15}$  and  $N_{127mw} = 0.013 \text{ppm}$  or  $6.2 \times 10^{16} \text{atoms/L}$  (Fehn et al., 2007a). The  $^{129}\text{I}/\text{I}$  ratio may then be expressed as:

$$R_{mix} = (X_{fw} R_{fw} N_{127fw} + X_{mw} R_{mw} N_{127mw}) / (X_{fw} N_{127fw} + X_{mw} N_{127mw}), \quad (4)$$

and

$$N_{127mix} = X_{fw} N_{127fw} + X_{mw} N_{127mw}. \quad (5)$$

The isotopic evolution of the diluted mixture is modeled (Fig. 5) using equation (3) and substituting  $R_{mix}$  for  $R_i$  and  $N_{127mix}$  for  $N_{127}$ .

# Climate change and tectonic uplift triggered the formation of the Atacama Desert's giant nitrate deposits

Alida Pérez-Fodich<sup>1,2</sup>, Martin Reich<sup>1,2\*</sup>, Fernanda Álvarez<sup>1,2</sup>, Glen T. Snyder<sup>3</sup>, Ronny Schoenberg<sup>4</sup>, Gabriel Vargas<sup>1,2</sup>, Yasuyuki Muramatsu<sup>5</sup>, and Udo Fehn<sup>6</sup>

<sup>1</sup>Department of Geology, Universidad de Chile, Plaza Ercilla 803, Santiago, Chile

<sup>2</sup>Andean Geothermal Center of Excellence (CEGA), Universidad de Chile, Santiago, Chile

<sup>3</sup>Department of Earth Science, Rice University, Houston, Texas 77251-1892, USA

<sup>4</sup>Department of Geoscience, University of Tübingen, Wilhelmstrasse 56, D-72074, 72074 Tübingen, Germany

<sup>5</sup>Department of Chemistry, Gakushuin University, Tokyo 171-8588, Japan

<sup>6</sup>Department of Earth and Environmental Sciences, University of Rochester, Rochester, New York 14627, USA

## ABSTRACT

The giant nitrate deposits of the hyperarid Atacama Desert (Chile) are one of the most extraordinary, yet enigmatic, mineral occurrences on Earth. These deposits are complex assemblages of highly soluble nitrates, chlorides, sulfates, perchlorates, iodates, and chromates, and their preservation is the result of prevalent hyperarid climate conditions in the Atacama Desert since the late Miocene, with average rainfall rates of <10 mm/yr in the past ~3 m.y. Although several hypotheses have been proposed since the mid-1800s, the formation of these extensive deposits still remains highly controversial despite the fact that recent studies have argued toward an atmospheric source for the nitrate, sulfate, and perchlorate components. In this report, we focus on the often overlooked and poorly studied iodine and chromium components of Atacama's nitrates. We present the first cosmogenic iodine ( $^{129}\text{I}$ ) and stable chromium ( $\delta^{53/52}\text{Cr}$ ) isotope data of nitrates showing that groundwater has played an unforeseen role in the formation of these massive deposits. The isotopic signature of I in the nitrates ( $^{129}\text{I}/\text{I} \sim 150\text{--}600 \times 10^{-15}$ ) share similarities with deep sedimentary (marine) pore waters and shales, deviating significantly from atmospheric iodine ( $^{129}\text{I}/\text{I} \sim 1500 \times 10^{-15}$ ), while the positive and highly fractionated  $\delta^{53/52}\text{Cr}_{\text{SRM979}}$  values (+0.7‰ to +3‰) are indicative of intense Cr redox cycling due to groundwater transport. Our evidence points toward a multi-source genetic model for the Atacama Desert nitrate deposits, where these extensive accumulations were the result of long-lived, near-surface mineral precipitation driven by groundwater (i.e., chromates, iodates) coupled with dry atmospheric deposition (i.e., nitrates, perchlorates) and sea spray inputs (i.e., sulfates, chlorides), triggered by increasing aridity and tectonic uplift.

## INTRODUCTION

Massive nitrate accumulations on Earth's surface are scarce and their existence is restricted to hyperarid environments like the Atacama Desert of northern Chile, although minor amounts of nitrate are present in other desert environments such as Death Valley (western United States), the Gobi Desert (Turpan-Hami area, northwestern China), and the McMurdo Dry Valleys (Antarctica) (Ericksen, 1981; Ericksen et al. 1988; Michalski et al., 2005; Qin et al., 2012). The Atacama deposits are unique in terms of their massive extent and diversity in chemical and mineralogical compositions. First, they are the largest nitrate accumulations in the world, making up an almost continuous ~700-km-long by ~20-km-wide belt (Fig. 1), and have been the premier source for natural nitrate since the 1800s. The nitrate deposits of Atacama are also singular due to the presence of unusual oxidized components such as iodates, chromates, and perchlorates, hosted by a complex mineral bed ~0.2–3 m thick composed of nitrates, sulfates, and chlorides. These unique features have puzzled geologists since Darwin's visit to Atacama in 1835, and several hypotheses have been proposed to explain their origin (Ericksen, 1981). Most recent studies have focused on the

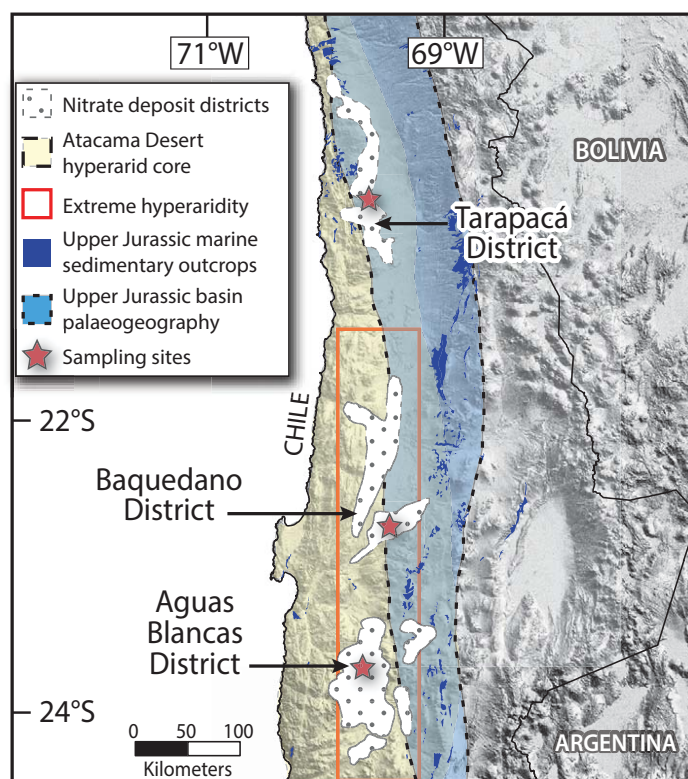


Figure 1. Map of Atacama's nitrate deposits displayed on digital elevation model of northern Chile. Location and distribution of nitrate deposits is shown in white dotted areas. Atacama Desert hyperarid core is shown in light yellow, and paleogeographic reconstruction of Jurassic Andean Basin (Vicente, 2006) is shown in light blue. Distribution of Upper Jurassic marine sedimentary outcrops (Mpodozis et al., 2005) is indicated in dark blue. Red rectangle shows extreme hyperarid area of Atacama Desert.

nitrogen, sulfur, and triple oxygen isotopic signatures from the abundant nitrate and sulfate mineral salts, and rare perchlorate compounds (Böhlke et al., 1997; Bao and Gu, 2004; Michalski et al., 2004). Oxygen, and to a lesser extent nitrogen, isotope data indicate that there is a significant atmospheric influence in nitrate formation related to dry deposition, while sulfur and oxygen data in sulfates indicate an influence of atmospheric, terrestrial, and marine sources (Böhlke et al., 1997; Rech et al., 2003; Michalski et al., 2004). Perchlorate, on the other hand, has a distinct atmospheric signature according to triple oxygen isotope values (Bao and Gu, 2004). Despite these recent advances, available geochemical and isotopic data on nitrate, sulfate, and perchlorate are not sufficiently diagnostic to yield a genetic model that explains the occurrence of all mineral components, including the exotic iodates and chromates. Iodine (I) occurrence

\*E-mail: mreich@ing.uchile.cl.

is so exceptional that Atacama's nitrates are currently the world's prime source for I, with concentrations in the range of hundreds to thousands of parts per million (ppm), ~3–4 orders of magnitude higher than the average I content of the continental crust. Chromium (Cr), on the other hand, is widespread in the Atacama nitrates in the range of tens of parts per million, but can also be sufficiently enriched as Cr(VI) to form chromate-bearing minerals. In this report, we propose a multi-source model for the genesis of the nitrate deposits of Atacama that (1) explains the presence of the exotic iodine and chromium components, (2) integrates their occurrence to the most common compounds, such as nitrate and sulfate, and (3) incorporates the previously unforeseen role of groundwater, constraining nitrate deposit formation to an outstanding convergence of tectonic, hydrologic, and climatic conditions that favored the long-lived fixation and accumulation of chemical components from the atmosphere and subsurface water.

## SAMPLES AND METHODS

We used  $^{129}\text{I}/\text{I}$  isotopic ratios measured in nitrate ores to determine the source of iodate as an expression of the deviation from the pre-anthropogenic meteoric/atmospheric value of  $1500 \times 10^{-15}$  [at·at $^{-1}$ ], typical of surficial reservoirs (meteoric water, seawater, and sea spray) uncontaminated with  $^{129}\text{I}$  from nuclear weapons testing and fuel reprocessing (Fehn et al., 2007). In addition, stable isotopes of Cr ( $\delta^{53/52}\text{Cr}$ ) were used to constrain the source of chromate in the nitrates, and to test the involvement of redox cycling between soluble Cr(VI) and insoluble Cr(III) in groundwater (Schoenberg et al., 2008).

To obtain  $^{129}\text{I}/\text{I}$  ratios, 30–50 g of powdered nitrate samples were diluted in 100 mL of deionized water, to release iodine as  $\text{IO}_3^-$ . Iodine was extracted into carbon tetrachloride, then back-extracted by a Na-bisulfite solution and precipitated as ~2 mg AgI targets. Iodine isotopic ratios were measured using accelerator mass spectrometry at the PRIME Lab, Purdue University (Indiana, USA).

To determine the  $\delta^{53/52}\text{Cr}$  values of chromate components in nitrate, 100–300 mg of sample was dissolved in 1.2 mL of deionized water, and was centrifuged to remove the minor detrital fraction. A  $^{50}\text{Cr}$ - $^{54}\text{Cr}$  spike solution of known composition was added to the supernate. Cr purification followed the anion-exchange and liquid-liquid extraction methods established by Schoenberg et al. (2008). Cr isotope analyses were performed on a Neptune Plus multicollector–inductively coupled plasma–mass spectrometer (MC-ICP-MS) at the University of Tübingen (Germany). Cr isotope data are given in the  $\delta$  notation relative to the chromium standard NIST SRM 979 (National Institute of Standards and Technology [NIST] standard reference material [SRM]).

## RESULTS AND DISCUSSION

The  $^{129}\text{I}/\text{I}$  ratios of nitrate samples from the Aguas Blancas and Baquedano districts in the hyperarid core of the Atacama Desert (Fig. 1) range between  $148.9 \pm 9.5 \times 10^{-15}$  and  $1580 \pm 244.1 \times 10^{-15}$ , but most of them are clustered within a narrow range, ~100–500  $\times 10^{-15}$  (average  $483.2 \pm 107.9 \times 10^{-15}$ ), deviating significantly from the pre-anthropogenic atmospheric value of  $1500 \pm 150 \times 10^{-15}$  (Fig. 2; Table DR1 in the GSA Data Repository<sup>1</sup>). These significantly low ratios rule out a prevalent atmospheric/eolian source for most of the I and point toward an old I source (Fehn et al., 2007; Fehn, 2012). Our results are in close agreement with  $^{129}\text{I}$  data from supergene enrichment zones of the giant Chuquicamata porphyry Cu deposit located ~100 km north east of the nitrate ore fields (Reich et al., 2013), strongly suggesting that the anomalous enrichment of I in the nitrates and in supergene Cu deposits shares a similar source.

<sup>1</sup>GSA Data Repository item 2014090, Table DR1 (iodine concentrations and isotopic ratios of nitrate samples) and Table DR2 (chromium concentrations and delta-chromium values of nitrate samples), is available online at [www.geosociety.org/pubs/ft2014.htm](http://www.geosociety.org/pubs/ft2014.htm), or on request from [editing@geosociety.org](mailto:editing@geosociety.org) or Documents Secretary, GSA, P.O. Box 9140, Boulder, CO 80301, USA.

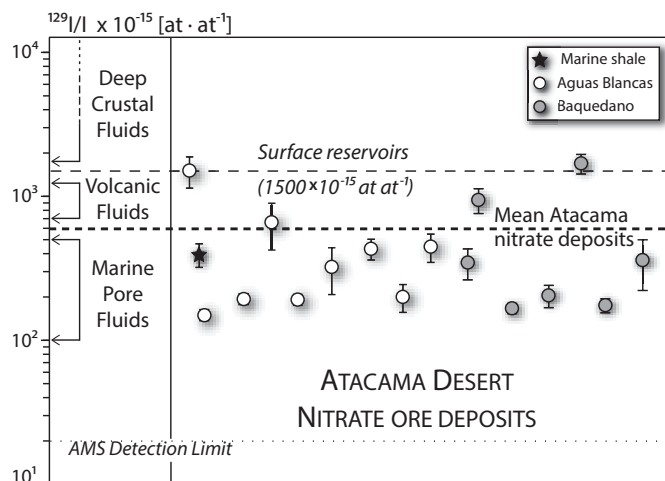


**Figure 2.**  $^{129}\text{I}/\text{I}$  ratios of nitrate samples from Atacama Desert (north-eastern Chile) (AMS—accelerator mass spectrometry). Left vertical axis shows  $^{129}\text{I}/\text{I}$  ratios for different Earth reservoirs (Fehn et al., 2007). Error bars are shown for each ratio. Thick horizontal dashed line shows average  $^{129}\text{I}/\text{I}$  ratio of the nitrates ( $483 \times 10^{-15}$ ), while light horizontal dashed line shows pre-anthropogenic surficial/atmospheric iodine ratios ( $1500 \times 10^{-15}$ ). White circles represent Aguas Blancas samples, and gray circles represent Baquedano samples. Black star shows  $^{129}\text{I}/\text{I}$  ratio of Jurassic marine shales from Atacama Desert.

Considering that the cosmogenic signal is accumulated in fluids related to organic matter (e.g., marine sediments; Fehn et al., 2007), the low  $^{129}\text{I}/\text{I}$  ratios (~100–500  $\times 10^{-15}$ ) reported here indicate that I was most likely leached from marine sedimentary rocks that form part of the Jurassic marine basin at the eastern border of the Atacama Desert (Vicente, 2006; Mpodozis et al., 2005) (Fig. 1), which can contain up to 90 ppm of I and show a distinct  $^{129}\text{I}/\text{I}$  isotopic ratio of  $\sim 393.1 \pm 73.5 \times 10^{-15}$  (Fig. 2). The higher  $^{129}\text{I}/\text{I}$  ratios (~600–1580  $\times 10^{-15}$ ) observed in a few samples are indicative of the influence of meteoric water with high pre-anthropogenic  $^{129}\text{I}/\text{I}$  ratios, most likely related to infrequent moisture and flooding events associated with increased precipitation in the High Andes, and subsequent groundwater recharge episodes that occurred since the formation of the nitrate deposits (e.g., 16–10 ka) (Nester et al., 2007).

The aforementioned I signal detected in the nitrates is consistent with Cr stable isotope data (Fig. 3; Table DR2). All nitrate samples have positive  $\delta^{53/52}\text{Cr}_{\text{SRM979}}$ , within a range of +0.050‰ to +3.088‰ (average of +1.104‰), showing a strong enrichment in the heavier Cr isotope compared to the mean value of silicate Earth reservoirs (Fig. 3). The  $\delta^{53/52}\text{Cr}_{\text{SRM979}}$  data for igneous and marine sedimentary rocks from the Atacama Desert are slightly negative as expected (–0.192‰ to –0.078‰), confirming that Cr isotopic fractionation involved in the Andean rock cycle is negligible. Cr in silicate Earth reservoirs is exclusively present in its trivalent oxidation state, Cr(III). It has been shown that Cr isotopes do not significantly fractionate during weathering and through oxidation from Cr(III) to Cr(VI) (Izbicki et al., 2008; Zink et al., 2010), while partial reduction of Cr(VI) to Cr(III) leads to isotopic fractionation in the per mil range on the  $^{53}\text{Cr}/^{52}\text{Cr}$  ratio. Therefore, the highly fractionated Cr isotope signature of chromate components in Atacama's nitrates with respect to common Cr sources such as igneous rocks and marine shales is strong evidence of extensive Cr redox cycling from its source to the final deposition in the nitrates. Our nitrate  $\delta^{53/52}\text{Cr}$  data are comparable to groundwater  $\delta^{53/52}\text{Cr}$  values from the Mojave Desert (Izbicki et al., 2008, 2012), and it is important to note that efficient natural Cr isotopic fractionation has only been reported associated to Cr reduction in groundwater, where softer chromate ( $\text{CrO}_4^{2-}$ ) and dichromate ( $\text{Cr}_2\text{O}_7^{2-}$ ) bonds of the lighter Cr isotopes are preferably broken, enriching the residual Cr(VI) in groundwater in heavier Cr isotopes. Therefore,

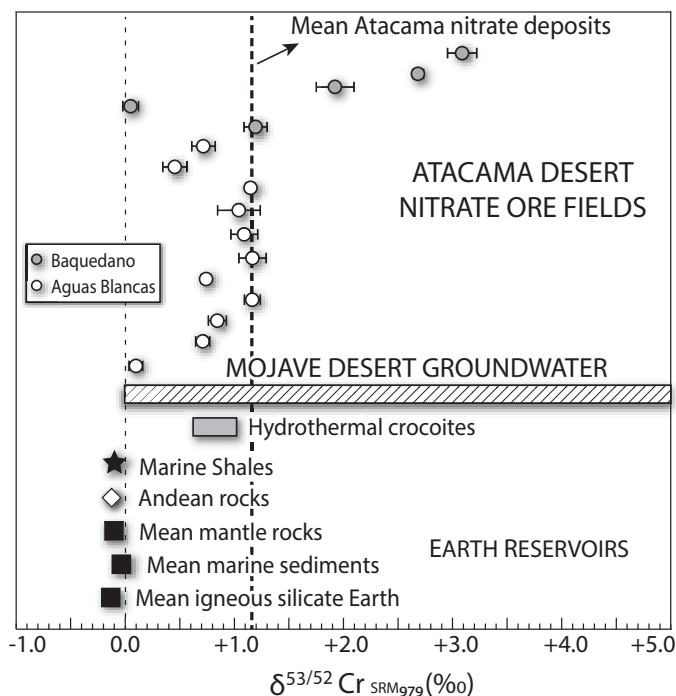


**Figure 3.**  $\delta^{53/52}\text{Cr}_{\text{SRM979}}$  of nitrate samples from Atacama Desert (northern Chile). White and gray circles represent Aguas Blancas and Baquedano samples, respectively. Error bars are shown for each value. Mojave Desert (western USA) groundwater  $\delta^{53/52}\text{Cr}$  values are displayed in hatched rectangle (Izbicki et al., 2008, 2012). Black star and white diamond show  $\delta^{53/52}\text{Cr}$  value of Jurassic marine shales and igneous rocks from Atacama, respectively. Mean values for igneous silicate Earth, marine sediments, mantle rocks, and hydrothermal crocoites are shown for comparison (Schoenberg et al., 2008). Thick vertical dashed line shows average  $\delta^{53/52}\text{Cr}$  value for nitrates (+1.104‰), and light dashed line represents 0.0‰ value.

we propose that Cr was leached as Cr(III) from its source upstream (e.g., Neogene volcanics and Jurassic shales in the Andes Mountains; Mpodozis et al., 2005), partially oxidized to Cr(VI), and released into groundwater that infiltrated westwards to the endorheic Central Basin, where decreasing dissolved  $\text{O}_2$  conditions and the presence of Fe(II)-bearing minerals partially reduced and removed Cr from solution leaving a progressively heavy  $\delta^{53/52}\text{Cr}$  signature downstream (Ellis et al., 2002). Within this framework, it is noteworthy that some previously reported non-marine values of sulfate and non-atmospheric nitrogen signatures of oxygen in the nitrate deposits (Böhlke et al., 1997; Rech et al., 2003; Michalski et al., 2004) are indicative of the various chemical inputs along the flow path, i.e., terrestrial sulfate from magmatic/geothermal fluids and sedimentary nitrogen contributions by microbial fixation in soils, into groundwater.

Our data provide new insights toward the understanding of the genesis of the enigmatic nitrate deposits of Atacama. Both  $^{129}\text{I}/\text{I}$  ratios and  $\delta^{53/52}\text{Cr}$  values point toward the important and previously unforeseen role played by groundwater during leaching and transport of the exotic I and Cr chemical components found in the Atacama nitrates. Based on our results and previously published O, N, and S stable isotope data, we propose an integrated, multi-source genetic model that explains the occurrence of all components found in the nitrate deposits and is consistent with the geological, hydrologic, and climatic evolution of this region (Fig. 4). Our model involves leaching of I and oxidized Cr from sedimentary rocks and volcanic sequences in the High Andes, which were then transported westwards along with other chemical species to the Central Basin by groundwater. Neogene climate change and tectonic uplift resulted in decreased precipitation rates from  $>200$  mm/yr to  $<20$  mm/yr between ca. 20 and 10 Ma, and to  $<3$  mm/yr today in its hyperarid core (Hartley and Chong, 2002; Reich et al., 2006, 2009; Amundson et al., 2012). This led to the development of an exclusively endorheic drainage system recharged in the High Andes (Magaritz et al., 1990), where increase in elevation of the Andean plateau due to uplift in the late Miocene (Allmendinger et al., 1997; Garzzone et al., 2008) would also have increased the hydraulic

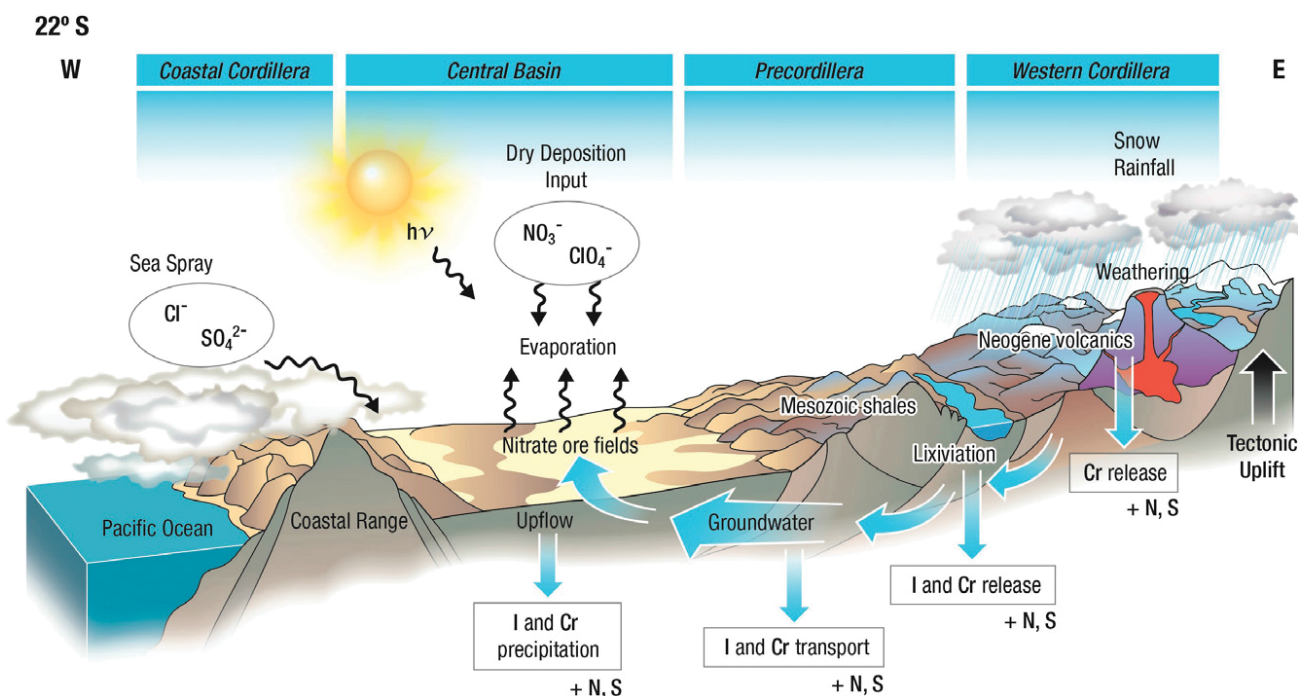


**Figure 4.** Multi-source genetic model for the formation of Atacama Desert's giant nitrate deposits. West-east section at latitude  $22^\circ\text{S}$  shows main structural domains: Coastal Cordillera, Central Basin, Precordillera, and Western Cordillera. Processes involved in formation of nitrate deposits are shown, i.e., atmospheric dry deposition, groundwater transport and precipitation, sea spray inputs, and evaporation. I—iodine as iodate ( $\text{IO}_3^-$ ) or iodide ( $\text{I}^-$ ); Cr—chromium as chromate ( $\text{CrO}_4^{2-}$ ), dichromate ( $\text{Cr}_2\text{O}_7^{2-}$ ), or Cr(III); S—sulfur as sulfate ( $\text{SO}_4^{2-}$ ); N—nitrogen as nitrate ( $\text{NO}_3^-$ ). Perchlorate ( $\text{ClO}_4^-$ ) and chloride ( $\text{Cl}^-$ ) are also shown.

potential between the wet Altiplano and the dry western slope, creating favorable conditions for increased groundwater flow toward the Central Basin (Hoke et al., 2004). The precipitation of iodate and chromate minerals (and probably some sulfate and nitrate) was favored downstream in the Central Basin by an “impermeable” barrier effect of the eastern slope of the Coastal Range (>1000 m above sea level at 10 Ma; Allmendinger and González, 2010) that allowed saline and reduced groundwater to efficiently rise, evaporate, and oxidize in the presence of a continuous dry deposition flux of atmospheric nitrate and perchlorate, and excursions of sulfate and/or chloride-bearing sea spray from the Pacific Ocean (Fig. 4).

## CONCLUDING REMARKS

We conclude that the large and almost continuous, ~700-km-long by ~20-km-wide belt of nitrate deposits of Atacama represent an unusual convergence of common physical-chemical processes with an ideal geologic, tectonic, hydrologic, and climatic setting that is specific to Atacama—that is, a convergent margin section undergoing rapid uplift since the late Miocene to elevations sufficient for exhumation and weathering of Jurassic marine sequences, and enhanced large-scale groundwater flow toward the Central Basin. The critical trigger for the formation of Atacama’s nitrate deposits was the concomitant increase in tectonic uplift and desiccation that allowed not only the precipitation of transported species from uprising groundwater in the Central Basin due to evaporation, but also the long-term accumulation and preservation of atmospheric nitrate.

## ACKNOWLEDGMENTS

The authors acknowledge funding by Fondo Nacional de Desarrollo Científico y Tecnológico (FONDECYT) 1100014 and Fondo de Financiamiento de Centros de Investigación en Áreas Prioritarias (FONDAP) 15090013 grants. We thank M. Caffee, I. Kleinhanns, and E. Reitter for their help with the I and Cr analysis, and two anonymous reviewers for their constructive comments.

## REFERENCES CITED

Allmendinger, R., and González, G., 2010, Neogene to Quaternary tectonics of the coastal Cordillera, northern Chile: *Tectonophysics*, v. 495, p. 93–110, doi:10.1016/j.tecto.2009.04.019.

Allmendinger, R.W., Jordan, T.E., Kay, S.M., and Isacks, B.L., 1997, The evolution of the Altiplano-Puna Plateau of the central Andes: *Annual Review of Earth and Planetary Sciences*, v. 25, p. 139–174, doi:10.1146/annurev.earth.25.1.139.

Amundson, R., Dietrich, W., Bellugi, D., Ewing, S., Nishizumi, K., Chong, G., Owen, J., Finkel, R., Heimsath, A., Stewart, B., and Caffee, M., 2012, Geomorphologic evidence for the late Pliocene onset of hyperaridity in the Atacama Desert: *Geological Society of America Bulletin*, v. 124, p. 1048–1070, doi:10.1130/B30445.1.

Bao, H., and Gu, B., 2004, Natural perchlorate has a unique oxygen isotope signature: *Environmental Science & Technology*, v. 38, p. 5073–5077, doi:10.1021/es049516z.

Böhlke, J.K., Erickson, G.E., and Revesz, K., 1997, Stable isotope evidence for an atmospheric origin of desert nitrate deposits in northern Chile and southern California, USA: *Chemical Geology*, v. 136, p. 135–152, doi:10.1016/S0009-2541(96)00124-6.

Ellis, A.S., Johnson, T.M., and Bullen, T.D., 2002, Chromium isotopes and the fate of hexavalent chromium in the environment: *Science*, v. 295, p. 2060–2062, doi:10.1126/science.1068368.

Erickson, G.E., 1981, *Geology and origin of the Chilean nitrate deposits*: U.S. Geological Survey Professional Paper 1188-B, p. 1–37.

Erickson, G.E., Hosterman, J.W., and St. Amand, P., 1988, *Chemistry, mineralogy and origin of the clay-hill nitrate deposits, Amargosa River valley, Death Valley region, California, U.S.A.*: *Chemical Geology*, v. 67, p. 85–102, doi:10.1016/0009-2541(88)90008-3.

Fehn, U., 2012, *Tracing crustal fluids: Applications of natural <sup>129</sup>I and <sup>36</sup>Cl*: *Annual Review of Earth and Planetary Sciences*, v. 40, p. 45–67, doi:10.1146/annurev-earth-042711-105528.

Fehn, U., Moran, J.E., Snyder, G.T., and Muramatsu, Y., 2007, The initial <sup>129</sup>I ratio and the presence of ‘old’ iodine in continental margins: *Nuclear Instruments and Methods in Physics Research Section B, Beam Interactions with Materials and Atoms*, v. 259, p. 496–502, doi:10.1016/j.nimb.2007.01.191.

Garzzone, C.N., Hoke, G.D., Libarkin, J.C., Whithers, S., MacFadden, B., Eiler, J., Ghosh, P., and Mulch, A., 2008, Rise of the Andes: *Science*, v. 320, p. 1304–1307, doi:10.1126/science.1148615.

Hartley, A.J., and Chong, G., 2002, Late Pliocene age for the Atacama Desert: Implications for the desertification of western South America: *Geology*, v. 30, p. 43–46, doi:10.1130/0091-7613(2002)030<0043:LPAFTA>2.0.CO;2.

Hoke, G.D., Isacks, B.L., Jordan, T.E., and Yu, J.S., 2004, Groundwater-sapping origin of the giant quebradas of northern Chile: *Geology*, v. 32, p. 605–608, doi:10.1130/G20601.1.

Izbicki, J.A., Ball, J.W., Bullen, T.D., and Sutley, S.J., 2008, Chromium, chromium isotopes and selected trace elements, western Mojave Desert, USA: *Applied Geochemistry*, v. 23, p. 1325–1352, doi:10.1016/j.apgeochem.2007.11.015.

Izbicki, J.A., Bullen, T.D., Martin, P., and Schroth, B., 2012, Delta Chromium-53/52 isotopic composition of native and contaminated groundwater, Mojave Desert, USA: *Applied Geochemistry*, v. 27, p. 841–853, doi:10.1016/j.apgeochem.2011.12.019.

Magaritz, M., Aravena, R., Peña, H., Suzuki, O., and Grilli, A., 1990, Source of ground water in the deserts of northern Chile: Evidence of deep circulation of ground water from the Andes: *Ground Water*, v. 28, p. 513–517, doi:10.1111/j.1745-6584.1990.tb01706.x.

Michalski, G., Böhlke, J.K., and Thiemens, M., 2004, Long term atmospheric deposition as the source of nitrate and other salts in the Atacama Desert, Chile: New evidence from mass independent oxygen isotopic compositions: *Geochimica et Cosmochimica Acta*, v. 68, p. 4023–4038, doi:10.1016/j.gca.2004.04.009.

Michalski, G., Bockheim, J.G., Kendall, C., and Thiemens, M., 2005, Isotopic composition of Antarctic Dry Valley nitrate: Implications for NO<sub>y</sub> sources and cycling in Antarctica: *Geophysical Research Letters*, v. 32, L13817, doi:10.1029/2004GL022121.

Mpodozis, C., Arriagada, C., Basso, M., Roperch, P., Cobbold, P., and Reich, M., 2005, Late Mesozoic to Paleogene stratigraphy of the Salar de Atacama Basin, Antofagasta, northern Chile: Implications for the tectonic evolution of the Central Andes: *Tectonophysics*, v. 399, p. 125–154, doi:10.1016/j.tecto.2004.12.019.

Nester, P.L., Gayó, E., Latorre, C., Jordan, T.E., and Blanco, N., 2007, Perennial stream discharge in the hyperarid Atacama Desert of northern Chile during the latest Pleistocene: *Proceedings of the National Academy of Sciences of the United States of America*, v. 104, p. 19,724–19,729, doi:10.1073/pnas.0705373104.

Qin, Y., Bao, H., Liu, F., Hou, K., Wan, D., and Zhang, C., 2012, Massive atmospheric nitrate accumulation in a continental interior desert, northwestern China: *Geology*, v. 40, p. 623–626, doi:10.1130/G32953.1.

Rech, J.A., Quade, J., and Hart, W.S., 2003, Isotopic evidence for the source of Ca and S in soil gypsum, anhydrite and calcite in the Atacama Desert, Chile: *Geochimica et Cosmochimica Acta*, v. 67, p. 575–586, doi:10.1016/S0016-7037(02)01175-4.

Rech, J.A., Currie, B.S., Michalski, G., and Cowan, A.M., 2006, Neogene climate change and uplift in the Atacama Desert, Chile: *Geology*, v. 34, p. 761–764, doi:10.1130/G22444.1.

Reich, M., Palacios, C., Vargas, G., Luo, S., Cameron, E.M., Leybourne, M.L., Parada, M.A., Zúñiga, A., and You, C., 2009, Supergene enrichment of copper deposits since the onset of modern hyperaridity in the Atacama Desert, Chile: *Mineralium Deposita*, v. 44, p. 497–504, doi:10.1007/s00126-009-0229-3.

Reich, M., Snyder, G.T., Alvarez, F., Pérez, A., Palacios, C., Vargas, G., Cameron, E.M., Muramatsu, Y., and Fehn, U., 2013, Using iodine to constrain supergene fluid sources in arid regions: Insights from the Chuquicamata oxide blanket: *Economic Geology and the Bulletin of the Society of Economic Geologists*, v. 108, p. 163–171, doi:10.2113/econgeo.108.1.163.

Schoenberg, R., Zink, S., Staubwasser, M., and von Blanckenburg, F., 2008, The stable Cr isotope inventory of solid Earth reservoirs determined by double spike MC-ICP-MS: *Chemical Geology*, v. 249, p. 294–306, doi:10.1016/j.chemgeo.2008.01.009.

Vicente, J.C., 2006, *Dynamic paleogeography of the Jurassic Andean Basin: Pattern of regression and general considerations on main features*: *Revista de la Asociación Geológica Argentina*, v. 61, p. 408–437.

Zink, S., Schoenberg, R., and Staubwasser, M., 2010, Isotopic fractionation and reaction kinetics between Cr(III) and Cr(VI) in aqueous media: *Geochimica et Cosmochimica Acta*, v. 74, p. 5729–5745, doi:10.1016/j.gca.2010.07.015.

Manuscript received 23 July 2013

Revised manuscript received 26 November 2013

Manuscript accepted 16 December 2013

Printed in USA

## Apéndice B. Resúmenes de congresos

### B.1 Annual Goldschmidt Conference, Prague, Czech Republic, 2011

#### The $^{129}\text{I}$ isotopic composition of supergene iodine minerals in Chile and Australia

Martin Reich <sup>a,b</sup>, Fernanda Álvarez <sup>a,b</sup>, Alida Pérez <sup>a,b</sup>, Glen Snyder <sup>c</sup>, Carlos Palacios <sup>a</sup>, Gabriel Vargas <sup>a,b</sup>, Yasuyuki Muramatsu <sup>d</sup>, Eron M. Cameron <sup>e</sup>, and Udo Fehn <sup>f</sup>

<sup>a</sup> Department of Geology, University of Chile, Santiago, Chile

<sup>b</sup> Andean Geothermal Center of Excellence (CEGA)

<sup>c</sup> Department of Earth Science, Rice University, Houston, TX, USA

<sup>d</sup> Chemical Department, Gakushuin University, Tokyo, Japan

<sup>e</sup> Eion Cameron Geochemical Inc., Carp, ON, Canada

<sup>f</sup> Department of Earth and Environmental Sciences, University of Rochester, Rochester, NY, USA

Because of its large ionic radius, iodine (I) is rarely incorporated into minerals and remains in the aqueous phase much longer than other halogens. Naturally-formed I minerals are very rare, but are found in the nitrate ore fields of the Atacama Desert in Chile and the supergene zones of base and precious ore deposits in extremely arid environments (Chile, Australia). The presence of I in Cu deposits in northern Chile has not been investigated previously, but provides the opportunity to apply the  $^{129}\text{I}$  system for the study of the tectonic history of the area and of climatic changes, particularly the desiccation of the Atacama region.

Here, we report the first  $^{129}\text{I}$  data of iodide minerals from supergene zones of Cu and Ag deposits from the hyperarid Atacama Desert. Two marshite (CuI) samples from the supergene zone of the Chuquicamata Cu deposit show  $^{129}\text{I}/\text{I}$  ratios of  $218 \pm 72$  and  $562 \pm 77$  ( $10^{-15}$  at-at<sup>-1</sup>), similar to the  $^{129}\text{I}$  isotopic signature of a geochemically anomalous, iodine rich soil sampled above the Spence porphyry Cu deposit ( $473 \pm 75$ ). Therefore, mineral and soil samples range between typical volcanic arc fluids ( $^{129}\text{I}/\text{I} \sim 700-1000$ ) and forearc fluids ( $^{129}\text{I}/\text{I} \sim 100-250$ ). In contrast, marshites and iodargyrites (AgI) from the Broken Hill Pb-Zn-Ag deposit in Australia and the Chañarcillo Ag deposit in Chile show a wider dispersion of  $^{129}\text{I}/\text{I}$  ratios, ranging from  $\sim 100$  to 2000, indicating a significant meteoric influence.

We suggest that I-rich fluids were involved in supergene enrichment and recycling of Cu in the Atacama region, revealing a complex link between multiple sources of fluids, active tectonics and climate change.

## B.2 XVIII Congreso Geológico Chileno, Antofagasta, Chile, 2012

### Origen del yodo en el Desierto de Atacama: $^{129}\text{I}$ como trazador de fluidos en procesos geodinámicos

Fernanda Álvarez <sup>a,b</sup>, Alida Pérez <sup>a,b</sup>, Glen Snyder <sup>c</sup>, Gabriel Vargas <sup>a,b</sup>, Yasuyuki Muramatsu <sup>d</sup>, Carlos Palacios <sup>a</sup>, Martin Reich <sup>a,b</sup>

<sup>a</sup> Departamento de Geología, Universidad de Chile, Santiago, Chile

<sup>b</sup> Centro de Excelencia en Geotermia de Los Andes, Universidad de Chile, Santiago, Chile

<sup>c</sup> Earth Sciences Department, Rice University, Houston, TX, USA

<sup>d</sup> Chemistry Department, Gakushuin University, Tokyo, Japan

**Resumen.** La distribución global del yodo (I) en la corteza terrestre está controlada por los sedimentos marinos del fondo oceánico. El I se encuentra fuertemente asociado a material orgánico, esto junto a la presencia del isótopo radiogénico  $^{129}\text{I}$ , permiten que el sistema isotópico del I sea útil para datar y trazar fluidos derivados de material orgánico. Para aplicar el sistema isotópico del yodo es importante conocer la razón inicial usada para el cálculo de edades  $R_i = 1500 \pm 150 \times 10^{-15} (\text{at}\cdot\text{at}^{-1})$ , la cual también ha sido utilizada para trazar fluidos relacionados a volcanes en zonas de subducción. En este estudio se presentan los primeros datos de concentraciones de I para cada reservorio en el Desierto de Atacama, los cuales indican que esta zona posee los valores más altos en la corteza terrestre. Por otro lado, resultados preliminares de razones isotópicas  $^{129}\text{I}/\text{I}$  son bastantes menores que la razón inicial, indicando que el I proviene de una o más fuentes profundas y habría sido movilizado por flujos subterráneos que ascienden a superficie por diferencias de presión. Estas razones isotópicas permiten estudiar el proceso de reciclaje de sedimentos en zonas de subducción.

Palabras Claves: yodo,  $^{129}\text{I}$ , nitratos, transporte de fluidos, fuentes, reservorios, reciclaje.

## B.3 AGU Meeting of the Americas, Cancun, Mexico, 2013

### Sources and sinks of natural and anthropogenic iodine in the hyperarid Atacama Desert of northern Chile

Fernanda Álvarez <sup>a,b</sup>, Alida Pérez <sup>a,b</sup>, Glen Snyder <sup>c</sup>, Gabriel Vargas <sup>a,b</sup>, Yasuyuki Muramatsu <sup>d</sup>, Martin Reich <sup>a,b</sup>

<sup>a</sup> Departamento de Geología, Universidad de Chile, Santiago, Chile

<sup>b</sup> Centro de Excelencia en Geotermia de Los Andes, Universidad de Chile, Santiago, Chile

<sup>c</sup> Earth Sciences Department, Rice University, Houston, TX, USA

<sup>d</sup> Chemistry Department, Gakushuin University, Tokyo, Japan

Iodine is a strongly biophilic element. Most of the global iodine budget concentrates in marine sediments, but in continental settings, the occurrence of iodine minerals is rare and restricted to hyper-arid environments. Currently, the Atacama Desert hosts the world's largest iodine crustal anomaly, where the occurrence of iodine minerals is constrained to the nitrate-iodine deposits located along the eastern side of the Coastal Range, and the supergene zones of copper deposits in the Central Depression and Precordillera. Although iodine enrichment has been documented for decades in this region, little is known about its setting, source and mechanism(s) of enrichment. In this study, we present the first survey of iodine concentrations and isotopic ratios ( $^{129}\text{I}/\text{I}$ ) of the different geochemical reservoirs in Atacama, including nitrate deposits, supergene copper ores, marine sedimentary rocks, geothermal fluids, groundwater and meteoric water.

Our results indicate that nitrate deposits contain the highest iodine concentrations of all reservoirs in Atacama, with a mean concentration of ~700 ppm. These anomalous values are followed by highly enriched soil samples above supergene copper deposits, and Mesozoic shales and limestones averaging ~50 ppm. On the other hand, the highest concentrations of iodine in fluids were measured in groundwater below nitrate ore fields (3.5-10 ppm). The  $^{129}\text{I}/\text{I}$  ratios in nitrate ores range from ~300 to ~400  $\times 10^{-15}$ . Supergene iodine minerals in copper deposits present values between 200 and 550  $\times 10^{-15}$  and ratios obtained from marine rocks averaging ~350  $\times 10^{-15}$ . Regarding isotopic ratios in fluids, seawater presents the highest  $^{129}\text{I}/\text{I}$  ratios (~11000  $\times 10^{-15}$ ).

In most of the reservoirs it is possible to identify a strong iodine enrichment compared to average crustal values. To reach these high concentrations it is necessary to have: (1) the presence of an enriched iodine source, (2) the removal of iodine by fluids from the source to the surficial reservoirs, and (3) the accumulation and preservation of iodine in these reservoirs. Isotopic ratios in nitrates and supergene iodine minerals are in agreement with previously reported  $^{129}\text{I}/\text{I}$  ratios in crustal fluids derived from organic material (200-400  $\times 10^{-15}$ ). Mesozoic shales are the most probable source for iodine because of the similar  $^{129}\text{I}/\text{I}$  ratios with rock reservoirs, high organic content and regional occurrence.



Finally, with respect to  $^{129}\text{I}/\text{I}$  ratios in fluids, most of the samples present values above the marine pre-anthropogenic value ( $1500 \pm 150 \times 10^{-15}$ ), and it is possible to identify a decreasing trend from sea to Western Cordillera. This indicates a more important marine influence in western samples and a meteoric component in eastern samples.

## B.4 Annual Goldschmidt Conference, Florence, Italy, 2013

### Sources, sinks and long-term cycling of iodine in a hyperarid continental margin

Fernanda Álvarez <sup>a</sup>, Martin Reich <sup>a,b</sup>, Alida Pérez <sup>a,b</sup>, Glen Snyder <sup>c</sup>, Gabriel Vargas <sup>a,b</sup>, Yasuyuki Muramatsu <sup>d</sup>, and Udo Fehn <sup>e</sup>

<sup>a</sup> Department of Geology, University of Chile, Santiago, Chile

<sup>b</sup> Andean Geothermal Center of Excellence (CEGA)

<sup>c</sup> Department of Earth Science, Rice University, Houston, TX, USA

<sup>d</sup> Chemical Department, Gakushuin University, Tokyo, Japan

<sup>e</sup> Department of Earth and Environmental Sciences, University of Rochester, Rochester, NY, USA

Iodine is a strongly biophilic element and its global distribution is dominated by marine sediments. Its strong association with organic material and the existence of a cosmogenic radioisotope (<sup>129</sup>I) make the iodine isotopic system suitable for the study of sediment recycling and fluid transport in subduction zones. In this work, we present the first comprehensive survey of iodine concentrations and isotopic ratios (<sup>129</sup>I/I) of different geochemical reservoirs in Atacama, including nitrate deposits, supergene copper ores, marine sedimentary rocks, geothermal fluids, groundwater and meteoric water. Nitrate deposits were found to have iodine concentrations significantly higher than mean values in the earth crust, with a mean concentration of ~700 ppm. These values are followed by soil samples above supergene copper deposits and Mesozoic sedimentary rocks (~50 ppm). Regarding the aqueous reservoirs, the highest concentrations were measured in groundwater below nitrate deposits (3.5-10 ppm) and in geothermal fluids (1-3 ppm). In most reservoirs, <sup>129</sup>I/I values are below the pre-anthropogenic input ratio of  $1500 \times 10^{-15}$ , demonstrating that recent anthropogenic additions are absent at solid reservoirs in Atacama. The majority of the ratios are between 150 and  $500 \times 10^{-15}$ . These ratios are in disagreement with subducted sediments being the source of iodine in the region, and suggest an older source located in the overlaying plate. However, there are some samples with higher values in nitrate deposits; we identified two additional clusters of ~800 and ~ $1500 \times 10^{-15}$ . The large variation observed in the isotopic ratios could be explained by a mixing of fluids from different organic and non-organic sources. Our results indicate an important fluid circulation in Chilean margin for at least 25 m.a., where deep water and shallower groundwater flow play an essential role in the iodine transport and accumulation. We suggest that the regional-scale iodine enrichment in Atacama is the result of a unique combination of geological, hydrological and tectonic conditions, and is strongly tied to large-scale groundwater flow over millions-of-years scales.

## B.5 Annual Goldschmidt Conference, Sacramento, USA, 2014

### Natural and anthropogenic iodine in Atacama: sources, sinks and cycling of iodine in a hyperarid continental margin

Fernanda Álvarez <sup>a</sup>, Martin Reich <sup>a,b</sup>, Alida Pérez <sup>a,b</sup>, Glen Snyder <sup>c</sup>, Gabriel Vargas <sup>a,b</sup>, Yasuyuki Muramatsu <sup>d</sup>, and Udo Fehn <sup>e</sup>

<sup>a</sup> Department of Geology, University of Chile, Santiago, Chile

<sup>b</sup> Andean Geothermal Center of Excellence (CEGA)

<sup>c</sup> Department of Earth Science, Rice University, Houston, TX, USA

<sup>d</sup> Chemical Department, Gakushuin University, Tokyo, Japan

<sup>e</sup> Department of Earth and Environmental Sciences, University of Rochester, Rochester, NY, USA

The Atacama region in northern Chile hosts the driest desert on Earth and is the world's premier iodine production province, only seconded by the Chiba brine fields in Japan. The origin of iodine enrichment in Atacama is controversial and fundamentally different processes have been invoked over the years, that involve marine, aeolian and more recently deep sedimentary and groundwater sources.

We present the first comprehensive survey of iodine concentrations and isotopic ratios ( $^{129}\text{I}/\text{I}$ ) of different geochemical reservoirs in Atacama, including nitrate deposits, supergene copper ores, marine sedimentary rocks, geothermal fluids, groundwater and meteoric water. Nitrate deposits were found to have iodine concentrations significantly higher than mean values in the earth crust ( $\sim 700$  ppm). These high values are followed by soil samples above supergene copper deposits and Mesozoic sedimentary rocks. In case of fluids, the highest concentrations were measured in groundwater below nitrates in the Central Depression (3.5-10 ppm) and in geothermal fluids in the volcanic arc (1-3 ppm).

In most solid reservoirs,  $^{129}\text{I}/\text{I}$  values are below the pre-anthropogenic input ratio of  $1500 \times 10^{-15}$ , demonstrating that anthropogenic additions are absent in them. Regarding fluids, seawater presents the highest  $^{129}\text{I}/\text{I}$  ratios ( $\sim 11000 \times 10^{-15}$ ), followed by groundwater below nitrates is  $\sim 10000 \times 10^{-15}$ , while  $^{129}\text{I}/\text{I}$  ratios in fluids from Western Cordillera are between 2000 and  $5000 \times 10^{-15}$ . The large variation observed in  $^{129}\text{I}/\text{I}$  ratios is explained by a mixing of fluids from different sources. Our results indicate an extensive fluid circulation in the Chilean margin for at least 25 m.a., where deep water and shallower groundwater flow play an essential role in the iodine transport and accumulation. We suggest that the regional-scale iodine enrichment in Atacama is the result of a unique combination of geological, hydrological and tectonic conditions, and is strongly tied to large-scale groundwater flow over millions-of-years scales.

